



University of Évora

Erasmus Mundus Master in ARCHaeological MATerials Science

Mestrado in Arqueologia e Ambiente (Erasmus Mundus - ARCHMAT)

Characterization of Medieval glass artefacts from Miranduolo site, Chiusdino, Italy

Ivona Posedi (m34322)

Professor Dr. Nicola Schiavon
(Supervisor – University of Évora)



Professor Dr. José António Paulo Mirão
(Co-supervisor – University of Évora)



Dr. Vittorio Fronza
(Co-supervisor – University of Siena)



Évora, September 2016



A tese não contém as críticas e sugestões do Júri

Abstract (English)

This archaeovitreological study deals with artefacts of Miranduolo site, Tuscany region (Italy), dated 1250-1350 AD. The Miranduolo site is a medieval hill-village dated from 7th to 14th century. The information obtained reveal that Miranduolo was under control of noble families, which displayed the social, economic and political power. It is marked by controlling the farmers and metal workers on the site, as well as having control over agricultural surpluses. No *in situ* glass workshop has been recovered, implying that the glass artefacts were imported.

One aim of this work is application of SEM-EDS to visualize textural characteristics and thickness of the pristine glass and corrosion layers. Preliminary qualification and semi-quantification of major and minor chemical elements will provide the data on the glass group present and fluxes employed. The data obtained will be integrated with the one obtained by more sensitive techniques such as PIXE/PIGE and LA-ICP-MS.

Twenty cross-sections of transparent glasses (colorless, azure, and different hues of yellow and) have been analyzed by VP-SEM. All the analyzed glasses display a homogenous matrix. Only four samples (MD 24, MD 139, MD 143, MD 259) show corrosion layers of various thickness with 2.25 μ m, 136-500 μ m, 26.8 μ m and 17.01 μ m. EDS linescan analyses indicate strong depletion in the corrosion layers of Na and K, while Ca depletes to a minor extent. In general, both glass composition and the burial conditions were favorable for preservation.

Samples can be classified as mainly plant ash Na-Ca-Si glasses made with both unpurified and purified Levantine ash. Only sample MD 243 is made from Barilla plant ash. Sample MD 139 cannot be classified into main compositional groups as K₂O is 1.33 wt% and MgO 5.92 wt%. In 8 samples MnO content is lower than 0.8 wt%, meaning that in these samples MnO is naturally present. In other 12 samples, MnO above 0.8 wt% indicates deliberate addition as a decolorant agent to intentionally obtain different hues or the amount added was not successful in making the glass transparent.

The results considering fluxes are compatible with archaeovitreological study from contemporary primary glass workshops in Tuscany. For determining the provenance of silica sources, further analysis with more sensitive techniques has to be carried out.

Resumo (Português)

Este estudo “arqueovitreologia” lida com artefatos do local Miranduolo, região da Toscana (Itália), datados de 1250-1350 AD. O sitio de Miranduolo é uma colina vila medieval datada do séc.VII ao séc.XIV. As informações obtidas revelam que Miranduolo estava sob o controle de famílias nobres, que exibiu o poder social, económico e político. É marcado por controlar os agricultores e trabalhadores do metal no sitio, bem como ter controlo sobre os excedentes agrícolas. Não há na oficina de vidro *in situ* foi recuperado, o que implica que os artefactos de vidro foram importados.

Um dos objetivos deste trabalho é a aplicação de SEM-EDS para visualizar características de textura e espessura das camadas de corrosão do vidro também como da áreas originais. qualificação preliminar e semi-quantificação de maiores e menores elementos químicos irá fornecer os dados sobre o grupo presente vidro e fluxos empregado. Os dados obtidos são integrados com os dados obtidos por meio de técnicas mais sensíveis, como PIXE / PIGE e LA-ICP-MS.

Vinte secções transversais de vidros transparentes (incolor, azul celeste, e diferentes tons de amarelo) foram analisados por VP-SEM. Todos os vidros analisados exibir uma matriz homogénea. Apenas quatro amostras (MD 24, MD 139, MD 143, MD 259) mostram camadas de corrosão de várias espessuras com 2,25 μ m, 136-500 μ m, 26,8 μ m e 17,01 μ m. Análises Linescan EDS indicam forte esgotamento nas camadas de corrosão de Na e K, enquanto Ca esgota, em menor grau. Em geral, tanto a composição de vidro e as condições de depósito foram favoráveis para a preservação.

As amostras podem ser classificados como vidros principalmente Na-Ca-Si feitas com cinzas de plantas do tipo levantino, não purificada e purificada. Apenas a amostra MD 243 é feita a partir de cinzas vegetais tipo “Barilla”. A amostra MD 139 não pode ser classificada em grupos principais de composição porque K₂O é 1,33% em peso e MgO 5,92% em peso. Em 8 amostras, o teor de MnO é menor do que 0,8% em peso, o que significa que nestas amostras MnO está naturalmente presente. Em outras 12 amostras, MnO acima de 0,8% em peso indica adição intencional como um agente de colorante para obter intencionalmente diferentes matizes ou o valor acrescentado não foi bem sucedido em fazer o vidro transparente. Os resultados, considerando os fluxos são compatíveis com o estudo “arqueovitreológico” com as principais oficinas de vidro contemporâneos na Toscana. Para determinar a origem das fontes de sílica, uma análise mais aprofundada com técnicas mais sensíveis tem de ser levada a cabo.

Table of contents

ACKNOWLEDGEMENTS	I
INTRODUCTION	1
1. ABOUT GLASS	5
1.1. DEFINITION, COMPOSITION, PROPERTIES AND BEHAVIOR OF GLASS.....	5
1.2. HISTORY OF GLASS PRODUCTION AND HISTORICAL DOCUMENTS	11
1.3. ARCHAEOVITREOLOGICAL CLASSIFICATION AND TERMINOLOGICAL ISSUES	14
2. THE ARCHAEOLOGICAL CONTEXT	20
2.1. THE ARCHAEOLOGICAL SITE OF MIRANDUOLO CASTLE.....	20
2.1.1. <i>Position</i>	20
2.1.2. <i>History</i>	21
2.1.3. <i>Excavation of Miranduolo castle</i>	22
2.1.4. <i>Miranduolo site catchment area</i>	24
2.1.5. <i>Periodization and development of the settlement</i>	24
2.1.6. <i>Excavation areas</i>	32
2.2. STATE OF THE ART OF ARCHAEOVITREOLOGY IN ITALY	35
3. MATERIALS AND METHODS	39
3.1. ANALYTICAL TECHNIQUES	39
3.1.1. <i>VP-SEM-EDS</i>	39
3.1.2. <i>PIXE/PIGE</i>	42
3.1.3. <i>LA-ICP-MS</i>	43
3.2. SAMPLING	47
3.3. EXPERIMENTAL METHODS	48
3.3.1. <i>VP-SEM-EDS</i>	48
3.3.2. <i>PIXE/PIGE</i>	49
3.3.3. <i>LA-ICP-MS</i>	51
4. RESULTS	54
4.1. SEM-EDS.....	54
4.1.1. <i>Elemental composition</i>	54
4.1.2. <i>Corrosion</i>	59
4.2. PIXE/PIGE	62
4.2.1. <i>Elemental composition</i>	62
4.2.2. <i>Corrosion</i>	66
4.3. LA-ICP-MS	76
4.3.1. <i>Elemental composition</i>	76
4.3.2. <i>Comparison of 50 μm and 15 μm laser ablation beam size</i>	89
4.3.3. <i>Corrosion</i>	93
5. DISCUSSION	100

6. CONCLUSION.....	109
APPENDIX 1 – MAPS AND FIGURES OF MIRANDUOLO.....	120
APPENDIX 2 – CATALOG OF GLASS ARTEFACTS FROM PERIOD II.....	131
APPENDIX 3 – VP-SEM-EDS PLOTS	138
APPENDIX 4 – PIXE/PIGE PLOTS AND CHEMICAL MAPS	143
APPENDIX 5 – LA-ICP-MS PLOTS	164
APPENDIX 6 – Fe_2O_3/MNO RATIO	184
APPENDIX 7 – COMPARISON OF RESULTS WITH CONTEMPORARY ITALIAN SITES	185

Acknowledgements

This work is a result of two years of gaining new knowledge. I take this opportunity to thank every person that in directly and indirectly provided their expertise and/or support.

I would like to express my deepest gratitude to my supervisor Professor Dr. Nick Schiavon, and co-supervisors Professor Dr. José Mirão and Dr. Vittorio Fronza for sharing their knowledge and giving input to make this thesis the best possible. Professor Dr. Nick Schiavon's role was not only as the thesis supervisor. The life lessons he taught me are highly appreciated and will not be forgotten.

I would like to thank the Department of Historical Sciences and Cultural Heritage, University of Siena, especially to Professor Dr. Marco Valenti for providing approval for the analyses, Dr. Alessandra Nardini and Dr. Vittorio Fronza for artefact handling and Manuele Putti for providing necessary archaeological data.

HERCULES Laboratory, which equipment has been used, is kindly acknowledged. I would especially like to show my appreciation to Dr. Pedro Barrulas for his LA-ICP-MS data acquisition and passing his knowledge for data treatment. I would also like to thank Dr. Massimo Beltrame and Dr. Milene Gil for their help with sample preparation.

Financial support by the Access to Research Infrastructures activity in the H2020 Programme of the EU (IPERION CH Grant Agreement) is gratefully acknowledged. I would like to express my gratitude to Dr. Zita Szikszai for the organization of the PIXE/PIGE analysis and to the whole ion beam staff at MTA Atomki, Debrecen who worked long night shifts: Dr. Anikó Angyal, Dr. László Csedreki, Dr. Enikő Furu, Dr. Róbert Huszánk, Dr. Zsófia Kertész, Dr. Enikő Papp and Dr. Zoltán Szoboszlai.

I would kindly like to thank Carla Soto for the advice on the selection of data treatment software and advice for data manipulation, which made data processing swift.

All the professors of the ARCHMAT consortium, which in one way or the other have been a part of my education, are kindly acknowledged.

I would like to thank Professor Dr. José Mirão, Luis Dias for SEM-EDS data acquisition, Sonia Costa for photography and Dr. Pedro Barrulas for LA-ICP-MS data acquisition within the Alentejo slate plaques project.

I would like to thank Professor Dr. Javier Campo for giving me the opportunity to do a summer internship at Instituto de Ciencia de Materiales de Aragón, CSIC - University of Zaragoza. I would also like to thank Professor Dr. Javier Campo and Professor Dr. Angel Larrea for the collaboration on the Cathedral of Cuenca stained glasses as well as the associated staff of the Institute, along with Professor Dr. Maria Pilar Alonso Abad from Department of Historical Sciences and Geography, University of Burgos.

As this thesis is an interdisciplinary study, the archaeological conclusions would not have been made without my previous education at the Department of Archaeology, University of Zadar. Thus, I would like to especially thank Dr. Jure Šučur for all the patience and knowledge he passed on to me.

I would like to thank all of my friends and colleagues who have literally been on my side through sickness and health, and through ups and downs of the thesis making. The support and kindness of Indrè Žalaitė, Carla Soto, Milan Marković, Guilhem Mauran, Ilona Viliūnaitė, Whitney Jacobs, Lenor Costa, Diego Badillo, Jure Šučur, Marica Milić, Helena Pille, Laura and Mirko Kovačević, Ivan Ljubičić, Dinko Capak, Tala Bdour, Guido Firmani, Celeste Massarotto, Andrea Musto, and Cristina Dias is especially acknowledged.

Last, but not least important, I would express my appreciation to my family for their love and support through all my life.

Introduction

Archaeometry is used as a scientific approach in order to understand not only chemical and physical properties of the recovered archaeological materials but to reconstruct the processes that occurred in the past. These includes questions like the procurement and processing of raw materials, production technology, use, distribution, trade and the social significance of the object. It aims to clarify the understanding of discovery, spread, adaptation and development of new technologies in a holistic manner, taking into consideration environmental, technological, socio-economic, political and ideological contexts [1].

As stressed out by [1], there is still a gap between the Humanities and Physical/Chemical sciences fields whereas the inappropriate technique is applied and non-informative data are being presented. On the other hand, one can lose sight of the main problem of the object investigated, focusing more on the optimization and usage of the technique[1]. Another issue currently present in archaeometrical investigations is the negligence of the importance of the descriptive and visual presentation of the object analyzed, as well as the context from which objects were recovered. I emphasize this issue as insufficient data on the aforementioned causes problems in interpretation of the obtained data, as well as the possibility of the data to be compared with other objects that are typologically equal or distinctive, dated to the same or other period of time, etc. Thus, the lack of basic information of the object itself makes the presented data useless to archaeologists. Therefore, one of the aims of this work is a presentation of a solid context of the glass artefacts analyzed, and a usage of scientific techniques in order to obtain data that will provide more information not only about the objects, but also the understanding of the past society through environmental, technological, socio-economic, political and ideological context.

Due to intensive research that has been done on vitreous and non-vitreous artefacts/fragments, there is a necessity to distinguish this field as a separate and autonomous part of Archaeology, in the same manner *Archaeometallurgy* has a distinguished position. Therefore, in the present study, a new term is proposed, *Archaeovitreology*, intended as the study of history and prehistoric use and production of: 1. man-made non-vitreous artefacts that are a product of glass

production, and 2. man-made vitreous products: glasses, glazes, enamels and faïences. It should be considered as a sub-discipline of Archaeology and Archaeometry (Archaeological Science) implying the use of physico-chemical methodologies and techniques in order to determine all the characteristic features that can reveal more information on environmental, technological, socio-economic, political and ideological contexts.

In ancient glass scientific literature, an issue already stressed by Rehren and Freestone is that authors develop their own compositional groupings that is characteristic of their analyzed assemblage, with few linkages to established groups [2]. The need for a uniform, consistent and applicable classification is a necessity that has to be discussed among the *archaeovitreologists* to reach a consensus upon the terminology and classification parameters for each glass group and sub-group. The necessity for a protocol of determination of each group and sub-group could be proposed through a coded name that could reveal all relevant information about the specimen analyzed. The code name would include the type of flux used, if plant ash used, specification of which plant ash, was the glass recycled, the provenance etc. The distinction between techniques used in order to classify needs to be pronounced and a protocol needs to be established. In other words, what we would be needed is a typology of glass artefacts based on technological and production markers. As comparison of data is an extensive work due to a large number of elements that one can analyze in a single glass sample with the large quantity of samples analyzed per archaeological site as well as the increasing number of sites, the inaccuracy of interpretation increases along with the probable increase in the different terminology for already established sub-groups. These issues encourage the necessity for an effort to produce an open access online database system for prehistoric and historic glasses. A database system that would allow every *archaeovitreologist* to upload their data and to immediately analyze and compare their data in binary or ternary plots. The database would need to be a joint effort of every *archaeovitreologist* to upload their data, hence in general leaving them more time to compare their results and it will increase the accuracy of the possible interpretation of the data.

Another relatively frequently encountered issue that is usually not stressed is the wide range of dates for a single specimen in the analyzed assemblage or the assemblage is analyzed as a single unit, usually encompassing few centuries.

The thesis is an *archaeovitreological* study of the artefacts from Period II of Miranduolo site, Chiusdino, Italy. Wide range of techniques that are available were taken into the account considering their limitations, advantages and the type of information they can provide. Thus, here VP-SEM-EDS, PIXE/PIGE and LA-ICP-MS techniques were used.

VP-SEM-EDS was used to visualize textural characteristics and thickness of the pristine glass and corrosion layers. Multipoint analysis will be used on the pristine glass to identify the chemical elements present and semi-quantify their abundance. Line scan will be used in the samples with corrosion layers in order to determine which chemical elements display enrichment and which depletion.

PIXE/PIGE non-invasively quantified and chemically mapped both the pristine glass and the corrosion where the corrosion layer was thick enough to analyze. Bromine can be successfully detected and quantified, which plotted with calcium oxide will confirm or cancel the premise if marine calcite (seashells) was added to the glass batch.

LA-ICP-MS micro-destructively quantified both pristine glass and two corrosion layers. Although micro-destructive, the technique provides better quantification results for minor and trace elements, along with the fact that it is the only technique used in this study that can determine Rare Earth Elements.

One aim of this work was to understand the chemical composition, physical properties of the glasses, what raw materials and production techniques were employed, what degradation processes were present and why, and what is the comparison of the results between VP-SEM-EDS, PIXE/PIGE, LA-ICP-MS. To my knowledge, this will be the first study that will do the chemical mapping of corrosion with PIXE/PIGE, and a quantification of the corrosion layers with LA-ICP-

MS, as well as the experiment with quantifications with diverse laser ablation beam sizes. The other aim is to determine socio-economical relevance of the glass finds present at Miranduolo and the possible trade routes from where the glass was imported.

Miranduolo is a settlement with a continuous habitation from 7th to mid-14th century AD. It displays the social evolution of the rural aristocracy and their display of control over the farmers and metalworkers. The dating of the site was done by more than 60 radiocarbon samples and the most extensive pottery sherds collection. Within the site major timeframes, called Period, have been identified, usually lasting approximately 100 years. Each Period is divided into two or three minor timeframes, called Phases, lasting approximately 20-50 years. Therefore, this thesis represents a pioneer work for: 1. the analysis of the possible differences in glasses that can display different social hierarchy by analyzing glass fragments from different social areas of the site, and 2. analyzing glass fragments from each phase of the site, enabling the possibility to determine if any change in glass production can be visible in a smaller timeframe or to confirm that the glass producing are centuries long traditions.

1. About glass

1.1. Definition, composition, properties and behavior of glass

Glass is a material obtained by polymerization or more commonly cooling from a liquid phase or by disordering solid phase, by avoiding occurrence of crystallization (Figure 1-1). In the literature there are many definitions of what is glass, and amongst them that it is “a non-crystalline solid”, “supercooled liquids frozen in a rigid state”, “an inorganic product of fusion which has cooled to a rigid condition without crystallization” [3]. Perhaps, more appropriate is defining glasses as “materials that can be cooled below their supercooling range and reversibly heated above, without the appearance of crystalline phases” [1], [4]–[12].

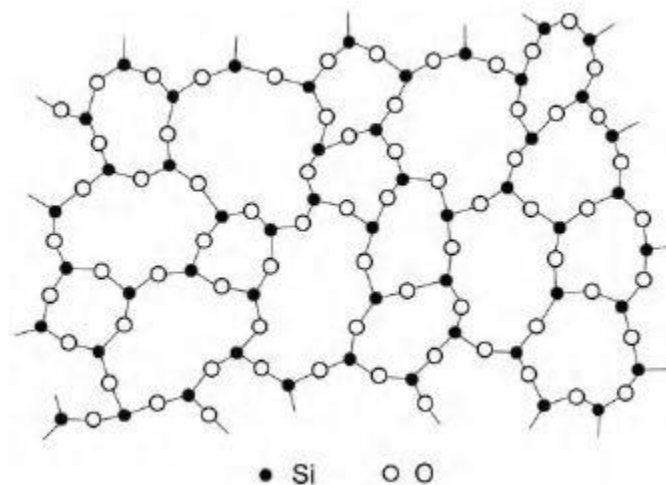


Figure 1-1 Structure of amorphous silica with Si-O tetrahedron unit which does not display a long-range periodicity as found in silica glass. From [3].

Although glass is a product of rapid cooling comparing to the crystallization time, there is no thermal point at which that change occurs. On the other hand, there are two points crucial for glass formation: a) **glass transition temperature (T_g)** and b) **glass transformation region**. Glass transition temperature is a thermal region at which the thermodynamic variables, such as volume, enthalpy and entropy, display a smooth continuous change. Glass transformation

region is a thermal interval between the enthalpy point of equilibrium liquid and enthalpy point of the frozen solid [1].

Glass families have been named according to the main component of the glass network formers. The largest group is the oxide glasses, and among them silicate glasses the most represented group of historical glasses is silicate glasses. Silica based glasses have a matrix of a covalently bonded Si – O in a non-regular network, with some ions, mainly Na, Ca, K, and Mg, found at irregular distances from each other [3]. Glass lowers its free energy by transforming into crystalline form that is completed with passing of time – a process called *devitrification*. Devitrification is manifested by breaking the covalent bonds which is very slow at the ambient temperature. Hence, the glasses, in this sense, stay thermodynamically stable for more than *ca* 70 years [1].

Diverse glass compositions may be obtained, but all the glasses are a mixture of several substances. These include: vitrifier, flux, stabilizers, intermediates, fining agents, colorants, decolorants and opacifiers. The latter three components are optional.

Vitrifier or **network former** is the main component of the glass structure. Silica¹ is used as a vitrifier, made from pure sands, quartz powder obtained by crushing quartz rocks or pebbles or diatomaceous earth. The pure sand contains some impurities as calcite (CaCO₃) and, magnesium oxide (MgO), or aluminum oxide (Al₂O₃) in other mineral phases which help the stabilization of the glass, while iron oxide (Fe₂O₃) causes tints [1], [3], [6], [9], [12]–[17].

Flux or **network modifier** is used in order to lower the melting temperature of silica. The addition of monovalent cations lowers the melting point of the silica, but the glass is prone to leaching, and it can be stabilized by addition of higher ionic strength cations such as alkaline earths. Several types of fluxes were used including *natron*, plant ash (halophytic plants, *Kali*, *Salsola*, *Salicornia*

¹ Other possible network formers are Boron oxide (B₂O₃), Lead oxide (PbO) and Phosphorus oxide (P₂O₅) [9].

sp.), wood ash and tartar. Natron ($\text{NaCO}_3 \cdot 10\text{H}_2\text{O}$) is found in the lakes of Wadi Natrun in Egypt [2], [3], [5], [6], [8]–[12], [14], [15], [17]–[26]. Because of its purity, natron cannot stabilize the glass, especially if a pure silica source is used as a network former. That is the reason why additional compounds, like limestone and seashells, were added, making the glass more resistant to deterioration. It has been used as a flux from 18th century BC to 18th century AD. Tartar from the wine barrels, used from 15th century AD, contained K. As plant and wood ashes contain impurities, the glassworkers could have applied the purification process in order to remove the non-soluble substances [1], [3], [5], [25], [27]–[29].

Stabilizers make the glass water resistant. Aluminum oxide (alumina; Al_2O_3) and Earth-alkali oxides are commonly found. Alumina is present through sand impurities and non-purified ashes, while magnesium oxides and calcium oxides through non-purified ashes [3], [9]–[12], [14], [15], [24], [30], [31].

Intermediates have an intermediate electronegative character between network former and network modifier. They can substitute Si in tetrahedral sites of the existing network. Those elements are Al, Ti and Zr [1], [6].

Fining agents help to remove glass bubbles and to make the glass homogeneous. The sulfates and chlorides impurities present in the raw materials, as well as nitre (KNO_3) and manganese oxide (MnO) served for this purpose [3].

The color of the glass is obtained due to the presence of transitional metal ions or metallic atoms present in the structure. It is dependable on the oxidation state of the element. Main ancient **colorants** are manganese (more than 0.8 wt%) for purple (Mn^{3+}) and brown (Mn^{2+}), cobalt (Co^{2+}) for blue; iron oxides for yellow to brown (Fe^{3+}) and green and blue color (Fe^{2+}); copper oxides for green and blue (Cu^{2+}) and red color (Cu^{+1} , Cu^0); silver for yellow to brown color (Ag^+); gold for ruby red; and a mixture of gold and silver for pink glasses. The unwanted coloring effect of the higher quantity of iron oxides introduced into the glass as an impurity has been removed by adding **decolorants**. From 7th century BC Antimony oxide (Sb_2O_3) was used, while since 2nd

century BC Manganese oxide (0.3/0.5 – 0.8 wt%) has become the main decolorant [1], [3], [5], [6], [8], [9], [12]–[14], [18], [19], [21], [23]–[25], [32]–[37].

Opacifiers were used to make the glass opaque. Calcium antimonite ($\text{Ca}_2\text{Sb}_2\text{O}_7$), tin dioxide (cassiterite; SnO_2) in the form of tin calx or lead/tin calx, lead stannate (Pb_2SnO_4 ; PbSnO_3) and lead antimonite ($\text{Pb}_2\text{Sb}_2\text{O}_7$) were mostly used. Arsenious trioxide (As_2O_3), realgar (AsS), orpiment (As_2S_3) and apatite (burnt bones; $\text{Ca}_5(\text{PO}_4)_3\text{F}$) were added less frequent, while gypsum ($\text{CaSO}_4 \cdot 2\text{H}_2\text{O}$) was used rarely [1], [3], [5], [9], [14], [15], [23], [35], [36], [38], [39].

Major changes that affect the original glass composition are corrosion, weathering and biodeterioration. *Biodeterioration* is the degradation of the material by bacteria, fungi and other microbes. *Weathering* is a special type of corrosion that is characterized by the attack of the atmospheric pollutants (CO_2 , SO_2 , NO_2 , O_3 , airborne particles) and gaseous water in the form of humidity, fog or rain. A thin water layer is absorbed on the surface leading to ion exchange. The pollutants may dissolve in this water layer leading to decrease of pH which stresses the ion diffusion. Variations in humidity and temperature might lead to the evaporation of this layer and precipitation of crystalline weathering products whose composition is dependent on the glass composition and air pollutants. Weathering crystals formed on both K-Ca-Si and Na-Ca-Si glasses are mainly gypsum ($\text{CaSO}_4 \cdot 2\text{H}_2\text{O}$) and syngenite ($\text{K}_2\text{SO}_4 \cdot \text{CaSO}_4 \cdot \text{H}_2\text{O}$) and non-crystalline hydrated silica. To a lesser extent arcanite (K_2SO_4), sylvite (KCl) and halite (NaCl) are found [3], [6], [9], [10], [33], [40], [41].

Corrosion is defined as degradation of the material due to external environmental or climatic conditions and/or internal factors like chemical composition and surface morphology which causes minor or major deterioration in the structure, functionality and/or shape. The speed and effect of chemical reactions occurring in the glass is dependent on the glass composition and the reactions that occur through different processes depending on the pH of the medium. Alkaline ions are easily attacked by aqueous media. In the **acidic** media the glass containing alkaline ions the attack starts with the ion exchange of the H^+ ions (more precisely *hydronium ion* H_3O^+) of the

medium and the alkaline ions of the glass at the surface. This results in a *dealkalinization* of the glass that slowly continues. Larger alkaline ions are weakly bonded with non-bridging oxygen atoms making them easily leach from the glass network. As K^+ ion is bigger than Na^+ this is the reason why K-Ca-Si glasses are more prone to degradation than Na-Ca-Si glasses. On the other hand, the double charge of the earth-alkaline ions keeps them strongly bonded to the network and they leach when the network shows sincere signs of deterioration. Therefore, Na-Ca-Si glasses are chemically most durable against most acid attack. As silicate glasses are strongly influenced by the hydrofluoric acid attack, dissolving the components of the network, forming SiF_4 and other alkaline and earth-alkaline fluorosilicates, it can affect the Na-Ca-Si glasses. Phosphoric acids also deteriorate these glasses but with less intensity. In the **basic** media, attack is the strongest, as OH^- groups are formed, e.g. with the presence of water. The **neutral** media helps the development of small dealkalinization. If the alkaline hydroxide is removed or diluted the attack is not severe, but if the water continues to be in contact with the surface for a longer period of time, preventing its vaporization, the concentration of the alkaline ions will increase, providing a strong basic medium. The long retention of the water, as in buried glasses, the dealkalization because of water penetration causes variations in volume near the glass surface. This stress is the reason for the accumulation of the cracks and detachments which result in the formation of stratification layers. The stratification layers interfere with the light causing the *iridescence* effect [1], [3], [6], [8], [19], [42], [43].

G.W. Morey noted that the corrosion resistance of glass is proportional to the alkali content. K-Ca-Si glasses are twice as prone to be attacked comparing to the Na-Ca-Si glasses [4]. The glasses that are richer in Al content did not display surface layer formation in acidic and basic conditions. It was explained as that all flux ions were bonded to aluminate network, which limits the release of Na ions. Ba and Sr leach to the same degree as Na, while Ca and Mg show minor leaching. In general, the amount of Si leached is also negligible. Significant leaching of both Si and alkali can be observed with $pH > 9$ [1], [3], [6], [8]–[11], [19], [40], [43], [44].

The corrosion of Roman and Medieval glass artefacts that were buried in the soil or seabed display a heterogeneous and laminated surface with pitting. These layers are thick from few microns to few millimeters. The composition of the glass in the corrosion displays enrichment in Si, Fe, Mn and Al and strong or complete depletion of alkali and alkaline-earth elements. Analysis of the 11th to 13th centuries Na-Ca-Si glasses with natron as a flux (MgO and $\text{K}_2\text{O} \leq 1.5$ wt%) display a more heterogeneous composition than plant ash glasses (MgO and $\text{K}_2\text{O} > 1.5$ wt%) [3], [6], [33], [40].

Thermal expansion coefficient is a key feature of the glass as it affects glass production, e.g. cooling rate during annealing, and it is a key point in soldering glass with other materials and in resistance of thermal shock. According to the thermal expansion coefficient, if $\alpha < 6 \times 10^{-6} \text{ K}^{-1}$ glasses are considered to be *hard*, if $\alpha > 6 \times 10^{-6} \text{ K}^{-1}$ glasses are considered to be *soft*. Therefore, with $\alpha = 8.7 - 9.0 \times 10^{-6} \text{ K}^{-1}$ Na-Ca-Si glasses are soft [3], [9].

Viscosity of the glass assures that the material does not crystallize when the melt is frozen during cooling. When the glass material is subjected to stress, glass displays ideal elastic behavior with a short deformation range. When the stress applied goes beyond the glass' short elasticity limit, it will break without residual deformation, characterizing the glass material as brittle. The stress needed in order to break the glass is also dependent if there are microcracks present, which can form by small stresses during cooling or by mechanical abrasion of the surface due to the usage. These semi-elliptic microcracks penetrate few microns inside the glass. As the microcracks grow, they reach the size at which the interatomic bonds break or open, making the glass fracture. The growth of the microcracks is assisted by mechanical stress applied, by aggressive chemical action, or by the combination of both. Water is one of the chemicals that favor microcrack growth, breaking the siloxane bonds, incorporating itself into the glass structure forming Si – OH groups. This is the reason why the glasses display better preservation state in dry conditions [3], [9].

1.2. History of glass production and historical documents

Natural glass (obsidian) was used since Palaeolithic times. The first known artefacts are East African sharp stone tools shaped by man. Due to the limiting availability, obsidian became a highly desirable material and an indicator of trade routes [3].

First man-made glass appeared on glazed stones in Egypt in 5th millennium BC, while faience production started at the end of 5th millennium BC in Syria and afterwards in Egypt [1], [5], [9], [17], [45]. The spread of faience to Crete, Cyprus, Rhodes and Greece happened at the end of 3rd millennium BC, while in the Caspian region, Poland, Slovakia, Italy, Switzerland, up to France and Britain in spread in the 1st half of 2nd millennium BC [1], [5], [46].

Glass beads appeared in the first half of 3rd millennium BC, but the industry was established around 1500 BC in Mesopotamia and Syria [1], [3]–[5], [9], [15], [17], [27], [45]. With victory of Tuthmosis III (1505 – 1450 BC) of these areas, primary glass production was established in Egypt. There it flourished until the 11th century BC. From 9th to 4th century BC Mesopotamia re-established their production. The spread of the glassmaking to European Mediterranean occurred in 7th century BC, with imported glass ingots that have been made into final objects in secondary glass workshops in Etruria, Istria, and Rhodes. The technique for producing glass beads included **stretching** of melted glass into threads which were wound upon a rod. In order to produce glass containers, **core-forming technique** was used. The wanted shape was modelled in clay, then covered with the glass material. After cooling the clay was scrapped out leaving the wanted shape in glass. The surface was smoothed and polished. All of the objects were opacified. Afterwards, glass was **molded**. The crushed glass was put into the mold and then heated, so that the glass would melt into the designed shape. The glass composition of the first object included plant ash Na-Ca-Si glasses, although lead has been used as a fusing agent. From early on the glass ingots have been transported to other sites to produce the final shape of the objects [1], [3], [4], [9], [15], [27], [46].

During the Hellenistic-Roman Period natron Na-Ca-Si glasses were produced, with prevalence of transparent glasses. **Free-blowing**, as a new production technique, has been introduced around 1st century BC and was the main technique until the Medieval Period. Glass **mold-blowing technique** was delivered by putting the molten glass into the mold where it cooled in 1st century AD. In Roman period beside the tableware, glass material was used for production of windows, *tesserae* and imitation of precious gems. In the 9th and 10th centuries AD the transition from natron to plant ash Na-Ca-Si has occurred, as evidenced in Islamic glass objects, due to loss of sources from Egypt. Although natron Na-Ca-Si glasses have appeared sporadically until 12th century AD. North of Alps (Central and Northern Europe), both natron and plant ash were not available, causing the decline of production and recycling the Roman natron glasses with wood ash² producing K-Ca-Si glasses [1], [3], [4], [9], [12], [13], [18], [19], [23]–[25], [27], [28], [31], [33], [34], [36], [45], [47]–[52].

Lead glass has sporadically been produced in 10th and 11th centuries AD in Islamic glasses and British Isles, and in 12th and 13th centuries AD in North-Western Europe.³ Usually tesserae, cups and bottles have been made. With the high content of lead, the content of alkali is lowered, especially K. The technique has been widely used only since 17th century AD [1], [3], [4], [9], [19], [25].

First historical documents regarding the glassmaking was confirmed on the 8th century BC Assyrian clay tablets, with the information that the glass was produced by melting a mixture of quartz and ash. Strabo, Pliny the Elder and Tacitus Cornelius provided large quantity of information about the glassmaking between 1st century BC and 1st century AD. They include the names of the regions for extracting the silica sand source, usage of specific fluxing agents, colorants, decolorants, the techniques and styles of production. 16th and 17th century copies of

² One of the oldest wood ash glasses fragments discovered are dated to 780 AD from imperial palace of Charlemagne at Paderborn [12].

³ The Mesopotamian cuneiform texts mention Pb as one of the ingredients as early as 2nd millennium BC [9].

7th to 9th centuries AD original manuscripts of Syrian alchemists Zozimo and Democrito reveal the glass recipes. Eraclius' work *De coloribus et artibus romanorum*, dated from 10th to 13th centuries AD describes the recipes for glass production, production of imitation of stone gems in glass and the techniques used in this period [3], [8], [9], [26]. Theophilus' *De diversibus artibus*, 12th century manuscript, encompasses a concise study of wall paintings, glass and metals [3], [39], [53]. A 14th century Ad Venetian glass painter Antonio da Pisa's *Secreti per lavorar li vetri secondo la dottrina de M.ro Antonio da Pisa, singolare in tal Arte* is a text that reveals preparation of colors, heat treatment, lead joining of stained glasses. Tuscan 14th and 15th centuries AD study *Dell' Arte del vetro per Musaico – tre trattatelli dei secoli XIV e XV ora per la prima volta publicati* was written by two anonymous writers and Benedetto Baldassare Obriachi. It describes the local recipes taken from the Venice on how to produce crystal and crystalline glass, enamels, white opaque glass, colored glass, mosaic glass, imitation of precious stones, and the purification of soda ash in order to obtain *cristallino* glass. For the first time usage of burnt bone ash as an opacifier and a recipe for chalcedony glass. 16th century AD *Segreti per colori* manuscript from Bologna also includes diverse glass recipes. 16th century AD *Recette per fare vetri colorati et smalti d'ogni sorte havute in Murano 1536*. Vannoccio Biringuccio's *De la Pirotechnia* from 1540 AD includes the information on glass production and furnaces. He mentions usage of *Salsola Kali* plant that was grown in Syria or near Rhone River in France and that other fluxes were made by burning lichens and ferns. Along with the production of *cristallo* lower quality glasses are mentioned. Other known documents are: 1556 AD Giorgio Agricola's *De re metallica*, 16th century AD manuscript *Ricettario anonimo del' 500*, 1612 AD Antonio Neri's *L'arte Vetraria*, 1644 AD Giovanni Darduin's *In nomine Domini Nostri Jesu Christi Beataeque Virginis Matris Mariae, anno a Nativitate Domini Millesimo Sexcentesimo Quadrigesimo Quarto, die secunda mensis Martii, Joannes Darduino quondam Nicolai : Copie de tutti li secreti de smalti cavate dalli libri et altre carte della buona memoria di mio padre* [3], [9], [23].

1.3. Archaeovitreological classification and terminological issues

In the extensive literature available, authors have tried to schematically represent the main compositional groups of glasses that were produced from prehistory to modern times [3], [54]. The issue lies in non-consistent terminology used for one compositional group and sub-groupings that are developed by some authors which is characteristic of their analyzed assemblage, with few linkages to established groups, or stressing that this is a new compositional sub-group. Meaning, when a new sub-group is presented for one site and the same sub-group is determined on another site, they can be named differently. This causes the lack of proper data interpretation. Here, the current terminology, compositional groups and sub-groups will be shortly outlined and a possible solution presented. It has to be stressed that a consensus on all of the aforementioned has to be reached in order to achieve uniform archaeovitreological terminology and a protocol for archaeovitreological classification.

There have been attempts to present an archaeovitreological classification protocol as in [54] as presented in Figure 1-2. In [54], and some other archaeovitreological papers [12], [13], [27], [37], [48], [55] the ratio of elements has been used as a parameter for determining the composition. In others, the quantity of oxides or elements are used as a parameter. In the latter, there is an inconsistency in using the same quantity for each oxide or element. For example, in [56] Na-Ca-Si glass with natron as a flux is defined by the content of both K_2O and MgO below 1 wt%, while in most of other papers such as [21], [24], [28], [45], [57], [58], it is determined that natron as a flux has been used if the aforementioned elements are below 1.5 wt%. Another issue encountered is the determination of values of oxides and/or elements as low, slightly high or high without defining the parameters for each value [12], [13], [27], [59], [60]. Presentation of data need to be re-evaluated and verified with experts as for the conclusion for the origin of silica source in form of sands, pebbles or flints as a plot of SiO_2 and Al_2O_3 content [22]. This has no geological support but such plots are being used to draw conclusions which, in the end, are not valid. A non-expert, as an Archaeologist, an Art Historian, or a Chemist will misuse the aforementioned data due to consideration that they are valid. Hence, interdisciplinarity and a

consensus on the classification protocol is obligatory. Otherwise, misinterpretations of the data will largely increase with time.

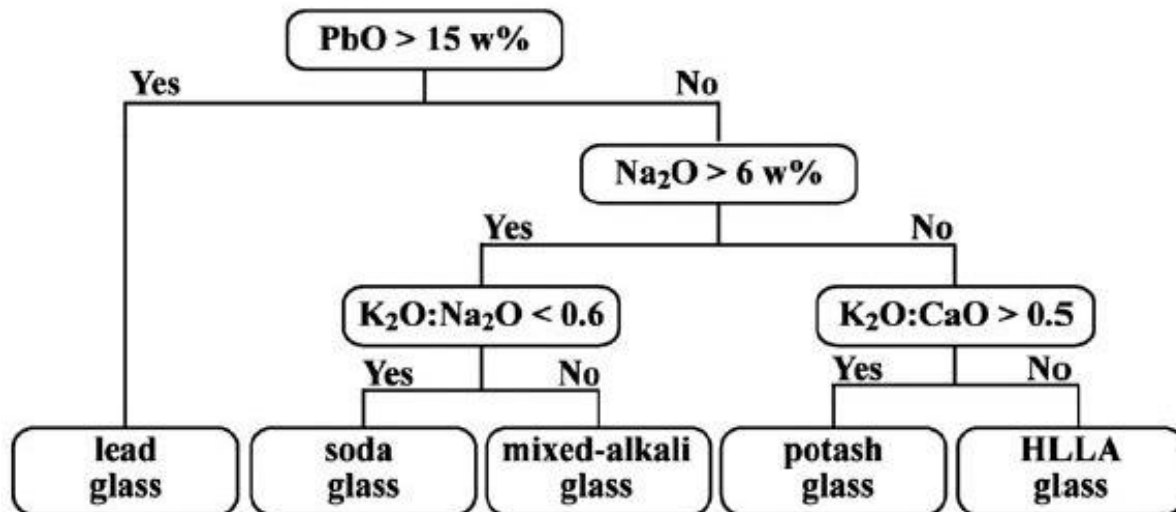


Figure 1-2 Protocol for classification of glass groups. From [54].

Terminological issues can arise from the inappropriate or undefined classification system of glass compositions. For example, according to Verità [51] and Henderson [60] Mixed-Alkali are defined as having comparable levels of Na₂O and K₂O, while according to Schalm *et al.* [54] the Mixed-Alkali group has a Na₂O content higher than 6 wt% and the ratio of K₂O and Na₂O is higher than 0.6.

An example of unsystematic terminology used in current studies for Na-Ca-Si glasses with natron and with plant ash as fluxes are presented in Table 1-1. The misuse of inappropriate terminology for K-Ca-Si glasses has already been stressed by Stern and Gerber [31]. Generally, in literature the term *Potash* is used as an alternative name for K-Ca-Si compositional group, which according to Stern and Gerber [31] should be referred as *Potassium*, *Potassium type* or *Potassium-Calcium* glasses. The authors stress the meaning of *potash* from Webster's New Encyclopedia as a *potassium carbonate from wood ashes*. In their study, the P₂O₅ content in the glasses have been proven to be a method of distinguishing whole ash (unpurified ash) from

potash (purified ash) K-Ca-Si glasses [31]. Therefore, this classification distinction should be put in practice to archaeovitreological terminology.

The code for each needs to be written from the main composition, inputting the information to the left (in the Table 1-2 up), then to the right from the main composition (in the Table 1-2 down), with each piece of information separated by hyphen (-). If multiple peculiarities are defined they are separated by slash (/). Values as very low, low, medium, high, very high need to be defined specifically for each oxide/element. An example for Fe₂O₃ values has been presented in Table 1-2. Also, for each oxide/element that has been intentionally added as a colorant, decolorant and/or opacifier values have to be defined. The definition of values for colorants, decolorants and opacifiers have to be defined separately for intentional and unintentional addition. An example of code for sample MD 243 and other samples are presented in Table 1-3.

Table 1-1 Presentation of terminology used by various authors for Na-Ca-Si glasses with natron and plant ash as a flux.

Composition	Terminology used by authors				
Na-Ca-Si glass with natron as a flux	LMG - Low Magnesium Glass (Sayre and Smith 1961; Henderson, 1985, 1988)	Natron glass (Brill 1992 and Cagno 2012)	Natron-based glass (Freestone, 2003)	Mineral soda-lime-silica glass (Gratuze, 2004)	Soda lime glass (Wedepohl, 2011)
Na-Ca-Si glass with plant ash as a flux	HMG - High Magnesium Glass (Sayre and Smith 1961; Henderson, 1985, 1988)	Plant ash glass (Freestone, 2003)	Mixed soda lime (Casellato et al, 2003)	Vegetable soda-lime-silica glass (Gratuze, 2004)	Soda ash glass (Wedepohl, 2011 and Cagno, 2012)

To avoid any terminological misuse I would suggest the coded terminology for defined groups and sub-groups as presented in Table 1-2.

There are three minor issues present. First one that arises is the presentation of major, minor and trace elements in tables in publications. There is no order of presenting the elements, whether it is alphabetically, according to the atomic number of the element, or according to any other specification. What I would suggest is the order of elements according to the columns of elements that are usually compared, indicating the following order for major, minor and trace oxides/elements: SiO₂, Na₂O, TiO₂, Fe₂O₃, Al₂O₃, MgO, CaO, K₂O, P₂O₅, SO₃, Cl⁻, MnO, Pb, Cr, Co, Cu, Zn, As, Rb, Br, Sr, Y, Zr, Nb, Sn, Sb, Cd, V, Ba, Bi, La, Ce, Pr, Nd, Sm, Eu, Gd, Tb, Dy, Ho, Er, Tm, Yb, Lu, Hf, Th and U. The oxides and Cl⁻ should be expressed in wt%, while elements in ppm. An element that is naturally present in the glass in ppm, when being input in larger quantities as in lead glasses, it should be presented as PbO in wt%. This principle should be followed for all the elements when the quantity of the elements exceeds 0.1 wt%.

Table 1-2 Proposal for a coded terminology for archaeovitreological classification. In the brackets are abbreviations for the code for each information.

Processing of the ash	Unpurified ash (U) with CaO ≥ 7 wt%, positive correlation of K ₂ O with CaO		Purified ash (P) with CaO < 7 wt%, no correlation of K ₂ O with CaO		
Ash (if used)/Other features	Levantine (L) with K ₂ O 1.5-4.5 wt% and MgO > 1.5 wt%)		Barilla (B) with K ₂ O > 4.5 wt%, and until ratio of K ₂ O and Na ₂ O is higher than 0.6; MgO > 1.5 wt%)		High Magnesium (HM) with K ₂ O ≤ 1.5 wt%, MgO ≥ 1.5 wt%)
Flux used	Plant ash (pa) with K ₂ O and MgO > 1.5 wt%				Natron (n) with K ₂ O and MgO ≤ 1.5 wt%; exception
Main composition	Na-Ca-Si				
Defining peculiarities (low, medium or high contents of oxides/elements)	Very low Iron (VLI) ≤ 0.5 wt% Fe ₂ O ₃	Low Iron (LI) 0.51-1.00 wt% Fe ₂ O ₃	Medium Iron (MI) 1-2.5 wt% Fe ₂ O ₃	High Iron (HI) 2.5-3.5 wt% Fe ₂ O ₃	Very high Iron (VHI) > 3.5 wt% Fe ₂ O ₃
Non-recycled or Recycled	Non recycled (nr) – 1-100 ppm of Cr, Co, Ni, Cu, Zn, Sn, Pb		Recycled (r) – 100-1000 ppm of Cr, Co, Ni, Cu, Zn, Sn, Pb		
Colorants, decolorants and/or Opacifiers	<p>Naturally colored+element (ncFe)</p> <p>Naturally colored with added decolorant (ncFe/adMn) - MnO ≥ 0.8 wt%</p> <p>Colorless glass+added decolorant (adMn) - MnO ≥ 0.8 wt%</p> <p>Intentionally colored+element (icCo) – colored with Cobalt</p> <p>Intentionally colored +elements (icAg+Au) – colored with Silver and Gold</p> <p>Intentionally colored+element with added decolorant (icCo/adMn) - - MnO ≥ 0.8 wt%</p> <p>Opacified+ chemical formula (oSnO₂)</p>				
Provenance	e.g. Egypt, Tuscany, France				

Table 1-3 Examples of writing the codes for archaeovitreological classification with a long description of the code.

Example	Code	Long description of the code
MD243	ULpa-Na-Ca-Si-VHI/VHM-nr-ncFe/adMn	Soda-Calcium-Silica glass made with unpurified Levantine ash as a flux, with very high Iron (III) oxide and Magnesium oxide content, naturally colored with Iron oxide but it has intentional addition of MnO

The elements known to be opacifiers should always be presented as elements in ppm as they are also naturally present in the glass, and generally usually not all of the glass samples have higher (than naturally present) amounts.

The second minor issue considers the determination of the terms *major*, *minor* and *trace elements*. In this study the term *major* implies that the element present has more than 1% intake in the glass, *minor* is defined by 0.1-1.0% and *trace elements* with intake ≤ 0.01 wt% (1000 ppm).

Finally, the third minor issue is the accessibility of the data from PDF articles that cannot be extracted as tables with every data in a separate cell. The data extraction can be, therefore, time consuming, especially for LA-ICP-MS analysis that usually include large number of elements. A suggestion to overcome this issue and to enable an easy access to the data is by setting up an online open-access data-base for archaeovitreological studies according to the technique used, with all the parameters (dating, color, type of artefact, instrument conditions) specified. It would be the responsibility of every archaeovitreologist to make their data accessible after the publication. This would make every research less time consuming and proper interpretations could be made.

2. The archaeological context

The questions that are posed strive to give us a better insight about the diverse contexts of the period in question. The answers can be only obtained as an amalgamation of both archaeological/historical context and understanding of the analytical results. This amalgamation can only give what we can then completely define as *interpretation*.

One of the aims of this study is to answer: what production technology was used for Miranduolo glasses? This includes providing answers about the glass composition, usage of (de)colorant/opacifiers, extent of recycling and is the information obtained compatible with the contemporary archaeovitreological studies.

The other aim includes the possibility of correlation of analytical with archaeological data (phase, area of recovery, stratigraphic unit, color) to understand the extent of imports and the commercial routes, to track an eventual change in production patterns and, possibly, to acquire data on socio-economic diversification within the settlement.

2.1. The archaeological site of Miranduolo castle

2.1.1. *Position*

Miranduolo castle (*Castello di Miranduolo*) is a multilayered medieval site (7th to 14th century AD) located on the Castagnoli slope (*Costa Castagnoli*), in the Municipality (*comune*) of Chiusdino, Province of Siena, Tuscany (*Toscana*) region, Italy (Map App.1-1). More precisely, 3.9 kilometers air distance south-southwest from Chiusino and 7 km air distance south-west from the San Galgano Abbey (*Abbazia di San Galgano*; Map App.1-2). The site has been first traced in the 1970's by Simonetta Bertini, but the wider area has been field surveyed in 1990's when Serena and Miranduolo castles have been precisely recorded. The site is settled on a hill-top with varying altitudes from 390 to 413 m above sea level (Map App.1-6). It is surrounded by two dried out streams from the north-east and south-west and a dense chestnut woodland. The extension of

the site is around 4650 m², from which 3900 m² is the village area with peasants' huts, metallurgical factory, church and cemetery and 750 m² is the summit area (*cassero*) with the palace of the ruling noble family and building related to storing surpluses [61]–[63].

2.1.2. History

According to historical writings there are over 1550 castles documented in Tuscany region, of which the majority are traceable today (Map App.1-3, Map App.1-4). The medieval settlements were erected as an establishment of rural aristocracy, by using the labor of peasants and accumulating agricultural goods, which has started to be archaeologically manifested from 8th century. The transition to the territorial sovereignty was gradual: with more severe investments and building actions, and when the settlement could be physically protected by defense [61], [62].

Miranduolo castle was one of the centers in the area of historical Val di Merse, which has been located between Siena and Volterra dioceses. Its location was important since one of the major roads of the time crossed the Val di Merse. Except the importance of geographical position, the area contains important mines with deposits of limonite, sphalerite, chalcopyrite and galena. Miranduolo itself, on the other hand, has been erected above the iron and copper deposits (Map App.1-5) [61], [62].

In total, there are 37 historical documents considering Miranduolo and its surrounding area recognized since beginning of 11th century to 14th century.⁴ The first historical document mentions the Gherardeschi noble family as initiators of Miranduolo's construction. Besides Miranduolo, Gherardeschi possessed 17 other castles (including Serena, Frosini, Sovioli) and 9

⁴ Out of 38 historical documents 1 from 11th century, 5 from 12th century, 20 from 13th century and 11 from 14th century [61]

churches located in southern and western Tuscany. The network of the castles (*castelli*) remained unaltered until the 12th century. Miranduolo is first mentioned as a castle in 1004 AD, when it is donated to the Abbey/Castle of Serena (which also belonged to the Gherardeschi family and was used by them as a center for the concentration of their properties). In 1128-1133, Miranduolo was heavily damaged by the bishop of Volterra as the result of a long lasting struggle over the rights on iron ores. The bishop destroyed the castle walls and prohibited their reconstruction. In fact, during this period Miranduolo becomes a minor unfortified rural settlement; the site will never really rise from this condition after 1133, even though it survived for at least two more centuries. In 1178 the Gherardeschi count of Frosini ceded half of the castle and the mines to Community of Siena. At that point the impact of the Gherardeschi family became unstable and the bishop of Volterra had expansionist ideas which subsequently led to a conflict in 1193 that resulted in destruction of Serena castle, causing also severe damage to Miranduolo castle. Afterwards, the bishop of Volterra returned all of the rights on Miranduolo and mines back to Gherardeschi family with the permission to rebuild the castle. The reconstruction works started soon afterwards, but archaeological excavations have shown how they were never completed: in fact, only a small part of the walls were restored before the enterprise was definitely and finally given up. Historical documents testify of events from the beginning of the conflict until the mid-13th century. Between 1257 and 1264 the Gherardeschi family sold all of the Miranduolo's rights to the Cantoni of Montieri noble family. In 1276 they re-sold it to Broccardi of Montieri noble family. In 1336/1337 Miranduolo, which has become a farm, has been put into the hands of the Community of Montieri, and shortly thereafter the site was abandoned [61], [62].

2.1.3. Excavation of Miranduolo castle

Historical documents only put a light on specific events that occurred. Hence, they are not sufficient to understand the social, political and economic context of formation and development of medieval society and material culture as a reflection of the society. Therefore, the excavations

were conducted to better understand the material culture, housing and urban planning, production and crafts, the hierarchical relationships within the site, and comparing their influence and connection with other sites. That is, throughout the life-span of the site to discern diverse economic and social processes, changes, conflicts and symbolisms. In order to be successful in interpretation of the site and proposing models the analysis of the building structures, all types of archeological and bio-archaeological artefacts, and geological data have been combined [61], [62].

First excavations started in 2001 and the excavation campaigns are continued to this day. In 2001, the investigation extent included the site and the surrounding territory in order to determine settlement limits and the extension of use of the surroundings, type of the settlement and economic practices. This was done by usage of GPS, total station, 3D scanner and GIS [61]–[63].

Due to seven centuries of continuation of occupation of the same area, some of the layers were overlapping while some are intact and in perfect state of preservation. Two fires that occurred between the 9th and the 11th century produced intact layers of perfectly preserved charred archaeobotanical remains and other housing facilities and artefacts. Archaeobotanical remains included micro-remains, partially charred timbers, charcoal, and other macro-remains. Analysis of the materials gave an insight into the agricultural practices and past vegetation cover. The organic residue analysis of Phosphorus, fatty acids and protein residues have indicated the usage of analyzed areas [61], [62], [64].

To date each period of the settlement more than 50 radiocarbon samples have been obtained and then crossed with stratigraphic sequence and the typology of archaeological finds (relative dating). The choice of sampling for radiocarbon dates have been carefully planned and the samples were taken from extremely well preserved stratigraphic conditions from all the medieval layers: 7th to 14th century. The analysis has been carried out in Robert Van der Graaf Laboratory, Faculty of Science at the University of Utrecht, Netherlands; in Mass Spectrometry Laboratory at the Department of Environmental, Biological and Pharmaceutical Sciences and Technologies

Department at Seconda Università degli Studi di Napoli, Italy; and at Department of Physics and Astronomy, Università degli Studi di Firenze, Italy. It has to be noted that radiocarbon dates obtained did not yield pleasing results. To lower the discrepancy of the dates obtained due to high interval of calibrated dates, contamination of the stratigraphic layers and re-use of materials analyzed, high amount of samples had to be encountered [61]–[63].

2.1.4. Miranduolo site catchment area

Thiessen polygons were utilized to understand the extent of the site catchment area. The Miranduolo site catchment area extends to 12 km². The area has been calibrated by geographical, hydrographical and archival data. The northern limit of the polygon is marked by the Masetana road and a river. The west boundary is limited by one of the Merse river tributaries. To the east and south-west it includes Cusa hill which had silver mines. In the central polygon area there is the Castellucio hill, with mines of limonite, sphalerite, chalcopyrite and galena. Here, ironworks have been archaeologically attested. The eastern area was covered with forest which is linked to the castle. Between the 11th and the 13th century, around 50 m north-west from the castle the area has been fully agriculturally exploited. Wooded areas north, south and east from the castle were used for forestry and pastoralism [61]–[63], [65].

2.1.5. Periodization and development of the settlement

Miranduolo castle has been continuously inhabited from the 7th to the 14th century, periods VIII-II. Every period is subdivided in phases (Table 2-1), except Period I, which is a contemporary and modern [61]–[63]. Here, shortly the development of the village will be presented through each period. As the glass artefacts analyzed come from Period II, that period will be in more detail described.

The earliest village, dated to **Period VIII (7th century)**, was characterized by scarce archaeological remains that include mostly wooden sunken-feature buildings, the so called *Grubenhäuser*. Miranduolo is a specialized village of ironworker. Importance of metallurgy was confirmed by demolition of two huts in order to access the surface vein. From **Period VII (8th century)**, the summit area was flattened and surrounded by palisade and terraces. The palisade protected the warehouse for agricultural goods, while on the terraces new ground level huts were erected along with the metallurgical processing workshop. In the central part of the settlement a wooden church was erected, while in the western area there were silos and granary pits protected with an another palisade. Generally, economy is based on agriculture, and the public and ecclesiastic elite starts to display its power and Miranduolo population of those periods must have been highly stratified, representing a hierarchical society [61]–[63], [66].

The village underwent major transformations with the start of the **Period VI (9th - late 10th c.)**. The hilltop has been isolated from the rest of the settlement by digging out two ditches and by putting up a palisade (Figure App.1-3, Figure App.1-4). This was to protect the *casa dominica*. With new protection, the summit area was accompanied by new buildings: warehouses for agricultural products and the dwellings of the lord and of his closest servants. Now, the settlement has become a manorial estate with a space of power on the hilltop (*casa dominica* marked by two ditches and a palisade). The space of power has direct control over the yield and surplus, and over the metallurgical workshop. Another palisade was enclosing the *pars dominica* (area where the landlord's serfs were residing). The terraces around the summit area again display habitation of peasants and metallurgical processing. The peasants' habitant area has been expanded by levelling three terraces. On the slopes of the hill *pars massaricia* was occupied by free farmers that were under strict power of the landlord. Right in front of the three newly flattened terraces a palisade has been erected, while below the terraces agricultural land spreads (Figure App.1-1). It is proposed that at this point Miranduolo had about 350-400 inhabitants. The end of this period is marked by a fire that mainly affected the main palace and the summit area. In general, Period VI displays visible changes that have a wide connotation in sense of diverse economy, display of different type of power and management strategies [61]–[63].

Due to the fire, reconstruction of the house of the dominus within the protected summit area and the rest of the settlement had occurred in **Period V (last quarter of the 10th - first quarter of the 11th century)**. It can be recognized that the influence and power of Gherardeschi family was equal or perhaps became stronger, displaying the social gap between the Miranduolo's inhabitants (Figure App.1-5). The control over the surpluses had controlled all the peasants, both artisans and farmers. It limited their contact with commercial channels and restricted any type of individuality. Two major transformations occurred: opening of the quarries in the western part of the site in order to utilize building materials and implementation of new building materials. The palisade has been constructed with a stone base onto which the poles were posted and covered with a thick layer of lime plaster. The same technique will be utilized in the construction of the lord's house, warehouses and several peasants' huts. The roofing was rebuilt in the old manner with straw, along with the new technique by using schist slabs. As with the previous period, Period V ends with a fire that primarily affected the main palace and summit area. It is important to stress that at this point, after all the development, Miranduolo still has the main features of the previous manorial village/estate, despite being attested as a castle in the written sources (in 1004 AD, as we have noted above). The masonry castle will be built only with the late 11th and early 12th century. In other words, the first castle was very similar, in terms of economy, topography and societal differentiation, to the *curtes* from previous periods [61]–[63].

After the fire, another reconstruction during **Period IV** (second of the half 11th - end of the 12th c.) had to be done. Now, the castle has reached its greatest extent and evolves into a fortified village with a new layout (Figure App.1-2). The Gherardeschi family have strengthened their power. Along with the agro-pastoralism, metallurgy became the main source of economy. This was the first systematic *in situ* exploitation of metals. A definitive shift towards masonry building techniques takes place in this period. The main palace is built and a circuit wall now completely encloses the settlement. Two gates were opened. One on the northern artificial terrace, about 1 m wide. The other, main gate, opened on the western side, about 6.5 m wide. The western area of the village has been expanded and a guarding/patrolling tower was added. There, after the main gates, follows a long corridor to access the summit area [61]–[63].

The central village area also goes through a major change when the stone church of Saint John Evangelist (*San Giovanni Evangelista*) has been constructed. The church was first attested in 1004. Around the church there was a cemetery, but few privileged individuals were buried inside the church. Below the stone church, there were two phases (respectively dating to the 8th and the 9th century, corresponding to Periods VII and VI), of a wooden church. Around the church there was an associated cemetery with privileged burials, dating from 9th to 12th century [61]–[63].

Few decennia after this reconstruction, the main palace has been renovated. With this renovation a tower and a cistern have been added in the summit area. Other houses on the terraces are mainly constructed with mixed materials, although some are completely reconstructed in stone [61]–[63].

Limitation of the area is a manifestation of the power and growth of wealth. All of these emphasize Miranduolo as one of the dominating castles of the area along with Serena, Sovioli and Frosini. This did not last long as Gherardeschi family found themselves in the middle of the confrontation with the bishop of Volterra. The war, 1125-1133, has left severe damage to Miranduolo. In the next few decades there will be a legal fight over the rights of the territory. This might be the reason for not taking any action in the reconstruction of the castle. Only after the legal issue has been settled, as evidenced by a historical document from 1193, any construction undertaking could be made [61]–[63].

Historical documents during the **Period III** refer Miranduolo as *Castellare* or a castle in ruins, which Miranduolo has been for sixty years. Only in the beginning of 13th century the Gherardeschi family invested in a limited reconstruction of the castle and of the defense walls. This was short-term and, as said before, the castle has been sold around 1257-1264 to Cantoni of Montieri noble family [61]–[63].

Period II is characterized by significant investments of the Cantoni of Montieri family which would represent the final phase of Miranduolo's revitalization. They tried to establish territory

territorial lordship. The main investment was in the summit area, which would affirm the Cantoni family socially and economically, displaying their elitist position in the society. Some parts of the wall have been repaired, but the rest of the site did not receive much investments. The tower in the summit area has been remodeled into a cistern and the main palace underwent significant changes. The palace, now higher than before, had a minimum of three floors and a height of at least 7 m (Figure App.1-7). The main entrance, located on the western wall, is marked by a pointed arch. Large wooden doors were supported by bronze nails and thick iron hinges. Locking system consisted of a metal stirrup. North from the wall, a metal ring for tying a horse was placed as well as a large stone mortar. A smaller entrance was located on the northern wall. The internal communication through the house was achieved by wooden staircases as the archaeological data do not reveal the existence of stone ones. The roofing was made out of schist slabs and was equipped with a stone gutter system. The outer façade has been completely remodeled, as well as the inner one displaying vaulted roofs and the usage of bricks to some extent. The usage of the bricks arrives very early if compared to other Tuscan rural sites and might be considered as an influence of the almost contemporary construction of the nearby San Galgano abbey. The ground floor flooring was made of beaten clay. After its destruction, it was covered by a layer of charcoal which preserved the bricks and medium sized wooden beams that have been spread in an irregular shape. The beams were a collapse from an upper floor, which is attested by numerous finds of nails. An additional burned layer located above the eastern wall is evidence of wooden structures that have collapsed in the ground floor. It is considered that the ground floor has been used for mangers and horse stables. In the last phase of use, a stone fireplace, made from re-used stones, has been added [61]–[63].

The recovery of the intact brick walls, with a large amount of bricks preserved in the lower portion of the collapse deposit indicates the existence of two successive floors. Right below there is a deposit of large stones and square blocks that are in connection with the eastern wall with a pointed arch which leads to a possibility that the first floor was divided in two smaller rooms. Not far away, in the south-western corner there is a brick vault indicating the roofing system. It is

assumed that the bricks were used for the flooring of the first floor. The first floor has been used as a living area of the Cantoni of Montieri family. As a small amount of earth has been recovered in the south-western part, the earth could have functioned as a binder for placing down the brick floors. Considering the size of the building, sequence of the collapsed layers, presence of accumulation of material above the arch, presence of numerous roofing slabs clearly indicate the existence of the third floor. It is assumed that the third floor had also a division of space which could be supported by the fragments of brick walls covered in plaster that have been recovered. It can be speculated that these rooms functioned as a dormitory [61]–[63].

The palace and the whole hilltop is connected with the rest of the village by a wooden bridge that has been constructed above the western ditch, while the stone stairways (built in phase 2) were enabling the access to the reconstructed stone building that is adjacent to the defense walls (Figure App.1-6) [61]–[63].

The investment in reconstruction was expensive, without the achievement of the desired result. The aim of the Cantoni family was to reconstruct the castle in the manner of the previous Gherardeschi one, to express their importance and role that they aspired to. Their project failed, as the castle was not repopulated. In 1276 the castle was resold to Broccardi of Montieri noble family. It was in their possession for about 40 years. The frequentation, on the basis of archaeological finds, is mostly dispersed in the summit area. As mentioned in the historical document from 1306, the building north from the palace was renovated, and the cistern was put in use. With the final sale in 1336, the site has been completely and finally abandoned [61]–[63].

Considering artefacts, pottery, coins, metal objects and glass artefacts were recovered [61]–[63]. The latter will be described in more detail in the next chapter.

In total, 2310 pottery shreds have been recovered, of which 1555 fine ware and 775 coarse ware. Their dispersal is mostly concentrated in the summit area, which is in correspondence with the fact that this area was the only area inhabited. The prevalence of fine ware over coarse ware is a major change comparing with previous periods. Before, probably perishable materials were

utilized as tableware and for storage. The change in larger quantity of fine pottery may indicate the abandonment of those materials during Period II. The pottery is made by hand and a fast pottery wheel. Only three types of cooking ware are represented: cooking pot (*olla*), pan (*tegame*) and pottery disc for flatbread (*testo*). Along with the common tableware, *maiolica arcaica* pottery was recovered. The matrix of all shreds seem to be similar and correspond to the matrix of the shreds recovered from the Ospedale Santa Maria dalla Scala site in Siena. Production of *maiolica arcaica* was initiated in Siena since the mid-13th century and was developed during 14th and 15th century. Therefore, it is hypothesized that the provenance of this pottery should be located in the Siena workshops [61]–[63].

Seven coins have been recovered from this period. Four of them are not found within a secure context (*denaro piccolo* from Lucca, Siena and Arezzo; *fiorino piccolo* from Firenze), while 3 are found within the layers of Area 1 and Area 4. In Area 1 a *fiorino piccolo* from Firenze and a *denaro piccolo* from Siena, while in Area 4 a *fiorino piccolo* from Firenze with markings of Filippo di Bonsignore [61]–[63].

A small amount of metal artifacts have been recovered during Period II, including an iron ring for tying a horse, iron nails and spurs, copper alloy nails and brooches, a bronze disc brooch, two bronze rings one of which had a collet for inserting a precious rock. The most interesting find is the lead pilgrim badge with a representation of Saint Peter and Saint Paul. This indicates a dwelling of the pilgrimage of Rome at Miranduolo [61]–[63].

Period I is modern and there are no evidence of re-settling. The site was only visited for re-usage of stone building material [61], [62].

Table 2-1 Periodization of Miranduolo castle [61]–[63].

Period	Years
Period VIII	600 – 700 AD
Phase 1	600 – 650 AD
Phase 2	650 – 690 AD
Phase 3	690 – 700 AD
Period VII	
	700 – 800 AD
Phase 1	700 – 750 AD
Phase 2	750 – 800 AD
Period VI	
	800 – 975 AD
Phase 1	800 – 875 AD
Phase 2	875 – 975 AD
Phase 3	ca. 975 AD
Period V	
	975 – 1025 AD
Phase 1	975 – 1025 AD
Phase 2	ca. 1025 AD
Period IV	
	1025 – 1150 AD
Phase 1	1025 – 1099 AD
Phase 2	1100 – 1133 AD
Phase 3	ca. 1133
Period III	
	1133 – 1250 AD
Phase 1	1150 – 1193 AD
Phase 2	1194 – 1250 AD
Period II	
	1250 – 1350 AD
Phase 1	1250 – 1278 AD
Phase 2	1278 – 1333 AD
Phase 3	1333 – 1350 AD
Period I	
	1350 – 20th century

2.1.6. Excavation areas

Due to the extent of the settlement and the longevity of excavation, multiple areas have been opened. In total, there are 17 areas, with 4652 m² excavated (Figure 2-1).⁵ Here, briefly the extent, location and main structures uncovered will be described.



Figure 2-1 Representation of excavated Areas at Miranduolo. Satellite image via www.maps.google.hr.

Area 1, located in the eastern part of the site has been excavated from 2001-2011 and it covers 885 m². It is the hilltop with the main palace, warehouse buildings, cistern and tower [61]–[63].

Area 2, located around the whole hill, it has been excavated in 2002 and it cover 168 m². It encompasses the defense wall [61]–[63].

⁵ What was primarily defined as area 13 has been merged with area 11. Also, the excavation area located at the last natural moat that surrounds Miranduolo hill, near modern road what was defined as area 16. This name has been discarded and named „test probe“. It was excavated in 2009 with an area of only 4 m² opened.

Area 3, located in the south-eastern part of the site, it has been excavated from 2001-2009 and it covers 228 m². The area includes a defense wall dated to end of 11th/beginning of 12th century which to the east extends to an artificial ditch from early 9th – last quarter of 10th century. On the north the wall is limited by the semi-terrace and a tower. The excavated deposits reveal a complete stratigraphic sequence and good preservation state [61]–[63].

Area 4, located south-western from the center of the site has been excavated in 2004 with an area of 104 m². The excavated area revealed stone walls of the castle houses and early medieval huts [61]–[63].

Area 5, located south-east from the settlement center, has been excavated from 2003-2005 and it covers 266 m². It is a plateau area west from the ditch, dated from 8th century to abandonment in 14th century [61]–[63].

Area 6, located west from Areas 1 and 3, has been excavated from 2003-2006 and it covers 131 m². This is the area of the 9th century ditch [61]–[63].

Area 7, located south from the center of the site, has been excavated in 2005 and it covers 107 m². It has a very poor deposit. It was the area for stone quarrying [61]–[63].

Area 8, located north from Area 2, has been excavated from 2005-2008 and it covers 274 m². The area comprises several levels of terraces with housing places dated from 8th century to abandonment in 14th century [61]–[63].

Area 9, located south from Area 5, has been excavated from 2005-2007 and it covers 140 m². It contains layers from 8th to 14th century when it was covered by up to 2 m thick layer of sand and stone in order to level the terrace, as it was implemented in a private road [61]–[63].

Area 10, located south of Area 9, has been excavated in 2009 and it covers 77 m². The area comprises early medieval evidences and 13th and 14th century deposits [61]–[63].

Area 11, located in the western part of the site, has been excavated since 2006 and it covers 308 m². The area includes the road to the main gate, part of the defense walls, early medieval huts, late 12th/early 13th century tower, and the traces of the 9th century outer palisade [61]–[63].

Area 12, located eastern from the defense walls, has been excavated in 2008 and it covers 830 m². The area is characterized by gorges cut into the rock, a summit area ditch, a road, mining area. This was probably linked to the northern part of the site used for mining in the 7th century [61]–[63].

Area 14, located on the northern part of the slope of the site and western from the Area 1 ditch, outside the castle walls, it has been excavated from 2009-2014 and it covers 130 m². Evidences of 7th century mines, 8th century farmer/blacksmith building with storage units, 9th century huts on posts, 10th century hut with stone base, 12th-13th century dump and construction site outside the defense walls [61]–[63].

Area 15, located west from Area 11, has been excavated from 2009-2013 and it covers 600 m². The area includes a rectangular shaped building related to metallurgical activities, dated to 13th century. Below it was the church of Saint John Evangelist (*San Giovanni Evangelista*) with an associated cemetery with privileged burials. Near the contemporary access road there was an 8th century silage area extending from area 11 and area 15. Also, early medieval huts were uncovered [61]–[63].

Area 17, located on the foot of the hill, north-northwest from the site, outside the defense walls has been excavated from 2010-2013 and it covers 180 m². The archaeological deposit contains artefacts from 8th century to modern times. The remains of a 10th-11th century road have been detected. A series of overlapping layers define the debris accumulated while re-building the castle from 11th to 13th century (period IV and III) [61]–[63].

Area 18, located south from area 14, has been excavated from 2012 to today and it covers 252 m². Here a metallurgical workshop has been recovered [61]–[63].

Area 19, located north from Area 15, has been excavated from 2013-2014 and it covers 140 m². The area has been covered by a levelling materials below which a 13th century shed was uncovered. Below the shed there were traces of a housing building and a warehouse. The area is mostly contemporary with the stone church (Area 15) although some elements are earlier like the 10th century burial, 9th century post holes of the outer palisade and a possible granary pit [61]–[63].

2.2. State of the art of archaeovitreology in Italy

In general, it is considered that the glass artefacts have a minor share among the archaeological artefacts, comparing to pottery and metal objects, due to the fact the glass has been re-melted (re-utilized) to make new objects [67]. Another hypothesis is that the glass objects were luxury items used only by privileged members of society. On the other hand, the archival documents from 14th and 15th centuries AD testify of relatively low cost of the production making relatively large quantities of products and with a wide variety of sizes and forms [67].

Venice (*Venezia*) was one of the most important production centers not only for Italy, but for the whole Western Europe [9], [30], [68], [69]. Venetian glass display amazing quality products (homogeneous, high transparency, variety of hues) with wide range of typological diversity and representing the skills of the artisans. The secret recipes that reveal which raw materials to use, which coloring agents and how to proceed with the preparation are kept in 15th century *Montpellier treatise* and *Anonimo*. Archaeological evidence of glass production (glassworking) in the Venetian lagoon and towns near Venice (Ferrara, Grado, Pieve di Bono near Trento and Torretta near Verona) are recognized and dated from 4th to 18th centuries. In Venice and the Torcello island the production has been noted from 7th-8th centuries. Since mid-13th century the Murano island glass workshop has been established. In this period the glassmaking starts, with the import of Levantine soda plant ash (Egyptian and Syrian) and from 16th century import of Spanish soda plant ash (*barilla*). Silica sand and pebble raw materials were imported from Crete

and Sicily sands. Import of quartz pebbles instead of sand after 1332 indicates the aspiration to have a high-purity silica source. The pebbles were imported from Ticino and Adige rivers in North Italy. Ticino river pebbles analysis prove their high-purity. Pyrolusite (MnO_2) was the decolorizer imported from Piemonte (NW Italy), Catalonia, Germany and France. By mid-15th century two qualities of glasses have been produced: *common glass (vetro commune)* with a slight green to yellow or blue natural hue and *vitrum blanchum*, a well decolorized glass; while *cristallo glass* appeared in mid-15th century. One of the secrets of producing *cristallo* glass was in the **purification of soda plant ash** by grounding it, sieving and dissolving in boiling water after which it was decanted, filtered, concentrated and dried until the *sale de cristallo/allume catino* was obtained. Glass samples analyzed that are dated from 13th to 14th centuries are mostly composed of plant ash (90%). As no wood ash glasses have not been detected, the connection with Levantine glassmaking should be proposed, due to the shortage of natron, plant ash has been re-introduced as a flux [1], [3], [4], [9], [20], [23], [25], [30], [56], [68].

Along with Venice, Altare near Genova in Liguria region was one of the most important glass workshop of the time [9], [20], [30], [52], [68]. In Liguria, around 20 glass workshops have been identified in the central part of the region, dated from 13th to 15th centuries. The glass materials have been analyzed from Monte Lecco (Passo della Bocchetta, 14th-15th centuries) and Veirera di Rossiglione (13th-14th centuries). In Monte Lecco local silica source of quartzite have been used. Documents evidence import of wood ash and soda plant ash from 14th to 16th centuries from Provence, south Italy, Spain and North Africa [3].

Although Venice produced large quantity and extremely high quality glass objects, Tuscany region had its own glass workshops. Archaeologically attested, those workshops have been practicing all the phases of glass production [3], [52]. Around 30 glass workshops have been recognized, but only small amount has been excavated. Compositional analysis of colorless, yellow and green glasses, dating from 9th-16th century, have been done. The analysis included samples from glass workshops (Gambassi, San Vettore, Germagnana, Orcia) and glass samples from settlements (Poggio Imperiale, Rocca di Campiglia, San Gimignano, San Giovanni Valdarno)

[22], [52], [69], [70].⁶ Considering the raw materials, historical sources mention the use of San Giovanni Valdarno near Florence sand and from Trequanda near Siena. There were small outcrops of sands in Gambassi and Montaione, which were used until the 20th century. Verrucano rock that was available in the vicinity of the workshops could be considered as a silica source. From 14th century, soda plant ash was used as a flux. It was imported from Provence and Pisa (originating from Syria), but local Tuscan production of the ash has been evidenced. Green glasses were unintentionally made in the 14th century at Germagnana and Santa Cristina glass workshops. The iron present in the sand as an impurity determined their color [3].

Tuscan glass vessel typology from 13th and 14th centuries can be classified due to comprehensive study of glass artifacts recovered from excavations of Casola (Massa Carrara), Pistoia, Prato, San Salvatore di Vaiano (Prato), Lucca, Pisa, Ripafratta (Pisa), Firenze, San Silvestro (Livorno), Porciano (Arezzo), San Giovanni Valdarno (Arezzo), Siena, Badia al Fango (Grosseto), Grosseto, Scarlino, Poggibonsi. That common tableware usually colorless and various hues of green, is represented by a larger amount of bubbles, diverse production of the rims and bottoms, widely produced forms for which it seems difficult to think about the import from distant production centers. Most of the artefacts belong to the common tableware, but sporadically lamps and pharmaceutical ampoules (*fiala da spezieria*). Among the common tableware open shapes like bowls (*coppa*, *ciotola*), plates (*piatti*), trays (*vassoio*), (*bacini*), closed forms and cups. Cups were a typical medieval form, while the goblets (*calice*) are scarce. During the 13th and 14th century the forms that appeared to be widely used are: truncated cone-conical and cylindrical smooth walled cups,

⁶ The dating of each site is as it follows: Gambassi from mid-16th century, San Vettore and Orcia from end of 13th-beginning of 14th century, Germagnana from end of 13th-mid-14th century, Poggio Imperiale glasses are dated from 1313, Rocca di Campiglia castle is dated from 11th-16th century while glasses analyzed from 13th-14th century, San Gimignano from 14th-16th century and San Giovanni Valderano to 15th century⁶⁸. Cagno, S., K. Janssens, and M. Medera, *Compositional analysis of Tuscan glass samples: in search of raw material fingerprints*. Analytical and Bioanalytical Chemistry 391, 2008: p. 1389-1395..

cups decorated with drops (*gocce*), globular body cups (*bicchiere*). Those forms have been introduced in the 11th century [67].

From 11th to 13th century bottles without the foot with conoid more or less pronounced. This type has been derived from early Medieval Venetian bottles. Another type of the bottom, from 12th to 14th century, is an empty or low ring foot. In 13th century, cups with small rounded decorations in horizontal lines, as noted in Sicily in 12th century. The body of the cups is truncated-conical and cylindrical. The bottles with narrow neck and pear-shaped and cylindrical bottles. 14th century small cylindrical pots (*vasetti*) without a foot or globular body with a marked neck – their function cannot be determined. Truncated cone-conical cups or cylindrical long-necked cups. There are also cups with the same shape but with the ring bottom and empty bottom [67].

Considering the decorations, from mid-12th to mid-13th century a change occurred whereas the cups have impressed decorations: diamonds, rhombs, quadrates, discs, and rib-like motifs repeating in series. In Germagnana, the type decorated with discs, diamonds and rib-like motifs has been produced [67].

Both Tuscan and Ligurian glasses, produced from 13th to 15th centuries, were mainly green and colorless Na-Ca-Si glass with plant ash used as a flux. In Valdelsa (Florence) workshop colored mosaic tesserae and flat glass was produced [18].

3. Materials and methods

3.1. Analytical techniques

In the literature [1], [3], [4], [71]–[74] one can find a wide range of available techniques that can be applied on glass depending on the research question that one wants to answer. Each of the techniques has advantages and disadvantages which have to be taken into consideration in order to obtain valid results and the results that will provide an answer for the posed question. Here, the techniques that have been used in the *archaeovitreological* study of Period II from Miranduolo site, will be presented, including SEM-EDS, PIXE/PIGE and LA-ICP-MS.

3.1.1. *VP-SEM-EDS*

SEM-EDS (Figure 3-1) is an analytical imaging tool based on the emission of electrons from the sample. The emission of electrons is induced by a strike of a focused electron beam[73]. High magnification, lateral resolution and large depth of focus along with the coupling with compositional mapping is the advantage of SEM-EDS in glass analysis. To reduce attenuation and scattering of the electron beam, the analysis is usually done under vacuum [3], [9], [75].

The electron beam is stretched over the sample irradiating array of points. As the electron beam hits the surface of the sample, the detector collects the interaction between beam and the surface as signals. Each of these signals can be recognized by a specialized detector, and not all of them are present in one instrument. The image can be formed by **backscattered electrons**, **secondary electrons**, **characteristic X-rays** and others (for thin samples the electrons emitted go through the sample like elastically scattered electrons, inelastically scattered electrons and transmitted electrons that are observed in TEM) [3], [76].

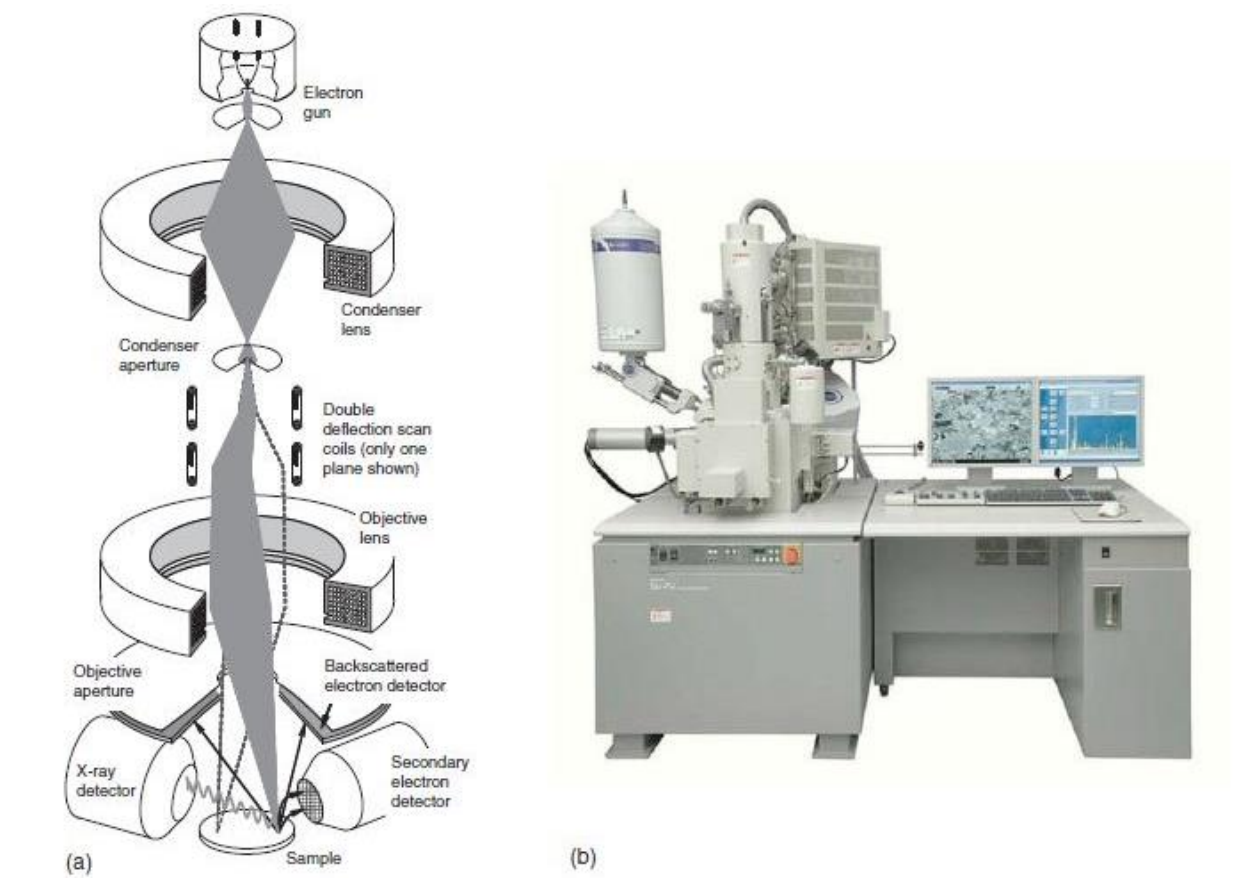


Figure 3-1 a) Schematic representation of SEM; b) photograph of SEM. From [3].

When the incident beam hits the surface it is backscattered as high energy electrons and it is a result of the interactions with the nucleus of atoms. The intensity recorded is proportional to the atomic weight meaning that the image contains chemical information. The higher Z elements will be displayed as lighter in color, since those elements backscatter stronger. As backscattered electrons escape from a greater depth than secondary electrons they do not reflect the topography. Secondary electrons, low in energy, are emitted from the loosely bound outer electronic orbitals of sample surface atoms. The emission of secondary electrons enables visualization of topographic features. The signal from characteristic X-rays (fluorescence X-rays) can be turned into chemical information of the analyzed area producing chemical maps [1], [3], [4], [6], [33], [74], [76].

In SEM-EDS the samples have to be prepared for the analysis. Firstly, the glass should be embedded in epoxy resin and polished to obtain a flat surface. The flat surface reduces the error of detected X-ray intensity, as inclination and surface roughness can affect the efficiency of the electron beam in the sample. As glass is a non-conductive material, a conductive layer (precious metal or carbon) of few nm needs to be applied, in order to avoid charging of the sample. Charging occurs as the electron beam hits the sample surface and the absorbed electrons are accumulated close to the surface, preventing the recording of the quality images. Charging can be prevented in low-vacuum mode by using a Variable Pressure SEM-EDS [3], [4], [6], [40], [74], [75], [77], [78]. As for VP-SEM, no sample preparation is needed [75], [76].

It is considered to be an accurate technique for analyzing glass particles down to 10 μm . Trace elements of oxides to 0.5 wt% can be detected although the quantification accuracy is poor. For nanoscopic investigations Transmission Electron Microscopy (TEM) is more appropriate, while for monitoring reaction of glass with water or for non-conductive samples that cannot be coated VP-SEM-EDS is usually employed [3], [9], [75], [76].⁷

Beam stimulated migration of alkali might occur during the analysis, due to the negative charge of the incident beam. Although the mechanism is not completely understood, the results of the alkali elements of the non-conducting samples may display analytical inaccuracies [18], [74].

In general, imaging techniques are used as preliminary mapping techniques of the present heterogeneities in the material that will induce which techniques should be further used [1], [6], [74], [77].

⁷ VP-SEM is also known as ESEM (Environmental Scanning Electron Microscopy), while EDS is also known as EDX (Energy Dispersive X-Rays) [76].

3.1.2. PIXE/PIGE

PIXE (Particle induced X-ray emission) and PIGE (Particle induced gamma emission) are non-destructive ion beam techniques that are based on the detection of radiation by a particle beam, with few MeV of energy [3], [6], [9], [10], [20], [72], [74], [79]. Protons are heavier and can be accelerated to a higher energy comparing to electrons. The protons loose less energy when passing through the sample, decreasing the Bremsstrahlung [6], [30], [72], [74]. The advantage of the ion beam techniques is in the insignificant irradiation of the sample. The techniques are non-invasive (no sampling required), non-destructive, and highly sensitive. When PIXE and PIGE are combined more information can be obtained [3], [6], [13], [19], [20], [72], [74].

PIXE is based on characteristic X-ray excitation through irradiation of protons, usually produced by a van der Graaff accelerator. The size of the incident beam is few microns [3], [6], [19], [72], [74]. The detection is limited to the surface, 5-10 μm , which is usually affected by degradation processes. In PIGE, proton beam excites the nucleus, that is, it penetrates deeper into the object: 20-30 μm . The gamma rays are emitted and detected by a detector. The gamma rays are characteristic of the element, and the measurements qualification and quantification data. The method is usually used for lighter elements (Li, F, Na, Mg, Al) and therefore it is usually used in combination with PIXE [3], [19], [30], [72], [74], [80].

The sensitivity is few $\mu\text{g/g}$ for transition metals, several hundred $\mu\text{g/g}$ for major elements and few hundred $\mu\text{g/g}$ for Na, Al, Si. REE (Rare Earth Elements) are rarely measurable because of the low intensity of K lines and the overlap of their L lines with high intensity K lines of other elements present in the glass [10], [14].

The analysis done in air only enables detection up to Si, in helium gas up to Na and in vacuum with a thin-window semiconductor up to C [3], [30], [72], [81].

Practically, PIXE/PIGE is used to characterize major and minor elements to define which fluxes, colorants, decolorants or opacifiers have been used. Trace elements will provide information of

the provenance of the raw materials. Also, corrosion processes can be studied [3], [10], [19], [30], [72], [74].

3.1.3. LA-ICP-MS

ICP-MS (Figure 3-2) is a micro-destructive analytical technique wide available since 1980's. The ablated aerosol of the sample is carried to the plasma torch where it is atomized and ionized. The ions move under the influence of magnetic or electrical field and are detected by mass spectrometer according to their mass-to-charge (m/z) ratio [74].

ICP-MS can be used to characterize the material through two modes of sample introduction: (a) liquid mode (solution mode) or (b) laser mode (LA). Laser mode is more appropriate for solid samples, it is only micro-destructive, and no sample preparation is necessary and spatial information is kept, comparing to the liquid mode. Another advantage of laser mode is that the corrosion layers present on the surface can be pre-ablated (no acquisition is done), regardless of the thickness of the corrosion layer, thus securing that the analysis will surely include pristine glass [3], [4], [73], [74], [82].

Different types of LA systems available, but majority is based on the ultra-violet (UV) Nd:YAG technology (Neodymium-doped Yttrium Aluminium Garnet). The Nd:YAG laser working at $\lambda=1066$ nm is considered obsolete due to chemical fractionation and low ablation field. Instead, 266 nm quadrupled or 213 nm quintupled frequency, or Excimer lasers working at 193 or 157 nm are used. The lower the wavelengths the lower the chemical fractionation and higher ablation yield. This enables the possibility of decreasing the diameter of the ablation spot and, therefore, increasing the spatial resolution. Generally, in Archaeometry 266 nm quadrupled or 213 nm quintupled frequencies are used [3], [73], [74], [82]–[84]

The sample must not exceed the sample chamber (*ca* 6 cm in diameter by *ca* 4 cm of depth). The sample's surface must be flat in order to keep the laser in focus during the ablation. Therefore, the sample can be embedded in a resin as for SEM-EDS analysis [6], [74].

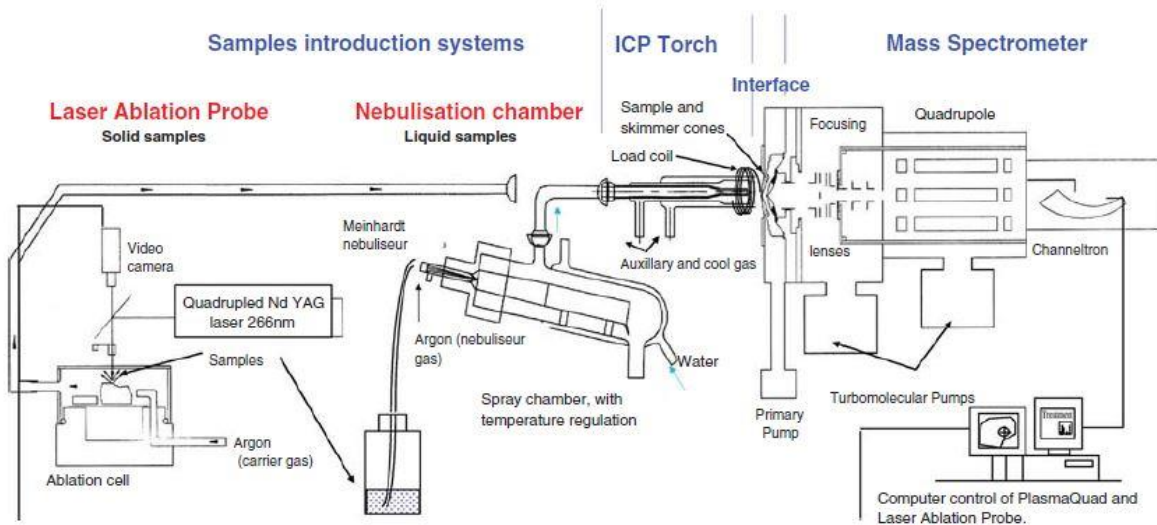


Figure 3-2 Schematic representation of LA-ICP-MS. From [3].

While ablating, the samples can be seen with a high-resolution CCD camera and color monitor. The laser beam is focused through window of a quartz sample cell. The repetition rate of the laser can be from 1 to 15 Hz, while the maximum energy of the beam is 2 mJ. The higher the repetition rate, the higher the sensitivity, but the fractionation increases. The fractionation can be partly corrected with the usage of glass standards. Otherwise, a balance between the repetition and fractionation should be maintained [3].

The ablation can be done in two modes: (a) with the ablation performed while the sample is mobile – line mode, and (b) with the immobile sample – spot mode. In the line mode, the ablation results with the line on the object's surface. This analysis can be used for characterization of enamels or glazes. In the case of the presence of the corrosion layers, the analysis will reflect its characterization. On the other hand, this mode has a lower fractionation. In the spot mode, the ablation results with a crater which depth depends on amount of the ablation time and laser

repetition rate. The amount of material sent with the spot mode to the torch is not constant, as with the liquid sample. Here, a peak at the beginning can be observed, with a plateau with the constant or slowly decreasing ion emission, before more prominent decreasing occurs. To obtain the maximum stability and reproducibility, the measurement should be recorded during the plateau, before the fractionation begins. The line mode gives a more linear signal, with a better sensitivity since the signal is measured at the pinnacle of the initial peak determined in spot mode. The disadvantage of the laser ablation is the absence of reproducibility of the raw signal that can be observed between ablations within the sample or between ablations between the samples. It is a consequence of variable interaction efficiency between the laser and the sample. This can be corrected by using isotopes as an internal standard and to account the ratios of the sample's signal to the signal of the internal standard [3]. The internal standard is usually one of the major or minor isotope present in the main glass components as ^{28}Si and ^{29}Si [3], [84]. For analyzing REE, ^{140}Ce is more appropriate [4].

Optical lenses and set of ceramic apertures adjust the diameter of the laser beam, making the spot size from 4 to 150 μm [3], [82], [83]. Determination of major chemical elements produces smaller craters, 40 to 80 μm . Minor and trace chemical elements determination produces larger craters, 80 to 200 μm [3].

In the ablation chamber a *ca* 1 L min^{-1} of argon or helium gas is introduced. The ablated aerosol is carried by argon or helium gas to the injector inlet of the plasma torch. There, the aerosol is atomized and ionized in the plasma flame at 8000°C. Sampling of the ions continues through a two-aperture cone system and channel electron multiplier assembly. The ions are selected according to their mass-to-charge ratio (m/z) using the mass filter. As the ions are separated they impact the detector. The signal is amplified through an external circuitry. In the quadrupole system the sensitivity can be increased with an additional pump to lower the pressure in the expansion chamber to 0.6-0,7 mbar [3], [73], [74], [82]–[84].

Two main mass spectrometers systems are employed: (a) low-resolution, and (b) high-resolution mass spectrometers. Low-resolution mass spectrometers are mainly quadrupole spectrometers which are used for elemental analysis. High-resolution spectrometers are used to avoid some isobaric interferences or to determine the isotopic ratios. With the LA mode the interferences are decreased, since there is no solvent effect as in liquid mode [3], [6], [85].

To ensure that the sample is homogeneous, several ablations are done within the same sample. Before each set of ablation, a blank signal is recorded to ensure that the baseline has returned to normal. The net signal is calculated by subtracting the blank value and a correction factor for the interferences, dividing it by the isotopic abundance and averaging multiple ablations. By dividing the net signal by the internal standard for the menu, a standardized signal for the elements is calculated. Then, a response coefficient factor is calculated for each element and for each menu using the standard glass reference materials. National Institute for Standards and Technology (NIST) 610, 611, 612, 614 and/or Corning A, B, C, D (Corning Museum of Glass) are the most used glass reference materials used. The analysis of standards is done regularly to correct the possible drifts of the instrument. As the elements present in the glass are in the oxide form, a correction factor is used. The concentrations of major and minor elements are normalized to 100% [3], [74], [83].

LA-ICP-MS has the sensitivity of 1-100 ppb, and the accuracy of 5-10%.⁸ Light chemical elements such as H, He, C, N, O, F, Ne, Cl, Ar and some actinides cannot be detected. The detection of REE is one of the advantages of the instrument in the glass analysis as the concentrations can help to determine the provenance of the sand source used [1], [4], [74].

⁸ In the liquid mode sensitivity reaches 50–1000 ppt, and accuracy 0.1-1.0 % [4].

3.2. Sampling

Sampling practices determine the success of the analysis, as they have to be appropriate in order to provide meaningful results [1], [4]. Theoretically, non-invasive⁹ techniques are the most desirable to use. In practice, those techniques sometimes might not give presentable data and/or surface of the object can be altered, as in glass, by degradation [1].

As every type of material contains some heterogeneities, larger or smaller dimensions, focused in the whole matrix or in individual areas. Therefore, the sampling area must be representative for the sample as whole [1].

During all the periods 572 glass fragments were recovered, while 86 of them belong to Period II.¹⁰ Twenty transparent samples have been chosen for this study, making *ca* 25% of the material being analyzed (Appendix 2 – Catalog of glass artefacts from Period II). This should be representative for the whole assemblage of the Period II. The fragments have been sampled by the principle of having a complete sequence of diverse colors of glass in each Area, and through all the Phases present in each Area. The glass fragments have been recovered from Area 1, 5, 8, 9, 10 and 11, but a single fragment from Area 5 has not been included in order to have the aforementioned sequence from other Areas through phases and colors (Figure 2-1). All the glasses recovered are transparent, and the colors range from various hues of green, yellow, azure and transparent. The classification of types of tableware consist mainly of cups, bowls, bottles,

⁹ Term non-invasive is used here as no sample is extracted from the original object, micro-invasive is determined as a micro-sample has been extracted, but the extraction is not visible to the naked eye, invasive as a sample had to be extracted from the original object. Non-destructive is determined as that the technique is not inducing changes in the sample, micro-destructive as micro destructions that are left on the sample but not visible on the sample by the naked eye, destructive as sample cannot be re-used in order to review the obtained results as in TGA.

¹⁰ The list of all fragments according to the inventory number, period, phase, structure, SU number, type, color, decorations and number of fragments can be found via [88].

closed forms, while few fragments are too small and non-distinctive to be classified. Hence, those fragments are labeled as non-identified.

The fragments obtained have already been washed. Prior to sampling, all of the fragments have been photographed from the external and internal side. The photographs have been processed in Adobe Photoshop CC 2014.

Macroscopically, air bubbles are visible in all the samples. The preservation state of the glasses on a macroscopic level can be generally defined as very well preserved. Sample MD 191 shows a slight iridescence effect, while samples MD 139 and MD 259 show a strong iridescence effect, and the glass is heavily flaking.

The area of the fragment that has been sampled in most of the samples is the wall of the tableware or non-identifiable object. Samples MD 173, MD 191 and MD 276 are ring bottoms of the cups.

The samples have been dry cut, set in epoxy resin blocks (epoxy resin/hardner 25:3 g), ground flat and polished using Si-C papers (P#220, P#320, P#500, P#800, P#1200, P#2000).

3.3. Experimental methods

3.3.1. *VP-SEM-EDS*

VP-SEM-EDS was used to determine the homogeneity of the glasses and deterioration products present. The thickness of the glasses have been measured in order to determine if it could be correlated with the type of the tableware, color, Phase and/or Area of recovery (Table 4-2). The bulk chemical qualification and semi-quantification was done by EDS to determine the major and minor glass components. The data obtained signified the usage of more sensitive techniques: PIXE/PIGE and LA-ICP-MS.

The blocks were analyzed with HITACHI S3700N Variable Pressure-SEM equipped with a Bruker AXS X-Flash® Silicon Drift Detector 5010 (129 eV Spectral Resolution at MnK α Full Maximum Half Width FMHW). Quantitative standardless PB/ZAF elemental analysis was made using the Bruker ESPRIT software. The operating conditions for EDS analysis were: backscattered electron mode (BSEM), pressure of 40 Pa, 20 kV accelerating voltage, 10-14 mm working distance. Each measurement was performed for 60 s in real time. The measurements had from 1.5 to 13.5 kcps. Elemental concentrations have been converted to weight percent (wt%) oxide concentrations.

3.3.2. PIXE/PIGE

The PIXE/PIGE analysis has been carried out at MTA Atomki, Debrecen, Hungary at the 0° beamline of the 5 MV Van de Graaff accelerator. The measurement setup included four detectors. For PIXE two X-Ray detectors were placed at 135° geometry to the incidence beam:

- a) an SDD detector with AP3.3 ultra-thin polymer window (SGX Sesortech) with 30 mm² active surface area for measurement of low and medium energy X-rays (0.2 – 12 keV, $Z > 5$);
- b) a Gresham type Be-window Si(Li) X-ray detector with 30 mm² active surface area equipped with an additional kapton filter of 125 μ m thickness for measurement of medium and high energy X-rays (3-30 keV, $Z > 19$).

For PIGE a Canberra HPGe 40% Gamma-Ray detector was placed at 45° with respect to the incidence beam direction and 11 cm distance from the sample, outside the vacuum chamber.

A particle detector of the chopper was used to measure the beam dose.

All the signals that have been recognized by the detectors have been recorded event by event in list mode by the Oxford type OMDAQ data acquisition system. Simultaneously, high quality PIXE

spectra were recorded with independent Camberra data acquisition system and with the SGX digital DPP.

The measurement conditions included an irradiating beam of 3.2 MeV focused down to $\sim 5 \mu\text{m} \times 5 \mu\text{m}$ with a current of 50-100 pA . Each sample measurement included 2-4 spots. The scan size of each spot was 1 mm x 1 mm. Firstly an elemental map of the aforementioned size was recorded, and if there was a necessity, a homogeneous area has been selected for a more accurate measurement. For samples MD 139, MD 143 and MD 259 that display corrosion layers, another map of the corrosion layer was made with a scan size adjusted to the size of the corrosion layer. The corrosion in sample MD 24 could not be measured since the beam size exceeded the size of the very thin corrosion layer ($2.25 \mu\text{m}$). The analysis of the corrosion layer was not performed as the results obtained would not present correct data.

Due to charging of the samples MD 12 and MD 243 the measurements had to be repeated using a lower beam current.

To test the quality and precision of the dose measurement and to determine the quantification parameters standard glass reference materials were used at the beginning and the end of each measurement campaign which typically contained 5 glass samples. Also, the calibration of the beam chopper was done at the beginning and the end of the measurement campaign. The standard glass reference materials included NIST 610, Corning A and Corning B[86, 87], and a series of pure metals and a layered sample ($6 \mu\text{m}$ thick Ti foil on $50 \mu\text{m}$ Ni).

The evaluation of the PIXE spectra has been done with GUPIXWIN software. Samples were treated as thick samples. Firstly, the matrix composition was determined from the SDD detector spectra using the iterative matrix solution method. Afterwards, the a Gresham type Be-window Si(Li) X-ray detector spectra were analyzed in trace mode, implementing the previously obtained matrix and the measured irradiation dose. In the 3.0 – 8.5 keV range are the intensive X-Ray lines as K K_{α} , Ca K_{α} , Ti K_{α} , Fe K_{α} and these were used for elemental concentration normalization. Generally, the concentration difference between the two PIXE detectors was 0 – 5%. Finally the

elemental concentrations were normalized to 100% where needed. The sum spectra was added to each sample to reduce the detection limits. This method reduced the detection limits by 30 – 50% comparing to the MDL of the spectra corresponding to one point analysis. This aided in the investigation of the homogeneity of the samples. The PIXE analytical uncertainty (including the fitting process uncertainty) for major elements is ~ 2 – 5%, while for minor and trace elements ~ 10 – 15%.

The data have been presented as oxides in wt% or as elements expressed in ppm. The table contains the fit error in % and the MDL in ppm or wt%, and the decision. Y represents the given element in a concentration that is more than one sigma above the 'quantization limit' (3.3 LOD + error), N represents a given element was found concentrations below LOD, and the '?' represents values in-between.

3.3.3. LA-ICP-MS

Due to usage of Laser ablation mode, no sample preparation was required. The ablation was performed by Cetac Technologies LSX-213 G2⁺ (213 nm Q-switched Nd:YAG laser with > 4 mJ source pulse energy and < 5 ns pulse width), with a laser working with 100% of energy, and a frequency of 20 Hz. The ablation was done in spot mode (600 shots), with He carrier gas flow of 1L/min. The conditions of the ablation included 15 s of gas blank, 30 s of ablation, and 10 s of wash out. The diameter of the beam was 50 μm for all the samples, except for the corrosion layers of sample MD 259, where the diameter of the beam was 15 μm . This beam size was chosen in order to focus on the corrosion layer while avoiding that of the pristine glass and the epoxy resin. Experimentally, as the pristine glass for the samples MD 143 and MD 259 were analyzed by 50 μm beam, the analysis of the pristine glass has been made with a 15 μm beam to investigate if there is a significant difference in accuracy and precision with respect to the beam diameter. The corrosion analyses results obtained will be compared with PIXE/PIGE.

NIST 610 and 612 have been used as glass standard certified materials [86]. Each measurement campaign consisted of 3 spot analyses for each glass standard material and 4 spot analyses for glass samples. Between 8-12 glass sample measurements, three replicates of the certified references materials were performed in order to check for any potential instrumental drift.

The ICP-MS analysis was performed by Agilent 8800 Triple Quadrupole Instrument in the MS/MS mode with no gas in the reaction cell. The working conditions included RF Power of 1550 W, RF Matching of 1.4 V, 4 mm of sample depth, Argon dilution gas flow of 0.7 L/min and Argon plasma flow of 15 L/min. The dwell times for all the isotopes analyzed are 5, 10 and 20 ms (Table 3-1).

Table 3-1 Dwell times in milliseconds (ms) for analyzed isotopes.

Dwell time (ms)	Isotopes
5	²³ Na, ²⁴ Mg, ²⁷ Al, ²⁸ Si, ³⁹ K, ⁴⁴ Ca, ⁵⁶ Fe
10	⁴³ Ca, ⁴⁷ Ti, ⁵² Cr, ⁵⁵ Mn, ⁵⁷ Fe, ⁵⁹ Co, ⁶⁰ Ni, ⁶³ Cu, ⁶⁶ Zn, ⁶⁷ Zn, ⁷⁵ As, ⁸⁵ Rb, ⁸⁸ Sr, ⁸⁹ Y, ⁹⁰ Zr, ¹¹⁸ Sn
20	³¹ P, ⁵¹ V, ⁹³ Nb, ¹²¹ Sb, ¹³⁷ Ba, ¹³⁹ La, ¹⁴⁰ Ce, ¹⁴¹ Pr, ¹⁴⁶ Nd, ¹⁴⁷ Sm, ¹⁵³ Eu, ¹⁴⁷ Gd, ¹⁵⁹ Tb, ¹⁶³ Dy, ¹⁶⁵ Ho, ¹⁶⁶ Er, ¹⁶⁹ Tm, ¹⁷² Yb, ¹⁷⁵ Lu, ¹⁷⁸ Hf, ²⁰⁸ Pb, ²³² Th, ²³⁸ U

The data set were analyzed using the data reduction software Glitter (version 4.4.2). Previous analysis by PIXE/PIGE provided the silica content that was converted into SiO₂ and used as internal standard for the quantification process by LA-ICP-MS.

The data evaluation for glass standard materials included the calculation of average, recovery (%) and drift (%). Recoveries of 90-110%, and a drift ≤10% have been accepted as a result that did not require any corrections.

Different CRM's ("Certified Reference Materials") were used due to the different concentration range of the targeted analytes in both standards and samples.

Due to higher concentrations in glass samples, Mg, P, K, Ti, Mn, Zn, Sr and Ba were calculated using NIST 610 as CRM. Remaining elements were quantified using NIST 612.

All the raw data have been obtained as elements in ppm. The major and minor elements (Na_2O_3 , MgO, Al_2O_3 , SiO_2 , P_2O_5 , K_2O , CaO, TiO_2 , MnO, Fe_2O_3) have been converted to oxides in wt%, while trace elements (V, Cr, Co, Ni, Cu, Zn, As, Rb, Sr, Y, Zr, Nb, Sn, Sb, Ba, La, Ce, Pr, Nd, Sm, Eu, Gd, Tb, Dy, Ho, Er, Tm, Yb, Lu, Hf, Pb, Th, U) are expressed in ppm.

4. Results

4.1. SEM-EDS

SEM analysis on the glass cross-section of resin-embedded blocks shows good homogeneity for all 20 samples, with no inclusions nor frequent presence of air bubbles. The major and minor elements have been measured with EDS and they are expressed as weight percent of oxides (wt%), except Cl⁻. Samples displaying corrosion layers were subjected to line-scan measurements in order to determine the magnitude of the depletion of monovalent and bivalent ions.

4.1.1. *Elemental composition*

VP-SEM-EDS is, as already stressed, a semi-quantifying method. In this study it has been used to have preliminary compositional results. The information obtained would be compared with contemporary Italian sites to conclude if the Miranduolo Period II glass artefacts fall within the general image of the glass compositions, while precise results would be obtained by PIXE/PIGE and LA-ICP-MS.

The average Miranduolo glass composition (Table 4-1) is 58.44 wt% (min. 53.87 – max. 61.65 wt%) of SiO₂, 17.46 wt% (min. 13.05 – max. 22.43 wt%) of Na₂O, 8.79 wt% (min. 2.98 – max. 12.28 wt%) of CaO, 2.76 wt% (min. 1.33 – max. 6.68 wt%) of K₂O, 3.67 wt% (min. 1.90 – max. 7.25 wt%) of MgO, 3.77 wt% (min. 2.03 – max. 5.74 wt%) of Al₂O₃ and 1.67 wt% (min. 0.5 – max. 2.51 wt%) of Fe₂O₃. In 2 samples the P₂O₅ concentration was below the detection limit, while for MnO it was in 4 samples. In majority of the samples SO₃ and TiO₂ concentrations were below the detection limit.

Table 4-1 Sample name, color, type of fragment analyzed and chemical elements analyzed by VP-SEM-EDS in wt%, except Cl. AM – amber, AZ – azure, C – colorless, G – green, Y – yellow, Y-G – yellow-green, nd – not identified.

Sample	color	type	SiO ₂	Na ₂ O	TiO ₂	Fe ₂ O ₃	Al ₂ O ₃	MgO	CaO	K ₂ O	P ₂ O ₅	SO ₃	Cl ⁻	MnO
MD12	G	cup	52.83	14.42	nd	1.34	5.50	7.25	12.28	2.83	0.65	nd	0.87	nd
MD21	G	bowl	54.40	13.53	nd	1.41	5.74	6.69	11.68	3.66	0.69	nd	0.94	nd
MD24	C	nd	61.65	18.85	nd	1.57	2.55	2.48	8.28	2.47	nd	nd	1.12	0.94
MD66	Y	cup	57.84	16.83	nd	1.62	3.10	3.48	10.81	2.63	0.60	nd	0.81	0.96
MD67	AM	nd	60.49	22.43	nd	2.51	4.14	2.24	2.98	1.91	0.16	nd	1.28	0.88
MD139	AZ	cup	56.81	15.34	nd	1.26	3.62	5.92	11.65	1.33	0.59	nd	0.99	nd
MD143	AZ	cup	54.80	14.83	nd	1.08	5.55	6.40	10.87	2.25	0.59	nd	0.94	nd
MD172	Y-G	bottle	58.89	21.00	nd	1.71	3.60	2.47	5.93	2.62	0.24	nd	1.02	0.91
MD173	Y	cup	63.62	14.72	0.16	1.13	2.86	3.52	10.34	2.66	0.38	0.16	0.71	0.49
MD191	Y-G	cup	60.12	18.14	nd	1.39	2.71	2.45	9.79	3.07	0.35	nd	0.94	1.13
MD193	Y	nd	59.52	20.06	nd	1.92	4.37	2.32	5.60	2.40	0.19	nd	1.08	0.54
MD222	G	nd	60.53	20.24	nd	1.63	3.79	2.36	6.03	2.47	0.15	nd	1.04	0.68
MD231	Y	cup	60.31	15.72	0.02	1.56	4.20	3.11	9.88	2.97	0.40	0.02	0.64	1.20
MD243	G	bowl	53.87	13.05	nd	3.16	3.23	3.65	10.79	6.68	0.88	nd	0.68	1.13
MD256	Y	nd	59.51	18.62	nd	2.31	4.12	2.38	6.61	3.92	0.26	nd	1.04	0.90
MD257	G	nd	58.41	19.13	0.02	2.21	4.00	3.04	7.32	2.11	0.12	0.02	0.94	1.33
MD259	C	cup	55.86	17.32	nd	0.50	2.03	4.63	11.03	2.70	0.21	nd	0.75	0.19
MD261	AZ	nd	59.91	20.03	nd	2.11	3.76	1.90	7.25	1.75	nd	nd	0.92	1.07
MD272	AM	cup	59.96	16.04	nd	1.43	3.25	4.38	8.92	1.89	0.44	nd	0.96	1.29
MD276	G	cup	59.52	18.85	nd	1.46	3.36	2.72	7.78	2.84	0.30	nd	0.77	1.06

According to the concentrations of K₂O and MgO (Figure 4-1, Table 4-1, Figure App.3-1), which are above 1.5 wt%, the samples can be classified as **plant ash Na-Ca-Si glasses (pa-Na-Ca-Si)**. The plant ash glasses can be classified according to the origin/K₂O concentrations. For glasses that have from 1.5 to 4.5 wt% of K₂O the glasses were made with **Levantine ash (Lpa-Na-Ca-Si)**, while from 4.5 to 8 wt% the so called **Barilla ash (Bpa-Na-Ca-Si)**; origin in western Mediterranean) has been used [69]. All of Miranduolo samples are made from Levantine ash, except MD 243, which is made from Barilla plant ash. The concentrations of CaO that are higher than 7 wt%, in bibliography imply the usage of unpurified ashes, while below 7 wt% imply production of glass

that implemented the purification procedure of plant ashes. Therefore, 6 of 18 Lpa-Na-Ca-Si glasses can further be classified as purified Levantine plant ash glasses (**PLpa-Na-Ca-Si**) and 13 as unpurified Levantine plant ash glasses (ULpa-Na-Ca-Si). The single Bpa-Na-Ca-Si glass is made from unpurified Barilla ash (**UBpa-Na-Ca-Si**). Sample MD 139 due to concentrations of 1.33 wt% of K_2O and 5.92 wt% of MgO cannot be classified into known glass groups (Figure App.3-4). In this work, this compositional occurrence will be proposed as a new compositional group called **High Magnesium natron (HMgn-Na-Ca-Si)**.

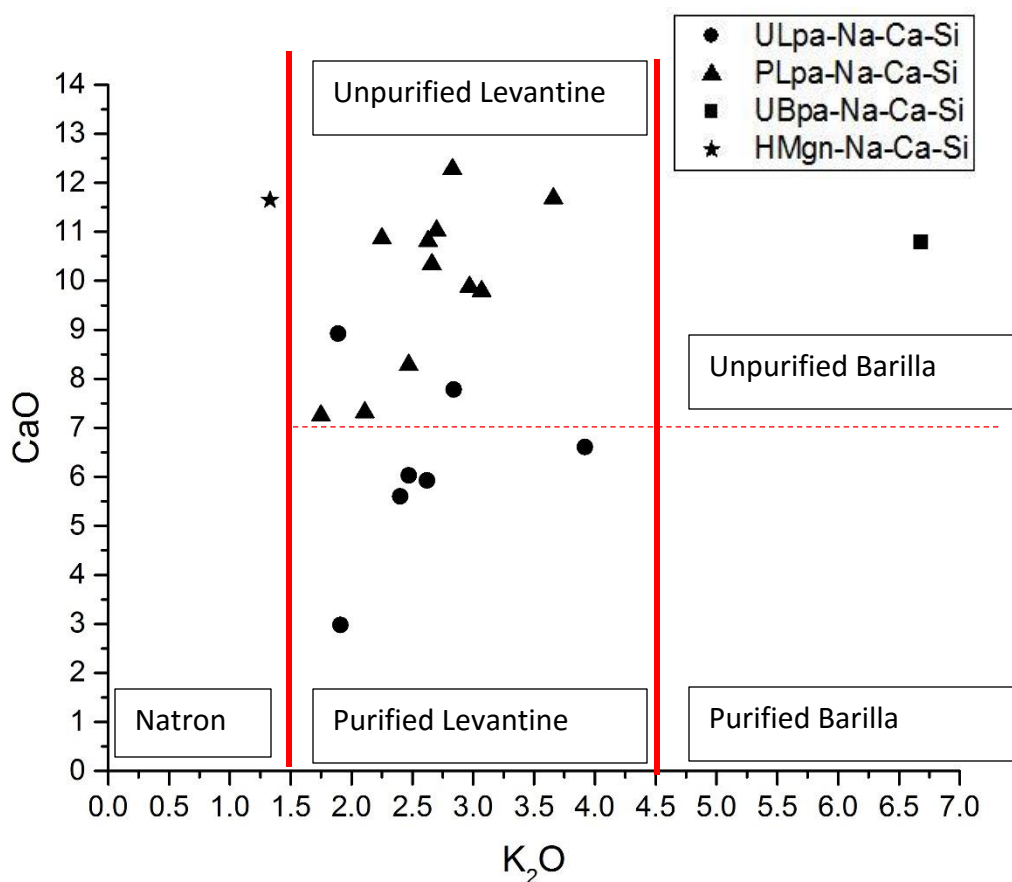


Figure 4-1 Bi-plot of K_2O and CaO (wt%) of Miranduolo samples with marked compositional groups.

The HMgn group has not been firstly encountered among Miranduolo glasses. Very few examples have been detected in Italian sites, but so far they have not been recognized as a glass type that should be specifically classified. For example, sample t_63 from 13th-14th century Rocca di Campiglia has 1.5 wt% of K₂O and 4.4 wt% MgO [22], sample 4121 from mid-13th century Savona has 1.37 wt% of K₂O and 4.09 wt% MgO [20], sample 52 from 6th-11th century San Genesio has 1.3 wt% of K₂O and 3.9 wt% MgO [50], sample v12 from 6th-7th century Piazza Bovio, Napoli has 0.63 wt% of K₂O and 1.71 wt% MgO [55]. 9th-12th century samples from Cordoba have also displayed this composition for the following samples: COR1 has 1.3 wt% of K₂O and 2.1 wt% MgO, COR14 has 0.92 wt% of K₂O and 1.74 wt% MgO, COR18 has 1.34 wt% of K₂O and 1.92 wt% MgO and COR24 has 1.46 wt% of K₂O and 3.21 wt% MgO [25]. Sample OF6a 10th-11th century Nogara has 0.92 wt% of K₂O and 2.28 wt% MgO, with other samples (OR3, PR2b, PR5 dated to 11th-12th century) that have a border value (1.5 wt%) of MgO [28]. Among Mixed-Alkali glasses analyzed by Henderson [60] there is one sample from La Négade (2, LN, *pu*, *v* as specified in Table 2 of the paper) which has a higher content of MgO (4.4 wt%) than of K₂O (1.0 wt%), which has not been recognized. From the archaeovitreological analysis of Siponto finds, there are 3 samples (7, 14, 22) display a value of K₂O higher than 1.5 wt%, and a lower value than 1.5 wt% of MgO [59].

On the other hand, the correlation of MgO and CaO seem to correspond to the intentional addition of calcite to Miranduolo glasses (Figure 4-2, Figure App.3-1). The results obtained with PIXE/PIGE and LA-ICP-MS will aid in determining the validity of this hypothesis. The correlation of Br with CaO would indicate the marine origin of calcite, possibly in the form of sea shells.

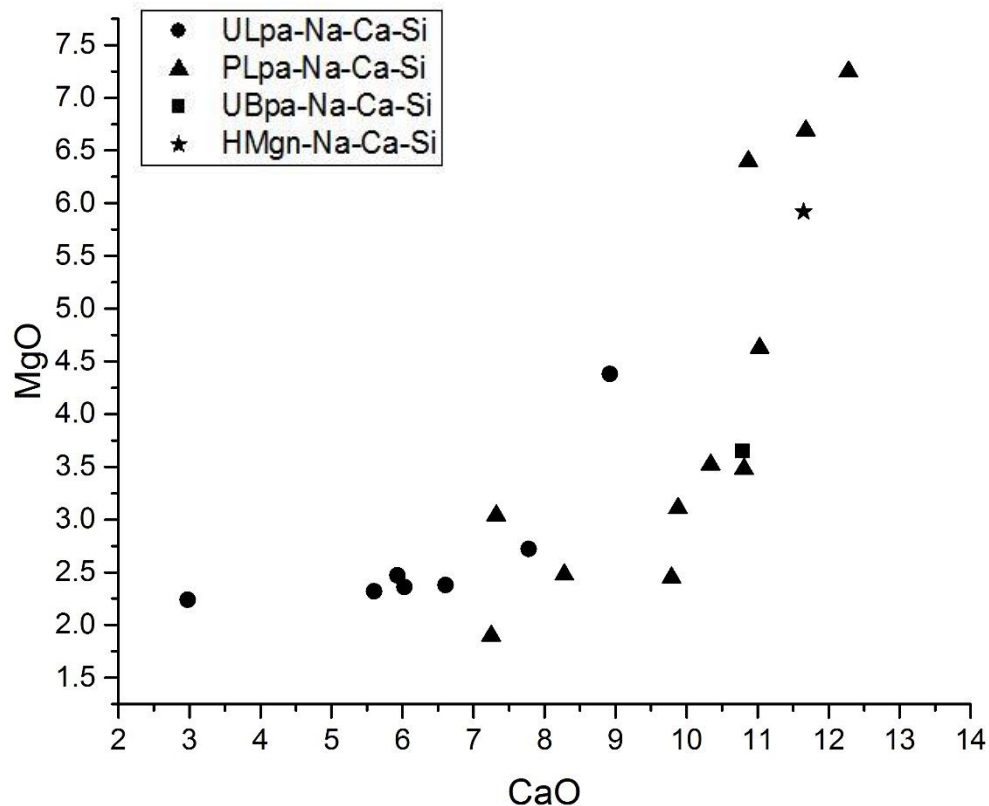


Figure 4-2 Bi-plot of CaO and MgO (wt%) of Miranduolo samples with marked compositional groups.

High concentrations of Fe_2O_3 (≥ 1 wt%) and Al_2O_3 (≥ 3 wt%) are to be considered as (Figure App.3-2, Figure App.3-5) the natural impurities of the raw silica source. This network former does not display a high SiO_2 content (average $\text{SiO}_2 < 60$ wt%). These lower SiO_2 concentrations along with only four corrosion layers was not consistent with all glass corrosion studies that claimed that for the glass to be less susceptible to degradation the SiO_2 concentrations need to be >60 wt%. Of course, the burial microenvironmental parameters should be considered as an important factor in glass deterioration. The feature of Miranduolo glasses to be corrosion resistant put a doubt on the SiO_2 quantification precision of VP-SEM-EDS in bibliography are not considered as glasses that stable and resistant to weathering and deterioration. Thus, the SiO_2 concentrations will be re-evaluated with PIXE/PIGE.

In 8 samples MnO content is lower than 0.5 wt% (in 4 samples it was not detected), meaning that in these samples MnO is naturally present. In other 12 samples, MnO above 0.5 wt% indicates deliberate addition as a decolorant agent to intentionally obtain different hues or the amount added was not successful in making the glass colorless (Figure App.3-3).

4.1.2. Corrosion

Out of 20 analyzed samples, in 16 of them only pristine glass could be recognized, while in 4 samples (MD 24, MD 139, MD 143, MD 259) corrosion layers can be distinguished. The thickness of the corrosion layer varies from 2.25 μm (MD 24), 136-500 μm (MD 139), 26.8 μm (MD 143) and 17.01 μm (MD 259).

Two different corrosion morphologies can be determined: a) parallel, and b) hemispherical (Figure 4-3). Their development is related to the type of progress of the corrosion. In parallel corrosion, the corrosion was developed slowly in time, without entrance of moisture into the glass through cracks or air bubbles. The hemispherical morphology appears as the final corrosion product. The corrosion has developed quickly in the glass where irregularities in form of air bubbles and/or mineral particles are present [14]. All corroded samples show the parallel morphology, while MD 139 also displays hemispherical morphology.

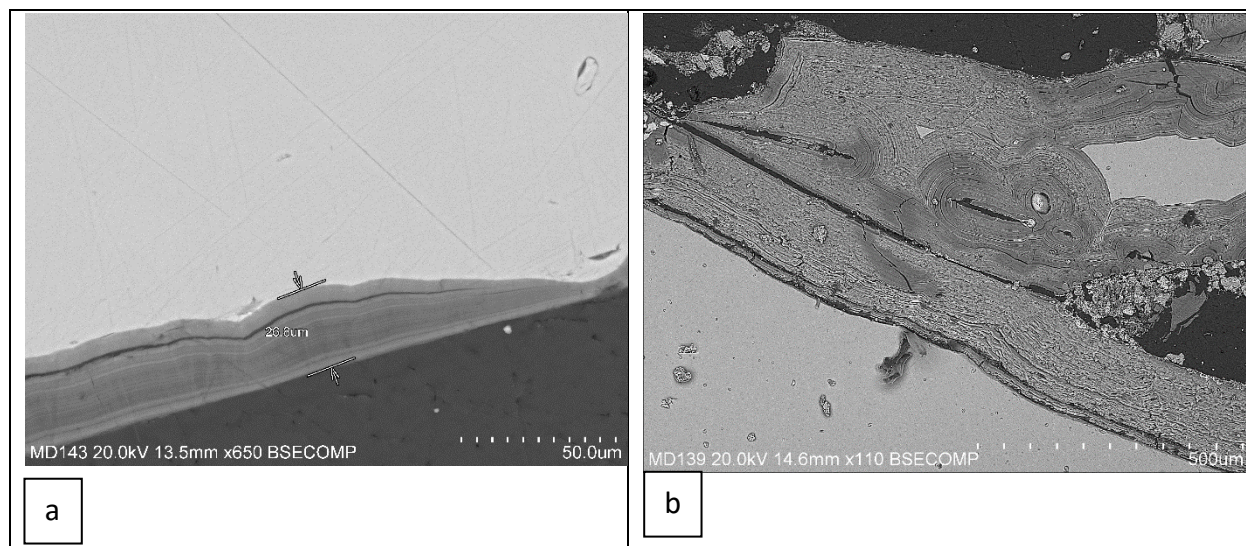


Figure 4-3 a) SEM image and measurement of parallel corrosion layer of sample MD 143; b) SEM image of parallel and hemispherical corrosion layers of sample MD 139.

The line-scan measurements determined that Na leaches heavily, indicating a complete depletion. On the other hand, Ca and K leach to a minor extent comparing to Na (Figure 4-4).

As mentioned before, the SiO₂ content below 60 wt% in glasses is not considered as favorable and resistant to weathering and deterioration. As VP-SEM-EDS is a semi-quantifying technique, the evaluation of the SiO₂ concentration will be done upon the results obtained with more precise instruments. On the other hand, the high concentrations of Al₂O₃ can be the cause for good preservation of Miranduolo glasses. It is considered that all flux ions were bonded to aluminate network, which limits leaching of Na ions in acidic and basic conditions. Again, the re-assessment of the quantification of the Al₂O₃ content need to be made before further conclusions can be made.

In general, as only four Miranduolo samples display corrosion products, this could imply that both glass composition and the burial conditions were favorable for their preservation.

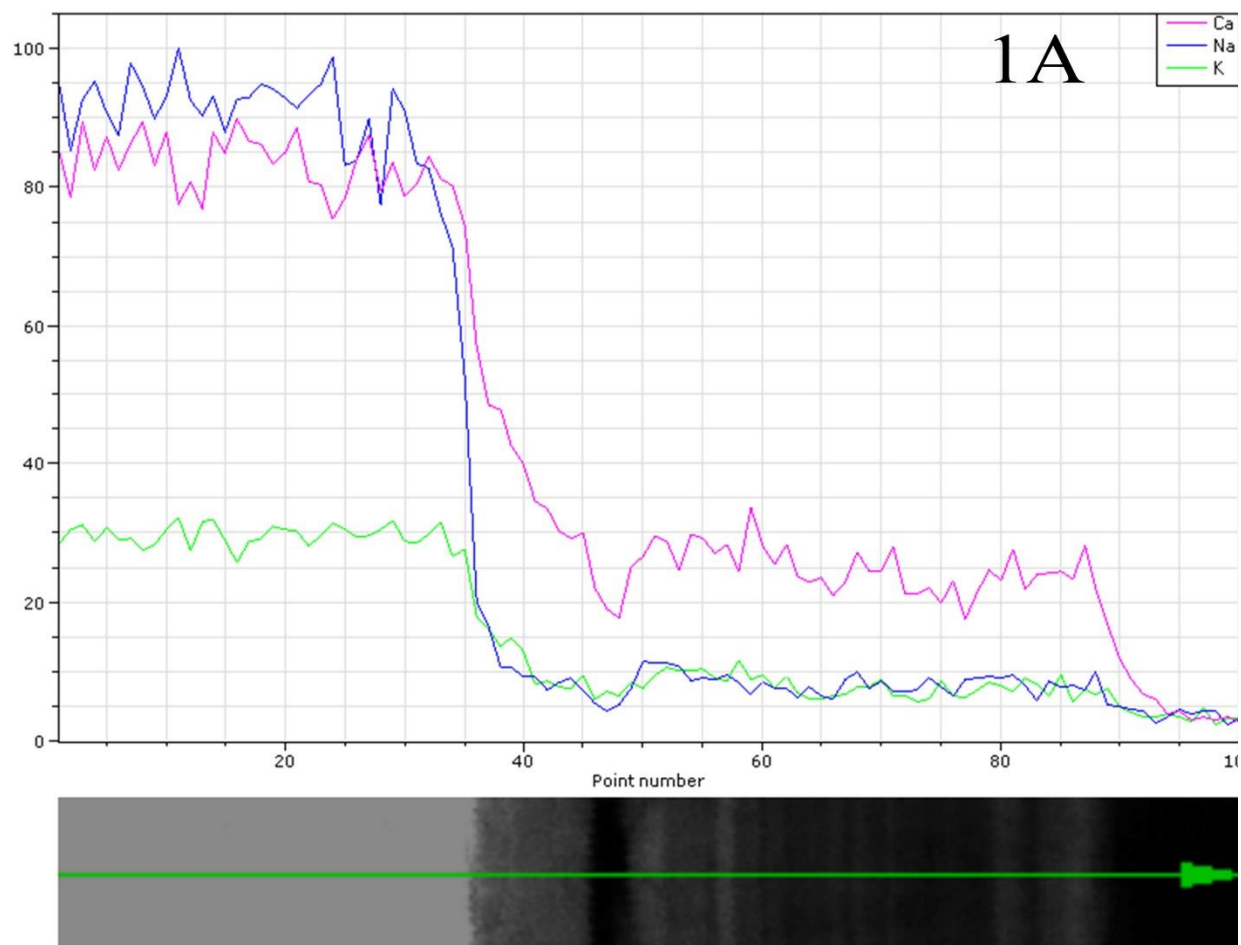


Figure 4-4 VP-SEM-EDS line scan of sample MD 143 displaying the depletion of Na, Ca and K.

Table 4-2 Color, type of fragment analyzed, part of the fragment sampled, thickness of the pristine glass and the corrosion layer. AM – amber, AZ – azure, C – colorless, G – green, Y – yellow, Y-G – yellow-green, nd – not identified, μm – micrometer, mm – millimeter, cm – centimeter.

Sample	color	type	Part sampled	Pristine glass thickness	Corrosion thickness
MD12	G	cup	Body	484 μm	nd
MD21	G	bowl	Body	1.11 mm	nd
MD24	C	nd	Body	526 μm	2.25 μm
MD66	Y	cup	Body	981 μm	nd
MD67	AM	nd	Body	1.32 mm	nd
MD139	AZ	cup	Body	1.93 mm	136-500 μm
MD143	AZ	cup	Body	702 μm	26.8 μm
MD172	Y-G	bottle	Body	3.12 mm	nd
MD173	Y	cup	Ring foot	2.85 mm	nd
MD191	Y-G	cup	Ring foot	5.14-6.00 mm	nd
MD193	Y	nd	Body	727 μm	nd
MD222	G	nd	Body	1.66 mm	nd
MD231	Y	cup	Body	1.40 mm	nd
MD243	G	bowl	Body	1.41 mm	nd
MD256	Y	nd	Body	830 μm	nd
MD257	G	nd	Body	1.23 mm	nd
MD259	C	cup	Bottom	349 μm	17.01 μm
MD261	AZ	nd	Body	1.02 mm	nd
MD272	AM	cup	Body	1.25 mm	nd
MD276	G	cup	Ring foot	1.5 cm	nd

4.2. PIXE/PIGE

For major elements PIXE/PIGE is considered to be most accurate [77] among the techniques used, while for minor and trace elements LA-ICP-MS is considered to be most accurate and precise among the techniques used in this study [1], [74].

4.2.1. Elemental composition

The chemical maps done for all glasses display their homogeneity as confirmed with VP-SEM-EDS. The results for major, minor and trace elements analyzed are represented in Table 4-3 and Table 4-4. The average Miranduolo glass composition is 63.94 wt% (min. 59.37 – max. 67.69 wt%)

of SiO₂, 15.76 wt% (min. 11.86 – max. 20.53 wt%) of Na₂O, 6.62 wt% (min. 2.17 – max. 9.41 wt%) of CaO, 2.43 wt% (min. 1.24 – max. 5.82 wt%) of K₂O, 3.42 wt% (min. 1.86 – max. 6.84 wt%) of MgO, 3.13 wt% (min. 1.57 – max. 4.99 wt%) of Al₂O₃ and 1.33 wt% (min. 0.55 – max. 1.95 wt%) of Fe₂O₃.

Comparing with the VP-SEM-EDS results, there are more samples with CaO ≤ 7 wt%. Namely, MD 24, MD 191, MD 257, MD 261, MD 272 and MD 276 can be according to PIXE/PIGE be classified as ULpa-Na-Ca-Si glasses. In total, there are 11 ULpa-Na-Ca-Si and 6 PLpa-Na-Ca-Si. Sample MD 139, as already proved, has a specific HMgn-Na-Ca-Si composition.

Positive correlation of CaO with MgO ($r = 0.8360$, $R^2 = 0.6989$; Figure App.4-1) and Sr ($r = 0.8519$, $R^2 = 0.7257$; Figure App.4-2), and no correlation of K₂O with CaO ($r = 0.2453$, $R^2 = 0.0602$) nor MgO ($r = 0.0824$, $R^2 = 0.0068$) indicates the addition of calcite in the batch.¹¹ When plotting CaO against Br, the positive correlation can be an indication of addition of the sea shells as a source of lime in the glass, as indicated in [15]. In total, there is a strong negative correlation of CaO and Br with $r = -0.6729$ and $R^2 = 0.4527$ (Figure 4-5, Figure App.4-1). This implies that the calcite was of continental origin.

¹¹ Strong positive correlation is considered from 0.5-1.0; Medium positive correlation is from 0.3-0.5 and small positive correlation is from 0.1-0.3 via [89].

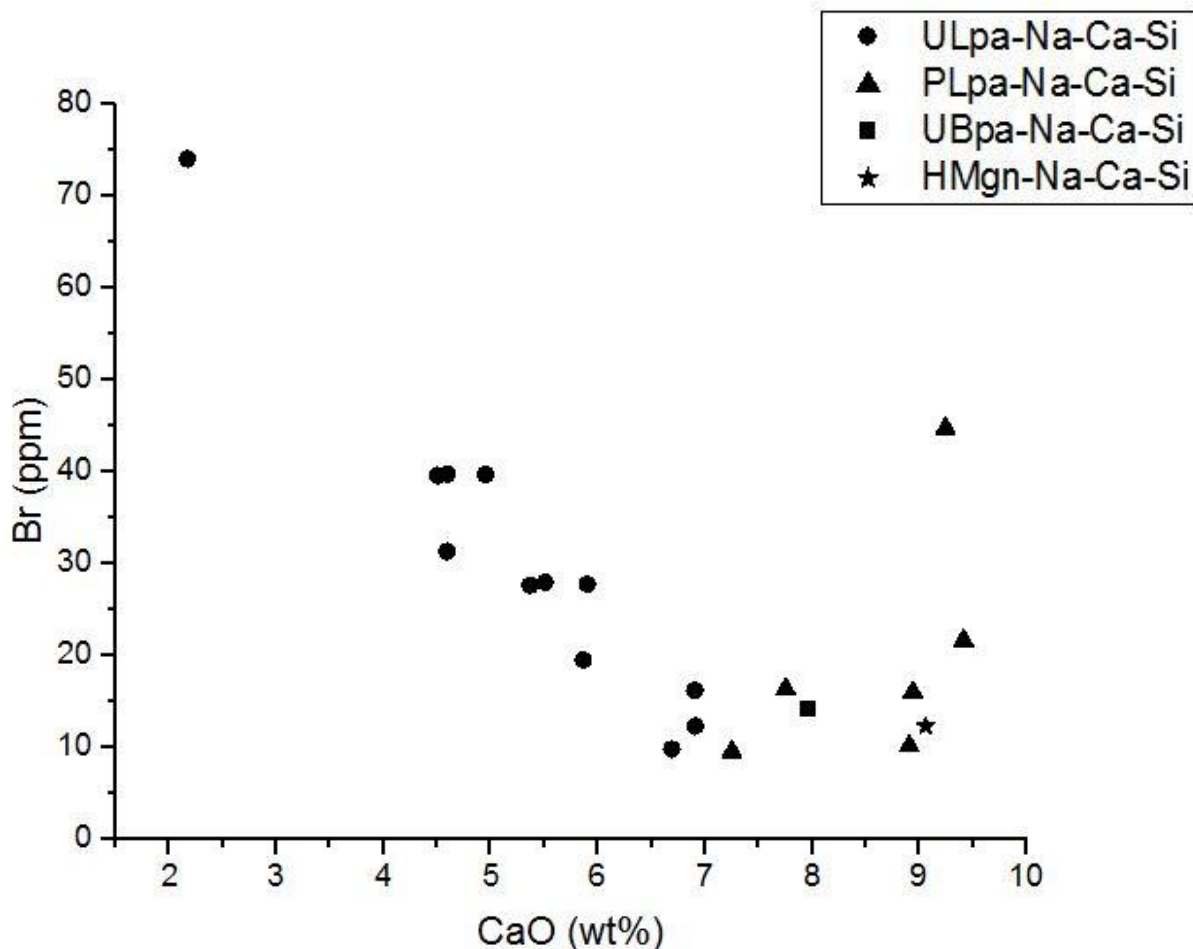


Figure 4-5 Bi-plot of CaO and Br of Miranduolo samples with marked compositional groups.

According to the glass groups, there is no apparent correlation with the silica source used, except for 3 ULpa-Na-Ca-Si glasses (MD 12, MD 21, MD 143) that have $\text{SiO}_2 \leq 62$ wt%, $\text{Al}_2\text{O}_3 \geq 4.5$ wt%. A distinction can be seen for the $\text{Fe}_2\text{O}_3/\text{Al}_2\text{O}_3$. Purer raw silica sources with $\text{Fe}_2\text{O}_3 \leq 1$ wt% have been used exclusively for PLpa-Na-Ca-Si glasses, while $1 \text{ wt}\% < \text{Fe}_2\text{O}_3 \leq 1.4 \text{ wt}\%$ is used for both Lpa-Na-Ca-Si glasses, but for ULpa more impure silica source has been used with $\text{Fe}_2\text{O}_3 > 1.4 \text{ wt}\%$ (Figure App.4-3, Figure App.4-4).

$\text{MgO} \leq 3.1$ wt% is determined for PLpa-Na-Ca-Si, except for MD 259 which has 4.10 wt%. For ULpa-Na-Ca-Si glasses $\text{MgO} > 3.2$ wt% (Figure 4-6, Figure App.4-1).

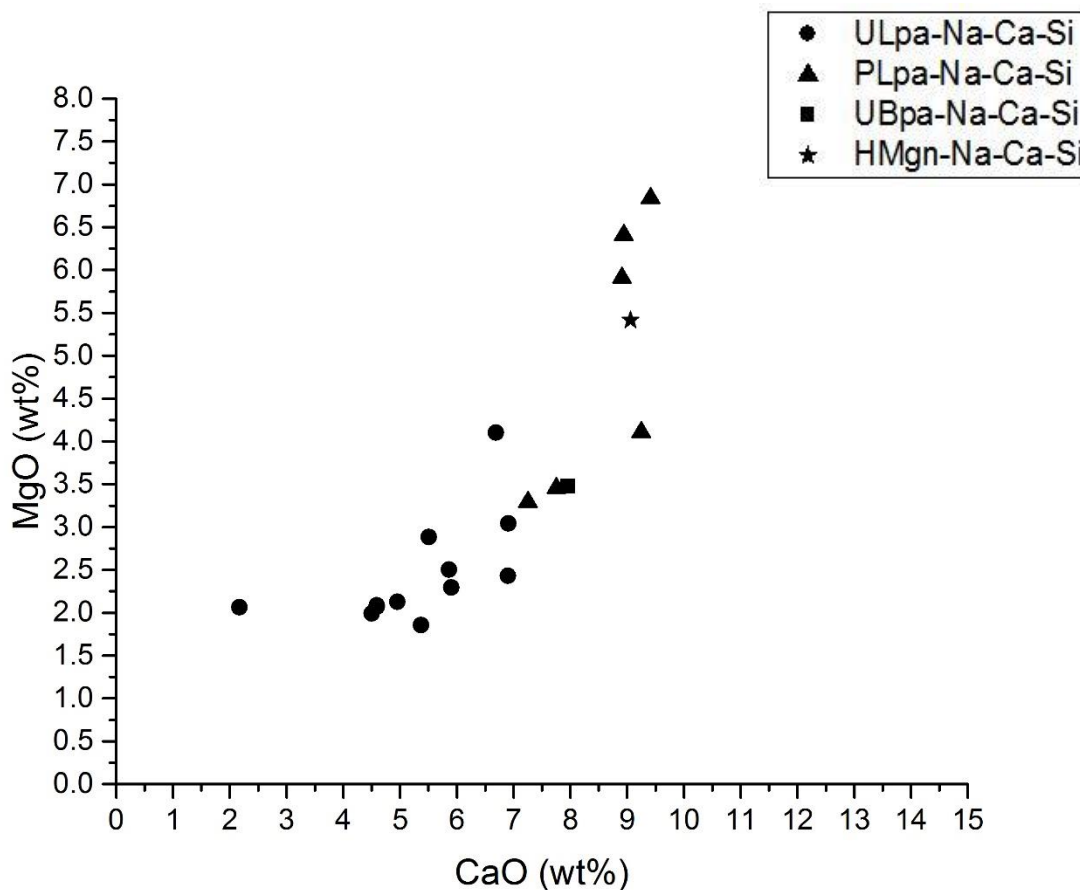


Figure 4-6 Bi-plot of CaO and MgO of Miranduolo samples with marked compositional groups.

$\text{Fe}_2\text{O}_3/\text{TiO}_2$ (Figure App.4-5) and TiO_2/Zr (Figure App.4-8) display a strong positive correlation, respectively $r = 0.7298$, $R^2 = 0.5326$ and $r = 0.7390$, $R^2 = 0.5462$. This should be investigated more with LA-ICP-MS due to higher sensitivity to Ti and Zr.

The $\text{Al}_2\text{O}_3/\text{Zr}$ plots indicate that for all glass types low (≤ 65 ppm) and medium (65-130 ppm) Zr values are common, while high Zr values (≥ 130 ppm) are only present in ULpa-Na-Ca-Si glasses.

Considering of the decolorization of the glasses, only two samples: MD 24 and MD 259 are colorless. Comparing the ratio of the $\text{Fe}_2\text{O}_3/\text{MnO}$ (Table App.6-1, Figure App.4-4) interesting results occur. This ratio has been taken into account due to the fact that iron impurities cause

tints in glass and MnO (0.3 – 0.8 wt% is intentional addition with a decolorizing effect). For colorless samples MD 24 the ratio is 1.52 and for MD 259 1.73. But the samples MD 66 has the ratio of 1.48 and MD 257 1.58, while MD 272 and MD 276 have the ratio of 1.30 and 1.29 and they are colored.

4.2.2. Corrosion

Out of four determined corrosion layers by VP-SEM-EDS only three (MD 139, MD 143 and MD 259) could be studied and chemically mapped. Due to thickness of 2.25 μm of MD 24 corrosion layer, the PIXE/PIGE beam size was not small enough to analyze and map only the corrosion without analyzing the glass and/or epoxy resin. Only for MD 259 there were two spots (*a* Figure App.4-11 and *b* Figure App.4-12, Figure App.4-21) with corrosions analyzed. The values are displayed in the Table 4-5, Table 4-6, Table 4-7, Table 4-8, Table 4-9 and Table 4-10. Comparing average composition of corrosion layers of MD 139 (Figure App.4-9), MD 143 (Figure App.4-10) and MD 259 (Figure App.4-13, Figure App.4-14) it is common for all of them enrichment of SiO_2 , TiO_2 , Al_2O_3 , Co; depletion of Na_2O , MgO, K_2O and Sr;. In MD 139 and MD 259 there is an enrichment of Fe_2O_3 and Zn and depletion of Cl^- and Br. In MD 139 and MD 143 enrichment of CaO and SO_3 , and depletion of Ni.

Table 4-3 PIXE-PIGE results of major, minor and trace elements. Oxides and Cl⁻ are represented in wt%, while elements in ppm. C - corrosion layer, avr - average.

Sample	wt%												ppm					
	SiO ₂	Na ₂ O	TiO ₂	Fe ₂ O ₃	Al ₂ O ₃	MgO	CaO	K ₂ O	P ₂ O ₅	SO ₃	Cl ⁻	MnO	Pb	Cr	Co	Ni	Cu	Zn
MD 12	59.37	12.42	0.12	1.04	4.81	6.84	9.41	2.57	0.76	0.11	0.84	0.12	42.41	13.84	65.48	20.14	36.16	90.67
MD 21	60.22	11.86	0.14	1.09	4.99	6.41	8.94	3.23	0.81	0.12	0.88	0.14	47.17	9.04	31.68	21.36	28.10	89.99
MD 24	66.02	16.22	0.11	1.11	2.08	2.29	5.90	2.08	0.39	0.14	0.99	0.73	1366.50	12.95	33.83	14.75	38.88	54.27
MD 66	63.47	14.37	0.11	1.17	2.69	3.46	7.75	2.25	0.76	0.17	0.79	0.79	375.20	8.23	nd	16.38	36.61	62.62
MD 67	64.80	20.53	0.28	1.95	3.39	2.06	2.17	1.59	0.35	0.09	1.19	0.80	158.82	28.54	45.68	28.18	39.11	45.36
MD 139	63.74	14.34	0.11	1.05	2.91	5.41	9.06	1.24	0.76	0.10	1.00	0.08	19.91	14.77	19.77	17.20	26.52	65.71
MD 139 – C	80.15	0.69	0.33	2.63	8.90	1.38	4.84	0.45	0.12	0.23	0.32	0.22	64.19	44.52	54.11	9.98	7.34	91.29
MD 143	61.52	12.61	0.11	0.96	4.78	5.91	8.91	2.18	0.66	0.10	0.95	0.16	41.50	10.35	30.08	16.07	22.97	69.41
MD 143 – C	76.98	8.91	0.12	0.61	7.85	4.23	9.46	1.93	0.64	0.18	1.66	0.08	0.00	24.62	31.88	8.90	8.01	28.84
MD 172	63.88	19.96	0.20	1.49	3.10	2.07	4.59	2.33	0.47	0.13	1.01	0.87	505.06	12.14	28.39	13.32	95.40	52.61
MD 173	67.69	13.03	0.09	0.81	2.32	3.30	7.25	2.20	0.57	0.31	0.66	0.39	74.37	nd	25.87	12.11	45.90	62.02
MD 191	64.72	15.63	0.11	1.03	2.22	2.43	6.90	2.56	0.63	0.15	0.91	0.77	117.61	13.41	36.66	11.36	47.46	54.24
MD 193	65.20	18.42	0.28	1.73	3.45	1.99	4.51	2.25	0.35	0.07	0.98	0.59	55.48	25.29	37.52	29.48	27.79	42.32
MD 222	65.48	18.44	0.22	1.43	2.93	2.09	4.59	2.10	0.40	0.08	0.97	0.64	318.79	49.06	39.59	15.82	75.25	35.78
MD 231	64.77	14.43	0.13	1.16	3.48	3.04	6.91	2.44	0.68	0.23	0.63	0.93	170.96	25.41	40.20	15.51	96.78	54.60
MD 243	61.23	13.17	0.16	2.51	2.71	3.48	7.95	5.82	0.99	0.17	0.66	1.02	192.89	19.74	42.54	23.54	69.03	98.64
MD 256	63.87	18.80	0.26	1.78	3.42	2.13	4.95	3.41	0.57	0.10	1.01	0.75	222.83	18.82	41.97	25.14	39.28	49.78
MD 257	63.39	14.11	0.24	1.78	3.43	2.88	5.51	1.84	0.40	0.10	0.92	1.13	723.94	11.38	29.00	13.84	111.28	54.45
MD 259	63.65	15.50	0.10	0.55	1.57	4.11	9.25	2.65	0.34	0.27	1.46	0.32	nd	41.63	nd	3.74	24.02	230.05
MD 259 – C avr	81.32	5.69	0.21	1.47	9.82	1.39	12.55	1.68	0.18	0.19	1.03	0.19	nd	33.25	56.63	13.70	23.15	164.42
MD 259 – C a 1a	92.11	0.41	0.19	1.46	14.41	0.80	13.58	0.73	0.05	0.25	1.23	0.05	nd	22.92	72.25	23.13	18.83	224.72
MD 259 – C a 1b	93.14	3.39	0.22	1.60	14.66	0.79	14.31	0.80	0.04	0.14	1.31	0.06	nd	46.70	53.08	8.44	24.57	218.50
MD 259 – C a 2	84.18	1.17	0.26	1.93	13.71	0.83	10.04	0.52	0.07	0.10	0.82	0.05	nd	3.89	38.24	6.29	19.75	59.19
MD 259 – C a 3	71.91	14.13	0.11	0.74	1.91	4.26	10.18	2.76	0.42	0.27	0.93	0.29	nd	76.80	77.71	22.44	35.39	222.38
MD 259 – C b 1	78.23	0.79	0.35	2.44	12.66	0.82	15.75	2.15	0.12	0.09	1.04	0.31	nd	7.54	41.88	18.16	16.33	31.71
MD 259 – C b 2	68.35	14.25	0.12	0.62	1.57	0.82	11.45	3.15	0.39	0.31	0.86	0.37	nd	41.63	nd	3.74	24.02	230.05
MD 261	64.86	18.03	0.21	1.61	3.19	1.86	5.37	1.48	0.31	0.17	0.85	0.78	1190.33	12.14	44.88	16.81	428.54	139.39
MD 272	65.62	15.68	0.14	1.22	2.52	4.10	6.69	1.70	0.59	0.13	0.93	0.93	59.90	22.94	34.49	17.20	25.63	59.03
MD 276	65.23	17.29	0.14	1.15	2.53	2.50	5.86	2.60	0.53	0.16	0.79	0.89	549.88	11.21	32.70	14.42	93.70	67.05

Table 4-4 Part 2 of PIXE-PIGE results trace element, presented in ppm. C - corrosion layer, avr – average, AM – amber, AZ- azure, C – colorless, G – green, Y – yellow, Y-G – yellow-green, nd – not identified.

Sample	ppm													Color	Type	Part preserved	Phase	Area
	As	Rb	Br	Sr	Y	Zr	Nb	Sb	Cd	V	Ba	Ga	Bi					
MD 12	nd	16.61	21.57	606.66	nd	34.63	nd	nd	40.45	31.19	200.99	nd	nd	G	cup	Body with the rim	3	1
MD 21	nd	33.19	15.94	540.67	9.78	66.86	nd	nd	nd	24.21	278.42	4.91	nd	G	bowl	Body with the rim	2	2
MD 24	nd	nd	27.73	418.27	nd	50.36	nd	nd	nd	20.26	97.05	nd	nd	C	nd	Body	2	1
MD 66	10.17	nd	16.30	469.49	3.67	71.13	nd	nd	nd	nd	138.49	4.83	nd	Y	cup	Body with the rim	2	1
MD 67	nd	nd	74.05	158.08	nd	56.83	9.46	nd	nd	25.90	nd	5.74	nd	AM	nd	Body	2	1
MD 139	nd	nd	12.22	502.92	nd	27.23	nd	nd	nd	nd	126.99	nd	nd	AZ	cup	Body	3	1
MD 139 – C	14.09	13.31	8.02	104.70	nd	93.15	nd	nd	nd	nd	nd	9.49	19.67			Body	3	1
MD 143	nd	28.80	10.07	552.84	nd	78.72	nd	nd	nd	17.70	230.28	4.25	nd	AZ	cup	Body	1	1
MD 143 – C	0.00	8.45	0.00	194.64	0.00	54.57	19.06	nd	nd	nd	193.68	2.15	nd	AZ	cup	Body	1	1
MD 172	nd	13.27	39.71	374.37	14.42	68.22	nd	nd	nd	29.90	137.24	nd	nd	Y-G	bottle	Body	2	9
MD 173	nd	7.19	9.49	454.01	nd	43.66	nd	226.69	nd	15.08	nd	5.17	nd	Y	cup	Ring foot	2	9
MD 191	nd	nd	16.13	496.11	nd	51.89	nd	nd	nd	16.84	108.61	4.31	nd	Y-G	cup	Ring foot	1	8
MD 193	nd	20.91	39.56	363.99	nd	217.70	nd	nd	nd	35.50	nd	5.92	nd	Y	nd	Body	1	8
MD 222	nd	11.49	31.27	358.75	12.63	147.01	nd	nd	nd	32.64	191.93	nd	nd	G	nd	Body	1	8
MD 231	nd	9.22	12.24	429.74	nd	71.95	nd	nd	nd	23.12	103.96	5.30	nd	Y	cup	Body with the rim	1	1
MD 243	14.57	20.02	14.27	462.29	9.82	95.84	nd	nd	nd	30.65	nd	nd	nd	G	bowl	Body with the rim	1	10
MD 256	nd	25.09	39.65	342.73	9.98	192.26	11.71	nd	nd	37.79	nd	nd	nd	Y	nd	Body	1	10
MD 257	nd	8.56	27.92	494.68	nd	155.81	nd	175.49	nd	23.20	189.59	5.84	nd	G	nd	Body	1	10
MD 259	8.21	14.27	44.69	455.71	nd	95.59	nd	nd	nd	nd	221.41	nd	nd	C	cup	Bottom	3	8
MD 259 – C avr	10.64	16.99	29.15	261.57	nd	118.35	nd	nd	nd	nd	911.07	14.95	nd	C	cup	Bottom	3	8
MD 259 – C a 1a	nd	nd	14.23	152.48	nd	151.41	nd	nd	nd	nd	1480.32	14.95	nd	C	cup	Bottom	3	8
MD 259 – C a 1b	13.30	nd	nd	191.98	nd	111.34	nd	nd	nd	nd	1290.82	nd	nd	C	cup	Bottom	3	8
MD 259 – C a 2	nd	nd	nd	157.73	nd	nd	nd	nd	nd	nd	863.68	nd	nd	C	cup	Bottom	3	8
MD 259 – C a 3	nd	16.99	nd	303.94	nd	63.23	nd	nd	nd	nd	277.22	nd	nd	C	cup	Bottom	3	8
MD 259 – C b 1	nd	nd	37.76	363.03	nd	223.47	nd	nd	nd	nd	1231.91	nd	nd	C	cup	Bottom	3	8
MD 259 – C b 2	7.98	nd	35.44	400.25	nd	42.32	nd	nd	nd	nd	322.48	nd	nd	C	cup	Bottom	3	8
MD 261	25.25	10.91	27.58	377.78	15.71	135.17	nd	1071.14	nd	24.18	214.15	nd	nd	AZ	nd	Body	3	11
MD 272	nd	nd	9.73	534.36	nd	66.45	nd	nd	nd	nd	nd	nd	nd	AM	cup	Body	3	11
MD 276	nd	19.43	19.45	469.50	nd	58.26	9.85	nd	nd	25.72	152.48	nd	nd	G	cup	Ring foot	1	11

Table 4-5 Depletion and enrichment (%) of selected elements in corrosion in comparison to pristine glass of MD 139 and MD 143. Oxides are expressed in wt% and elements in ppm.

MD 139					MD 143					
Unit	Oxide/Element	Pristine	Corrosion	Depleted amount from pristine (%)	Unit	Oxide/Element	Pristine	Corrosion	Depleted amount from pristine (%)	
wt%	Na ₂ O	14.34	0.69	4.84	wt%	Na ₂ O	12.60534	8.90947	29.32	
	MgO	5.41	1.38	25.50		Fe ₂ O ₃	0.96304	0.61219	36.43	
	CaO	9.06	4.84	53.41		MgO	5.91158	4.23206	28.41	
	K ₂ O	1.24	0.45	36.28		K ₂ O	2.17812	1.93182	11.31	
	P ₂ O ₅	0.76	0.12	16.02		P ₂ O ₅	0.65977	0.63936	3.09	
	Cl	1.00	0.32	32.28		MnO	0.16364	0.0802	50.99	
ppm	Ni	17.20	9.98	58.04	ppm	Ni	16.07431	8.89797	44.64	
	Cu	26.52	7.34	27.68		Cu	22.97048	8.00818	65.14	
	Br	12.22	8.02	65.67		Zn	69.40659	28.84426	58.44	
	Sr	502.92	104.70	20.82		Rb	28.8046	8.45307	70.65	
						Sr	552.84157	194.64316	64.79	
						Zr	78.72108	54.57423	30.67	
						Ba	230.27889	193.67921	15.89	
						Ga	4.24749	2.15034	49.37	
Unit	Oxide/Element	Pristine	Corrosion	Enriched amount from pristine (%)		Unit	Oxide/Element	Pristine	Corrosion	Enriched amount from pristine (%)
wt%	SiO ₂	63.74	80.15	25.74		wt%	SiO ₂	61.51769	76.98211	25.14
	TiO ₂	0.11	0.33	208.19			TiO ₂	0.11421	0.11576	1.36
	Fe ₂ O ₃	1.05	2.63	151.58			Al ₂ O ₃	4.77752	7.84672	64.24
	Al ₂ O ₃	2.91	8.90	206.07			CaO	8.90863	9.46363	6.23
	SO ₃	0.10	0.23	126.32			SO ₃	0.10281	0.18419	79.16
	MnO	0.08	0.22	179.78	Cl		0.95431	1.6565	73.58	
ppm	Pb	19.91	64.19	222.34	ppm	Cr	10.34784	24.61773	137.90	
	Cr	14.77	44.52	201.38		Co	30.08193	31.8844	5.99	
	Co	19.77	54.11	173.73						
	Zn	65.71	91.29	38.94						

Table 4-6 Depletion and enrichment (%) of selected elements in corrosion of MD 259 – C avr and MD 259 – C b avr in comparison to pristine glass of MD 259. Oxides are expressed in wt% and elements in ppm.

MD 259									
Unit	Oxide/Element	Pristine	Corrosion avr	Depleted amount from pristine (%)	Unit	Oxide/Element	Pristine	Corrosion b avr	Depleted amount from pristine (%)
wt%	Na ₂ O	15.50	5.69	36.71	wt%	Na ₂ O	15.50	7.52	51.48
	MgO	4.11	1.39	33.71		MgO	4.11	0.82	80.15
	K ₂ O	2.65	1.68	63.57		P ₂ O ₅	0.34	0.26	25.55
	P ₂ O ₅	0.34	0.18	53.20		SO ₃	0.27	0.20	27.09
	SO ₃	0.27	0.19	70.82		Cl ⁻	1.46	0.95	34.98
	Cl ⁻	1.46	1.03	70.60		Br	44.69	36.60	18.11
	MnO	0.32	0.19	59.16		Sr	455.71	381.64	16.25
ppm	Br	44.69	29.15	65.21					
	Sr	455.71	261.57	57.40					
Unit	Oxide/Element	Pristine	Corrosion avr	Enriched amount from pristine (%)	Unit	Oxide/Element	Pristine	Corrosion b avr	Enriched amount from pristine (%)
wt%	SiO ₂	63.65	81.32	27.76	wt%	SiO ₂	63.65	73.29	15.14
	TiO ₂	0.10	0.21	111.08		TiO ₂	0.10	0.23	136.48
	Fe ₂ O ₃	0.55	1.47	165.34		Fe ₂ O ₃	0.55	1.53	177.58
	Al ₂ O ₃	1.57	9.82	525.09		Al ₂ O ₃	1.57	7.12	352.92
	CaO	9.25	12.55	35.75		K ₂ O	2.65	2.65	0.03
ppm	Co	25.60	56.63	121.24	ppm	CaO	9.25	13.60	47.12
	Ni	9.17	13.70	49.43		MnO	0.32	0.34	6.96
	Cu	12.19	23.15	89.84		Co	25.60	59.80	133.61
	Zn	29.59	164.42	455.71		Ni	9.17	20.30	121.44
	As	8.21	10.64	29.59		Cu	12.19	25.86	112.07
	Rb	14.27	16.99	19.03		Zn	29.59	127.04	329.37
	Zr	95.59	118.35	23.82		Zr	95.59	132.90	39.03
						Ba	221.41	777.20	251.03

Table 4-7 Depletion and enrichment (%) of selected elements in corrosion of MD 259 – C b1 and MD 259 – C b2 in comparison to pristine glass of MD 259. Oxides are expressed in wt% and elements in ppm.

MD 259									
Unit	Oxide/Element	Pristine	Corrosion b2	Depleted amount from pristine (%)	Unit	Oxide/Element	Pristine	Corrosion b1	Depleted amount from pristine (%)
wt%	Na ₂ O	15.50	14.25	8.04	wt%	Na ₂ O	15.50	0.79	94.92
	Al ₂ O ₃	1.57	1.57	0.04		MgO	4.11	0.82	80.15
	MgO	4.11	0.82	80.15		K ₂ O	2.65	2.15	18.98
	Cl ⁻	1.46	0.86	40.99		P ₂ O ₅	0.34	0.12	64.98
	As	8.21	7.98	2.81		SO ₃	0.27	0.09	67.00
ppm	Br	44.69	35.44	20.70	ppm	Cl ⁻	1.46	1.04	28.97
	Sr	455.71	400.25	12.17		MnO	0.32	0.31	2.84
	Zr	95.59	42.32	55.72		Br	44.69	37.76	15.51
						Sr	455.71	363.03	20.34
Unit	Oxide/Element	Pristine	Corrosion b2	Enriched amount from pristine (%)	Unit	Oxide/Element	Pristine	Corrosion b1	Enriched amount from pristine (%)
wt%	SiO ₂	63.65	68.35	7.38	wt%	SiO ₂	63.65	78.23	122.91
	TiO ₂	0.10	0.12	20.86		TiO ₂	0.10	0.35	352.10
	Fe ₂ O ₃	0.55	0.62	12.70		Fe ₂ O ₃	0.55	2.44	442.46
	CaO	9.25	11.45	23.87		Al ₂ O ₃	1.57	12.66	805.89
	K ₂ O	2.65	3.15	19.04		CaO	9.25	15.75	170.37
ppm	P ₂ O ₅	0.34	0.39	13.88	ppm	Co	25.60	77.71	303.60
	SO ₃	0.27	0.31	12.81		Ni	9.17	22.44	244.78
	MnO	0.32	0.37	16.77		Cu	12.19	35.39	290.23
	Co	25.60	41.88	63.63		Zn	29.59	222.38	751.57
	Ni	9.17	18.16	98.11		Zr	95.59	223.47	233.79
	Cu	12.19	16.33	33.91		Ba	221.41	1231.91	556.40
	Zn	29.59	31.71	7.16					
	Ba	221.41	322.48	45.65					

Table 4-8 Depletion and enrichment (%) of selected elements in corrosion of MD 259 – C a avr and MD 259 – C a3 in comparison to pristine glass of MD 259. Oxides are expressed in wt% and elements in ppm.

MD 259										
Unit	Oxide/Element	Pristine	Corrosion a avr	Depleted amount from pristine (%)	Unit	Oxide/Element	Pristine	Corrosion a3	Depleted amount from pristine (%)	
wt%	Na ₂ O	15.50	4.78	69.19	wt%	Na ₂ O	15.50	14.13	8.84	
	MgO	4.11	1.67	59.36		SO ₃	0.27	0.27	1.64	
	K ₂ O	2.65	1.20	54.66		Cl ⁻	1.46	0.93	36.35	
	P ₂ O ₅	0.34	0.15	57.43		MnO	0.32	0.29	9.35	
	SO ₃	0.27	0.19	30.22		Ni	9.17	6.29	31.43	
	Cl ⁻	1.46	1.07	26.61		ppm	Sr	455.71	303.94	33.31
	MnO	0.32	0.11	64.74			Zr	95.59	63.23	33.85
ppm	Sr	455.71	201.53	55.78						
Unit	Oxide/Element	Pristine	Corrosion a avr	Enriched amount from pristine (%)	Unit	Oxide/Element	Pristine	Corrosion a3	Enriched amount from pristine (%)	
wt%	SiO ₂	63.65	85.33	34.07	wt%	SiO ₂	63.65	71.91	112.98	
	TiO ₂	0.10	0.20	98.39		TiO ₂	0.10	0.11	116.06	
	Fe ₂ O ₃	0.55	1.43	159.22		Fe ₂ O ₃	0.55	0.74	133.71	
	Al ₂ O ₃	1.57	11.17	611.18		Al ₂ O ₃	1.57	1.91	121.87	
	CaO	9.25	12.03	30.07		MgO	4.11	4.26	103.71	
ppm	Co	25.60	54.52	112.99	ppm	CaO	9.25	10.18	110.04	
	Ni	9.17	10.40	13.42		K ₂ O	2.65	2.76	104.11	
	Cu	12.19	21.79	78.72		P ₂ O ₅	0.34	0.42	122.92	
	Zn	29.59	183.12	518.88		Co	25.60	38.24	149.37	
	Zr	95.59	108.66	13.68		Cu	12.19	19.75	162.00	
	Ba	221.41	978.01	341.73		Zn	29.59	59.19	200.03	
						Rb	14.27	16.99	119.03	
				Ba	221.41	277.22	112.98			

Table 4-9 Depletion and enrichment (%) of selected elements in corrosion of MD 259 – C a2 and MD 259 – C a1 avr in comparison to pristine glass of MD 259. Oxides are expressed in wt% and elements in ppm.

MD 259									
Unit	Oxide/Element	Pristine	Corrosion a2	Depleted amount from pristine (%)	Unit	Oxide/Element	Pristine	Corrosion a1 avr	Depleted amount from pristine (%)
wt%	Na ₂ O	15.50	1.17	7.56	wt%	Na ₂ O	15.50	1.90	87.74
	MgO	4.11	0.83	20.20		MgO	4.11	0.79	80.67
	K ₂ O	2.65	0.52	19.47		K ₂ O	2.65	0.76	71.12
	P ₂ O ₅	0.34	0.07	20.48		P ₂ O ₅	0.34	0.05	86.55
	SO ₃	0.27	0.10	37.18		SO ₃	0.27	0.20	28.21
	Cl ⁻	1.46	0.82	55.79		Cl ⁻	1.46	1.27	12.93
ppm	MnO	0.32	0.05	15.00	ppm	MnO	0.32	0.06	82.31
	Ni	9.17	8.44	92.07		Sr	455.71	172.23	62.21
	Sr	455.71	157.73	34.61					
Unit	Oxide/Element	Pristine	Corrosion a2	Enriched amount from pristine (%)	Unit	Oxide/Element	Pristine	Corrosion a1 avr	Enriched amount from pristine (%)
wt%	SiO ₂	63.65	84.18	132.25	wt%	SiO ₂	63.65	92.62	45.52
	TiO ₂	0.10	0.26	268.16		TiO ₂	0.10	0.20	104.66
	Fe ₂ O ₃	0.55	1.93	349.18		Fe ₂ O ₃	0.55	1.53	177.00
	Al ₂ O ₃	1.57	13.71	872.42		Al ₂ O ₃	1.57	14.54	825.21
	CaO	9.25	10.04	108.61		CaO	9.25	13.94	50.80
ppm	Co	25.60	53.08	207.36	ppm	Cu	12.19	21.42	75.70
	Cu	12.19	24.57	201.49		Zn	29.59	227.39	668.52
	Zn	29.59	218.50	738.47		Zr	95.59	131.38	37.44
	Ba	221.41	863.68	390.09		Ba	221.41	1385.57	525.80
						Ni	9.17	13.43	46.53

Table 4-10 Depletion and enrichment (%) of selected elements in corrosion of MD 259 – C a1a and MD 259 – C a1b in comparison to pristine glass of MD 259. Oxides are expressed in wt% and elements in ppm.

MD 259									
Unit	Oxide/Element	Pristine	Corrosion a1b	Depleted amount from pristine (%)	Unit	Oxide/Element	Pristine	Corrosion a1a	Depleted amount from pristine (%)
wt%	Na ₂ O	15.50	3.39	78.14	wt%	Na ₂ O	15.50	0.41	97.34
	MgO	4.11	0.79	80.78		MgO	4.11	0.80	80.57
	K ₂ O	2.65	0.80	69.82		K ₂ O	2.65	0.73	72.43
	P ₂ O ₅	0.34	0.04	87.56		P ₂ O ₅	0.34	0.05	85.55
	SO ₃	0.27	0.14	48.25		SO ₃	0.27	0.25	8.18
	Cl ⁻	1.46	1.31	10.19		Cl ⁻	1.46	1.23	15.68
ppm	MnO	0.32	0.06	81.64	ppm	MnO	0.32	0.05	82.98
	Sr	455.71	191.98	57.87		Ni	9.17	3.74	59.24
						Br	44.69	14.23	68.15
						Sr	455.71	152.48	66.54
Unit	Oxide/Element	Pristine	Corrosion a1b	Enriched amount from pristine (%)	Unit	Oxide/Element	Pristine	Corrosion a1a	Enriched amount from pristine (%)
wt%	SiO ₂	63.65	93.14	46.33	wt%	SiO ₂	63.65	92.11	44.71
	TiO ₂	0.10	0.22	120.58		TiO ₂	0.10	0.19	88.74
	Fe ₂ O ₃	0.55	1.60	189.42		Fe ₂ O ₃	0.55	1.46	164.59
	Al ₂ O ₃	1.57	14.66	832.99		Al ₂ O ₃	1.57	14.41	817.42
	CaO	9.25	14.31	54.74		CaO	9.25	13.58	46.87
ppm	Co	25.60	72.25	182.24	ppm	Cu	12.19	24.02	96.98
	Ni	9.17	23.13	152.30		Zn	29.59	230.05	677.53
	Cu	12.19	18.83	54.41		Zr	95.59	151.41	58.40
	Zn	29.59	224.72	659.50		Ba	221.41	1480.32	568.60
	As	8.21	13.30	61.99					
	Zr	95.59	111.34	16.48					
	Ba	221.41	1290.82	483.01					

In general, the chemical maps of the corrosion layers display that they are very heterogeneous (Figure App.4-15, Figure App.4-16, Figure App.4-17, Figure App.4-18, Figure App.4-19, Figure App.4-20). The chemical maps of spot *a* done for sample MD 259 clearly displays three distinctive stratification layers with diverse composition (Figure 4-7, Figure App.4-19). All three layers have been separately measured with layer *a 1* and *a 2* (and an average has been calculated and marked as *a 1 avr*). When comparing all three layers *a 1 avr*, *a 2* and *a 3* the quantification data indicate a slow progression of the corrosion with enrichment and depletion that is generally common for only several elements. For spot *b* two stratification layers can be distinguished, although the map of Si displays three layers (Figure App.4-20).

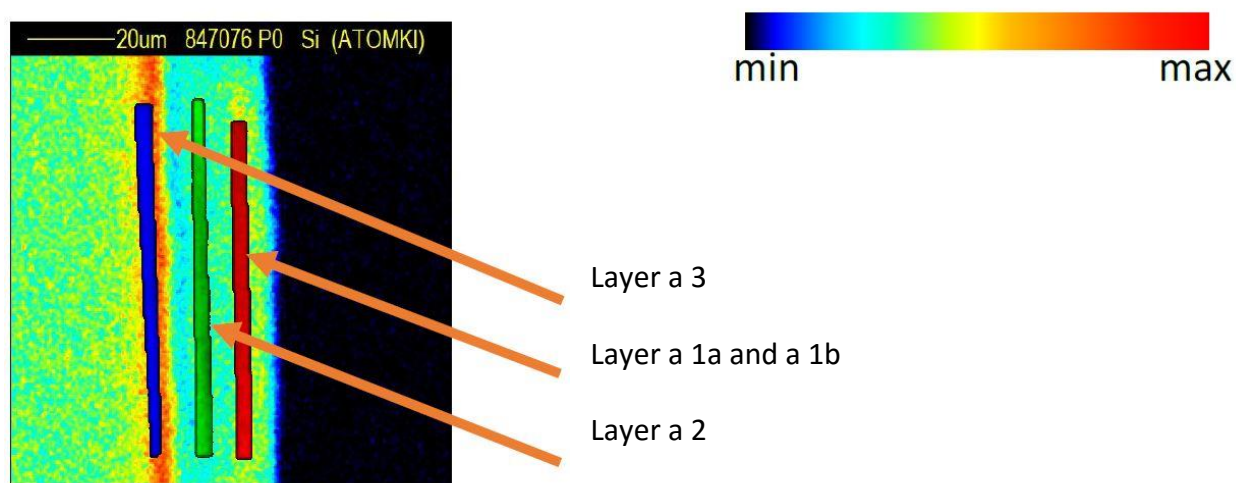


Figure 4-7 PIXE chemical map of spot *a* of sample MD 259 with marked stratification of corrosion layers that has been quantified.

The comparison of enrichment/depletion patterns indicate only a certain number of elements displaying common patterns for all samples, while other elements display an ambivalent behavior. The latter, quantification and the maps strongly prove the homogeneity of the corrosion layers which does not seem to be dependent on the chemical composition of the glass.

4.3. LA-ICP-MS

LA-ICP-MS technique is mainly used as a precise technique for quantifying minor and trace elements. Major, minor and trace elements will be presented, and in the discussion compared with EDS and PIXE/PIGE results.

4.3.1. *Elemental composition*

The general composition is consistent with VP-SEM-EDS and PIXE/PIGE results. The results for major, minor and trace elements analyzed are represented in Table 4-11 and Table 4-12. The average Miranduolo glass composition is 66.62 wt% (min. 62.75 – max. 80.47 wt%) of SiO₂, 15.94 wt% (min. 11.63 – max. 22.80 wt%) of Na₂O, 7.94 wt% (min. 2.84 – max. 11.92 wt%) of CaO, 2.43 wt% (min. 1.24 – max. 7.05 wt%) of K₂O, 2.80 wt% (min. 1.60 – max. 5.58 wt%) of MgO, 3.43 wt% (min. 1.57 – max. 5.36 wt%) of Al₂O₃ and 1.22 wt% (min. 0.41 – max. 2.15 wt%) of Fe₂O₃.

Table 4-11 LA-ICP-MS results of major, minor and trace elements. Oxides are represented in wt%, while elements in ppm. The beam size was 50 µm, except when noted differently. C - corrosion layer.

Sample	SiO ₂	Na ₂ O	TiO ₂	Fe ₂ O ₃	Al ₂ O ₃	MgO	CaO	K ₂ O	P ₂ O ₅	MnO	Pb	Cr	Co	Ni	Cu	Zn	As	Rb	Sr	Y	Zr	Nb	Sn	Sb
MD 12	65.12	13.01	0.11	1.08	4.30	5.58	10.44	2.90	0.63	0.12	75.7	19.7	6.0	17.5	39.0	94.2	2.2	26.4	606.7	6.5	48.5	3.2	11.4	0.8
MD 21	80.47	12.57	0.15	1.15	5.36	5.50	10.79	3.89	0.65	0.15	56.1	23.3	6.9	19.4	30.5	102.4	2.6	39.0	594.4	8.7	71.9	3.9	7.9	1.6
MD 24	62.75	17.72	0.12	1.16	4.64	1.95	7.51	2.69	0.31	0.79	1447.6	15.3	5.0	13.6	45.8	65.3	4.9	11.2	455.5	6.0	82.9	2.7	15.8	19.9
MD 66	62.75	16.87	0.11	1.33	2.73	2.89	9.80	2.74	0.62	0.87	505.0	16.2	5.9	20.8	47.1	80.2	5.2	16.3	519.4	6.9	55.9	3.1	8.5	15.0
MD 67	69.69	22.80	0.30	2.15	4.04	1.73	2.84	1.99	0.28	0.85	198.6	34.7	8.5	25.4	45.6	53.9	2.5	8.7	172.9	8.8	68.6	5.1	7.3	3.8
MD 139	65.20	15.44	0.11	1.19	3.38	4.63	11.92	1.52	0.59	0.09	36.5	18.5	6.0	17.6	31.4	73.3	3.5	9.6	590.4	7.0	43.2	2.9	9.3	1.6
MD 139 – C	68.75	0.31	0.16	1.89	6.86	0.69	3.19	0.19	0.01	0.01	75.2	47.2	0.2	0.9	1.8	35.1	19.2	8.0	65.5	1.0	72.1	4.5	24.7	14.0
MD 143	65.98	13.23	0.10	0.98	4.64	4.85	9.91	2.41	0.51	0.16	62.4	17.1	6.7	15.6	26.2	73.7	2.5	28.7	554.0	7.5	59.3	3.1	15.8	1.0
MD 143 (15 µm)	66.37	14.62	0.12	0.76	5.66	5.22	10.61	2.52	0.60	0.17	61.4	20.7	7.8	20.3	29.7	64.0	6.0	29.0	656.4	10.5	78.2	4.0	17.5	2.4
MD 172	65.92	18.72	0.20	1.58	3.23	1.70	5.62	2.70	0.34	0.87	602.9	23.9	9.6	19.7	99.2	56.1	6.5	14.8	389.2	7.4	77.2	4.0	29.6	23.0
MD 173	61.71	12.46	0.09	0.85	2.35	2.32	8.29	2.36	0.40	0.39	94.0	12.7	3.6	10.9	52.1	56.0	3.8	10.3	472.7	5.0	57.7	2.5	4.6	72.1
MD 191	65.01	16.20	0.10	1.15	2.15	1.92	7.86	2.80	0.45	0.91	136.5	17.0	5.2	12.3	54.8	64.4	4.3	9.7	511.3	4.5	48.0	2.7	10.0	3.2
MD 193	64.61	17.03	0.27	1.70	3.84	1.60	4.97	2.40	0.24	0.54	50.0	26.3	6.1	19.1	27.9	39.9	2.2	15.8	322.8	10.3	221.3	5.6	2.3	2.3
MD 222	64.96	15.91	0.18	1.37	3.14	1.48	5.12	2.20	0.24	0.59	331.2	20.7	5.6	14.8	78.6	36.6	2.9	13.5	348.9	7.8	143.9	4.1	9.6	40.5
MD 231	64.96	14.27	0.14	0.86	3.98	2.48	8.34	2.88	0.54	0.97	259.0	18.2	6.4	19.5	109.3	76.7	3.7	15.6	496.7	7.5	72.1	3.7	7.6	38.1
MD 243	74.41	11.63	0.17	1.76	2.86	2.71	9.78	7.05	0.76	1.04	276.0	22.5	6.7	18.7	72.1	132.5	4.0	27.3	493.1	7.0	110.0	3.4	8.4	19.1
MD 256	66.17	14.92	0.23	1.15	3.18	1.70	5.01	3.80	0.44	0.74	234.4	25.4	6.1	19.6	41.0	53.1	3.1	22.8	309.4	7.9	162.9	4.6	4.7	9.7
MD 257	66.93	18.70	0.26	1.46	3.90	2.53	7.00	2.30	0.31	1.23	880.7	29.0	7.4	20.2	131.6	69.0	4.1	16.1	522.7	11.2	203.3	5.7	23.3	110.3
MD 259	66.31	15.49	0.10	0.41	1.57	3.44	11.37	3.05	0.25	0.34	12.5	12.1	9.6	9.2	16.1	32.1	2.6	17.3	466.7	5.1	81.0	2.2	2.5	1.2
MD 259 (15 µm)	64.96	15.75	0.10	0.41	1.58	3.56	11.09	2.99	0.28	0.35	12.0	12.7	10.4	9.2	16.8	31.0	5.7	16.2	519.1	5.9	84.7	2.2	2.3	1.2
MD 259 - C (15 µm)	74.41	5.44	0.12	1.04	8.13	1.55	7.03	1.24	0.14	0.14	17.7	28.5	3.7	6.2	34.9	154.1	5.1	12.9	252.2	3.0	107.4	2.7	8.6	1.6
MD 261	66.17	19.41	0.22	1.32	3.66	1.54	6.84	1.83	0.22	0.85	1691.0	26.8	11.2	16.8	502.7	166.4	10.1	19.2	419.7	10.1	168.9	4.7	143.1	1224.6
MD 272	66.93	15.60	0.13	0.95	2.47	3.48	7.91	1.97	0.47	0.97	75.2	20.6	7.1	18.7	27.4	74.4	4.0	7.7	517.8	5.2	62.3	3.3	2.5	0.8
MD 276	66.31	16.73	0.15	0.88	3.13	1.99	7.40	2.96	0.38	0.93	626.9	18.1	8.4	17.3	97.6	63.7	4.5	18.6	475.7	7.2	82.4	3.7	17.9	87.9

Table 4-12 Part 2 of LA-ICP-MS results of trace elements in ppm. The beam size was 50 µm, except when noted differently. C - corrosion layer, AM – amber, AZ-azure, C – colorless, G – green, Y – yellow, Y-G – yellow-green, nd – not identified.

ppm	V	Ba	La	Ce	Pr	Nd	Sm	Eu	Gd	Tb	Dy	Ho	Er	Tm	Yb	Lu	Hf	Th	U	Color	Type	Part preserved	Phase	Area
MD 12	15.5	240.3	11.3	20.8	2.4	8.4	1.5	0.3	1.2	0.2	1.2	0.2	0.6	0.1	0.7	0.1	1.2	2.6	1.7	G	cup	Body with the rim	3	1
MD 21	18.2	275.8	14.8	24.5	2.9	10.7	1.9	0.4	1.6	0.2	1.4	0.3	0.8	0.1	1.0	0.1	1.8	3.3	1.7	G	bowl	Body with the rim	2	2
MD 24	16.2	145.2	6.9	13.3	1.6	6.6	1.3	0.3	1.1	0.2	1.1	0.2	0.6	0.1	0.6	0.1	2.0	1.8	0.7	C	nd	Body	2	1
MD 66	17.6	170.8	7.2	15.3	1.8	6.8	1.5	0.4	1.5	0.2	1.3	0.2	0.6	0.1	0.6	0.1	1.5	1.7	0.8	Y	cup	Body with the rim	2	1
MD 67	38.8	126.3	8.7	17.9	2.1	8.4	1.8	0.5	1.7	0.3	1.7	0.3	0.9	0.1	0.9	0.1	1.8	1.8	0.6	AM	nd	Body	2	1
MD 139	16.9	107.8	9.6	17.4	2.1	8.2	1.5	0.3	1.3	0.2	1.3	0.2	0.7	0.1	0.7	0.1	1.1	2.7	1.2	AZ	cup	Body	3	1
MD 139 – C	7.7	22.8	1.1	1.2	0.3	1.2	0.3	0.1	0.2	0.0	0.2	0.0	0.1	0.0	0.2	0.0	1.9	3.1	0.2			Body	3	1
MD 143	13.5	240.8	10.4	19.6	2.3	8.2	1.4	0.3	1.3	0.2	1.3	0.3	0.8	0.1	0.9	0.1	1.4	2.8	1.8	AZ	cup	Body	1	1
MD 143 (15 µm)	15.2	269.3	13.0	22.9	2.5	9.3	1.5	0.4	2.1	0.3	1.7	0.3	0.7	0.2	0.8	0.2	2.1	3.4	1.7	AZ	cup	Body	1	1
MD 172	26.4	295.8	8.0	16.0	1.9	7.7	1.5	0.4	1.5	0.2	1.3	0.3	0.7	0.1	0.8	0.1	2.0	1.9	0.6	Y-G	bottle	Body	2	9
MD 173	12.5	159.0	6.0	11.9	1.4	5.5	1.1	0.2	1.0	0.2	1.0	0.2	0.5	0.1	0.5	0.1	1.7	1.7	0.7	Y	cup	Ring foot	2	9
MD 191	18.8	96.2	6.1	13.0	1.5	5.4	1.0	0.3	0.9	0.1	0.8	0.2	0.4	0.1	0.5	0.1	1.2	1.4	0.6	Y-G	cup	Ring foot	1	8
MD 193	31.0	99.6	12.3	24.0	2.9	11.1	2.2	0.5	2.0	0.3	1.9	0.4	1.1	0.2	1.1	0.2	5.7	3.0	1.0	Y	nd	Body	1	8
MD 222	21.6	161.3	9.1	17.2	2.1	8.2	1.7	0.4	1.6	0.2	1.5	0.3	0.8	0.1	0.8	0.1	3.8	2.3	0.8	G	nd	Body	1	8
MD 231	19.1	169.9	8.2	15.5	1.9	7.4	1.6	0.4	1.4	0.2	1.4	0.3	0.7	0.1	0.8	0.1	1.9	2.3	0.8	Y	cup	Body with the rim	1	1
MD 243	21.0	162.4	9.3	15.6	2.0	7.8	1.6	0.3	1.4	0.2	1.3	0.2	0.7	0.1	0.7	0.1	2.8	2.1	0.7	G	bowl	Body with the rim	1	10
MD 256	28.0	217.3	11.5	21.6	2.6	9.3	1.8	0.4	1.5	0.2	1.5	0.3	0.8	0.1	0.9	0.1	4.3	2.4	0.9	Y	nd	Body	1	10
MD 257	30.0	174.6	12.6	24.3	2.8	11.7	2.1	0.5	2.1	0.3	2.0	0.4	1.1	0.2	1.1	0.2	4.8	3.0	1.2	G	nd	Body	1	10
MD 259	11.2	243.0	6.5	12.2	1.5	5.9	1.0	0.2	1.0	0.1	0.9	0.2	0.5	0.1	0.4	0.1	2.1	1.4	0.5	C	cup	Bottom	3	8
MD 259 (15 µm)	11.7	255.6	6.3	12.3	1.8	6.5	1.1	0.1	0.9	0.1	0.8	0.1	0.5	0.1	0.4	0.1	2.1	1.7	0.5	C	cup	Bottom	3	8
MD 259 - C (15 µm)	5.7	274.2	3.3	5.8	1.0	2.8	0.5	0.2	1.1	0.1	0.4	0.1	0.2	0.1	0.5	0.0	3.7	2.2	0.2			Bottom	3	8
MD 261	28.2	347.1	10.9	21.4	2.5	9.9	2.0	0.4	1.8	0.3	1.6	0.4	1.0	0.2	0.9	0.1	4.1	2.6	1.2	AZ	nd	Body	3	11
MD 272	18.9	271.2	7.0	16.5	1.7	6.3	1.2	0.3	0.9	0.2	1.1	0.2	0.5	0.1	0.5	0.1	1.5	1.7	1.0	AM	cup	Body	3	11
MD 276	19.1	96.9	8.1	15.8	1.8	7.3	1.5	0.3	1.4	0.2	1.3	0.3	0.7	0.1	0.7	0.1	2.2	2.1	0.8	G	cup	Ring foot	1	11

As determined with PIXE/PIGE, there is a strong positive correlation of CaO with MgO ($r=0.7870$, $R^2=0.6194$; Figure App.5-4) and Sr ($r=0.8827$, $R^2=0.7782$; Figure App.5-5), with the lack of correlation of K₂O with CaO ($r=0.2202$, $R^2=0.0485$; Figure App.5-2) and MgO ($r=0.0661$, $R^2=0.0044$; Figure App.5-3).

The quantity of MgO and Sr are dependent on the flux employed in the glass production. For the PLpa-Na-Ca-Si, $MgO \leq 1.8$ wt% and $Sr \leq 420$ ppm, while for ULpa-Na-Ca-Si, UBpa-Na-Ca-Si and HMgn-Na-Ca-Si $MgO > 1.8$ wt% and $Sr > 420$ ppm (with MD 257 having a bordering quantity of 7 wt% of CaO).

For the sample MD 139 (HMgn-Na-Ca-Si) the quantity of K₂O is 1.5 wt%, but with VP-SEM-EDS the quantity of K₂O is 1.31 wt%, and with PIXE/PIGE is 1.24 wt%. As this amount is on the border with LA-ICP-MS, other techniques indicate usage of natron as a flux, while usage of local silica raw materials and addition of calcite has increased the amount of CaO and MgO. The sample MD 139 is the only one with the highest thickness of corrosion layer, and it has been proven that n-Na-Ca-Si is more prone to corrosion than pa-Na-Ca-Si glasses, and this fact is supporting the fact that sample MD 139 was made with natron as a flux hence classifying it as HMgn-Na-Ca-Si glass.

The results obtained indicate the correlation of CaO/MgO and CaO/Sr for ULpa-Na-Ca-Si, UBpa-Na-Ca-Si and HMgn-Na-Ca-Si, while no correlation of K₂O/CaO nor K₂O/MgO is present (Figure App.5-3). This indicates that the CaO in the glass originates from the addition of calcite. For the PLpa-Na-Ca-Si there is no correlation of CaO/MgO ($r=0.3888$; $R^2=0.1512$) nor CaO/K₂O ($r=-0.0626$; $R^2=0.0039$) indicating that possibly purification process has been involved and all the correlations have been affected by this process.

In Cagno [22], plot of K₂O/Rb has been used for Lpa-Na-Ca-Si glasses as a dating discriminant: a) $Rb \leq 30$ ppm dated to 13th-14th century AD; b) $Rb > 30$ ppm dated to 15th-16th century AD. The one 13th-14th century AD Bpa-Na-Ca-Si sample (t_90 from San Vettore) has Rb 54 ppm, while MD 243 has Rb 27 ppm. The Rb quantity of Lpa-Na-Ca-Si Miranduolo samples are all below 30 ppm, except MD 21 which has Rb 39 ppm (Figure 4-8, Figure App.5-1). Sample t_62 is also an exception with

Rb 47 ppm. As the results for Lpa-Na-Ca-Si 13th-14th century samples from Tuscan sites and Miranduolo are consistent, there might be a possibility that sample MD 21 and t_62 were not archaeologically correctly dated. More 13th-14th century analysis should be performed to confirm this, as well as for Bpa-Na-Ca-Si glasses, as there are only 2 samples in total recovered providing ambiguous data. If Rb values are also applicable to Bpa-Na-Ca-Si glasses, the t_90 sample from San Vettore might not be archaeologically correctly dated.

Considering silica sources $\text{SiO}_2/\text{Al}_2\text{O}_3$ (Figure App.5-9) and $\text{Fe}_2\text{O}_3/\text{Al}_2\text{O}_3$ (Figure App.5-6) plot indicates pureness of silica source used. There is a distinctive pattern for PLpa-Na-Ca-Si glasses, whereas they exclusively employ more impure silica source, with $\text{Al}_2\text{O}_3 \geq 3.00$ wt% and $\text{Fe}_2\text{O}_3 \geq 1.00$ wt%. ULpa-Na-Ca-Si is more widely dispersed, Al_2O_3 : ca 2.0 -5.5 wt%, and Fe_2O_3 : ca 0.8 – 1.4 wt%. Only one ULpa-Na-Ca-Si (MD 259) with an Al_2O_3 1.57 wt% and Fe_2O_3 : 0.41 wt % indicates a possible different provenance.

The correlation of $\text{Fe}_2\text{O}_3/\text{TiO}_2$ (Figure App.5-8) for Miranduolo samples is $r = 0.74197$; $R^2 = 0.55052$, indicating a strong positive correlation between the two and implying the presence of Fe_2O_3 as a silica source impurity.

Indicated in [14], the $\text{Fe}_2\text{O}_3/\text{TiO}_2$ positive correlation is explained with the association of Fe and Ti in ilmenite (FeTiO_3) which is a heavy mineral constituting fluvial sands. On the other hand, hematite (Fe_2O_3) and magnetite (Fe_3O_4) can be selectively enriched with titanium oxides as rutile or brookite in fluvial sand placer deposits which is a result of similar sedimentation process.

TiO₂/Zr has strong positive correlation of $r = 0.72862$; $R^2 = 0.5309$ which can increase up to $r = 0.9619$; $R^2 = 0.9253$ when two outliers (MD 67 and MD 172) are not included (Figure 4-9). This is to be expected due to deposition of zircon (ZrSiO₄) which is selectively deposited with ilmenite grains in fluvial sedimentary deposits.

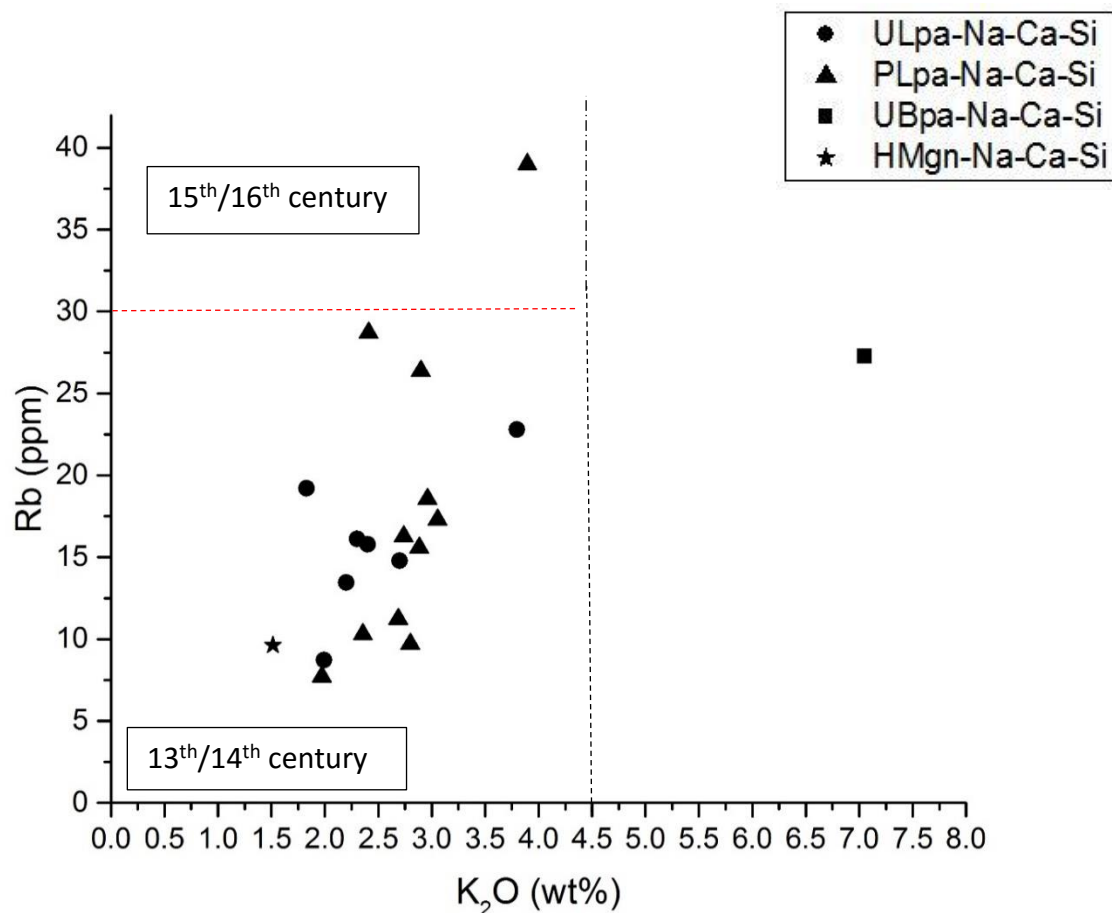


Figure 4-8 Bi-plot of K₂O and Rb of Miranduolo samples with marked glass groups and possible chronological determination

Positive correlations between Fe₂O₃/TiO₂ and TiO₂/Zr have been used as a discriminant for the local availability, indicating the probability of usage of local silica sand source and presence of iron content as a natural impurity and not an addition of it for modification of the glass

composition [14]. In Cagno [22] the correlation of different silica sources have been made with the $\text{Al}_2\text{O}_3/\text{Zr}$. Miranduolo samples show medium positive correlation of Zr with the Al_2O_3 content ($r = 0.3724$; $R^2 = 0.1387$).

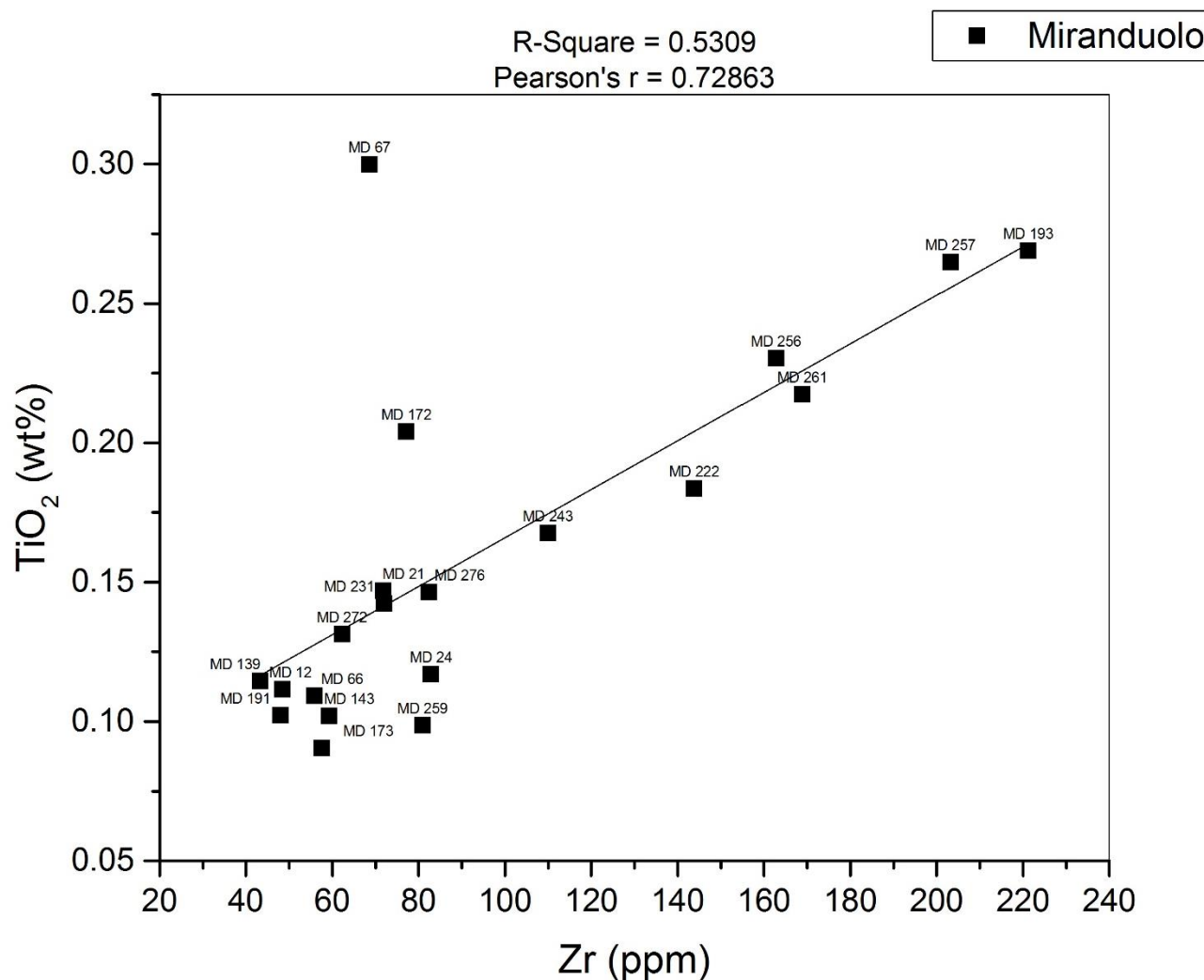


Figure 4-9 Bi-plot of Zr and TiO_2 of Miranduolo samples with marked sample numbers and r and r^2 values.

The Low $\text{Zr} \leq 65$ ppm and TiO_2 0.09-0.13 wt% is correlated with ULpa-Na-Ca-Si glasses; the medium Zr from 65-130 ppm. TiO_2 0.09-0.30 wt% is correlated with both ULpa-Na-Ca-Si and PLpa-Na-Ca-Si, while high $\text{Zr} \geq 130$ are correlated only with PLpa-Na-Ca-Si glasses. In general, $\text{Zr} \geq 140$ ppm and

$TiO_2 \geq 18$ ppm are correlated with PLpa-Na-Ca-Si, with MD 67 and MD 172 as outliers; while $Zr \leq 85$ ppm and $TiO_2 \leq 15$ ppm are correlated with ULpa-Na-Ca-Si. Therefore, here the concentrations of Zr and TiO_2 can be considered compositionally indicative. Strong positive correlation of TiO_2/Nb with $r = 0.9414$; $R^2 = 0.8862$ are noted in Miranduolo samples (Figure 4-10). Again, concentrations of Nb can be distinguished for PLpa-Na-Ca-Si $Nb \geq 4$ ppm and $Nb < 4$ ppm for ULpa-Na-Ca-Si. Positive correlation of TiO_2/Nb along with the strong positive correlation TiO_2/Zr and Fe_2O_3/TiO_2 are explained as mineral impurities in the sandy raw material.

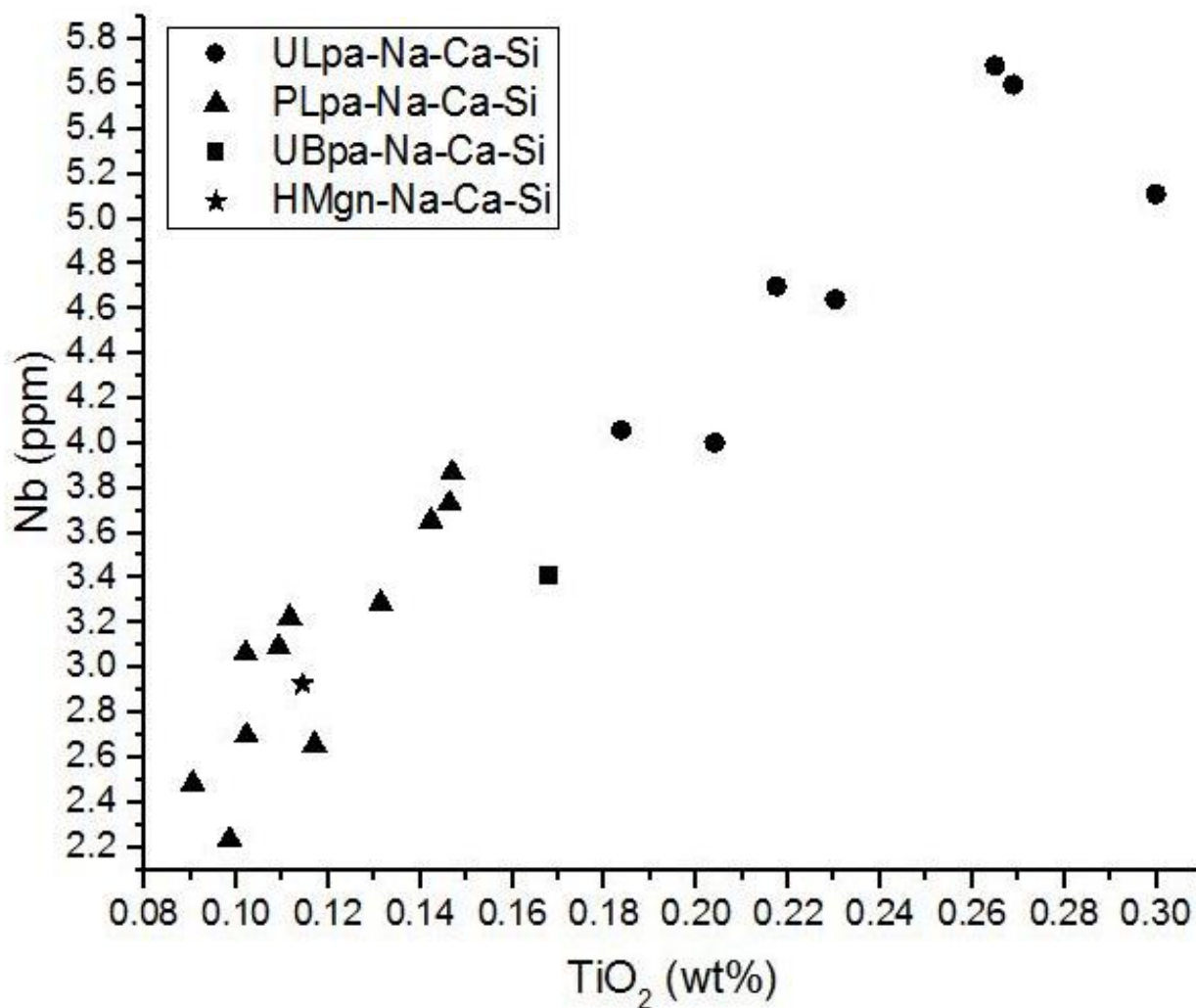


Figure 4-10 Bi-plot of TiO_2 and Nb of Miranduolo samples with marked glass groups, and r and r^2 values.

Columbite (FeNb_2O_6), a Nb-containing mineral, can be found selectively deposited with Fe-Ti bearing oxide minerals, including zircon and ilmenite. They are found in sedimentary deposits as heavy mineral placers, as they display high resistivity to erosion. Columbite-bearing mineral deposits are common for granitic rocks and outcrops. On the other hand, no significant granite outcrops are present in Miranduolo area nor near San Vettore and Germagnana glass factories [86]. Zr/Hf are strongly correlated with $r = 0.9966$ and $R^2 = 0.9931$ (Figure 4-11, Figure App.5-9). In geochemistry this phenomenon is known and explained. Hf can be found as a substitute for Zr in Zr-bearing minerals.

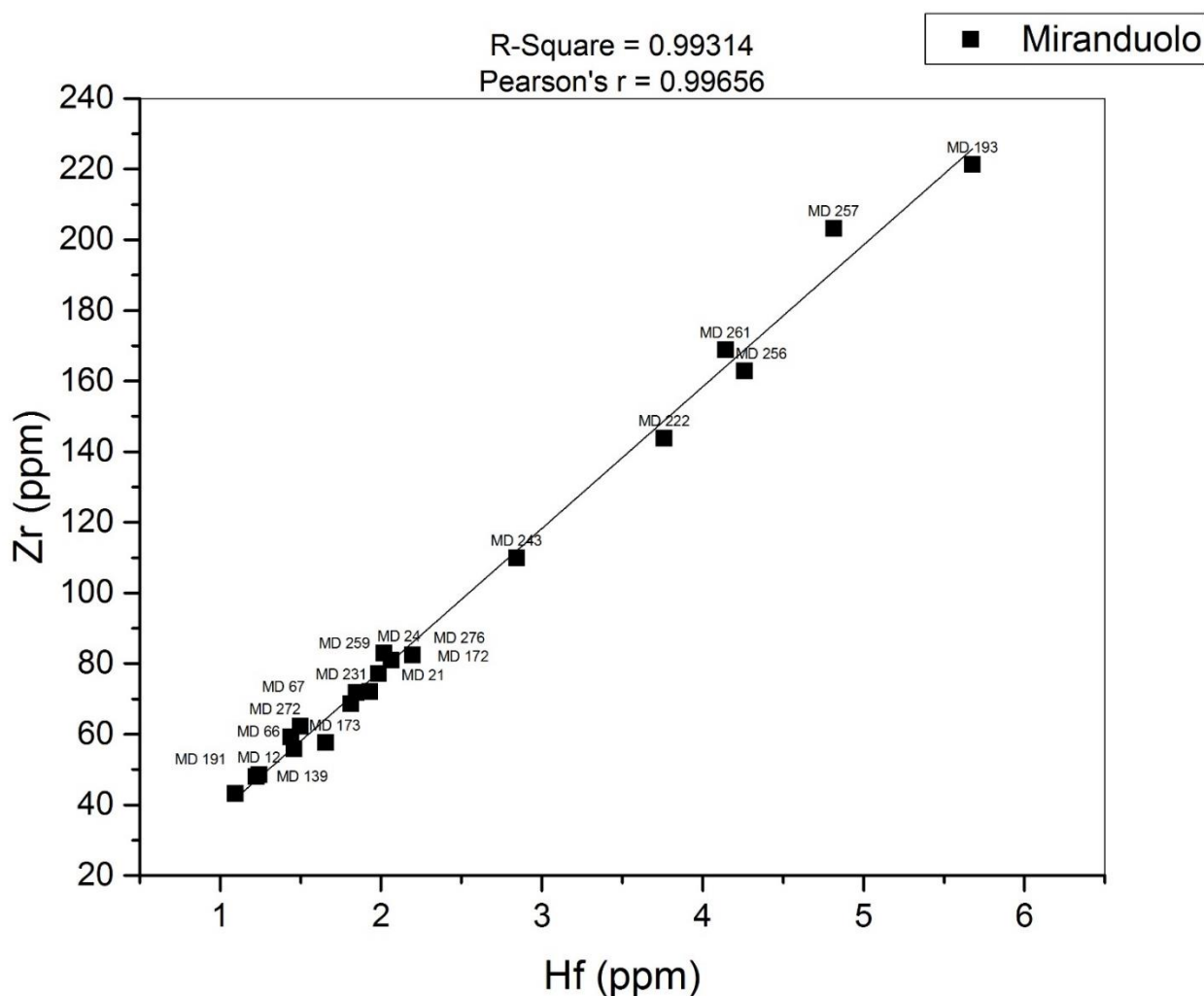


Figure 4-11 Bi-plot of Hf and Zr of Miranduolo samples with marked sample numbers, and r and r^2 values.

To further analyze silica sources for P- and ULpa-Na-Ca-Si concentrations of Co, Ni, Ti, Cr and V are examined due to their correlation with Fe_2O_3 of the raw material. Considering Co and Ni there is no distinction in concentration according to the flux used, but Ti, Cr and V display discrepancies between the two compositions. PLpa-Na-Ca-Si $\text{TiO}_2 \geq 0.18$ wt%, $\text{Cr} \geq 23.5$ ppm, $\text{V} \geq 21$ ppm ; ULpa-Na-Ca-Si $\text{TiO}_2 \leq 0.15$ wt%, $\text{Cr} < 23.5$ ppm, $\text{V} \leq 20$ ppm.

LA-ICP-MS can provide information on REE (Rare Earth Elements): La, Ce, Pr, Nd, Sm, Eu, Gd, Tb, Dy, Ho, Er, Tm, Yb and Lu. It is considered to be a raw material fingerprint. Miranduolo's REE have been divided by Wedepohl's continental crust data (Figure 4-12, Figure App.5-10, Figure App.5-11) [88, 89] and by chondrite concentrations (Figure App.5-12, Figure App.5-13, Figure App.5-14) [90]. When the sum of REE for each sample have been plotted against CaO there is no correlation ($r = -0.2687$; $R^2 = 0.0722$). While observing Miranduolo samples with $\text{CaO} \leq 7$ wt% (PLpa-Na-Ca-Si glasses) do not show a positive correlation ($r = 0.4277$; $R^2 = 0.1830$). On the other hand, samples with $\text{CaO} > 7$ wt% (ULpa-Na-Ca-Si, UBpa-Na-Ca-Si and HMgn-Na-Ca-Si glasses), the correlation is strongly positive ($r = 0.8079$; $R^2 = 0.6527$) thus giving the limestone signature (Figure 4-13).

The two colorless samples MD 24 and MD 259 display the results that have been noted for PIXE/PIGE, only with a slightly different $\text{Fe}_2\text{O}_3/\text{MnO}$ ratios (Table App.6-1, Figure App.5-7). For colorless samples MD 24 the ratio is 1.47 and for MD 259 1.22 and MD 259 (15 microns) 1.19. But the samples MD 66 has the ratio of 1.51 and MD 257 1.19, while MD 272 and MD 276 have the ratio of 0.98 and 0.95. The latter means that the amount of MnO exceeds the amount of Fe_2O_3 .

What could have been noted that $\text{Sn} \leq 30$ ppm, $\text{Sb} \leq 120$ ppm nor $\text{Pb} \leq 1500$ ppm do not have a decoloring effect on the colored glasses, nor coloring effect on the decolorized glasses. For the colored samples with the $\text{Fe}_2\text{O}_3/\text{MnO}$ ratio above 1 (MD 66 and MD 257) in both samples the quantity of Cr, Ni, Cu, Zn exceeds the one in the colorless samples. For the colored samples with the $\text{Fe}_2\text{O}_3/\text{MnO}$ ratio below 1 (MD 272 and MD 276) three elements of the Cr, Ni, Cu, Zn have

higher values than the colorless samples. As the quantity of the samples is not representative, future investigation of this matter for pa-Na-Ca-Si glasses have to be conducted in order to confirm or disprove the possible influence of the quantity of Cr, Ni, Cu and Zn to the quantity of MnO and the ratio of Fe₂O₃ for coloring and decoloring glasses. As stressed in [3] the final color of the glass artefact is also dependent on the furnace atmosphere, melting time, etc.

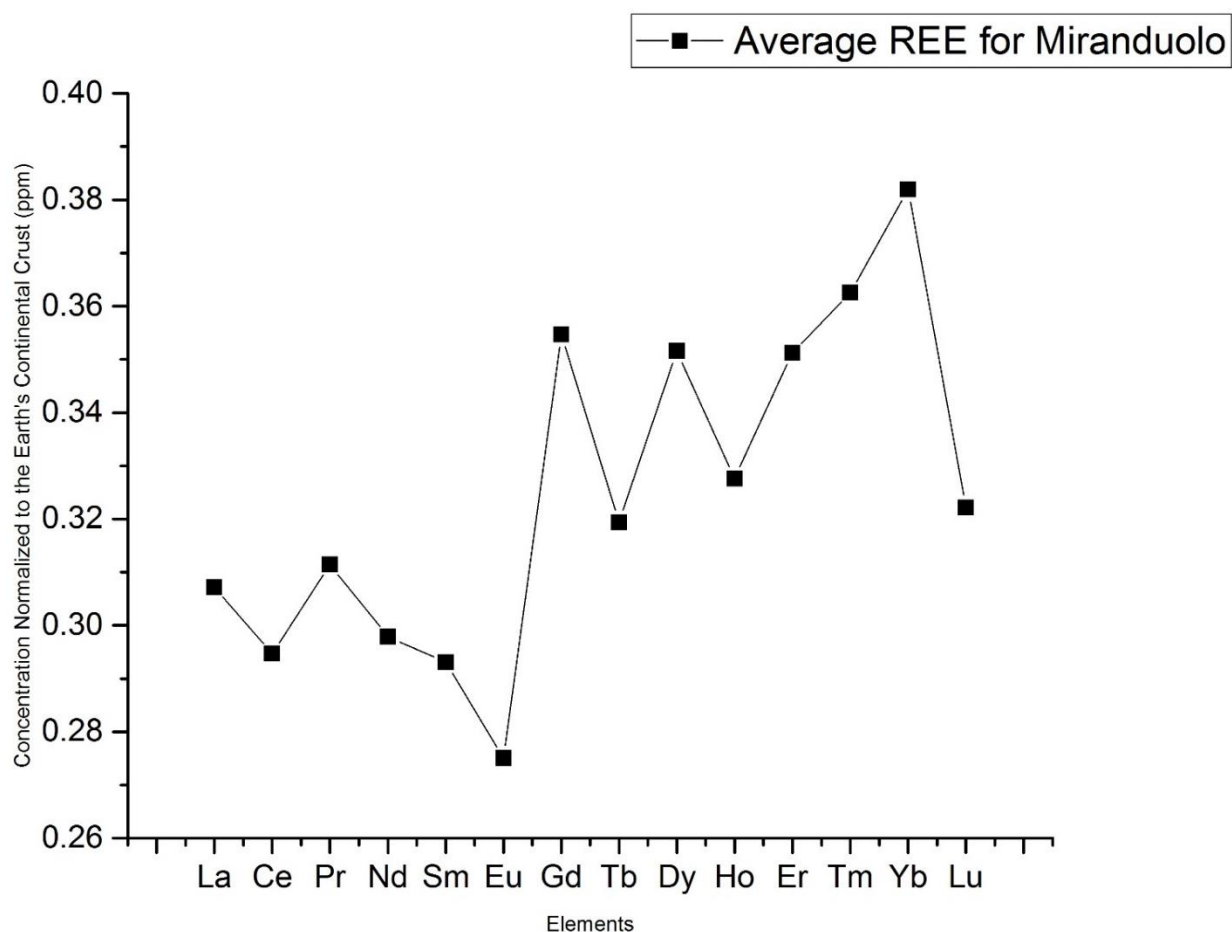


Figure 4-12 Average concentration of Miranduolo REE. The concentration has been normalized to Earth Continental Crust (ppm).

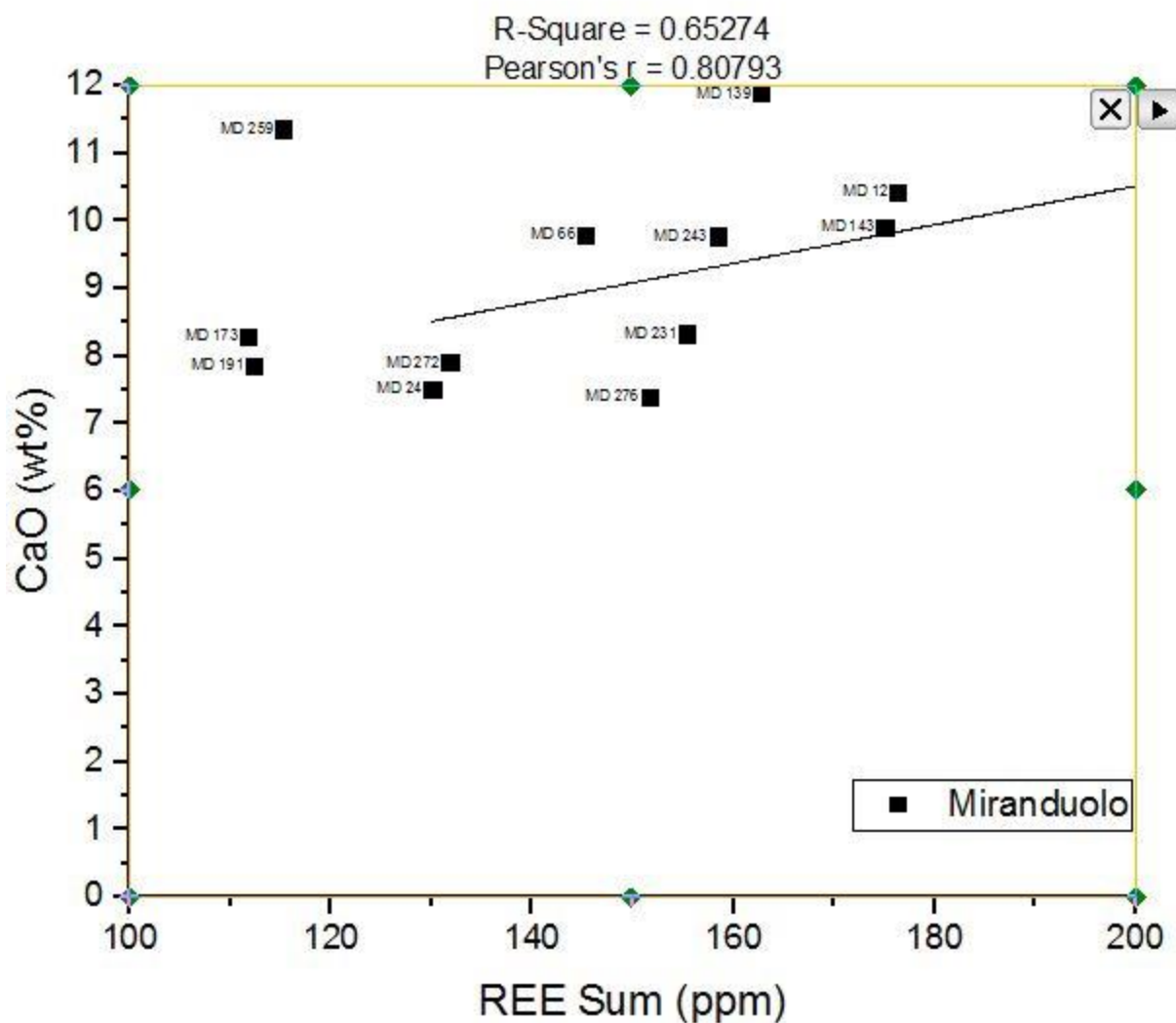


Figure 4-13 Bi-plot and correlation of Miranduolo samples with $\text{CaO} > 7\text{wt}\%$ (ULpa-Na-Ca-Si, UBpa-Na-Ca-Si and HMgn-Na-Ca-Si glasses) displaying the limestone signature.

The extent of recycling of Miranduolo samples is 65%, meaning 13 samples display recycling concentrations of Pb, Cu, Zn, Sb, Sn (Figure 4-14, Figure App.5-15, Figure App.5-16). Recycling concentrations are considered those in the 100-1000 ppm range as indicated in [34]. The samples that have not been recycled are: MD 12, MD 139, MD 143, MD 173, MD 193, MD 259 and MD 272. Recycled samples with $\text{Pb} \geq 100$ ppm are MD 24 ($\text{Pb} > 1000$ ppm), MD 66, MD 67, MD 172,

MD 191, MD 222, MD 256, MD 276. Recycled sample with $Zn \geq 100$ ppm is MD 21, while sample with both Pb and $Zn \geq 100$ ppm is MD 243. Pb and $Cu \geq 100$ ppm is present in MD 231, and Pb, Cu, $Sb \geq 100$ ppm is determined in MD 257, possibly implying the usage of blue cullet. Sample MD 261 displays Cu, Zn, $Sn > 100$ ppm and Pb, $Sb > 1000$ ppm, possibly indicating recycling of the tesserae.

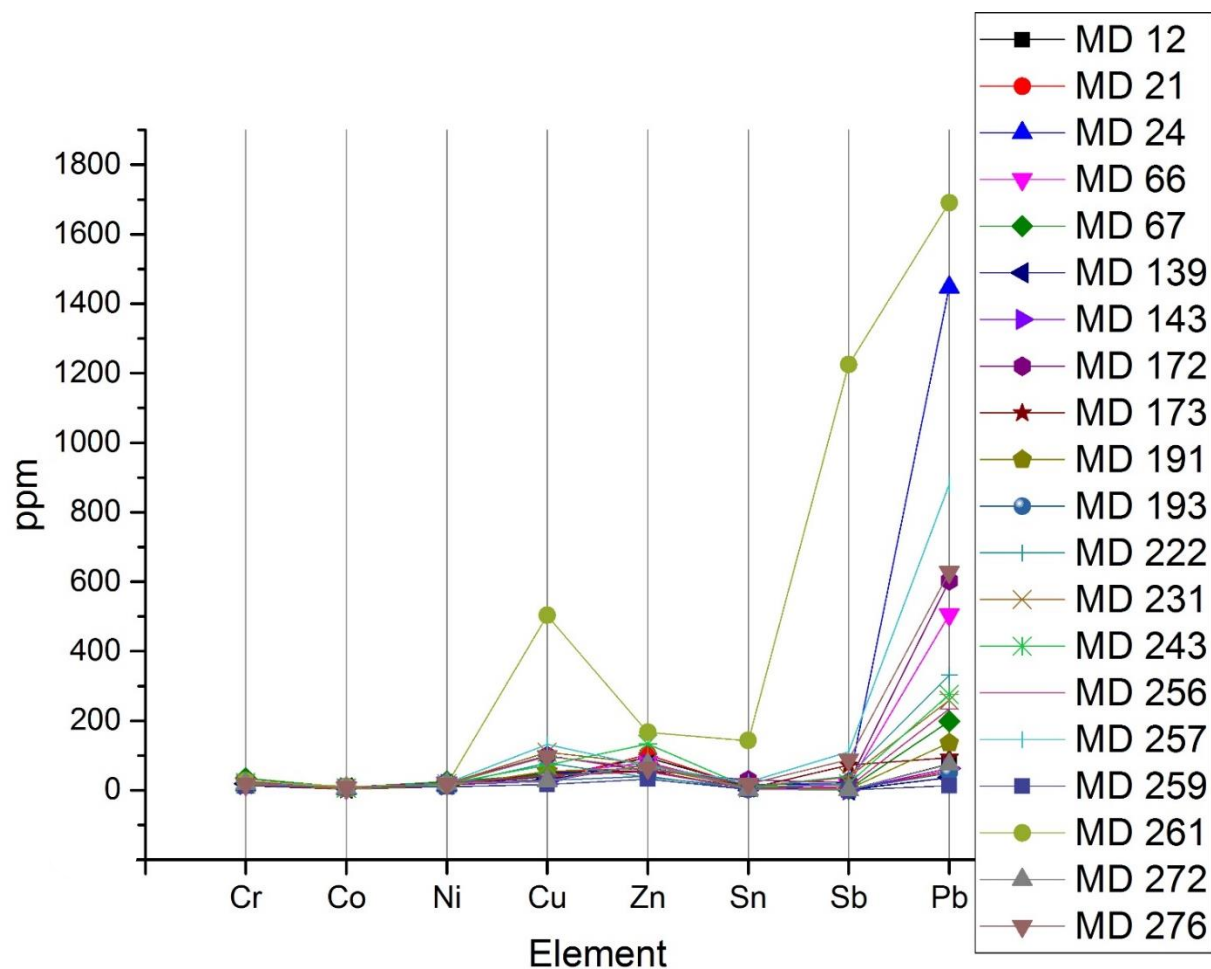


Figure 4-14 Representation of elements which are indicators for recycling for all Miranduolo samples.

Thus, it seems like the first Tuscan factories experimented and/or knowingly used all the possible raw materials (fluxes) and procedures (ash purifications and addition of calcite).

4.3.2. Comparison of 50 μm and 15 μm laser ablation beam size

Due to different thicknesses of the corrosion layers, the beam size had to be reduced from 50 μm to 15 μm . To confirm the validity of the corrosion results, the reproducibility of the data of the pristine glasses had to be verified with both 50 μm and 15 μm laser beam size. The results are presented in Table 4-13.

For MD 143 ablation with 15 μm laser beam (Figure App.5-17) gave higher values for Na_2O , MgO , Al_2O_3 , SiO_2 , P_2O_5 , K_2O , CaO , TiO_2 , MnO , V , Cr , Co , Ni , Cu , As , Rb , Sr , Y , Zr , Nb , Sn , Sb , Ba , La , Ce , Pr , Nd , Sm , Eu , Gd , Tm , Dy , Ho , Tm , Lu , Hf , Th . Lower values are noted for Fe_2O_3 , Zn , Er , Yb , Pb , U with an average difference of 10.86%. Higher values display more discrepancies, with average difference of 18.50%, while Sn and As display a difference of over 50%. The average beams size difference for MD 143 is 14.58%.

For MD 259 ablation with 15 μm laser beam (Figure App.5-18) gave higher values for Na_2O , MgO , Al_2O_3 , P_2O_5 , TiO_2 , MnO , Fe_2O_3 , V , Cr , Co , Ni , Cu , As , Sr , Y , Zr , Sb , Ba , Ce , Pr , Nd , Sm , Lu , Th , U . The average difference is 9.63%, while As and Lu display a difference over 40%. Lower values observed with a 15 μm laser beam are for SiO_2 , K_2O , CaO , Zn , Rb , Nb , Sn , La , Eu , Gd , Tb , Dy , Ho , Er , Tm , Yb , Hf , Pb , with an average of 10.20%. The average beams size difference for MD 259 is 9.91%.

Comparing MD 143 and MD 259 (Figure 4-15) the higher values with 15 μm laser ablation beam are for Na_2O , MgO , Al_2O_3 , P_2O_5 , TiO_2 , MnO , V , Cr , Co , Ni , Cu , As , Sr , Y , Zr , Sb , Ba , Ce , Pr , Nd , Sm and Lu . Lower values in both samples are for Zn , Er , Yb and Pb . There is no apparent pattern in the elements that display higher and lower values when using a smaller laser beam. As both glasses are made classified as ULpa-Na-Ca-Si glasses, the compositional difference could not be taken into account as a source for this discrepancies. Future investigations on more abundant collection should be made to draw valid and widely applicable conclusions.

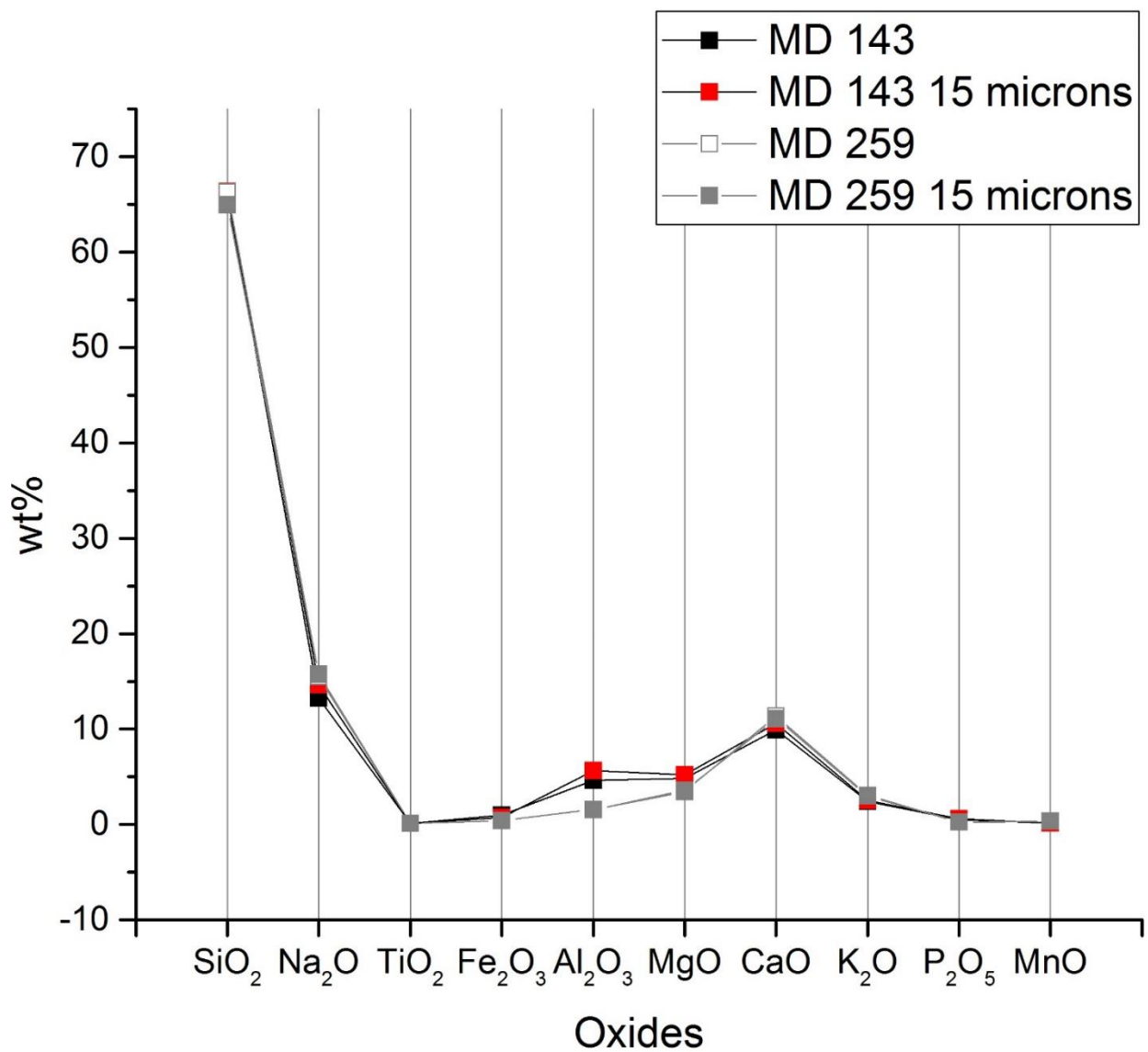


Figure 4-15 Comparison of quantification data between 50 μm and 15 μm laser beam size in samples MD 143 and MD 259.

Table 4-13 Comparison of results obtained by 50 μm and 15 μm laser beam size of MD 143 and MD 259. The difference between the two beams sizes are displayed in %. Total average is the average of samples MD 143 and MD 259.

MD 143					MD 259					
Units	Oxides/elements	50 μm	15 μm	Difference between beam sizes (%)	Units	Oxides/elements	50 μm	15 μm	Difference between beam sizes (%)	
wt%	Na ₂ O	13.23	14.62	9.48	wt%	Na ₂ O	15.49	15.75	1.66	
	MgO	4.85	5.22	7.15		MgO	3.44	3.56	3.45	
	Al ₂ O ₃	4.64	5.66	18.05		Al ₂ O ₃	1.57	1.58	0.50	
	SiO ₂	65.98	66.37	0.59		P ₂ O ₅	0.25	0.28	8.84	
	P ₂ O ₅	0.51	0.60	14.09		TiO ₂	0.10	0.10	5.84	
	K ₂ O	2.41	2.52	4.54		MnO	0.34	0.35	3.54	
	CaO	9.91	10.61	6.55		Fe ₂ O ₃	0.41	0.41	0.37	
	TiO ₂	0.10	0.12	17.59		ppm	V	11.20	11.67	4.05
	MnO	0.16	0.17	5.47			Cr	12.09	12.67	4.56
ppm	V	13.52	15.19	11.01	Co		9.55	10.40	8.20	
	Cr	17.10	20.65	17.21	Ni		9.20	9.22	0.24	
	Co	6.67	7.78	14.30	Cu		16.06	16.78	4.33	
	Ni	15.62	20.35	23.21	As		2.60	5.68	54.31	
	Cu	26.23	29.69	11.68	Sr		466.73	519.06	10.08	
	As	2.50	5.96	58.06	Y		5.08	5.91	13.97	
	Rb	28.69	29.02	1.14	Zr		80.95	84.66	4.37	
	Sr	553.95	656.36	15.60	Sb		1.16	1.22	4.73	
	Y	7.47	10.53	29.10	Ba		255.61	274.19	6.77	
	Zr	59.32	78.20	24.15	Ce		12.22	12.29	0.55	
	Nb	3.07	3.99	23.18	Pr		1.53	1.77	13.44	
	Sn	15.81	17.48	9.54	Nd		5.87	6.48	9.38	
	Sb	1.03	2.40	57.10	Sm		1.04	1.12	7.16	
	Ba	240.76	269.35	10.61	Lu	0.06	0.11	42.12		
	La	10.38	13.00	20.19	Th	1.36	1.67	18.47		
Ce	19.58	22.86	14.36	U	0.46	0.50	9.77			

MD 143					MD 259					
Oxides/elements	50 µm	15 µm	Difference between beam sizes (%)		Oxides/elements	50 µm	15 µm	Difference between beam sizes (%)		
Pr	2.29	2.54	10.13		Average					9.63
Nd	8.25	9.34	11.67							
Sm	1.43	1.53	7.01		wt%	SiO ₂	66.31	64.96	2.04	
Eu	0.29	0.37	20.65			K ₂ O	3.05	2.99	2.15	
Gd	1.30	2.14	39.56			CaO	11.37	11.09	2.48	
Tb	0.19	0.30	36.71		ppm	Zn	32.05	31.01	3.26	
Dy	1.28	1.66	22.62			Rb	17.28	16.23	6.10	
Ho	0.26	0.29	8.98			Nb	2.24	2.19	2.24	
Tm	0.12	0.15	20.85			Sn	2.49	2.26	9.15	
Lu	0.12	0.18	33.85			La	6.49	6.33	2.50	
Hf	1.44	2.08	30.48			Eu	0.24	0.14	38.51	
Th	2.77	3.38	17.91			Gd	1.04	0.85	17.83	
Average			18.50			Tb	0.14	0.10	27.39	
						Dy	0.86	0.77	9.94	
wt%	Fe ₂ O ₃	0.98	0.76	22.56		Ho	0.15	0.13	13.37	
ppm	Zn	73.72	64.00	73.72		Er	0.51	0.51	1.17	
	Er	0.78	0.67	0.78		Tm	0.09	0.07	25.84	
	Yb	0.87	0.81	0.87		Yb	0.45	0.38	16.01	
	Pb	62.42	61.41	62.42		Hf	2.07	2.06	0.24	
	U	1.77	1.67	1.77		Pb	12.47	12.05	3.37	
Average				10.67	Average				10.20	
Average MD 143 (%)				14.58	Average MD 259 (%)				9.91	
Average total (%)					12.25					

4.3.3. Corrosion

LA-ICP-MS has been performed on corrosion layers to possibly determine if there is a notable pattern in depletion or enrichments of elements. Due to the fact that the corrosion layer of MD 24 is 2.25 μm the minimum laser ablation beam size was not small enough only to ablate the corrosion layer. The corrosion layer of sample MD 143 was not successfully ablated. Hence, the results of the MD 143 is not included.

Corrosion analysis of MD 139 (Figure App.5-19) and MD 259 (Figure App.5-20) has been successfully carried out. It has to be noted that the pristine glass and the corrosion layer in MD 139 have been ablated with 50 μm beam size and MD 259 with 15 μm beam size. The results obtained are displayed in Table 4-14, Table 4-15, Table 4-17, Table 4-16, Table 4-18 and Table 4-19.

From sample MD 139 Na_2O , K_2O , CaO , MgO , P_2O_5 , MnO , V , Co , Ni , Cu , Zn , Rb , Sr , Ba , Y , La , Ce , Pr , Nd , Sm , Eu , Gd , Tb , Dy , Ho , Er , Tm , Yb , Lu , U started to deplete, while SiO_2 , Al_2O_3 , TiO_2 , Fe_2O_3 , Cr , As , Zr , Nb , Sn , Sb , Hf , Pb , Th show enriched values. From sample MD 259 Na_2O_3 , K_2O , CaO , MgO , P_2O_5 , MnO , V , Co , Ni , As , Rb , Sr , Y , La , Ce , Pr , Nd , Sm , Tb , Dy , Ho , Er , Tm , Lu , U have depleted, and SiO_2 , Al_2O_3 , TiO_2 , Fe_2O_3 , Cr , Cu , Zn , Zr , Nb , Sn , Sb , Ba , Eu , Gd , Yb , Hf , Pb , Th display enriched concentrations compared to pristine glass.

In both compositional groups the following elements occur: Na_2O , K_2O , CaO , MgO , P_2O_5 , MnO , V , Co , Ni , Rb , Sr , Y , La , Ce , Pr , Nd , Sm , Tb , Dy , Ho , Er , Tm , Lu and U . For all the aforementioned elements, the larger depletion is notable in MD 139, except for Y , with only 3.1% difference in depletion. For all the other elements the depletion is on average 35.47% more pronounced in MD 139. The enrichment of SiO_2 , Al_2O_3 , TiO_2 , Fe_2O_3 , Cr , Zr , Nb , Sb , Sn , Hf , Th , Pb are common for both samples. The larger enrichment of SiO_2 , Al_2O_3 , Fe_2O_3 , Sn , Hf , Th with the average of 91.62% more pronounced enrichment in MD 259, while for TiO_2 , Cr , Zr , Nb , Sb , Pb on average 119.16% the enrichment is more pronounced in MD 139.

Table 4-14 Depletion (%) of selected elements in corrosion in comparison to pristine glass of MD 139. Oxides are expressed in wt% and elements in ppm.

MD 139				
Unit	Oxide/Element	Pristine	Corrosion	Depleted amount from pristine (%)
wt%	Na ₂ O	15.44	0.31	97.97
	MgO	4.63	0.69	85.19
	P ₂ O ₅	0.59	0.012	98.04
	K ₂ O	1.52	0.19	87.51
	CaO	11.92	3.19	73.20
	MnO	0.09	0.01	88.24
ppm	V	16.95	7.66	54.79
	Co	5.97	0.18	96.92
	Ni	17.56	0.90	94.86
	Cu	31.38	1.82	94.22
	Zn	73.29	35.14	52.05
	Rb	9.63	8.04	16.52
	Sr	590.44	65.49	88.91
	Ba	107.77	22.79	78.86
	Y	7.03	1.05	85.10
	La	9.56	1.07	88.84
	Ce	17.37	1.24	92.84
	Pr	2.09	0.31	85.17
	Nd	8.21	1.22	85.17
	Sm	1.52	0.28	81.63
	Eu	0.30	0.05	82.19
	Gd	1.30	0.22	82.86
	Tb	0.20	0.03	83.66
	Dy	1.27	0.21	83.08
	Ho	0.24	0.04	81.21
	Er	0.69	0.13	81.18
	Tm	0.09	0.02	83.59
Yb	0.72	0.15	78.60	
Lu	0.10	0.02	82.03	
U	1.22	0.24	80.18	

Table 4-15 Enrichment (%) of selected elements in corrosion in comparison to pristine glass of MD 139. Oxides are expressed in wt% and elements in ppm.

MD 139				
Unit	Oxide/Element	Pristine	Corrosion	Enriched amount from pristine (%)
wt%	Al ₂ O ₃	3.38	6.86	102.84
	SiO ₂	65.20	68.75	5.45
	TiO ₂	0.11	0.16	37.02
	Fe ₂ O ₃	1.19	1.89	59.01
ppm	Cr	18.50	47.17	154.94
	As	3.52	19.19	444.71
	Zr	43.24	72.06	66.63
	Nb	2.93	4.47	52.78
	Sn	9.25	24.65	166.49
	Sb	1.62	14.03	765.90
	Hf	1.09	1.94	77.08
	Pb	36.49	75.15	105.97
	Th	2.68	3.08	14.95

Table 4-16 Enrichment (%) of selected elements in corrosion in comparison to pristine glass of MD 259. Oxides are expressed in wt% and elements in ppm.

MD 259				
Unit	Oxide/Element	Pristine	Corrosion	Enriched amount from pristine (%)
wt%	Al ₂ O ₃	1.58	8.13	416.33
	SiO ₂	64.96	74.41	14.54
	TiO ₂	0.10	0.12	16.10
	Fe ₂ O ₃	0.41	1.04	150.89
ppm	Cr	12.67	28.49	124.91
	Cu	16.78	34.86	107.70
	Zn	31.01	154.05	396.87
	Zr	84.66	107.43	26.90
	Nb	2.19	2.69	23.11
	Sn	2.26	8.64	282.87
	Sb	1.22	1.60	31.69
	Ba	274.19	347.07	26.58
	Eu	0.14	0.15	6.80
	Gd	0.85	1.05	23.56
	Yb	0.38	0.52	37.33
	Hf	2.06	3.74	81.55

	Pb	12.05	17.70	46.95
	Th	1.67	2.15	29.33

Table 4-17 Depletion (%) of selected elements in corrosion in comparison to pristine glass of MD 259. Oxides are expressed in wt% and elements in ppm.

MD 259				
Unit	Oxide/Element	Pristine	Corrosion	Depleted amount from pristine (%)
wt%	Na ₂ O	15.75	5.44	65.44
	MgO	3.56	1.55	56.38
	P ₂ O ₅	0.28	0.14	47.90
	K ₂ O	2.99	1.24	58.62
	CaO	11.09	7.03	36.62
	MnO	0.35	0.14	58.80
ppm	V	11.67	5.65	51.57
	Co	10.40	3.71	64.37
	Ni	9.22	6.17	33.15
	As	5.68	5.12	9.86
	Rb	16.23	12.93	20.34
	Sr	519.06	252.23	51.41
	Y	5.91	2.96	49.87
	La	6.33	3.34	47.21
	Ce	12.29	5.81	52.75
	Pr	1.77	0.98	44.74
	Nd	6.48	2.78	57.15
	Sm	1.12	0.52	53.17
	Tb	0.10	0.07	29.20
	Dy	0.77	0.35	54.55
	Ho	0.13	0.12	5.27
	Er	0.51	0.16	68.71
	Tm	0.07	0.05	20.45
	Lu	0.11	0.04	66.43
U	0.50	0.15	69.72	

Table 4-18 Comparison of depletion of elements in MD 139 and MD 259 corrosions, expressed in %.

Corrosion depletion of elements (MD 139 vs MD 259)				
Unit	Element	MD 139 depletion (%)	MD 259 depletion (%)	Depletion difference between MD 139 and MD 259 (%)
wt%	Na ₂ O	97.97	65.44	32.53
	MgO	85.19	56.38	28.80
	P ₂ O ₅	98.04	47.90	50.14
	K ₂ O	87.51	58.62	28.88
	CaO	73.20	36.62	36.57
	MnO	88.24	58.80	29.44
ppm	V	54.79	51.57	3.21
	Co	96.92	64.37	32.55
	Ni	94.86	33.15	61.71
	Sr	88.91	51.41	37.50
	Y	85.10	49.87	35.23
	La	88.84	47.21	41.62
	Ce	92.84	52.75	40.09
	Pr	85.17	44.74	40.43
	Nd	85.17	57.15	28.02
	Sm	81.63	53.17	28.46
	Tb	83.66	29.20	54.46
	Dy	83.08	54.55	28.53
	Ho	81.21	5.27	75.93
	Er	81.18	68.71	12.47
	Tm	83.59	20.45	63.13
	Lu	82.03	66.43	15.60
	U	80.18	69.72	10.46
	Average depletion difference (%)			35.47
ppm	Rb	16.52	20.34	3.83

Table 4-19 Comparison of enrichment of elements in MD 139 and MD 259 corrosions, expressed in %.

Corrosion enrichment of elements (MD 139 vs MD 259)				
Unit	Oxide/element	MD 139 enrichment (%)	MD 259 enrichment (%)	Enrichment difference between MD 139 and MD 259 (%)
wt%	Al₂O₃	102.84	416.33	313.49
	SiO₂	5.45	14.54	9.10
	Fe₂O₃	59.01	150.89	91.88
ppm	Sn	166.49	282.87	116.39
	Hf	77.08	81.55	4.48
	Th	14.95	29.33	14.38
	Average enrichment difference (%)	70.97	162.59	91.62
ppm	Pb	105.97	46.95	59.02
wt%	TiO₂	37.02	16.10	20.91
ppm	Cr	154.94	124.91	30.03
	Zr	66.63	26.90	39.73
	Nb	52.78	23.11	29.66
	Sb	765.90	31.69	734.21
	Average enrichment difference (%)	197.20	44.94	119.61

As MD 139 is compositionally n-NM-Na-Ca-Si, while MD 259 is ULpa-Na-Ca-Si glass, it might be the cause for different pattern of depletion/enrichment of elements in the corrosion layer, as well as the extent of the depletion/enrichment. As the sample number is not representative, further investigations have to be conducted to confirm or disprove the aforementioned conclusions.

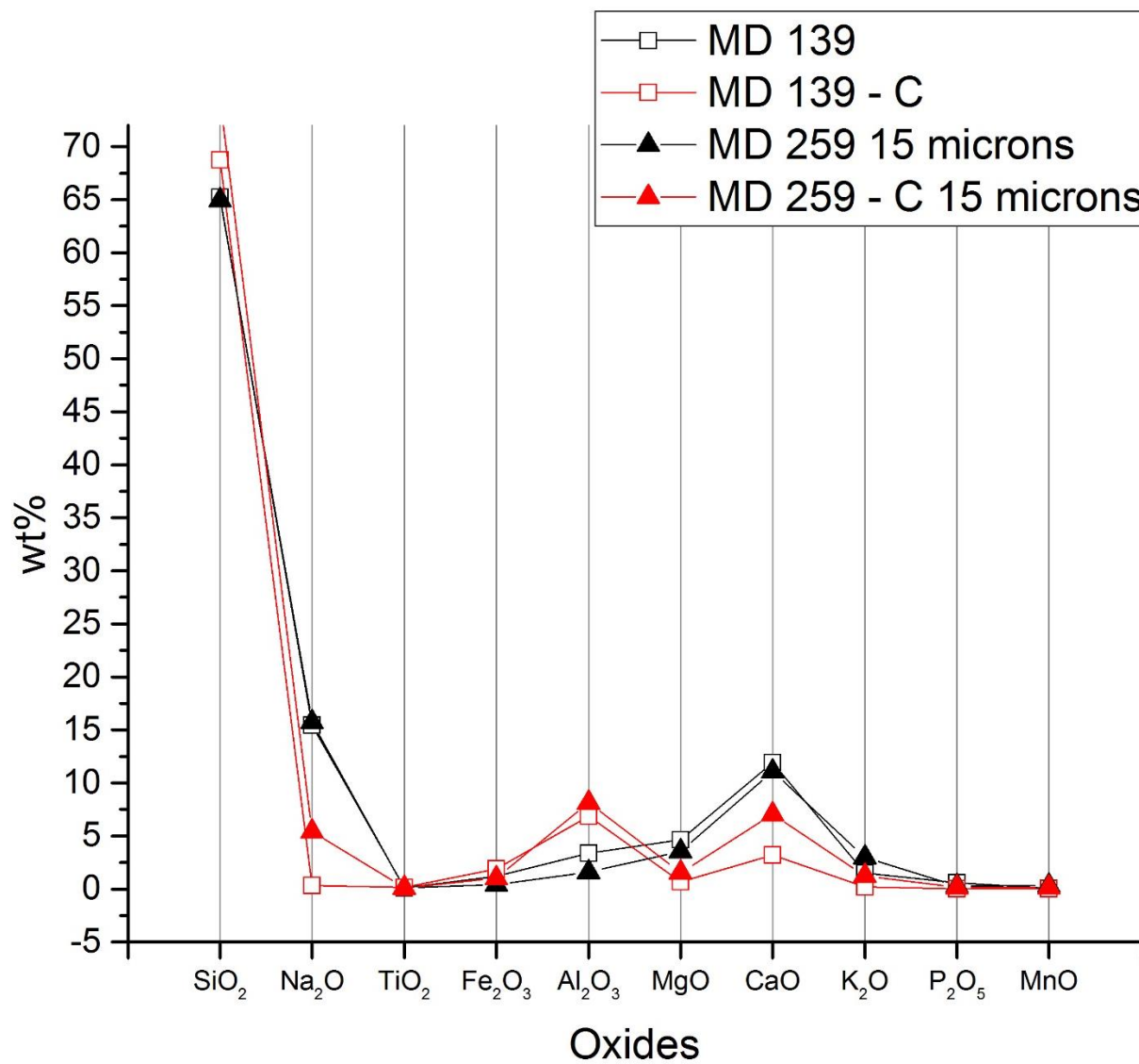


Figure 4-16 Comparison of pristine glass and corrosion layer (C) of samples MD 139 and MD 259.

5. Discussion

VP-SEM-EDS imaging showed that all Miranduolo glasses are homogeneous. This was confirmed by PIXE/PIGE chemical maps and by LA-ICP-MS results for each spot taken in a sample. The distinction between the amount of K_2O over CaO and MgO can be noted. The K_2O is discriminating for the plant ash (Levantine if $K_2O \leq 4.5$ wt%; Barilla if $K_2O > 4.5$ wt%) used.

The amount of $CaO \leq 7$ wt% should be an indication that a purification process of the plant ash has been employed, which is confirmed by the lack of correlation of K_2O/CaO and K_2O/MgO . On the other hand, $CaO > 7$ wt% indicates that purification process has also been employed, but additional calcite has been added to the batch as CaO is strongly correlated to MgO , while no correlation of K_2O with MgO is present. The assumption that on these glasses purification of ash has been done, is based on the fact that the studies have proven the existence of correlation of K_2O with CaO and MgO in *Salsola* genus. In fact, the 6-9 wt% of CaO and 0.5 wt % of MgO can be solely introduced with plant ash[26, 28]. But the authors provided results plant ash analyses with the aforementioned CaO values, while K_2O and MgO are exceedingly higher, notably from *ca* 10-40 wt% and 1-10 wt%. The plant ash P_2O_5 values are also higher, from 0.35-3.50 wt%, comparing to the average amount usually found in glasses. As the percentages of raw materials input in the batch differs to the output (finished glass objects) due to chemical processes occurring during manufacturing process of the glass, the CaO content should also be lower. All of the aforementioned information leaves the doubt that CaO content can be high as 6-9 wt% due to plant ash.

In Miranduolo PLpa-Na-Ca-Si glasses there is no strong positive correlation of CaO with MgO and Sr , nor K_2O with CaO implying that a purification process could have been used.

ULpa-Na-Ca-Si glasses there is a strong positive correlation of CaO with MgO and Sr , while there is no correlation of K_2O with CaO . This implies that the plant ash is not responsible for the quantity of CaO , but that the additional calcite had to be input in the batch. Comparing the correlation of CaO with Br , as it is not positive the marine source of calcite, namely seashells, can be excluded.

Hence, the calcite added had a continental origin. Interestingly, for PLpa-Na-Ca-Si glasses there is a strong negative correlation of CaO and Br.

Generally, the glass composition portrays the prevalence of Lpa-Na-Ca-Si glasses, with the usage of both purified and unpurified ashes as a flux. Only MD 243 is Bpa-Na-Ca-Si glasses and MD 139 has a specific composition. The latter is a non-recycled glass made with natron as flux. But the choice of raw material had an impact on overall MgO value in this glass, making it higher than 1.5 wt%. This has classified this glass type as High Magnesium natron soda lime silica glass (HMgn-Na-Ca-Si). Existence of thick 500 μm corrosion layer, was a confirmation of the usage of natron as a flux, as these thick corrosion layers frequently occur in Roman n-Na-Ca-Si glasses. There are two contemporary samples with the same range of values of K_2O and MgO as in Rocca di Campiglia and Savona in Italy. The usage of natron as a flux is rare in 13th-14th century but it has been reported in Nogara and Venice glasses [3], [28].

There have been diverse raw sources used for PLpa-Na-Ca-Si and ULpa-Na-Ca-Si glasses which is pronounced in concertation of several elements, indicating the purity of the raw material.

For the PLpa-Na-Ca-Si the following concentrations apply: $\text{TiO}_2 \geq 0.18$ wt% (MD 67 and MD 172 are outliers), $\text{Fe}_2\text{O}_3 \geq 1.00$ wt%, $\text{Al}_2\text{O}_3 \geq 3.00$ wt%, $\text{Zr} \geq 140$ ppm $\text{MgO} \leq 1.8$ wt%, $\text{Sr} \leq 420$ ppm, $\text{Nb} \geq 4$ ppm, $\text{Cr} \geq 23.5$ ppm and $\text{V} \geq 21$ ppm.

ULpa-Na-Ca-Si displays the concentrations as it follows: $\text{TiO}_2 \leq 0.15$ wt%, Fe_2O_3 ca 0.8 – 1.4 wt% and Al_2O_3 ca 2.0 -5.5 wt% (MD 257 is an outlier for Fe_2O_3 and Al_2O_3 contents), $\text{Zr} \leq 85$ ppm, $\text{MgO} > 1.8$ wt%, $\text{Sr} > 420$ ppm, $\text{Nb} < 4$ ppm, $\text{Cr} < 23.5$ ppm and $\text{V} \leq 20$ ppm. There is no distinction between the two groups according to the Co and Ni concentrations.

For sample MD 257 lower CaO values < 7 wt% as detected by PIXE/PIGE, while EDS and LA-ICP-MS recognized higher value $\text{CaO} \geq 7$ wt%. Could the MgO and Sr content be used as a discriminant to determine to which compositional group MD 257 belongs to when the CaO results are ambiguous?

MD 259 has distinctively low concentration of Fe_2O_3 0.41 wt%, along with the lowest Al_2O_3 , Th, U, Cr, Ni, Zn, V, Nb, As, Pb concentrations comparing to other Miranduolo samples. Comparison of this sample to post-medieval glasses that used Ticino river raw materials was done due to low concentrations of the aforementioned elements and the known concentration of Fe_2O_3 (around 0.50 wt%) and specific low trace elements values: REE and $\text{Ce} < 10$ ppm, $\text{Ti} < 70$ ppm, $\text{Zr} < 65$ ppm and $\text{Hf} < 2$ ppm in glasses that used Ticino siliceous pebbles as network former [23]. The MD 259 displays higher values than those glasses, hence disproving the possibility of Ticino pebbles as a source for Miranduolo glasses.

The concentrations of Rb for Lpa-Na-Ca-Si glasses have been used in [22], as a dating discriminant. The $\text{Rb} \leq 30$ ppm date the glasses to 13th-14th century AD, while $\text{Rb} > 30$ ppm date to 15th-16th century AD. In general, the data obtained from Miranduolo and other Tuscan sites fit, except for samples MD 21 and t_62 (Rocca di Campiglia) that show Rb of 39 ppm and 47 ppm. This leaves the possibility that those samples were not archaeologically correctly dated. On the other hand, MD 243 and t_90 (San Vettore) samples are UBpa-Na-Ca-Si glasses, showing ambiguous data 27 ppm and 54 ppm. This could lead to three possibilities. First, there is no apparent pattern for UBpa-Na-Ca-Si glasses; second, the pattern that exists is the same as for Lpa-Na-Ca-Si, meaning that the 13th-14th century glasses have $\text{Rb} \leq 30$ ppm; third, the pattern that exists is the opposite from the Lpa-Na-Ca-Si glasses, meaning that the 13th-14th century glasses have $\text{Rb} > 30$ ppm. Due to only two samples that have been analyzed, further conclusions cannot be made, until appropriate number of analyzed glasses are confirming one of the theoretical possibilities.

The strong positive correlation of $\text{Fe}_2\text{O}_3/\text{TiO}_2$ indicates the presence of Fe_2O_3 as a silica source impurity and is associated with ilmenite (FeTiO_3) which is a heavy mineral constituting fluvial sands. This is supported by the strong positive correlation of TiO_2/Zr , which is expected due to deposition of zircon (ZrSiO_4) which is selectively deposited with ilmenite grains in fluvial sedimentary deposits. Positive correlation of TiO_2/Nb along with the strong positive correlation TiO_2/Zr and $\text{Fe}_2\text{O}_3/\text{TiO}_2$ are explained as mineral impurities in the sandy raw material. Columbite

(FeNb_2O_6), a Nb-containing mineral, can be found selectively deposited with Fe-Ti bearing oxide minerals, including zircon and ilmenite. They are found in sedimentary deposits as heavy mineral placers, as they display high resistivity to erosion. Columbite-bearing mineral deposits are common for granitic rocks and outcrops. Zr/Hf are strongly correlated which, in geochemistry, is a phenomenon that is known and explained. Hf can be found as a substitute for Zr in Zr-bearing minerals. $\text{Fe}_2\text{O}_3/\text{TiO}_2$ and TiO_2/Zr have been used as a discriminant for the local availability, indicating the probability of usage of local silica sand source and presence of iron content as a natural impurity and not an addition of it for modification of the glass composition.

The REE results obtained are the first ones done on Tuscan mid-13th to mid-14th century AD glasses. Thus, the results cannot be compared with other contemporary sites. Strong positive correlation of REE with CaO can be seen for the samples with $\text{CaO} > 7\text{wt}\%$ (meaning mainly ULpa-Na-Ca-Si glasses) which provided a limestone signature.

Miranduolo glasses MD 66, MD 257, MD 272, MD 276 have $\text{MnO} > 0.8\text{ wt}\%$. In literature [1], [3], [5], [6], [8], [9], [12]–[14], [18], [19], [21], [23]–[25], [32]–[37] it is considered that MnO can be used as a decolorant (0.3-0.8 wt%) and a colorant ($>0.8\text{ wt}\%$). But, this is not necessarily valid in practice, as the sample 8 from Siena cathedral with $\text{MnO} \geq 0.8\text{ wt}\%$ is colorless [18]. On the other hand, the difference in the quantity of MnO between colorless and colored samples, is lower than 0.1 wt%. The addition of MnO should propagate either purple or brown color, but the aforementioned Miranduolo samples are yellow (MD 66), green (MD 257 and MD 276) and amber (MD 272). Generally, the pattern of this MnO color propagation and decoloration in these concentrations can be seen in Siena cathedral samples with very low content of iron oxide ($\leq 0.50\text{ wt}\%$), but for higher amounts of iron oxides ($\geq 0.51\text{ wt}\%$) there is no apparent pattern.

The colorless glasses MD 24 and MD 259 have the $\text{MnO} \leq 0.8\text{ wt}\%$. The ratio $\text{Fe}_2\text{O}_3/\text{MnO}$ for PIXE/PIGE to obtain colorless glass seems to be from 1.5-2.0, and for LA-ICP-MS from 1.0-1.5, with $\text{MnO} \leq 0.8\text{ wt}\%$ (Table App.6-1).

What could have been noted that $\text{Sn} \leq 30$ ppm, $\text{Sb} \leq 120$ ppm nor $\text{Pb} \leq 1500$ ppm do not have a decoloring effect on the colored glasses, but might have a coloring effect on the decolorized glasses. For the colored samples (MD 66 and MD 257) with the $\text{Fe}_2\text{O}_3/\text{MnO}$ ratio 1.0-1.5 (LA-ICP-MS) or 1.48-1.58 (PIXE/PIGE) with $\text{MnO} > 0.8$ wt% in both samples the quantity of Cr, Ni, Cu, Zn (LA-ICP-MS) exceeds the one in the colorless samples. For the colored samples (MD 272 and MD 276) with the $\text{Fe}_2\text{O}_3/\text{MnO}$ ratio below 1 three elements of the Cr, Ni, Cu, Zn have higher values than the colorless samples. As the quantity of the samples is not representative, future investigation of this matter for pa-Na-Ca-Si glasses have to be conducted in order to confirm or disprove the possible influence of the quantity of Cr, Ni, Cu and Zn to the quantity of MnO and Fe_2O_3 and the $\text{Fe}_2\text{O}_3/\text{MnO}$ ratio for coloring and decoloring glasses. As stressed in [4] the final color of the glass artefact not solely dependent on the colorants and decolorants amount and/or ratio but also on the furnace atmosphere, melting time, etc.

The extent of recycling of Miranduolo samples is 65%, meaning 13 samples display recycling concentrations of $100 \text{ ppm} \leq \text{Pb}$, Cu, Zn, Sb, $\text{Sn} \leq 1000$ ppm. The recycling concentrations are indicated in [48]. The samples that have not been recycled are: MD 12, MD 139, MD 143, MD 173, MD 193, MD 259 and MD 272. Recycled samples are MD 24, MD 66, MD 67, MD 172, MD 191, MD 222, MD 231, MD 243, MD 256, MD 257, MD 261 and MD 276. The recycling of blue cullet into the batch is possible for samples MD 231 and MD 257 due to recycling amount of Cu. There is no elevation of concentration of Zn that would indicate addition of bronze to the batch. On the other hand MD 261 displays Cu, Zn, $\text{Sn} > 100$ ppm and Pb, Sb > 1000 ppm, possibly indicating recycling of the tesserae. As Nogara samples generally have values around 1000 ppm for the glass fragments, could this be an indication that those samples have been recycled multiple times, while Miranduolo once or few?

As determined through an extensive archaeovitreological corrosion studies, plant ash glasses with $\text{SiO}_2 > 60$ wt% are the least prone to be heavily affected by degradation. Glass components such as Na_2O , K_2O , MgO and CaO when present in higher quantities seem not effectively resist the corrosion as those elements leach out of the glass the easiest and abundantly [42]. The results

obtained with VP-SEM-EDS gave multiple samples with $\text{SiO}_2 \leq 60$ wt%, but the corrosion was present in only 4 samples. Hence, the quantification of the EDS did not seem accurate.

Mid-13th to mid-14th century Miranduolo glasses reveal the following information: Miranduolo glasses are very stable and are not susceptible to degradation. MD 139 with HMgn-Na-Ca-Si composition displays both corrosion morphologies and the thickest corrosion layers. Out of 19 pa-Na-Ca-Si Miranduolo glasses, only three of them display very thin corrosion layers, 2.25 μm to 26.8 μm . All of the corroded glasses were made with Levantine ash, possibly all with unpurified Levantine ash. None of the samples have been found in the same context (meaning stratigraphic unit, *SU*), disabling to assess or precisely determine if the low corrosion rate is dependent on composition, burial conditions or both.

A parallel could possibly be made with Byzantine painted bracelets, dated 11th-13th century, from a site near Isaccea, Romania. Two types could have been distinguished: a) corroded glasses covered in white layer, with exfoliation and reduced transparency; b) glasses that show no signs of deterioration. The authors state that corroded and non-corroded bracelets were buried for thousands of years in the same soil and that they have undergone the same weathering processes [87]. Unfortunately, to make a valid comparison, no chemical data on the glass composition of the bracelets have been published, nor there is more detail on the context of their recovery, as they could all possibly be recovered from a diverse *SU*.

A possible explanation for diminishing the deterioration of the glass is the higher Al_2O_3 content. Solely, the higher Al_2O_3 content (≥ 2 wt%) does not seem to be the only factor, but possibly might include the $\text{Fe}_2\text{O}_3 \geq 1$ wt%, with a specific ratio of $\text{Al}_2\text{O}_3/\text{Fe}_2\text{O}_3$, including the effect of burial conditions.

PIXE/PIGE chemical mappings of the corrosion layers confirm their morphologies detected with VP-SEM-EDS. Although it was acknowledged that the corruptions are considered to be heterogeneous, the quantification of each layer of the corrosion patina further confirms it. Interestingly, the CaO content in each stratification layer of sample MD 259 is higher than in the

pristine glass, as in the corrosion layer of MD 143. The Ca is considered to leach out of the glass, with depleting values in the corrosion layer. Such is confirmed for the corruptions analyzed with LA-ICP-MS. Could this indicate that the accuracy of CaO content with the PIXE/PIGE might be lower than those obtained by LA-ICP-MS? If so, the CaO contents should not be considered for the compositional determination. In general the average results of corrosion layers of MD 139 and MD 259 analyzed with both techniques are in good agreement.

What can be concluded for the values obtained with 50 μm and 15 μm laser ablation beam for MD 143 and MD 259 is that higher values are for Na_2O , MgO , Al_2O_3 , P_2O_5 , TiO_2 , MnO , V , Cr , Co , Ni , Cu , As , Sr , Y , Zr , Sb , Ba , Ce , Pr , Nd , Sm and Lu when ablated with 15 μm . Lower values in both samples are for Zn , Er , Yb and Pb . Other elements do not display a recognizable pattern. As both glasses are classified as ULpa-Na-Ca-Si glasses, the compositional difference could not be taken into account as a source for this discrepancies.

Only few archaeovitreological studies have compared the results of diverse analytical techniques that have been used. The importance of the accuracy and precision between techniques is crucial as the composition of the glass is referenced to other known glasses. The quantification deviation between techniques of even few percent can theoretically mean a different glass composition. Therefore, the quantification accuracy and precision of each technique needs to be included when interpreting the results and drawing conclusions.

Finally, a correlation was tried to be established between the physico-chemical features or glass composition of Miranduolo glass fragments and any possible archaeological parameter, such as the phase, typology, area, or context of the finds. No such correlation nor distinction could have been made.

Comparing the results to archaeovitreological studies of the contemporary fragments/objects generally those studies have samples of a wider time frame, encompassing few centuries. The ones that have been compared are 13th-14th century. Only Val Gargassa, Genova is being dated from 13th-16th century. The data have been compared according to each technique that has been

used in this study. Therefore, EMPA results from Rocca di Asolo and Cathedral of Siena would not be implemented.

Another issue encountered in these analyses is that not all the elements that have been analyzed as in Miranduolo glasses, making the complete comparison not possible.

The VP-SEM-EDS results that have been compared with Miranduolo are Santa Cristina and Val Gargassa, Genova. It seems that the basic glass recipe used was widely dispersed. Santa Cristina seems improbable as a glassmaking workshop that provided glasses to Miranduolo due to concentration of $\text{CaO} > 12 \text{ wt\%}$, and a general usage of purer raw materials, with $\text{Fe}_2\text{O}_3 < 0.5 \text{ wt\%}$ and $\text{Al}_2\text{O}_3 < 1 \text{ wt\%}$. The already mentioned sample MD 259 that has low Fe_2O_3 content, was tried to be correlated with Santa Cristina glasses, but due to $\text{Al}_2\text{O}_3 2.03 \text{ wt\%}$ of MD 259 this seems improbable. The concentrations of Fe_2O_3 , Al_2O_3 and MgO of Val Gargassa near Genova (Liguria) samples do not display the same pattern as Miranduolo pattern. Hence, that glass workshop can also be disregarded as a probable production center for Miranduolo glasses.

PIXE/PIGE data could only be compared with Savona near Altare (Liguria). The data presented display a Fe_2O_3 content which is usually $< 1 \text{ wt\%}$, while $\text{Al}_2\text{O}_3 > 4 \text{ wt\%}$ and $\text{MgO} > 3 \text{ wt\%}$, which is not consistent with Miranduolo samples. Although there is a strong positive correlation of $\text{Fe}_2\text{O}_3/\text{TiO}_2$, there is no TiO_2/Zr strong positive correlation, indicating a different local silica source used, probably a regional Ligurian. There is not a correlation of CaO with MgO nor Sr . Trace elements differentiate in concentrations from Miranduolo glasses, with the most pronounced results for Rb and Nb values. In Savona samples $\text{Rb} \geq 50 \text{ ppm}$, $\text{Nb} \geq 40 \text{ ppm}$, in Miranduolo $\text{Rb} \leq 30 \text{ ppm}$, $\text{Nb} \leq 20 \text{ ppm}$ (except one sample). Thus, all of the data discriminate the possibility of Altare provenance. What has to be stressed is sample 1421 which is not recycled HMgn-Na-Ca-Si glass the same as MD 139.

The LA-ICP-MS results could be compared with Tuscan sites (Rocca di Campiglia, San Vettore, Germagnana, Poggio Imperiale and Santa Cristina), and Nogara, Verona samples only for Cr , Co , Ni , Cu , Zn , As . The ICP-MS data for Santa Cristina are scarce and not conclusive. Nogara samples

display $\text{Cu} > 300$ ppm and $\text{As} > 5$ ppm, while Miranduolo glasses do not have as high values, again making Nogara an improbable place of production for Miranduolo glasses.

The data from the Tuscan sites (excluding Santa Cristina), seem corresponsive to Miranduolo glasses. Sample t_63 from Rocca di Campiglia is compositionally HMgn-Na-Ca-Si glass as MD 139. The Fe_2O_3 , Al_2O_3 , MgO values are in the frame of Miranduolo glasses. The extent of the recycling is not pronounced. Only 3 out of 10 Tuscan samples have been recycled. Only elevated Pb concentrations and in one sample Pb and Sn concentrations are present. Only t_90 from San Vettore has extremely high Pb concentrations which surpass 4000 ppm. Interestingly, the t_63 is not a recycled glass as MD 139. The concentrations of other trace element suggest the same provenance, although the Sr and Ba concentrations are somewhat higher. This could indicate the addition of different calcites into the batch.

6. Conclusion

This thesis is a successful example of an archaeovitreological study, which combines both the scientific methodology and archaeological interpretation, being a solid bridge between Science and Humanities. The sole purpose of the analyses is not only determining the glass composition, but our aim is to do our best effort in revealing any aspect of the history that the fragments/objects we are analyzing are linked to.

More attention is needed in making a consensus on determining the protocol and concentrations/ratios of oxides/elements for glass classification. Due to this non-existent protocol, terminological issues occur. That combined with not precisely dated contexts has misinterpretations of results as a consequence. The need for coded classification is stressed as a possible solution.

Comparing VP-SEM-EDS to PIXE/PIGE and LA-ICP-MS, it proved to be a semi-quantifying method, giving the insight into a general glass composition. It has been a tremendously helpful technique for detecting corrosion layers, measuring the glasses' thickness and the size of the bubbles, and accurately portraying the glass consistency as homogeneous. The latter was confirmed by PIXE/PIGE chemical maps and comparing the quantification results between spots for one sample with LA-ICP-MS.

More accurate and precise techniques such as PIXE/PIGE and LA-ICP-MS are a necessity to determine the in-depth information on the glasses. Those include the purity and provenance of raw materials used, the production technique (usage of purification processes of ashes, addition of calcite, origin of calcite), effect of the addition of the (de)colorants, extent of recycling, extent of import of raw materials and/or finished glass objects, etc.

Miranduolo site is among first settlements, if not the first, where the samples have been distinctively selected according to the typology, colors, phases and areas they have been recovered from, along with the socio-economic and political features that are distinctive on the

site: the dominant and ruling area of the noble family of Cantieri stressed out with ditches; the surrounding village. The life of the village was on decline, comparing to the previous periods. The distinction between the ruling and the ruled has been more prominent in the anteceding periods, as with the distinction of animal bone concentration that has been extremely higher in the noble family area and with having the monopole over the crops by placing the silos' under immediate surveillance of the noble family. The gap is less visible in the Period II, as the site has been only used possibly as a getaway residence. Hence, the glass artefacts do not display any differentiation between the phases nor areas that they have been unearthed from. Possibly, the information obtained that reveals that no connection between any archaeological and scientific factor can be distinguished, hence only indicating that the glass as a product was a luxury item of the time, present in small number of fragments and dispersed randomly throughout extension of Miranduolo. Archaeovitreological studies should be done on the artefacts from Period III to Period VIII as it would possibly be an indication of the two different socio-economic and political classes.

Although local factories have been erected in the period investigated, it is clear that the Cantieri family was not following any tradition of glass procurement, for example an import of highly appreciated Venetian glass.

What can be induced is that the glass masters have been highly skilled. They used local silica and possibly calcite sources, knew the ash purification processes, possibly consciously added certain amounts of decolorants to obtain different hues, recycled the glass, added calcite into the batch to make the glass more stable and simultaneously more expensive. The addition of calcite risen the melting temperature of the glass and more fuel was need to obtain such temperatures. A clear proof of the use of different silica sources between ULpa-Na-Ca-Si and PLpa-Na-Ca-Si also indicates different production practices for different glass sub-types. They generally produced high quality glasses which were not prone to corrode with standardized 13th-14th century tableware typology. Finally, their skills were accentuated with possibility of making decorations, highly homogeneous matrix and the ability to blow the glass as thin as *ca* 300 μm . Due to the fact

that no distinction in production can be made temporally, through phases, the same glassmaking procedures were used at least a century.

All of these could lead to a conclusion that the establishment of Tuscan glassmaking factories was a well-thought economical decision, possibly only aimed at a specific market. The market that includes prominent individuals with the socio-economic and political power, which is displayed in owning numerous properties: noble families, such as Cantieri, which has extravagant properties all around Tuscany. If this type of buyers were the main target, skillful glass masters with experience would have been employed.

“Equal” composition (at least for Fe_2O_3 , Al_2O_3 , MgO , P_2O_5 wt%) can be distinguished for 13th-14th Venetian glasses. This possibly implies a general “recipe” trend or that the Venetian glass masters were the ones who placed in these new Tuscan glassmaking workshops. Although the basic glass recipe seems to be dispersed in mid-13th to mid-14th century AD Venice, Liguria and Tuscany regions, some of the glass factories seem improbable as Miranduolo’s glass suppliers. It includes both Ligurian glass factories, Val Gargassa near Genova and Savona near Altare and Santa Cristina. Compositional similarity can be distinguished between Miranduolo and glass artefacts from Poggio Imperiale, Rocca di Campiglia, San Vettore and Germagnana. The two latter are glass factories. Thus, San Vettore and Germagnana seem probable candidates as Miranduolo’s glass supplier. On the other hand, one should take in consideration the possibility of other Tuscan glass factories that have not been unearthed and that could have used local raw material sources as did San Vettore and Germagnana.

Interestingly, the HMgn-Na-Ca-Si glass has been proven to be made completely as a new glass, not imputing any cullets nor tesserae, and being made with local raw materials, both in Tuscany and Liguria. This implies possibly a uniform knowledge for production of this compositional group, at least for those two regions.

7. Bibliography

- [1] G. Artioli, *Scientific methods and cultural heritage: an introduction to the application of materials science to archaeometry and conservation science*. Oxford: Oxford University Press, 2012.
- [2] T. Rehren and I. Freestone, "Pattern in Glass Use in the Roman and Byzantine Worlds: A Report on Current Research at the Institute of Archaeology and UCL Qatar," *Archaeol. Int.*, vol. 17, no. 17, pp. 74–78, 2014.
- [3] K. Janssens, Ed., *Modern Methods for Analysing Archaeological and Historical Glass*. Chichester: Wiley, 2013.
- [4] T. D. Price and J. H. Burton, *An Introduction to Archaeological Chemistry*. New York: Springer, 2011.
- [5] G. Rapp, *Archaeomineralogy*. Heidelberg: Springer-Verlag, 2009.
- [6] M. A. Pollard and C. Heron, *Archaeological Chemistry*, vol. 1. Cambridge: The Royal Society of Chemistry, 2008.
- [7] R. H. Shackelford, J. F.; Doremus, Ed., *Ceramic and Glass Materials: Structure, Properties and Processing*. New York: Springer Science+Business Media, LLC, 2008.
- [8] G. Salviulo, A. Silvestri, G. Molin, and R. Bertinello, "An archaeometric study of the bulk and surface weathering characteristics of Early Medieval (5th-7th century) glass from the Po valley, northern Italy," *J. Archaeol. Sci.*, vol. 31, pp. 295–306, 2004.
- [9] S. Davison, *Conservation and Restoration of Glass*. Oxford: Butterworth-Heinemann, 2003.
- [10] T. Calligaro, "PIXE in the study of archaeological and historical glass," *X-Ray Spectrom.*, vol. 37, pp. 169–177, 2008.
- [11] B. Gómez-Tubío, M. Á. Ontalba Salamanca, I. Ortega-Feliu, M. Á. Respalda, F. Amores Carredano, and D. González-Acuña, "PIXE-PIGE analysis of late roman glass fragments," *Nucl. Instruments Methods Phys. Res. Sect. B Beam Interact. with Mater. Atoms*, vol. 249, no. 1–2 SPEC. ISS., pp. 616–621, 2006.
- [12] K. H. Wedepohl, K. Simon, and A. Kronz, "Data on 61 chemical elements for the characterization of three major glass compositions in late antiquity and the middle ages,"

- Archaeometry*, vol. 53, no. 1, pp. 81–102, 2011.
- [13] A. Zucchiatti, L. Canonica, P. Prati, A. Cagnana, S. Roascio, and A. C. Font, “PIXE analysis of V-XVI century glasses from the archaeological site of San Martino di Ovaro (Italy),” *J. Cult. Herit.*, vol. 8, no. 3, pp. 307–314, 2007.
- [14] N. Schiavon, A. Candeias, T. Ferreira, M. Da Conceicao Lopes, A. Carneiro, T. Calligaro, and J. Mirao, “A Combined Multi-Analytical Approach for the Study of Roman Glass from South-West Iberia: Synchrotron micro-XRF, External-PIXE/PIGE and BSEM-EDS,” *Archaeometry*, vol. 54, no. 6, pp. 974–996, 2012.
- [15] I. Freestone, “Looking into Glass,” in *Science and the Past*, S. Bowman, Ed. London: British Museum Press, 1991, pp. 37–57.
- [16] P. Degryse, I. Freestone, S. Jennings, and J. Schneider, “Technology and provenance study of Levantine plant ash glass using Sr-Nd isotope analysis,” in *Glass in Byzantium – Production, Usage, Analyses*, D. Drauke, J. Keller, Ed. Mainz: Römisch-Germanisches Zentralmuseum, 2010, pp. 83–91.
- [17] M. Tite, A. Shortland, and S. Paynter, “The Beginnings of Vitreous Materials in the Near East and Egypt,” *Acc. Chem. Res.*, vol. 35, pp. 585–593, 2002.
- [18] E. Basso, M. P. Riccardi, B. Messiga, M. Mendera, D. Gimeno, M. Garcia-Valles, J. L. Fernandez-Turiel, F. Bazzocchi, M. Aulinas, and C. Tarozzi, “Composition of the base glass used to realize the stained glass windows by Duccio di Buoninsegna (Siena Cathedral, 1288-1289 AD): A geochemical approach,” *Mater. Charact.*, vol. 60, no. 12, pp. 1545–1554, 2009.
- [19] N. Carmona, I. Ortega-Feliu, B. Gómez-Tubío, and M. A. Villegas, “Advantages and disadvantages of PIXE/PIGE, XRF and EDX spectrometries applied to archaeometric characterisation of glasses,” *Mater. Charact.*, vol. 61, no. 2, pp. 257–267, 2010.
- [20] S. Cagno, M. Brondi Badano, F. Mathis, D. Strivay, and K. Janssens, “Study of medieval glass fragments from Savona (Italy) and their relation with the glass produced in Altare,” *J. Archaeol. Sci.*, vol. 39, pp. 2191–2197, 2012.
- [21] A. Aerts, B. Velde, K. Janssens, and W. Dijkman, “Change in silica sources in Roman and post-Roman glass,” *Spectrochim. Acta - Part B At. Spectrosc.*, vol. 58, pp. 659–667, 2003.
- [22] S. Cagno, M. Mendera, T. Jeffries, and K. Janssens, “Raw materials for medieval to post-medieval Tuscan glassmaking: new insight from LA-ICP-MS analyses,” *J. Archaeol. Sci.*, vol. 37, pp. 3030–3036, 2010.

- [23] M. Verità, "Secrets and innovations of Venetian glass between the 15th and the 17th centuries: raw materials, glass melting and artefacts," in *Proceedings of the Study Days on Venetian Glass, Approximately 1600's*, 2014, pp. 53–68.
- [24] I. Freestone, M. J. Hughes, and C. P. Stapleton, *The composition and production of Anglo-Saxon glass*. London: The British Museum, 2008.
- [25] C. N. Duckworth, R. C. de la Llave, E. W. Faber, D. J. G. Edwards, and J. Henderson, "Electron Microprobe Analysis of 9th-12th Century Islamic Glass from Córdoba, Spain," *Archaeometry*, vol. 57, no. 1, pp. 27–50, 2015.
- [26] I. Freestone, "The provenance of ancient glass through compositional analysis," in *Materials Research Society Symposium Proceedings*, 2005, vol. 852, p. 008.1.1-008.1.13.
- [27] F. Gallo, "Glass in Northern Adriatic area from Roman to Medieval period: a geochemical approach for provenance and production technologies," University degli Studi di Padova, 2012.
- [28] A. Silvestri and A. Marcante, "The glass of Nogara (Verona): a ' window ' on production technology of mid- Medieval times in Northern Italy," *J. Archaeol. Sci.*, vol. 38, pp. 2509–2522, 2011.
- [29] Y. Barkoudah and J. Henderson, "Plant ashes from Syria and the manufacture of ancient glass: ethnographic and scientific aspects," *J. Glass Stud.*, vol. 48, pp. 297–321, 2008.
- [30] Ž. Šmit and M. Kos, "Investigations of Medieval Glass by a Combined PIXE/PIGE Method: Glassmaking a facon de Venise," in *X-rays for Archaeology*, I. Uda, M.; Demortier, G.; Nakai, Ed. Dodrecht: Springer, 2005, pp. 133–122.
- [31] W. B. Stern and Y. Gerber, "Ancient Potassium-Calcium Glass and its Raw Materials (Wood-Ash, Fern-Ash, Potash) in Central Europe," *Mitteilungen der Naturforschenden Gesellschaften beider Basel*, vol. 11, pp. 107–122, 2009.
- [32] S. Quartieri, M. P. Riccardi, B. Messiga, and F. Boscherini, "The ancient glass production of the Medieval Val Gargassa glasshouse: Fe and Mn XANES study," *J. Non. Cryst. Solids*, vol. 351, pp. 3013–3022, 2005.
- [33] R. Bertoncetto, L. Milanese, U. Russo, D. Pedron, P. Guerriero, and S. Barison, "Chemistry of cultural glasses: The early medieval glasses of Monselice's hill (Padova, Italy)," *J. Non. Cryst. Solids*, vol. 306, pp. 249–262, 2002.
- [34] A. Silvestri, G. Molin, and G. Salviulo, "Roman and medieval glass from the Italian area: Bulk characterization and relationships with production technologies," *Archaeometry*,

- vol. 47, no. 4, pp. 797–816, 2005.
- [35] N. Schibille and I. Freestone, “Composition, Production and Procurement of Glass at San Vincenzo al Volturno: An Early Medieval Monastic Complex in Southern Italy,” *PLoS One*, vol. 8, no. 10, pp. 1–13, 2013.
- [36] M. Ubaldi and M. Verità, “Scientific Analyses of Glasses from Late Antique to Early Medieval Archaeological Sites in Northern Italy,” *J. Glass Stud.*, vol. 45, pp. 115–137, 2003.
- [37] N. Schibille, A. Sterrett-Krause, and I. Freestone, “Glass groups, glass supply and recycling in late Roman Carthage,” *Archaeol. Anthropol. Sci.*, pp. 1–19, 2016.
- [38] M. Tite, T. Pradell, and A. Shortland, “Discovery, production and use of tin-based opacifiers in glasses, enamels and glazes from the Late Iron Age onwards: A reassessment,” *Archaeometry*, vol. 50, no. 1, pp. 67–84, 2008.
- [39] I. Freestone, “Theophilus and the composition of Medieval glass,” *Mater. Issues Art Archaeol. III*, vol. 267, pp. 739–745, 1992.
- [40] M. Melcher and M. Schreiner, “Evaluation procedure for leaching studies on naturally weathered potash-lime-silica glasses with medieval composition by scanning electron microscopy,” *J. Non. Cryst. Solids*, vol. 351, pp. 1210–1225, 2005.
- [41] V. Kontozova-Deutsch, F. Deutsch, R. H. M. Godoi, R. Van Grieken, and K. De Wael, “Urban air pollutants and their micro effects on medieval stained glass windows,” *Microchem. J.*, vol. 99, no. 2, pp. 508–513, 2011.
- [42] B. Messiga and M. P. Riccardi, “Alteration behaviour of glass panes from the medieval Pavia Charterhouse (Italy),” *J. Cult. Herit.*, vol. 7, no. 4, pp. 334–338, 2006.
- [43] J. T. van Elteren, A. Izmer, M. Šala, E. F. Orsega, V. S. Šelih, S. Panighello, and F. Vanhaecke, “3D laser ablation-ICP-mass spectrometry mapping for the study of surface layer phenomena – a case study for weathered glass,” *J. Anal. At. Spectrom.*, vol. 28, no. 7, pp. 994–1004, 2013.
- [44] M. De Bardi, R. Wiesinger, and M. Schreiner, “Leaching studies of potash-lime-silica glass with medieval composition by IRRAS,” *J. Non. Cryst. Solids*, vol. 360, no. 1, pp. 57–63, 2013.
- [45] A. Shortland, L. Schachner, I. Freestone, and M. Tite, “Natron as a flux in the early vitreous materials industry: Sources, beginnings and reasons for decline,” *J. Archaeol. Sci.*, vol. 33, no. 4, pp. 521–530, 2006.

- [46] J. Henderson, "Glass production and Bronze Age Europe," *Antiquity*, vol. 62, no. 236, pp. 435–451, 1988.
- [47] F. Gallo and A. Silvestri, "Medieval glass from Rocca di Asolo (Northern Italy): an archaeometric study," *Archaeometry*, vol. 54, no. 6, pp. 1023–1039, 2012.
- [48] K. H. Wedepohl and K. Simon, "The chemical composition of medieval wood ash glass from Central Europe," *Chemie der Erde - Geochemistry*, vol. 70, pp. 89–97, 2010.
- [49] M. P. Riccardi, V. Marchesi, and B. Messiga, "Melting path-ways of medieval glass from Certosa di Pavia (Italy)," *Thermochim. Acta*, vol. 425, pp. 127–130, 2005.
- [50] S. Cagno, L. Favaretto, M. Mendera, A. Izmer, F. Vanhaecke, and K. Janssens, "Evidence of early medieval soda ash glass in the archaeological site of San Genesio (Tuscany)," *J. Archaeol. Sci.*, vol. 39, no. 5, pp. 1540–1552, 2012.
- [51] M. Verità, A. Renier, and S. Zecchin, "Chemical analyses of ancient glass findings excavated in the Venetian lagoon," *J. Cult. Herit.*, vol. 3, no. 4, pp. 261–271, 2002.
- [52] U. Casellato, F. Fenzi, P. Guerriero, S. Sitran, P. A. Vigato, U. Russo, M. Galgani, M. Mendera, and A. Manasse, "Medieval and renaissance glass technology in Valdelsa (Florence). Part 1: Raw materials, sands and non-vitreous finds," *J. Cult. Herit.*, vol. 4, no. 4, pp. 337–353, 2003.
- [53] P. Theophilus and R. (Trans. . Hendrie, *Theophili, qui et Rugerus, presbyteri et monachi, libri III. de diversis artibus: seu, Diversarum artium schedula*. London: Londini, J. Murray, 1847.
- [54] O. Schalm, K. Janssens, H. Wouters, and D. Caluwé, "Composition of 12–18th century window glass in Belgium: Non-figurative windows in secular buildings and stained-glass windows in religious buildings," *Spectrochim. Acta - Part B At. Spectrosc.*, vol. 62, pp. 663–668, 2007.
- [55] A. M. De Francesco, R. Scarpelli, F. Del Vecchio, and D. Giampaola, "Analysis of early medieval glass from excavations at 'Piazza Bovio', Naples (Italy)," *Archaeometry*, vol. 56, no. SUPPLS1, pp. 137–147, 2014.
- [56] I. Freestone, "Primary glass sources in the mid first millennium AD," in *AIHV Annales du 15e Congrès, 2001*, 2001, pp. 111–115.
- [57] R. H. Brill, *Chemical Analyses of Early Glasses*, vol. 1. Corning, N.Y.: Corning Museum of Glass, 1999.

- [58] R. H. Brill, *Chemical Analyses of Early Glasses*, vol. 2. Corning, N.Y.: Corning Museum of Glass, 1999.
- [59] A. Genga, M. Siciliano, A. Tepore, A. Mangone, A. Traini, and C. Laganara, "An archaeometric approach about the study of medieval glass from Siponto (Foggia, Italy)," *Microchem. J.*, vol. 90, pp. 56–62, 2008.
- [60] J. Henderson, "Electron Probe Microanalysis of Mixed-Alkali Glasses," *Archaeometry*, vol. 30, no. 1, pp. 77–91, 1988.
- [61] M. Valenti, Ed., *Miranduolo in alta Val di Merse (Chiusdino -SI). Archeologia su un sito di potere del Medioevo toscano*. Firenze: All'Insegna del Giglio s. a. s., 2008.
- [62] M. Valenti, Ed., *Miranduolo in alta Val di Merse (Chiusdino – SI). Archeologia su un sito di potere del Medioevo toscano.*, Ebook. University of Siena, 2010.
- [63] "Castello di Miranduolo." [Online]. Available: <http://archeologiamedievale.unisi.it/miranduolo/mediacenter>. [Accessed: 31-Aug-2016].
- [64] G. Di Pasquale, A. Pecci, S. Ricciardi, G. Di Falco, M. P. Buonincontri, and C. Lubritto, "Dal paesaggio alla funzione delle strutture: primi risultati delle analisi archeobotaniche e chimiche a Miranduolo (Siena)," *IV Congr. Naz. di Archeol. Mediev. (Scriptorium dell'Abbazia, Abbazia di San Galgano, Chiusdino-Siena, 26-30 settembre 2006)*, pp. 41–46, 2006.
- [65] C. Renfrew and P. Bahn, "How societies were organized? Social archaeology," in *Archaeology: Theories, Methods and Practice*, 3rd ed., London: Thames & Hudson, 2000, pp. 173–224.
- [66] M. Valenti, "Miranduolo (Chiusdino, SI). Il 'quartiere' di un fabbro di VIII secolo.," 2013. [Online]. Available: <http://www.fastionline.org/docs/FOLDER-it-2013-299.pdf>. [Accessed: 31-Aug-2016].
- [67] D. Stiaffini, "La diffusione del vasellame vitreo da mensa d'uso comune in Toscana durante il Medioevo: il contributo archeologico," in *I Congresso Nazionale di Archeologia Medievale Terza ristampa*, 2015, pp. 416–420.
- [68] M. Kos and Ž. Šmit, "Glassmaking in the Venetian Manner," in *X-rays for Archaeology*, M. Uda, G. Demortier, and I. Nakai, Eds. Dodrecht: Springer, 2005, pp. 159–162.
- [69] S. Cagno, K. Janssens, and M. Mendera, "Compositional analysis of Tuscan glass samples: In search of raw material fingerprints," *Anal. Bioanal. Chem.*, vol. 391, no. 4, pp. 1389–1395, 2008.

- [70] S. Bianchin, N. Brianese, U. Casellato, F. Fenzi, P. Guerriero, P. A. Vigato, L. Nodari, U. Russo, M. Galgani, and M. Mendera, "Medieval and renaissance glass technology in Valdelsa (Florence). Part 2: Vitreous finds and sands," *J. Cult. Herit.*, vol. 6, no. 1, pp. 39–54, 2005.
- [71] M. Aucouturier and E. Darque-Ceretti, "The surface of cultural heritage artefacts: physicochemical investigations for their knowledge and their conservation.," *Chem. Soc. Rev.*, vol. 36, no. 10, pp. 1605–1621, 2007.
- [72] G. Demortier, "Ion Beam Techniques for the Non-destructive Analysis of Archaeological Materials," in *X-rays for Archaeology*, M. Uda, G. Demortier, and I. Nakai, Eds. Dodrecht: Springer, 2005, pp. 67–100.
- [73] J. Pisonero and B. Fern, "Critical revision of GD-MS , LA-ICP-MS and SIMS as inorganic mass spectrometric techniques for direct solid analysis," vol. 24, no. 9, 2009.
- [74] M. Pollard, C. Batt, B. Stern, and S. M. M. Young, *Analytical Chemistry in Archaeology*. Cambridge: Cambridge University Press, 2007.
- [75] E. Doehne and D. C. Stulik, "Application of the environmental scanning electron microscope to conservation science," *Scanning Microsc.*, vol. 4, no. 2, pp. 275–286, 1990.
- [76] G. Danilatos, "Environmental scanning electron microscopy and microanalysis," *Microchim. Acta*, vol. 155, pp. 143–155, 1994.
- [77] P. Kuisma-Kursula, "Accuracy, precision and detection limits of SEM-WDS, SEM-EDS and PIXE in the multi-elemental analysis of medieval glass," *X-Ray Spectrom.*, vol. 29, no. 1, pp. 111–118, 2000.
- [78] R. Falcone, G. Sommariva, and M. Verità, "WDXRF, EPMA and SEM/EDX quantitative chemical analyses of small glass samples," *Microchim. Acta*, vol. 155, no. 1–2, pp. 137–140, 2006.
- [79] J. L. Campbell, G. K. Czamanske, L. MacDonald, and W. J. Teesdale, "Quantitative analysis of major elements in silicate minerals and glasses by micro-PIXE," *Nucl. Instruments Methods Phys. Res. Sect. B*, vol. 130, no. 1–4, pp. 608–616, 1997.
- [80] Ž. Šmit, P. Pelicon, G. Vidmar, B. Zorko, M. Budnar, G. Demortier, B. Gratuze, S. Šturm, M. Nečemer, P. Kump, and M. Kos, "Analysis of medieval glass by X-ray spectrometric methods," *Nucl. Instruments Methods Phys. Res. Sect. B Beam Interact. with Mater. Atoms*, vol. 161, pp. 718–723, 2000.
- [81] Ž. Šmit, P. Pelicon, M. Holc, and M. Kos, "PIXE/PIGE characterization of medieval glass,"

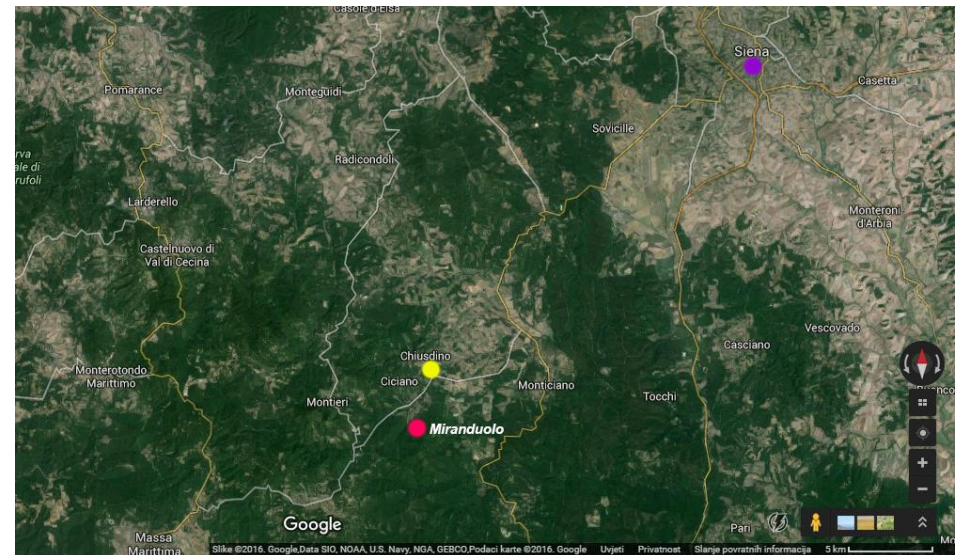
- Nucl. Instruments Methods Phys. Res. Sect. B Beam Interact. with Mater. Atoms*, vol. 189, no. 1–4, pp. 344–349, 2002.
- [82] A. J. G. Mank and P. R. D. Mason, “A critical assessment of laser ablation ICP-MS as an analytical tool for depth analysis in silica-based glass samples,” *J. Anal. At. Spectrom.*, vol. 14, no. 8, pp. 1143–1153, 1999.
- [83] I. Horn, M. Guillon, and D. Günther, “Wavelength dependant ablation rates for metals and silicate glasses using homogenized laser beam profiles - Implications for LA-ICP-MS,” *Appl. Surf. Sci.*, vol. 182, no. 1–2, pp. 91–102, 2001.
- [84] D. Guenther and C. A. Heinrich, “Comparison of the ablation behaviour of 266 nm Nd:YAG and 193 nm ArF excimer lasers for LA-ICP-MS analysis,” *J. Anal. At. Spectrom.*, vol. 14, no. 9, pp. 1369–1374, 1999.
- [85] “U.S. Geological Survey.” [Online]. Available: <http://crustal.usgs.gov/laboratories/icpms/index.html>. [Accessed: 31-Aug-2016].
- [86] A. Constantini, F. A. Decandia, A. Lazzarotto, D. Liotta, R. Mazzei, V. Pascucci, G. Salvatorini, and F. Sandrelli, *Note Illustrative della Carta Geologica d'Italia alla scala 1:50.000. Foglio 296- Siena*. Roma: Università degli Studi di Siena e ISPRA-Servizio Geologico d' Italia, 2005.
- [87] B. Constantinescu, R. Bugoi, G. Niculescu, D. Popovici, and G. Manacu-Adamesteanu, “Studies on Pigments for Ancient Ceramics and Glass Using X-ray Methods,” in *X-rays for Archaeology*, M. Uda, G. Demortier, and I. Nakai, Eds. Dodrecht: Springer, 2005, pp. 163–172.
- [88] “Reperti vitrei Castello di Miranduolo.” [Online]. Available: http://archeologiamedievale.unisi.it/miranduolo/lo-scavo/documentazione/i-materiali/vetri?field_num_inv_vetri_value=&field_area_rif_ceramica_nid=All&field_us_reference_nid=All&field_periodo_ceramica_nid=All&field_struttura_rif_ceramica_nid=All&field_forma_vetri_value_many_to_one=All&field_decoraz_vetri_value_many_to_one=All. [Accessed: 31-Aug-2016].
- [89] “Paerson Correlation Coefficient StatisticsI Guide.” [Online]. Available: <https://statistics.laerd.com/statistical-guides/pearson-correlation-coefficient-statistical-guide.php>.

Appendix 1 – Maps and figures of Miranduolo

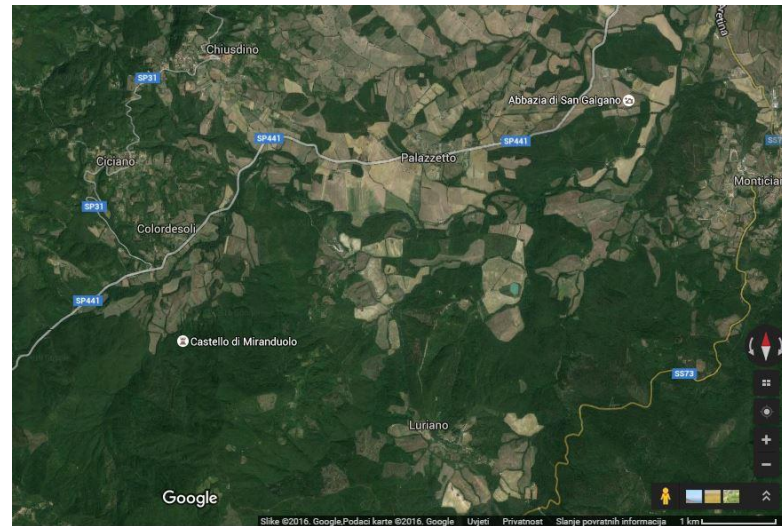
a



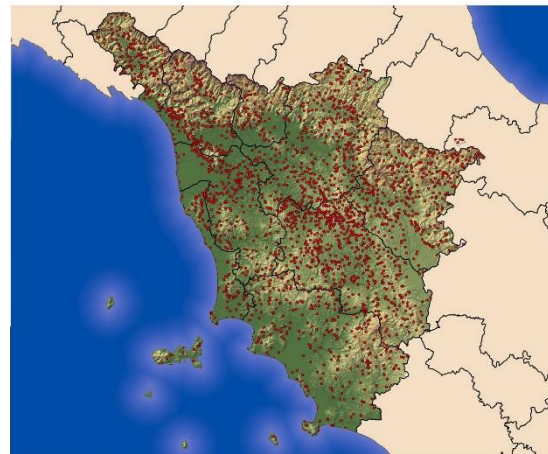
b



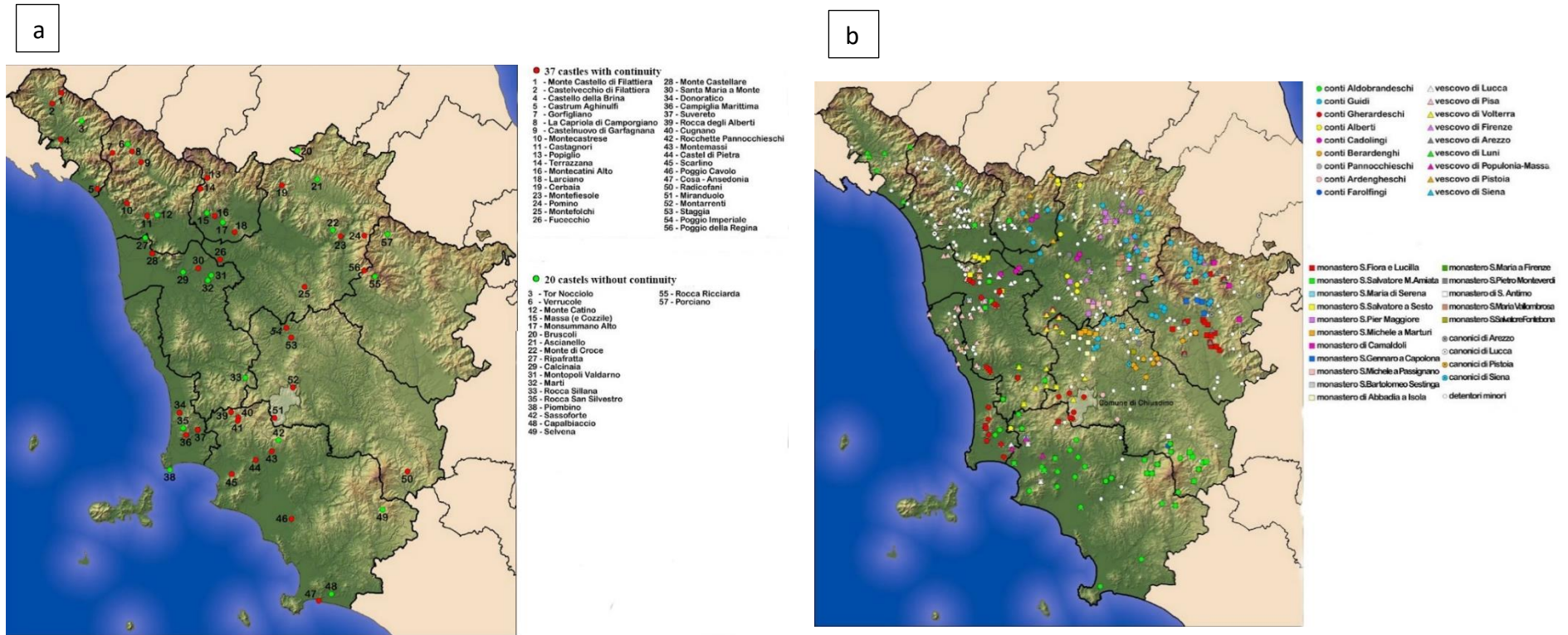
Map App.1-1 – a) In the upper right corner, the map of Italy with a red outline of the Tuscany region. Map with an outlined Tuscany region; b) Position of Miranduolo: 30 km air distance south-west from Siena and 3.9 km air distance south-southwest from Chiusdino. Satellite image via www.maps.google.hr



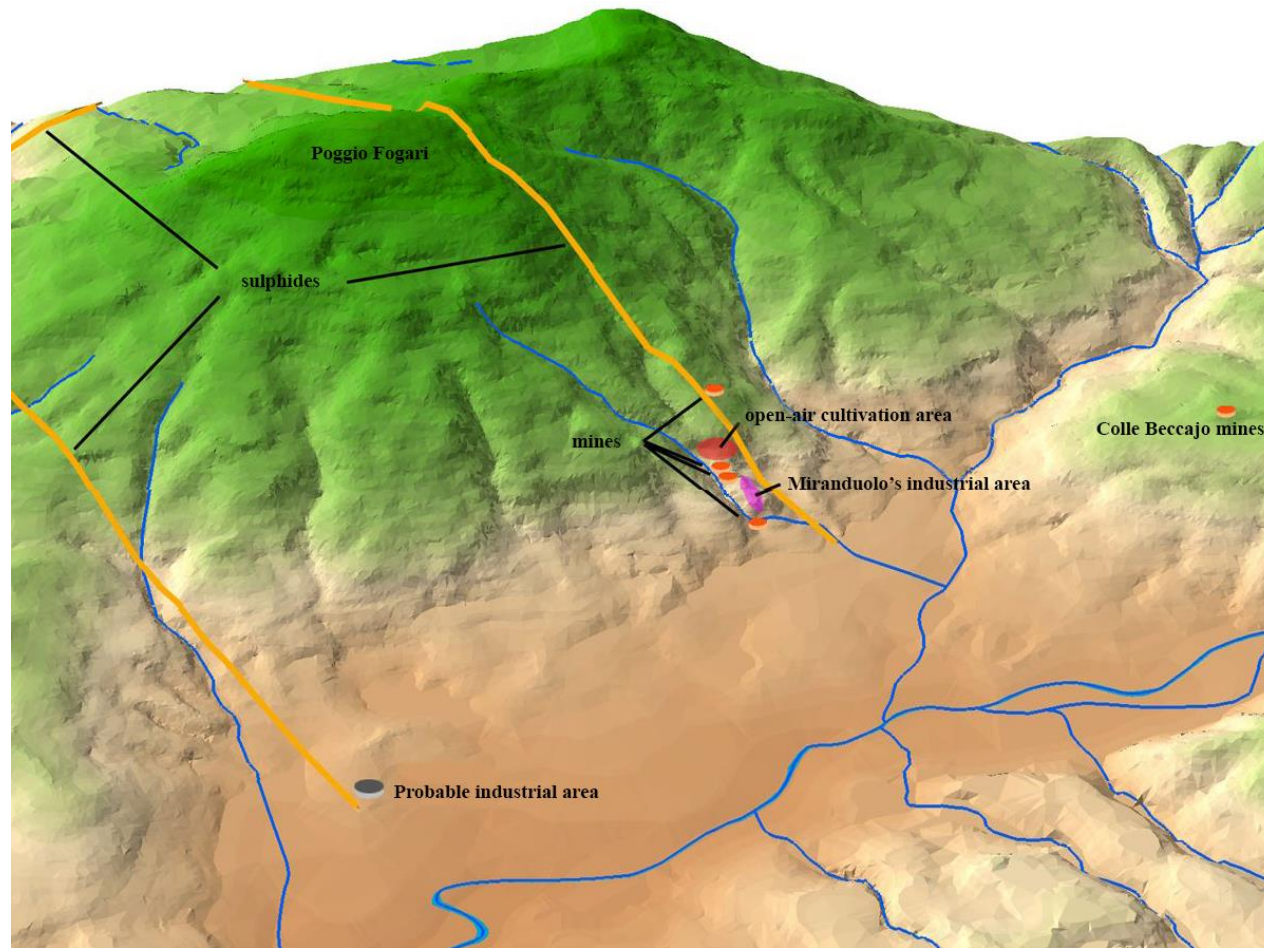
Map App.1-2 - Position of Miranduolo: 3.9 km air distance south-southwest from Chiusdino and 7 km air distance south-west from San Galgano Abbey. Satellite image via www.maps.google.hr



Map App.1-3 - Map of Tuscan fortified hill-sites: 2266 attested, from which 1554 are castles via <http://archeologiamedievale.unisi.it/miranduolo/territorio/cartografia/cartografia-archeologica/contesto-toscana>



Map App.1-4 – a) Map of archaeologically investigated castles. There are 37 castles that show continuation from Early Medieval Period and 20 without continuation from the previous period via <http://archeologiamedievale.unisi.it/miranduolo/territorio/cartografia/cartografia-archeologica/contesto-toscano>; b) Reconstructive map of the “power” in the Tuscan region between 11th and 12th century via <http://archeologiamedievale.unisi.it/miranduolo/territorio/cartografia/cartografia-archeologica/contesto-toscano>



Map App.1-5 Representation of mines around and at Miranduolo via <http://archeologiamedievale.unisi.it/miranduolo/territorio/studio-del-comprensorio/paesaggio-minerario>

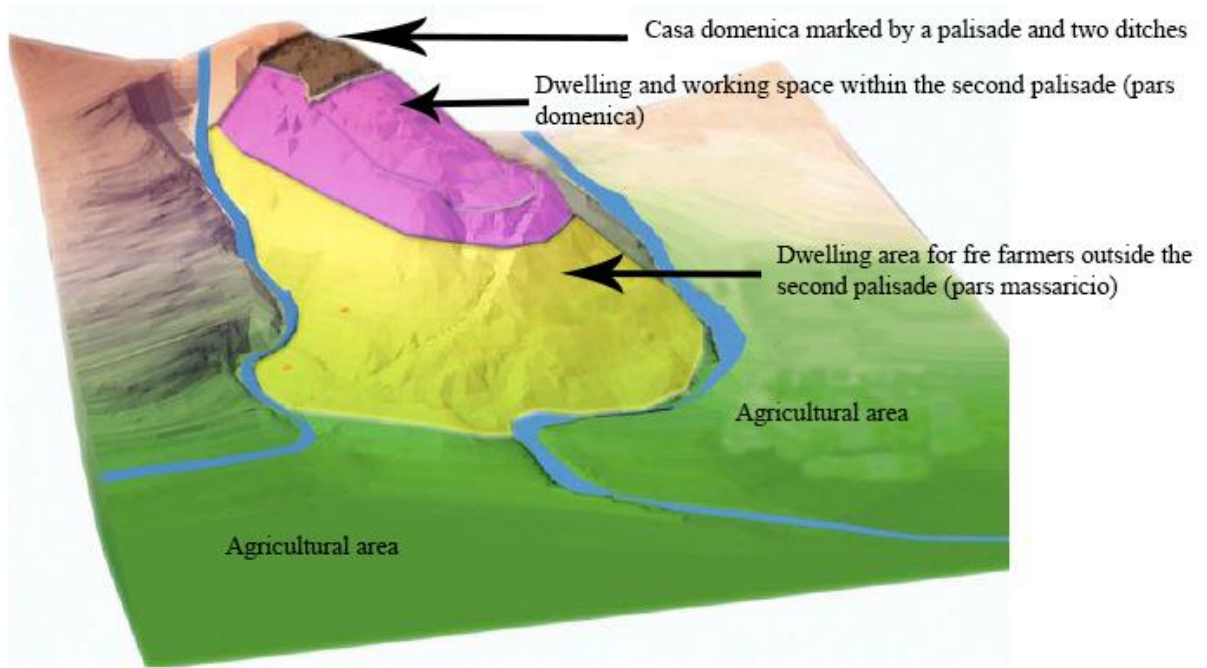


Figure App.1-1 - Reconstruction of the Miranduolo hill dwelling areas from[1].

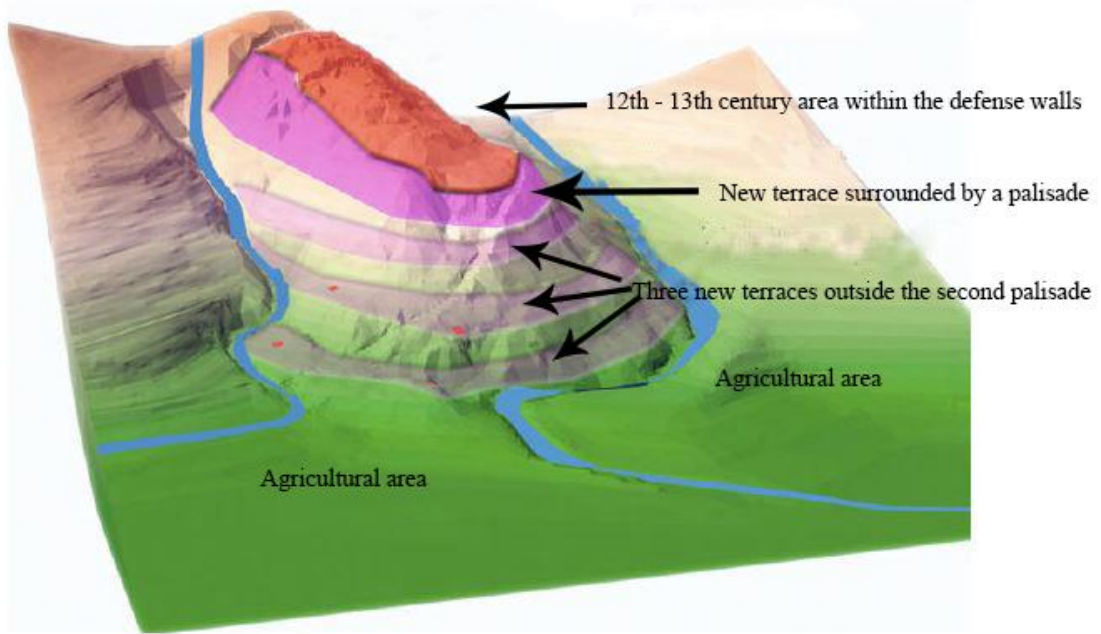


Figure App.1-2 - Reconstruction of 12th-13th century Miranduolo hill from[1].

Appendix 1 – Maps and figures of Miranduolo



Map App.1-6 – Aerial view of Miranduolo. Satellite image via www.maps.google.hr



Map App.1-7 – Representation of the excavated areas at Miranduolo. Areas marked in italics and bold are from where the samples for this study were recovered. Satellite image via www.maps.google.com

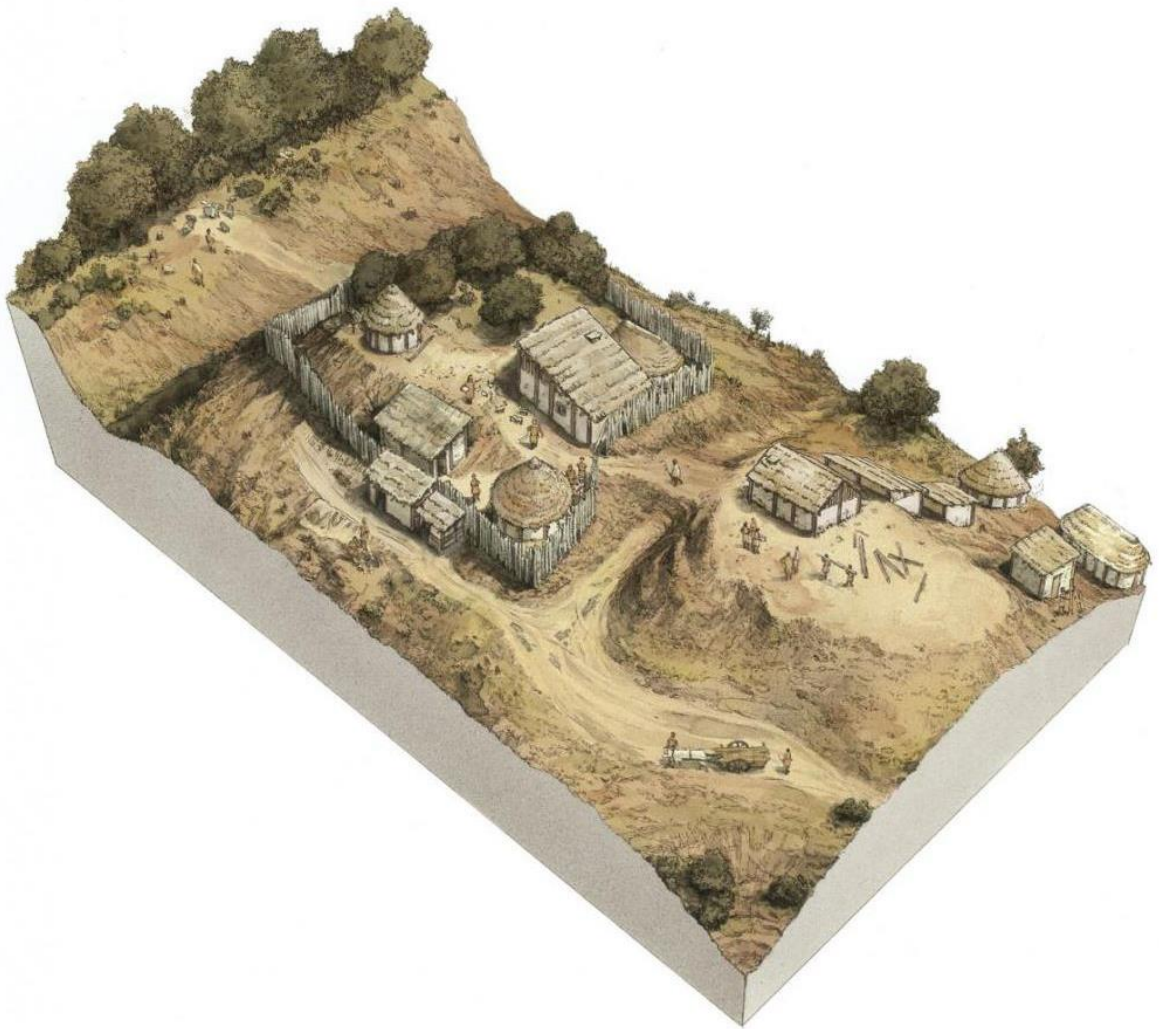


Figure App.1-3 - Reconstruction of 9th century Miranduolo site via <http://archeologiamedievale.unisi.it/miranduolo/la-valorizzazione/ricostruzioni-grafiche>



Figure App.1-4 - Reconstruction of the 10th century Miranduolo site via <http://archeologiamedievale.unisi.it/miranduolo/la-valorizzazione/ricostruzioni-grafiche>

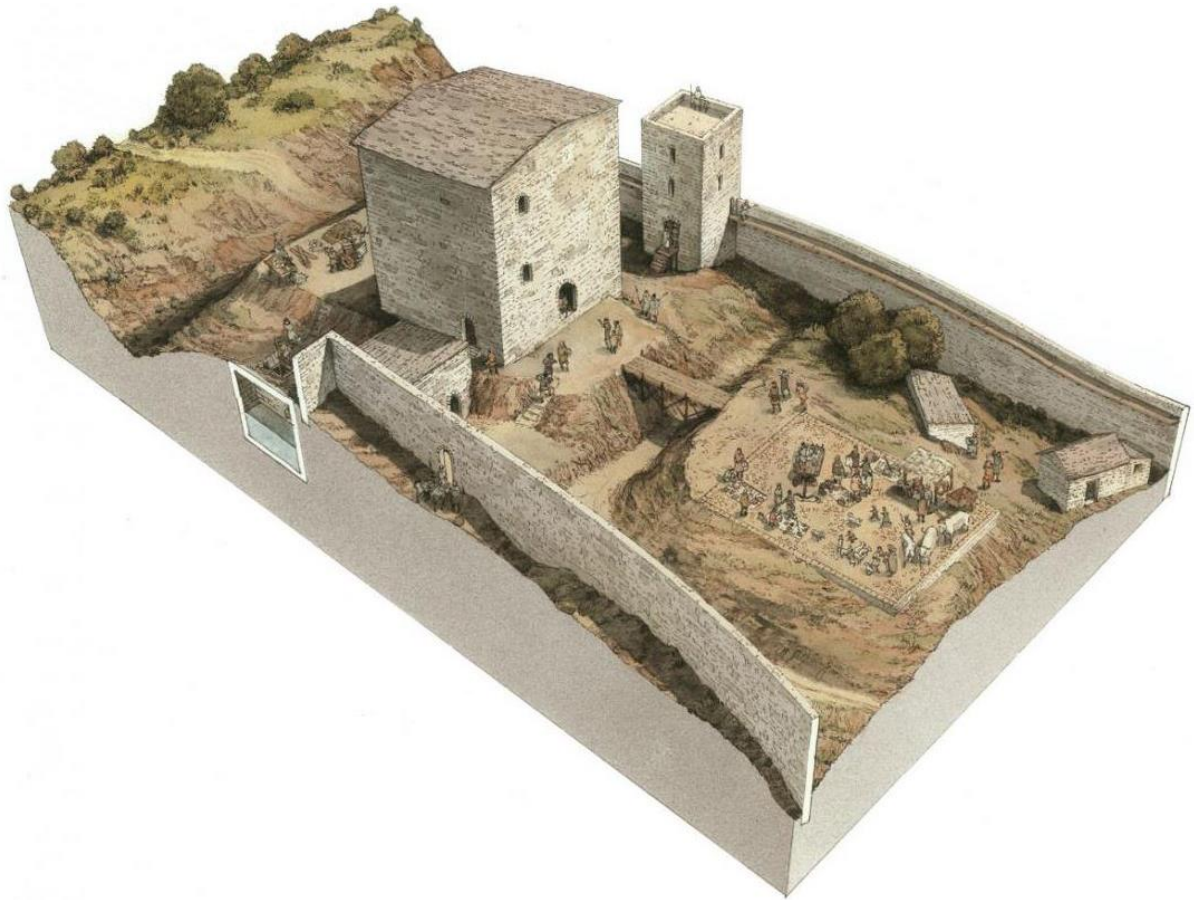


Figure App.1-5 – Reconstruction of 11th-12th century Miranduolo site via <http://archeologiamedievale.unisi.it/miranduolo/la-valorizzazione/ricostruzioni-grafiche>

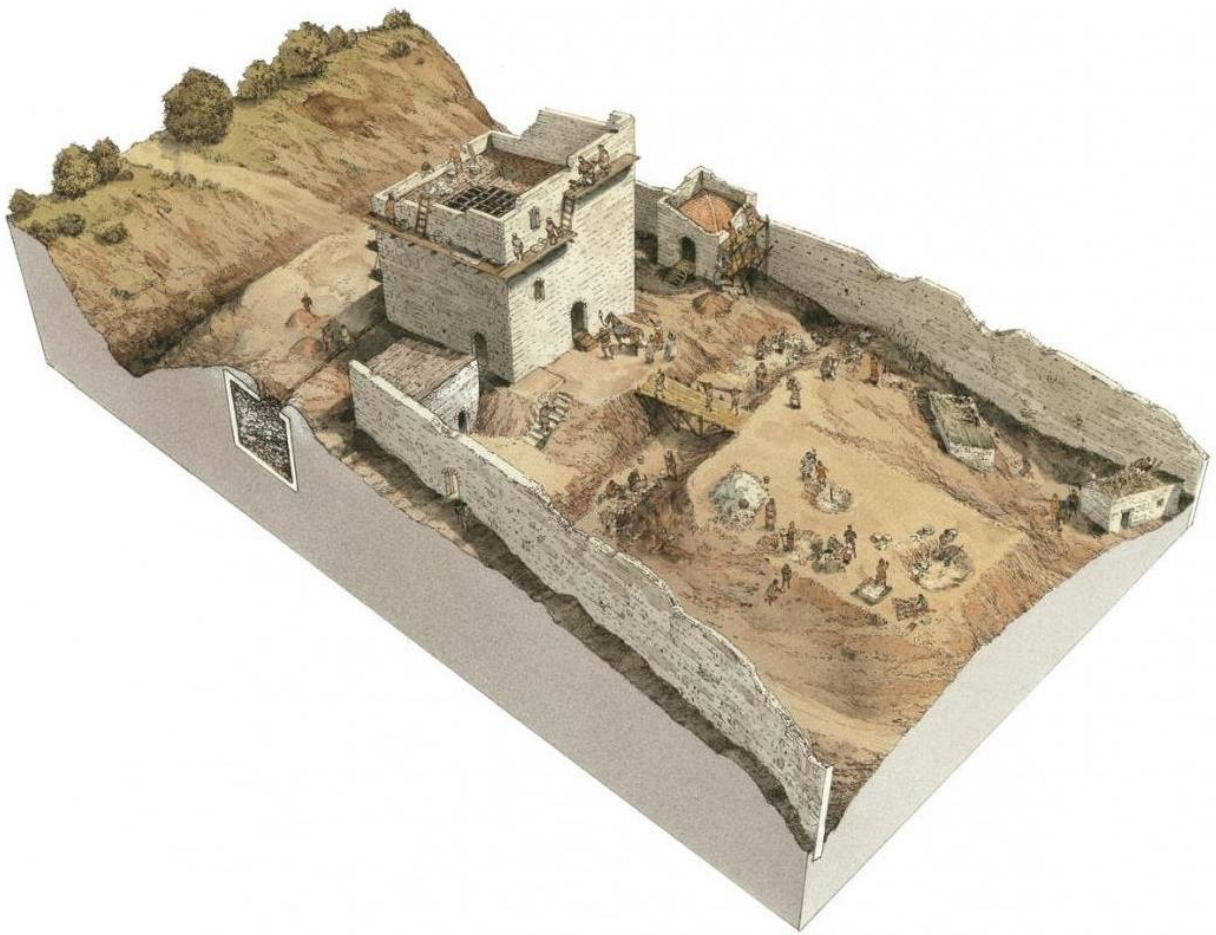


Figure App.1-6 – Reconstruction of 13th century Miranduolo site via <http://archeologiamedievale.unisi.it/miranduolo/la-valorizzazione/ricostruzioni-grafiche>

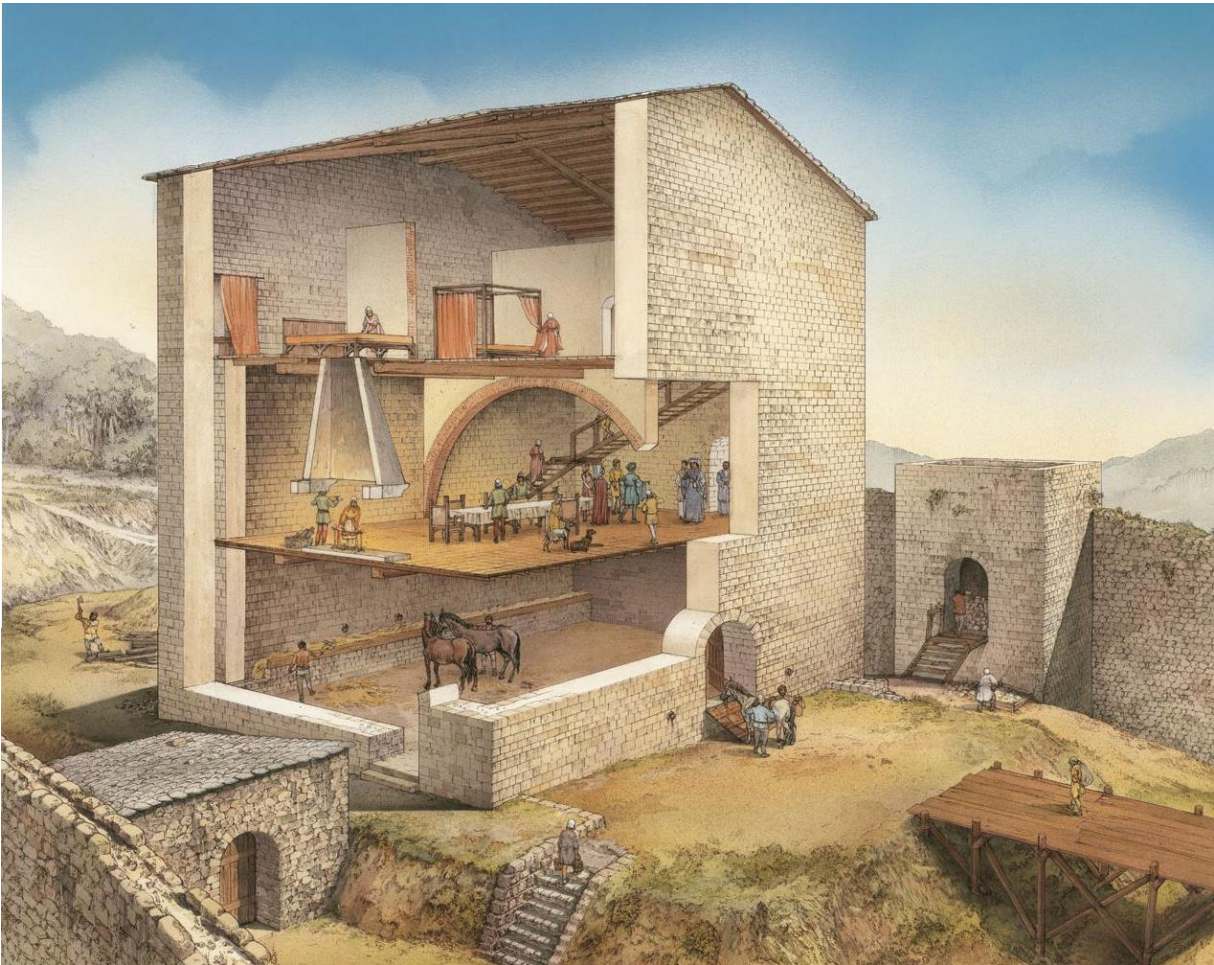
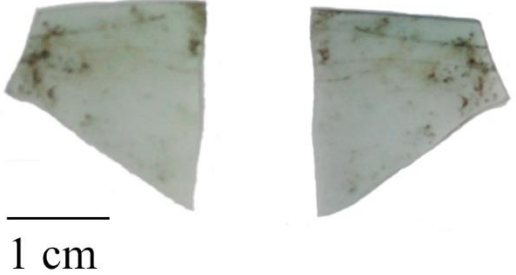

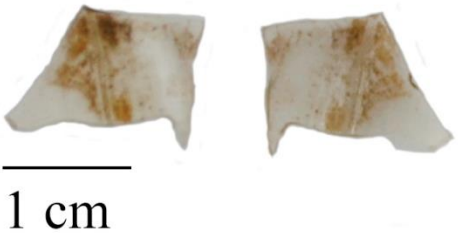


Figure App.1-7 – Reconstruction of the 13th-14th century Cantoni casa dominica via <http://arheologiamedievale.unisi.it/miranduolo/lo-scavo/interpretazioni/castello-tra-xiii-xiv-secolo>


Appendix 2 – Catalog of glass artefacts from Period II


Sample number:	MD 12	
Inventory number:	NI 12	
Object type:	Cup	
Area:	1	
Period:	2	
Phase:	3	
SU:	16	
Structure:	ED05	
Color:	Light Green	
Decorations:	No	
No. of fragments:	1	
Excavation year:	2001	

Sample number:	MD 21	
Inventory number:	NI 21	
Object type:	Bowl	
Area:	1	
Period:	2	
Phase:	2	
SU:	38	
Color:	Green	
Decorations:	No	
No. of fragments:	1	
Excavation year:	2001	

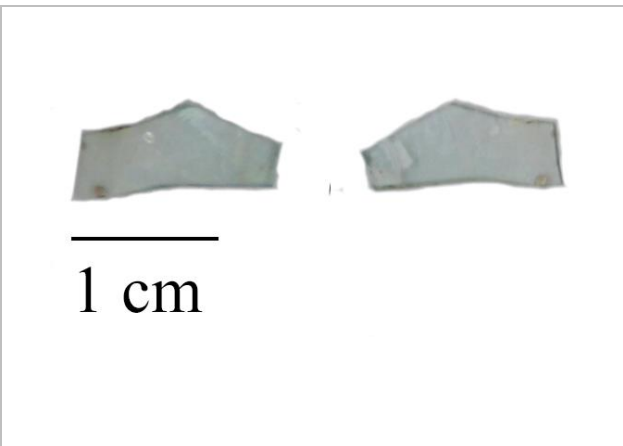
Sample number:	MD 24	
Inventory number:	NI 24	
Object type:	Non-identifiable	
Area:	1	
Period:	2	
Phase:	2	
SU:	28	
Color:	Colorless	
Decorations:	No	
No. of fragments:	2	
Excavation year:	2001	


Appendix 2 – Catalog of glass artefacts from Period II


Sample number:	MD 66	
Inventory number:	NI 66	
Object type:	Cup	
Area:	1	
Period:	2	
Phase:	2	
SU:	375	
Color:	Yellow	
Decorations:	No	
No. of fragments:	1	
Excavation year:	2003	

Sample number:	MD 67	
Inventory number:	NI 67	
Object type:	Non-identifiable	
Area:	1	
Period:	2	
Phase:	2	
SU:	375	
Color:	Amber	
Decorations:	No	
No. of fragments:	1	
Excavation year:	2003	

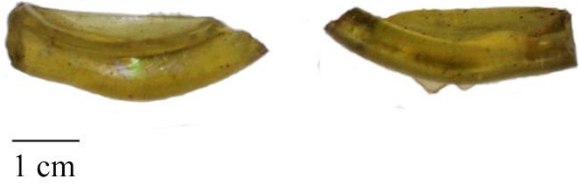
Sample number:	MD 139	
Inventory number:	NI 139	
Object type:	Cup	
Area:	1	
Period:	2	
Phase:	3	
SU:	2008	
Color:	Azure	
Decorations:	No	
No. of fragments:	2	
Excavation year:	2005	


Sample number:	MD 143	
Inventory number:	NI 143	
Object type:	Cup	
Area:	1	
Period:	2	
Phase:	1	
SU:	2020	
Color:	Azure	
Decorations:	No	
No. of fragments:	6	
Excavation year:	2005	

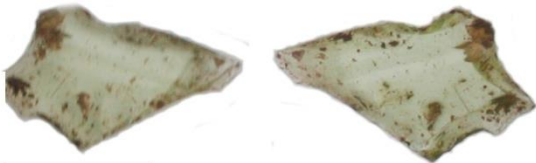
Sample number:	MD 172	
Inventory number:	NI 172	
Object type:	bottle	
Area:	9	
Period:	2	
Phase:	2	
SU:	7	
Color:	Yellow/Green	
Decorations:	No	
No. of fragments:	1	
Excavation year:	2005	

Sample number:	MD 173	
Inventory number:	NI 173	
Object type:	Cup	
Area:	9	
Period:	2	
Phase:	2	
SU:	7	
Color:	Light Yellow	
Decorations:	No	
No. of fragments:	1	
Excavation year:	2005	


Appendix 2 – Catalog of glass artefacts from Period II


Sample number:	MD 191	
Inventory number:	NI 191	
Object type:	Cup	
Area:	8	
Period:	2	
Phase:	1	
SU:	196	
Color:	Yellow/Green	
Decorations:	No	
No. of fragments:	2	
Excavation year:	2006	


Sample number:	MD 193	
Inventory number:	NI 193	
Object type:	Non-identifiable	
Area:	8	
Period:	2	
Phase:	1	
SU:	196	
Color:	Yellow	
Decorations:	No	
No. of fragments:	1	
Excavation year:	2006	


Sample number:	MD 222	
Inventory number:	NI 222	
Object type:	Non-identifiable	
Area:	8	
Period:	2	
Phase:	1	
SU:	196	
Color:	Light Green	
Decorations:	No	
No. of fragments:	7	
Excavation year:	2006	

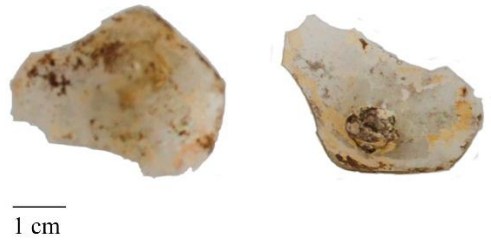
Appendix 2 – Catalog of glass artefacts from Period II

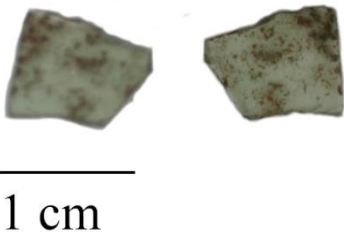
Sample number	MD 231	
Inventory number:	NI 231	
Object type:	Cup	
Area:	1	
Period:	2	
Phase:	1	
SU:	2204	
Structure:	GL01	
Color:	Light Yellow	
Decorations:	No	
No. of fragments:	1	
Excavation year:	2006	

Sample number:	MD 243	
Inventory number:	NI 243	
Object type:	Bowl	
Area:	10	
Period:	2	
Phase:	1	
SU:	2	
Structure:	GL01	
Color:	Dark Green	
Decorations:	No	
No. of fragments:	1	
Excavation year:	2007	

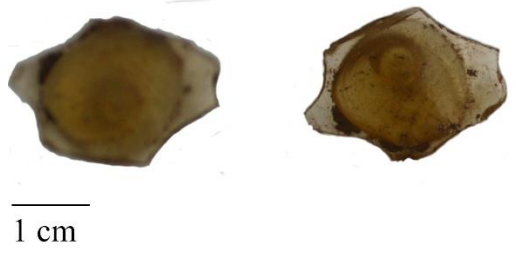
Sample number:	MD 256	
Inventory number:	NI 256	
Object type:	Non-identifiable	
Area:	10	
Period:	2	
Phase:	1	
SU:	66	
Color:	Light Yellow	
Decorations:	No	
No. of fragments:	2	
Excavation year:	2008	


Sample number:	MD 257	
Inventory number:	NI 257	
Object type:	Closed form	
Area:	10	
Period:	2	
Phase:	1	
SU:	47	
Color:	Olive Green	
Decorations:	No	
No. of fragments:	1	
Excavation year:	2008	

Sample number:	MD 259	
Inventory number:	NI 259	
Object type:	Cup	
Area:	8	
Period:	2	
Phase:	3	
SU:	568	
Color:	Colorless	
Decorations:	No	
No. of fragments:	1	
Excavation year:	2008	

Sample number:	MD 261	
Inventory number:	NI 261	
Object type:	Closed form	
Area:	11	
Period:	2	
Phase:	3	
SU:	2	
Color:	Azure	
Decorations:	No	
No. of fragments:	2	
Excavation year:	2008	

Appendix 2 – Catalog of glass artefacts from Period II

Sample number:	MD 272	
Inventory number:	NI 272	
Object type:	Cup	
Area:	11	
Period:	2	
Phase:	3	
SU:	8	
Color:	Amber	
Decorations:	Drops	
No. of fragments:	1	
Excavation year:	2008	

Sample number:	MD 276	
Inventory number:	NI 276	
Object type:	Cup	
Area:	11	
Period:	2	
Phase:	1	
SU:	19	
Structure:	V12c	
Color:	Green	
Decorations:	No	
No. of fragments:	3	
Excavation year:	2008	

Appendix 3 – VP-SEM-EDS plots

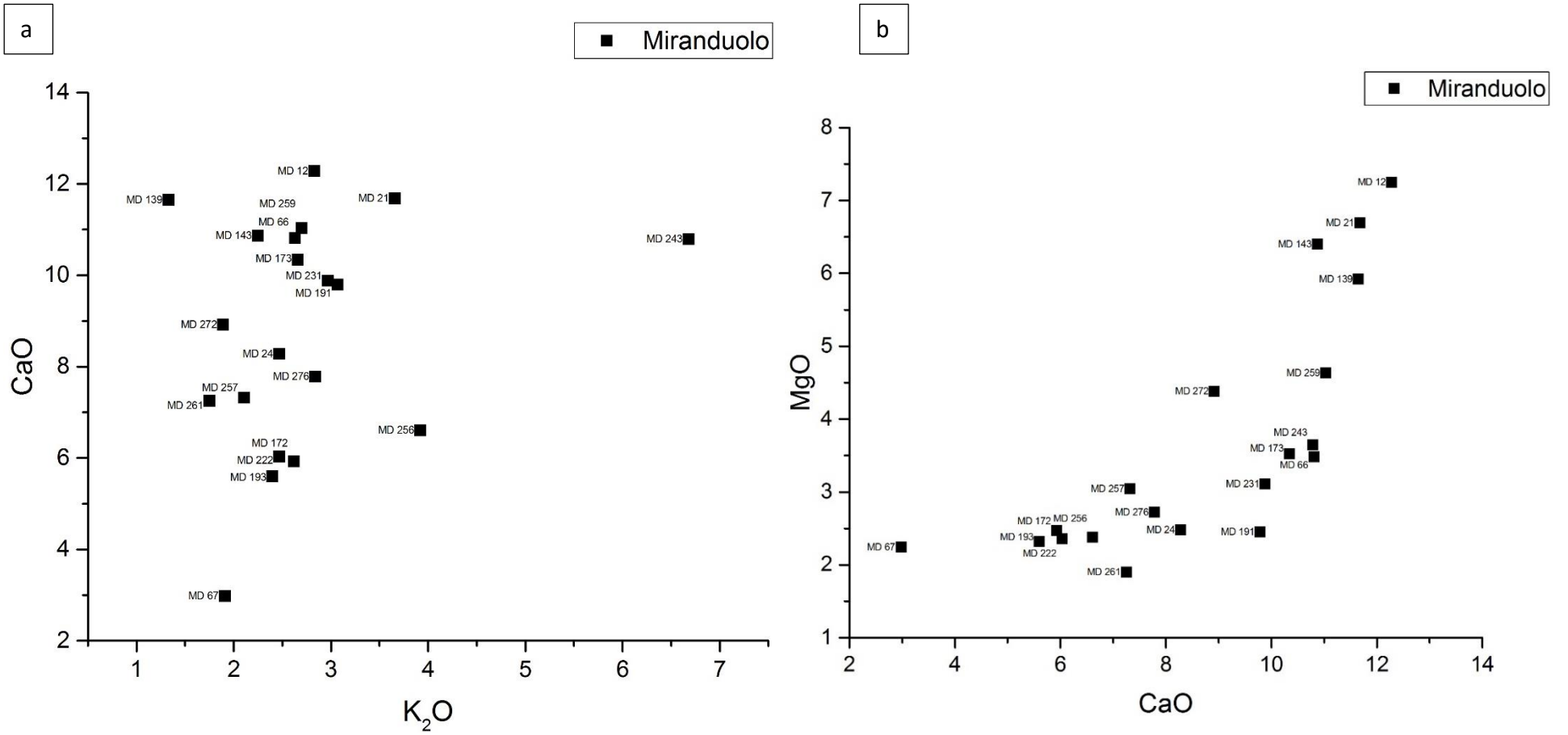


Figure App.3-1 a) Bi-plot of K₂O and CaO with marked Miranduolo sample names; b) Bi-plot of CaO and MgO with marked Miranduolo sample names. The concentrations are presented in wt%.

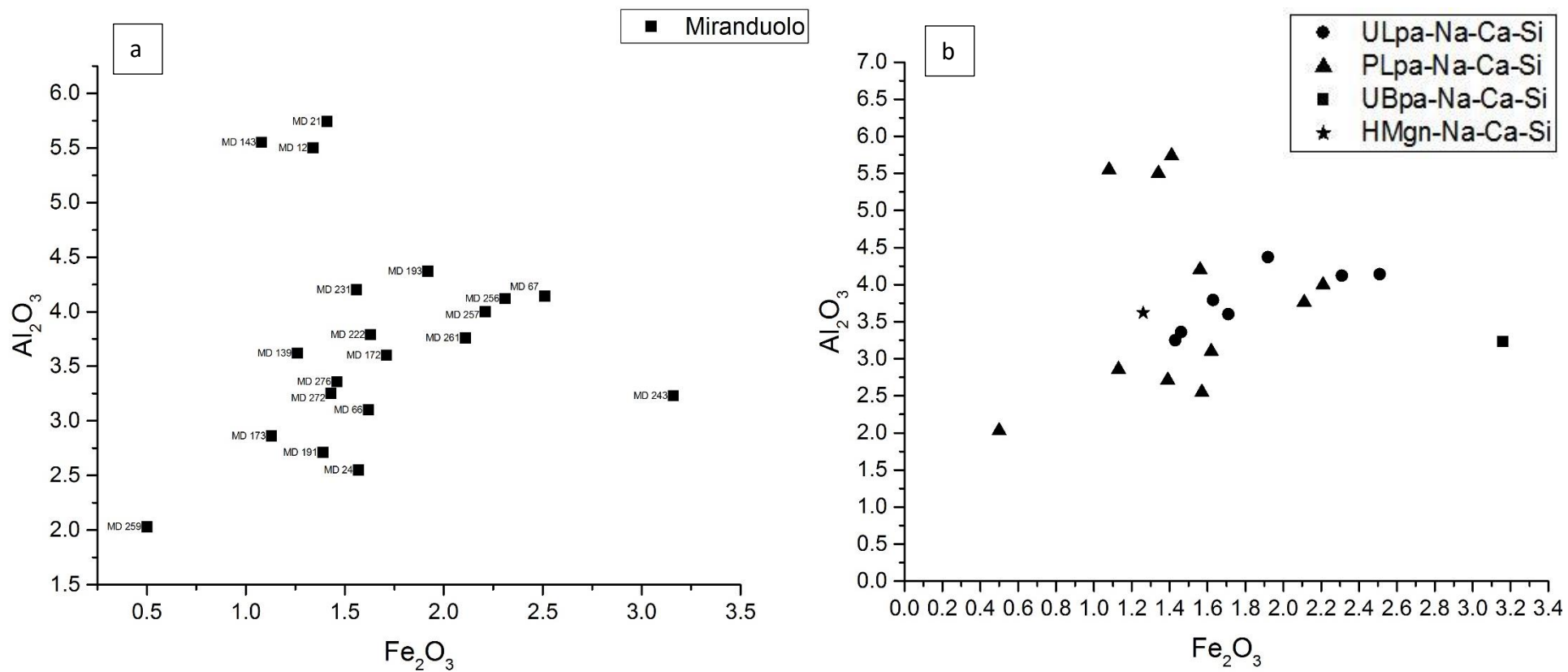


Figure App.3-2 a) Bi-plot of Fe_2O_3 and Al_2O_3 with marked Miranduolo sample names; b) Bi-plot of Fe_2O_3 and Al_2O_3 of Miranduolo samples with marked compositional groups. The concentrations are in wt%.

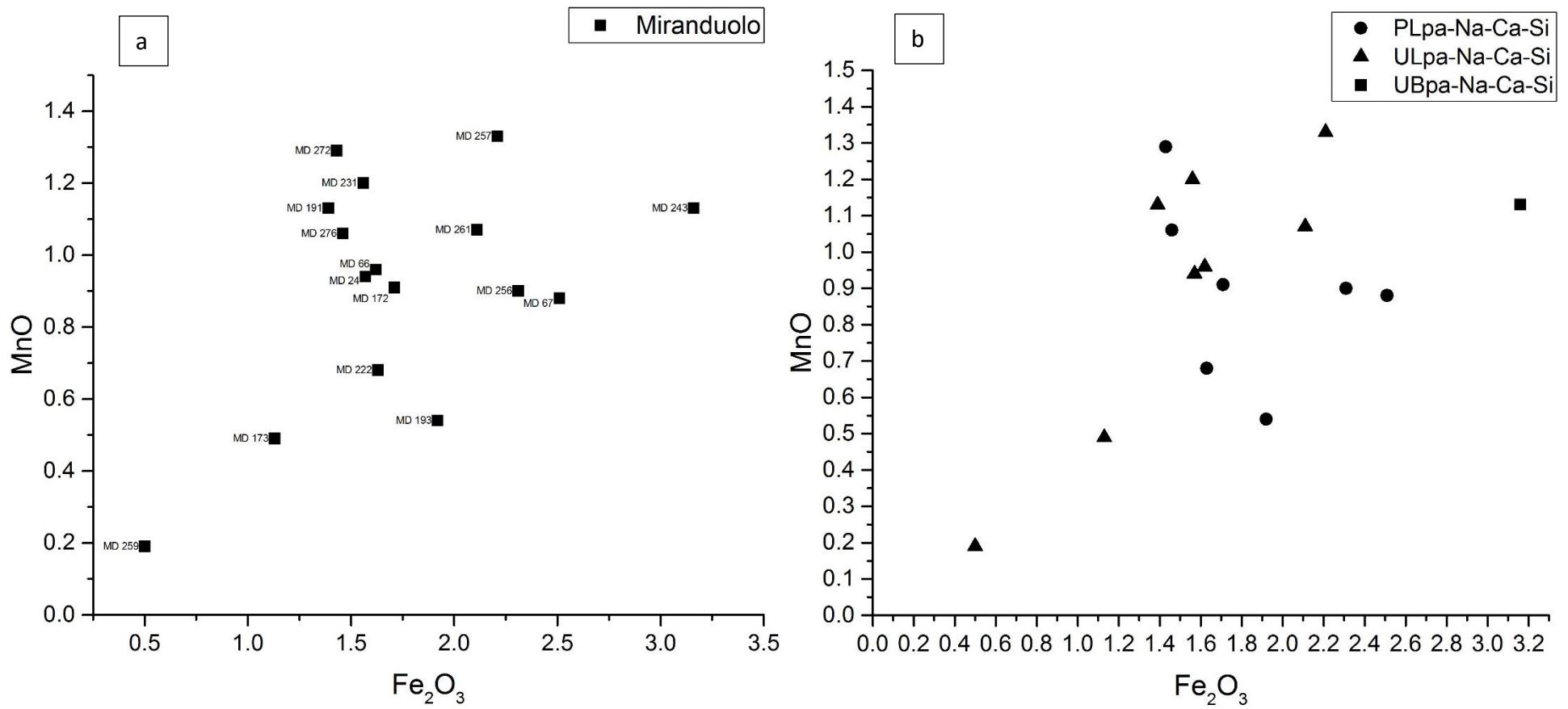


Figure App.3-3 a) Bi-plot of Fe₂O₃ and MnO with marked Miranduolo sample names; b) Bi-plot of Fe₂O₃ and MnO of Miranduolo samples with marked compositional groups. The concentrations are in wt%.

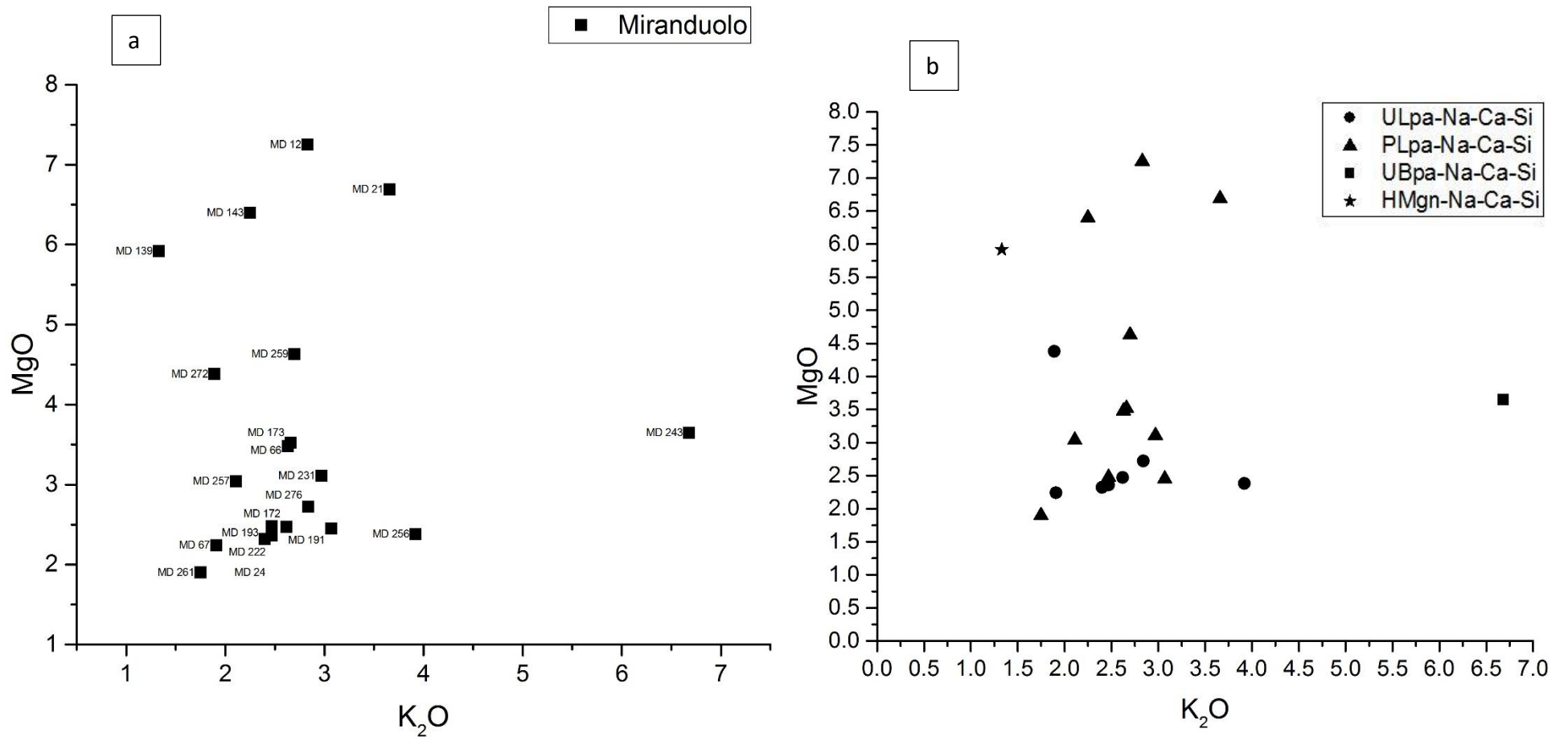


Figure App.3-4 a) Bi-plot of K_2O and MgO with marked Miranduolo sample names; b) Bi-plot of K_2O and MgO of Miranduolo samples with marked compositional groups. The concentrations are in wt%.

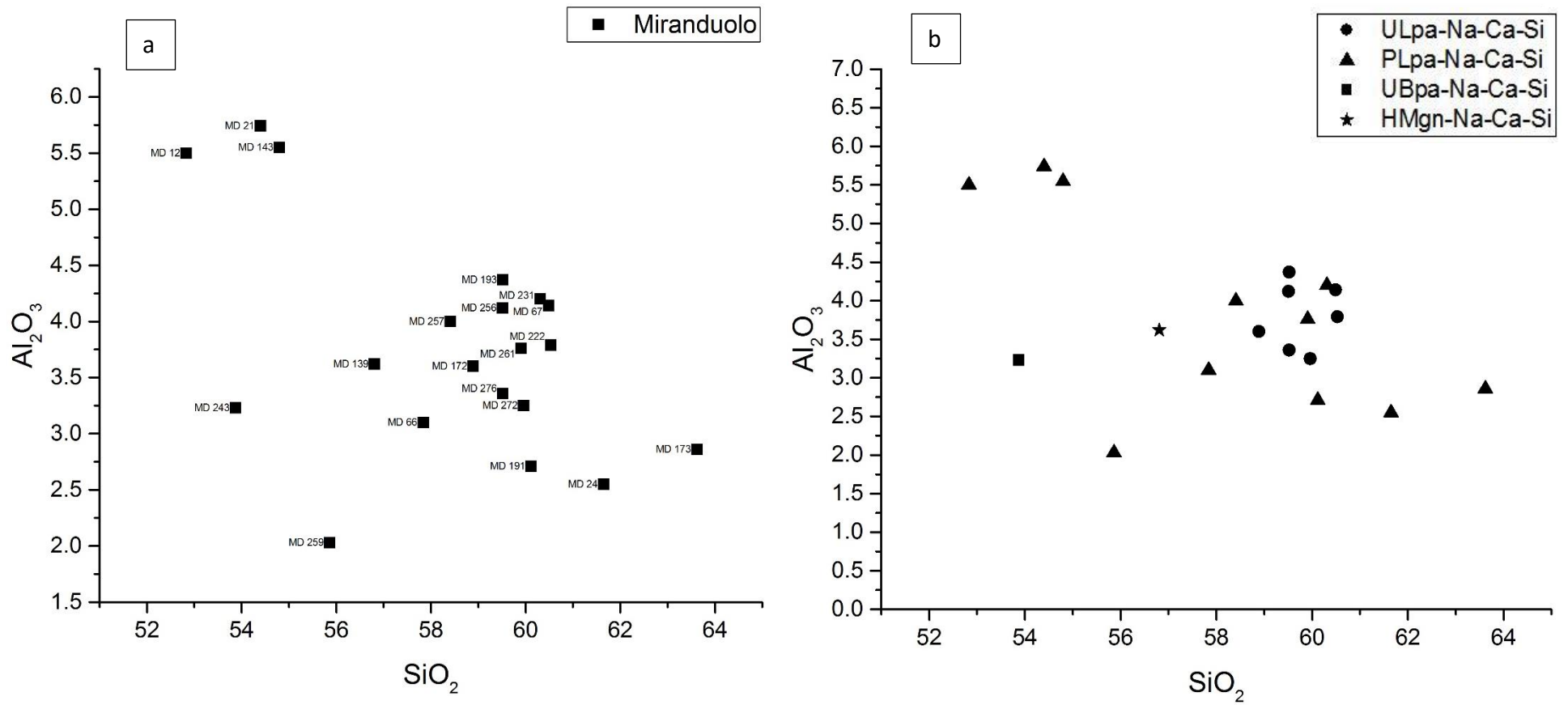


Figure App.3-5 a) Bi-plot of SiO_2 and Al_2O_3 with marked Miranduolo sample names; b) Bi-plot of SiO_2 and Al_2O_3 of Miranduolo samples with marked compositional groups. The concentrations are in wt%.

Appendix 4 – PIXE/PIGE plots and chemical maps

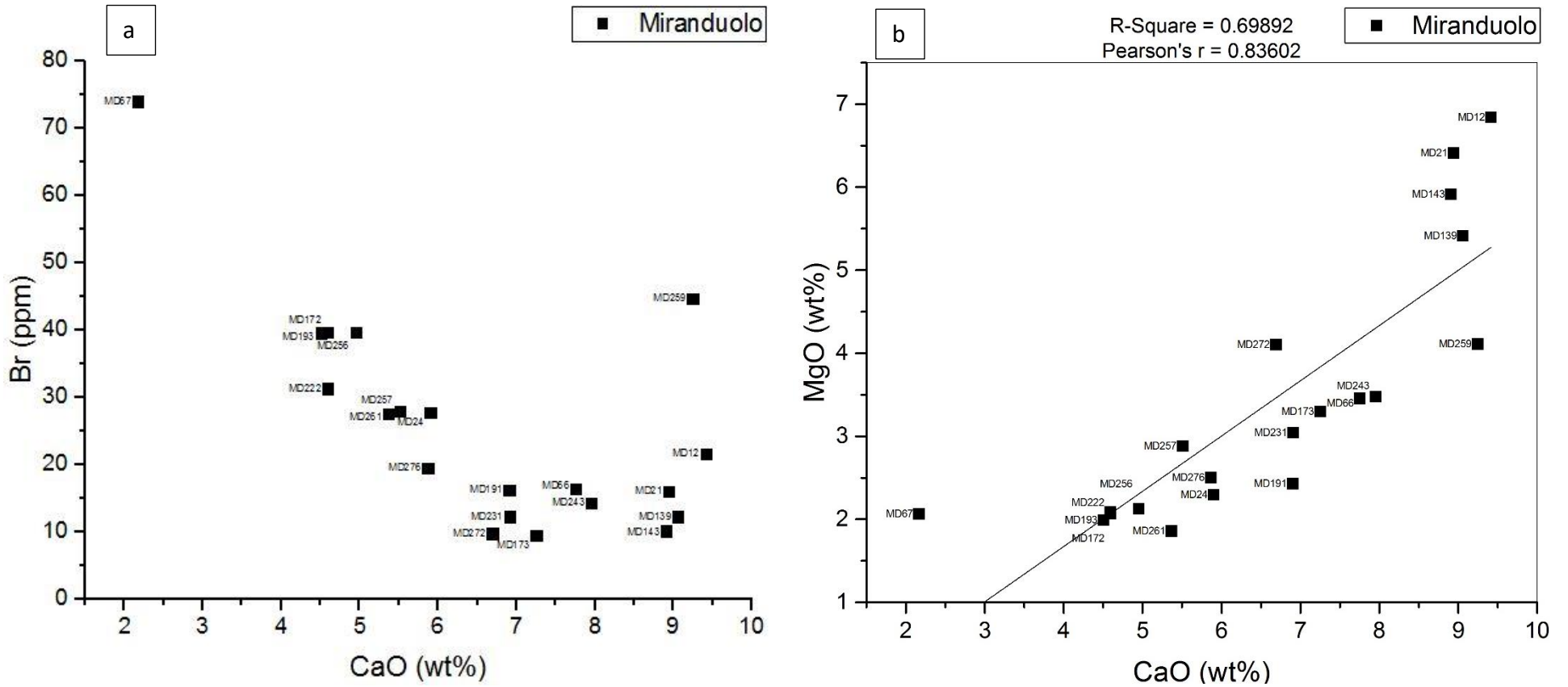


Figure App.4-1 a) Bi-plot of CaO and Br with marked Miranduolo sample names; b) Bi-plot of CaO and MgO with marked Miranduolo sample names and r and r² values.

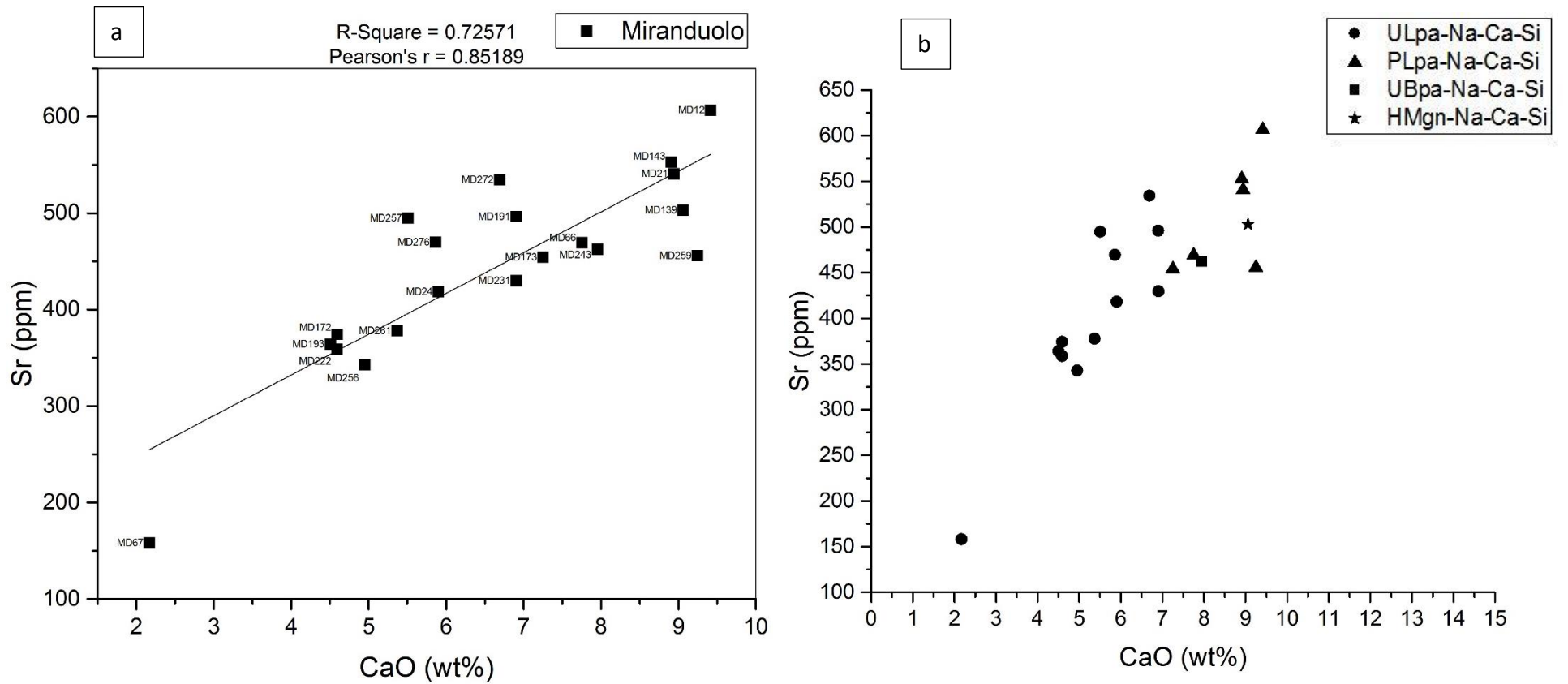


Figure App.4-2 a) Bi-plot of CaO and Sr with marked Miranduolo sample names and r and r^2 values; b) Bi-plot of CaO and Sr of Miranduolo samples with marked compositional groups.

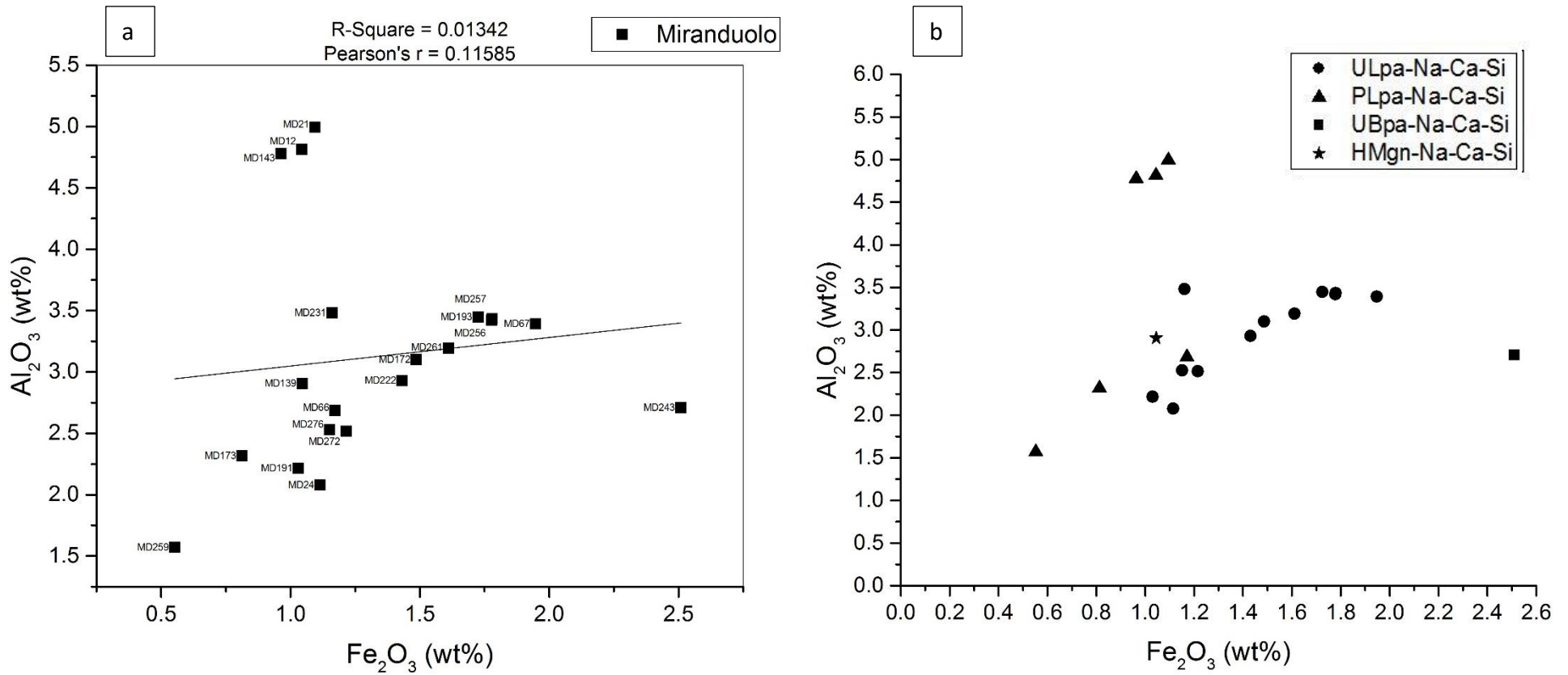


Figure App.4-3 a) Bi-plot of Fe_2O_3 and Al_2O_3 with marked Miranduolo sample names and r and r^2 values; b) Bi-plot of Fe_2O_3 and Al_2O_3 of Miranduolo samples with marked compositional groups.

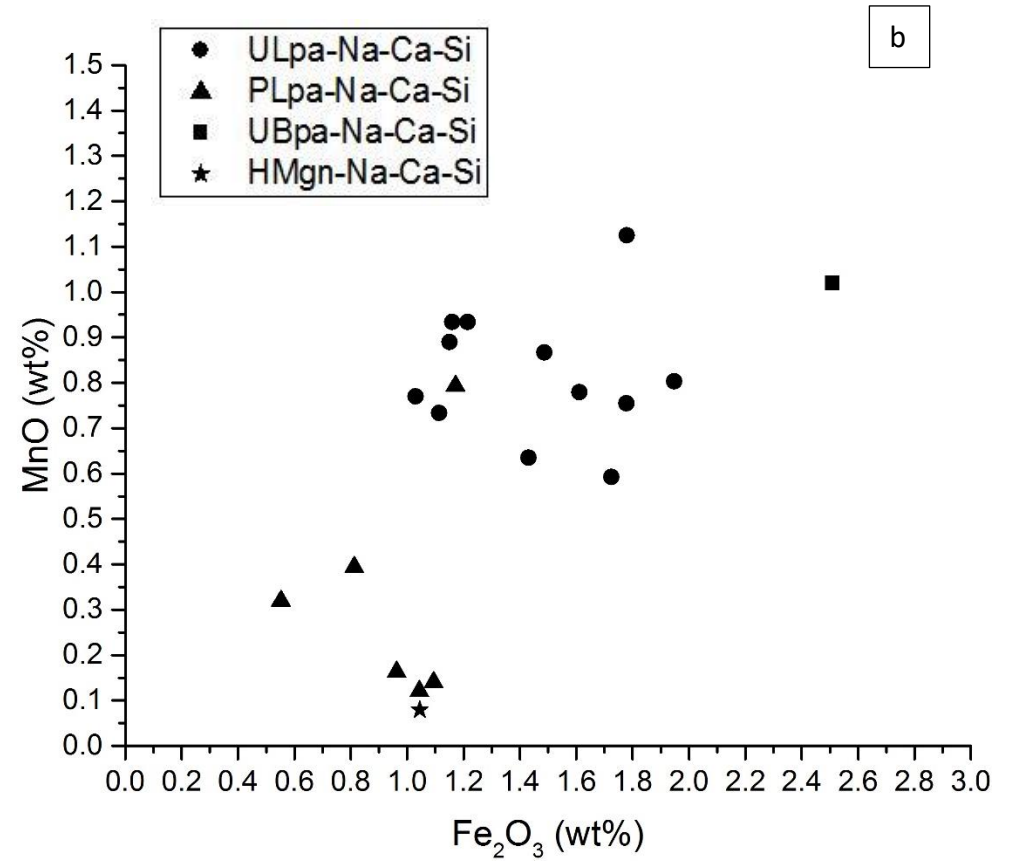
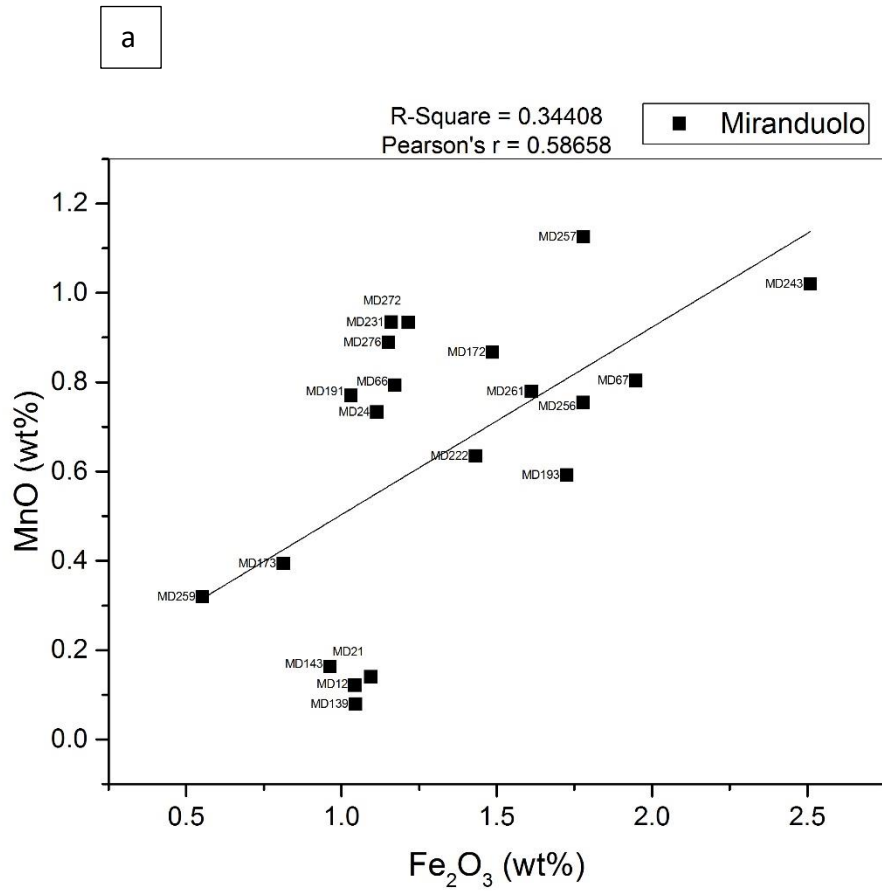


Figure App.4-4 a) Bi-plot of Fe₂O₃ and MnO with marked Miranduolo sample names and r and r² values; b) Bi-plot of Fe₂O₃ and MnO of Miranduolo samples with marked compositional groups.

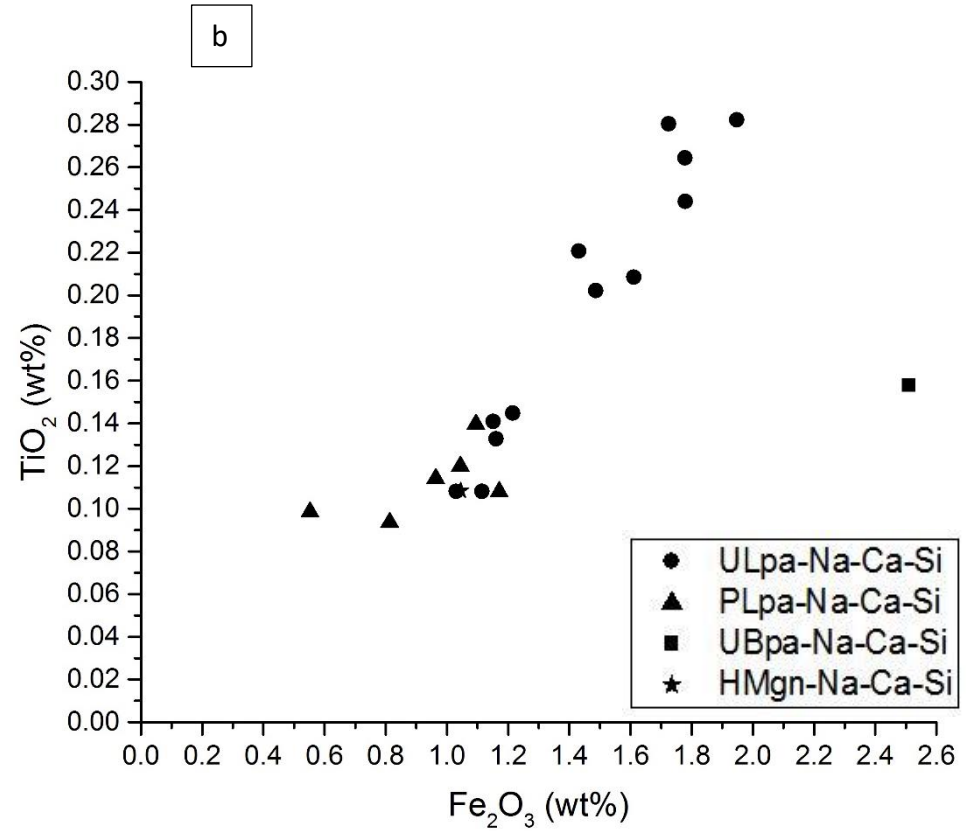
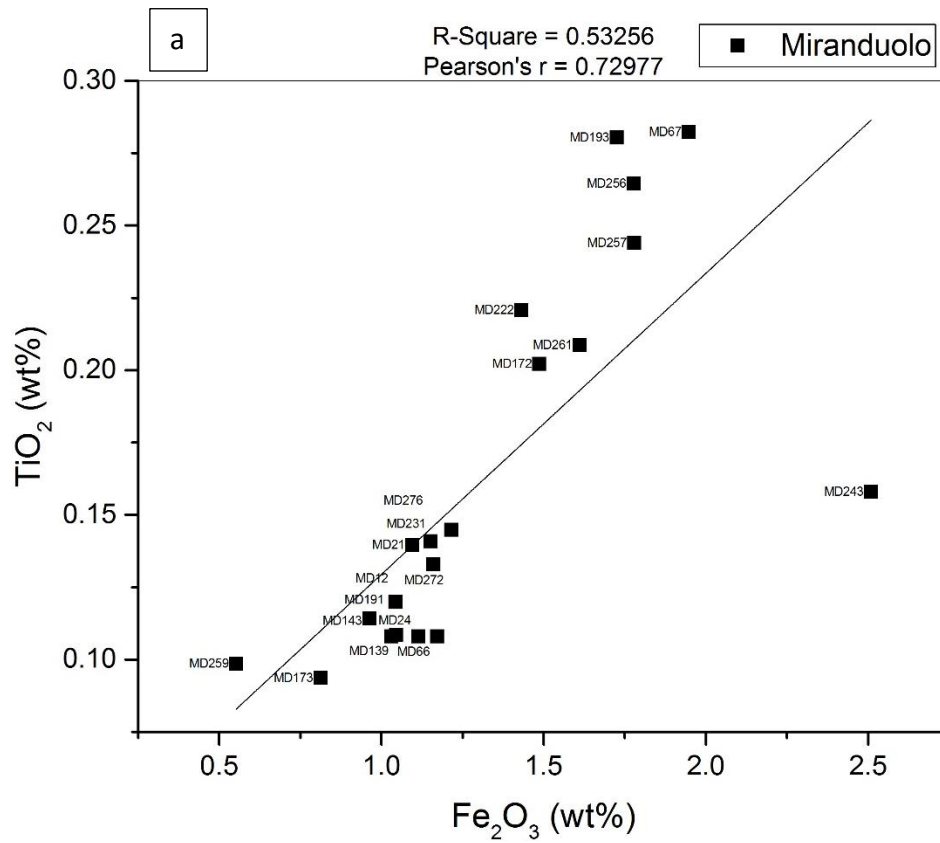


Figure App.4-5 a) Bi-plot of Fe_2O_3 and TiO_2 with marked Miranduolo sample names and r and r^2 values; b) Bi-plot of Fe_2O_3 and TiO_2 of Miranduolo samples with marked compositional groups.

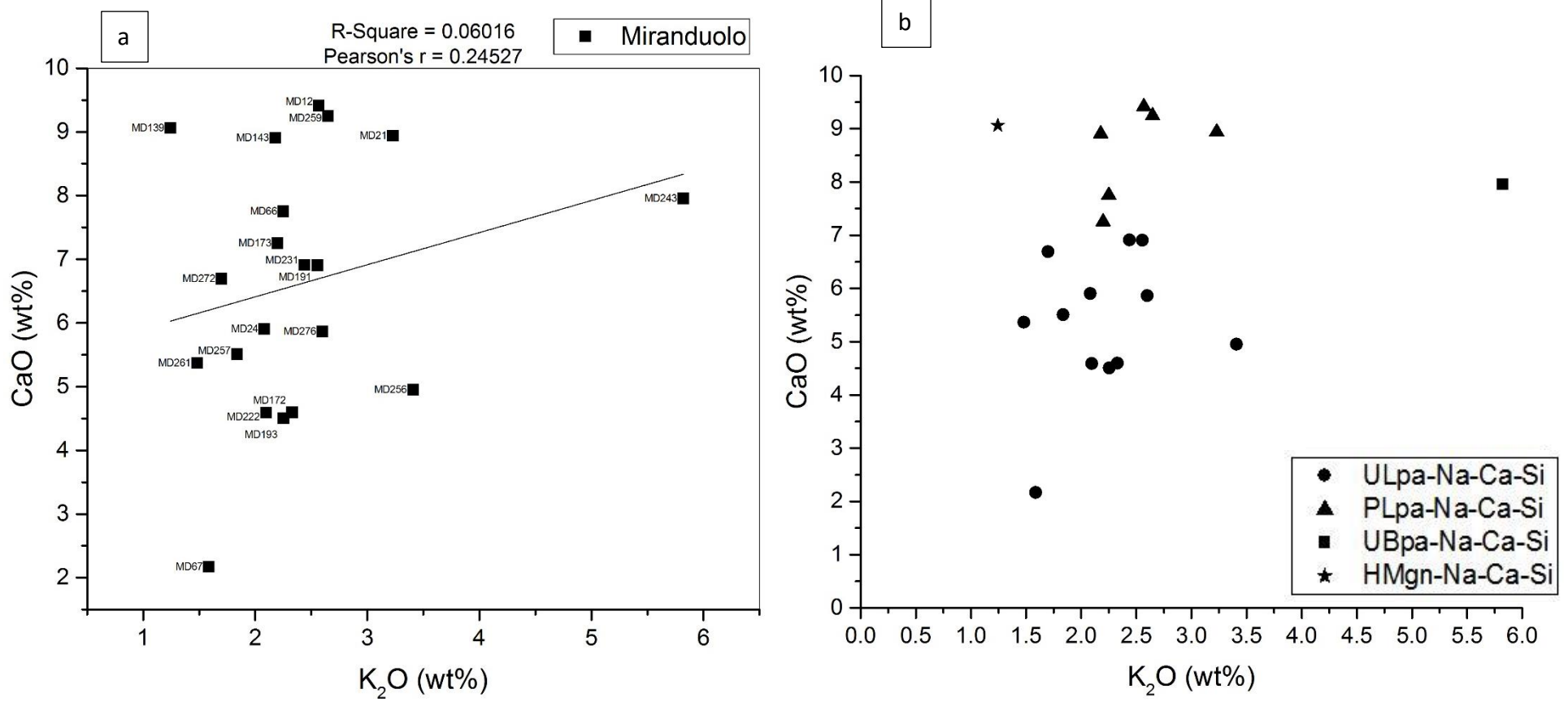


Figure App.4-6 a) Bi-plot of K₂O and CaO with marked Miranduolo sample names and r and r² values; b) Bi-plot of K₂O and CaO of Miranduolo samples with marked compositional groups.

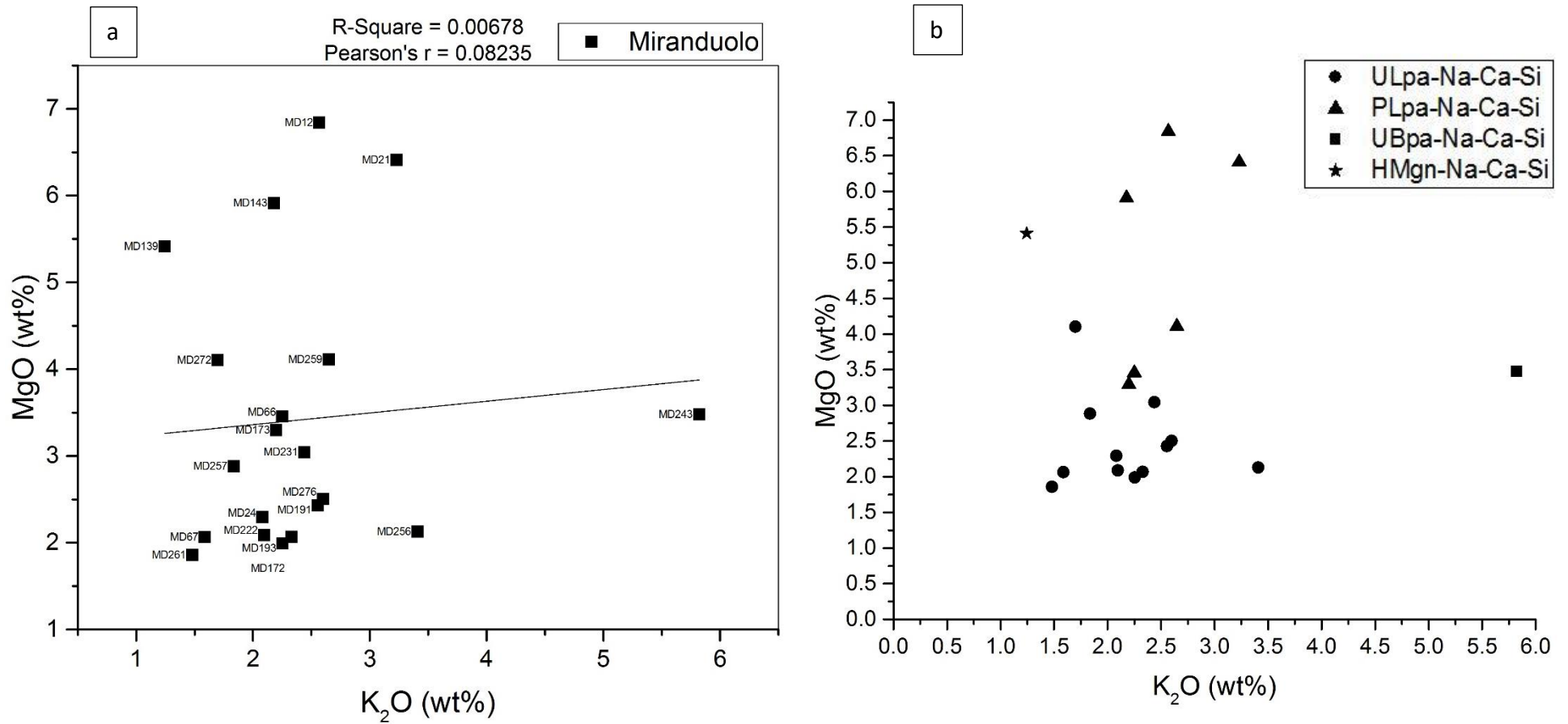


Figure App.4-7 a) Bi-plot of K_2O and MgO with marked Miranduolo sample names and r and r^2 values; b) Bi-plot of K_2O and MgO of Miranduolo samples with marked compositional groups.

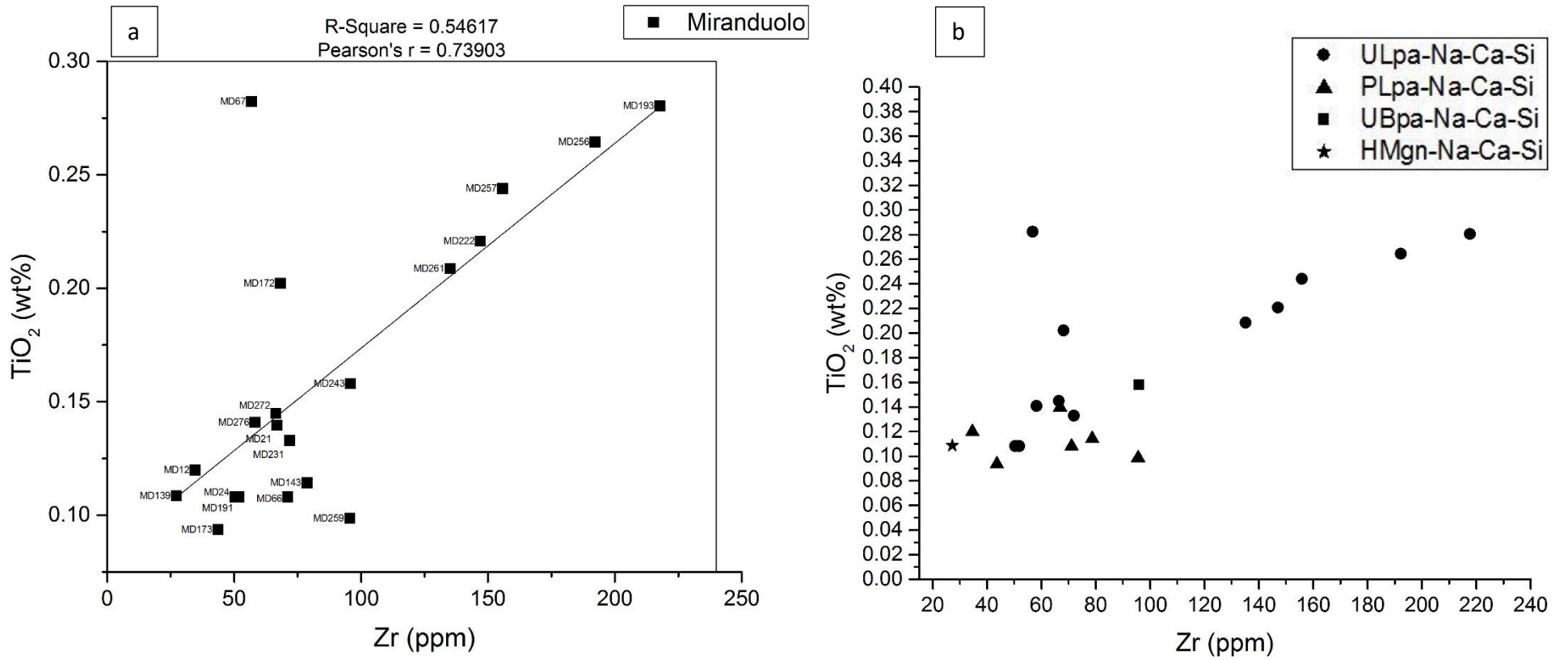


Figure App.4-8 a) Bi-plot of Zr and TiO₂ with marked Miranduolo sample names and r and r² values; b) Bi-plot of Zr and TiO₂ of Miranduolo samples with marked compositional groups.

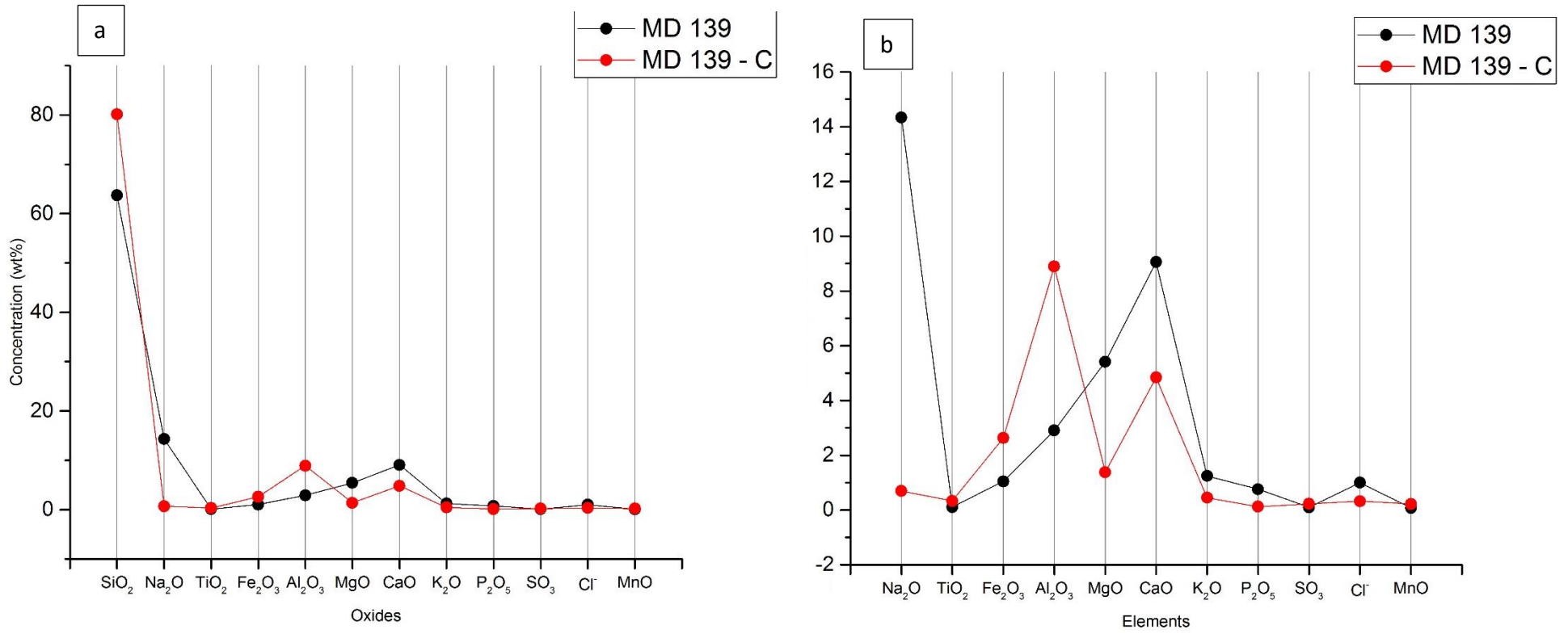


Figure App.4-9 a) and b) Comparison of selected major and minor elements of pristine glass and corrosion layer of MD 139. C – corrosion layer.

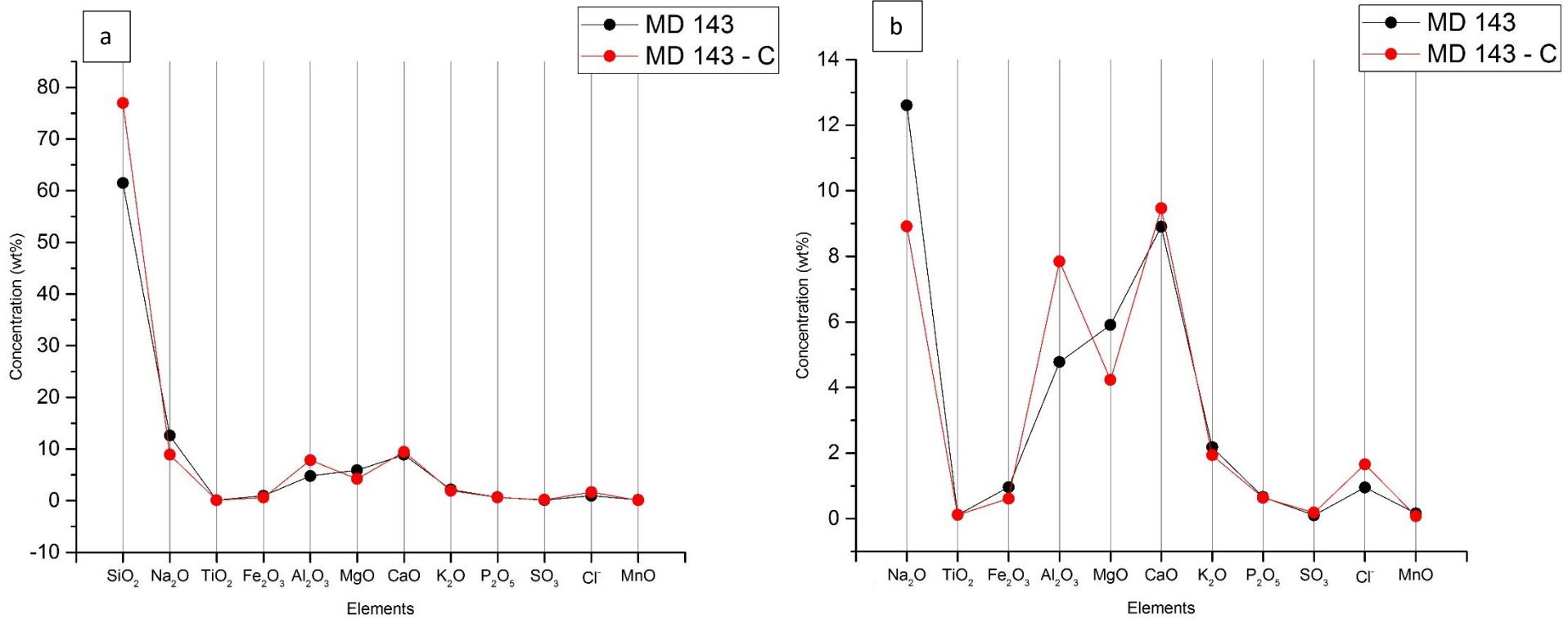


Figure App.4-10 a) and b) Comparison of selected major and minor elements of pristine glass and corrosion layer of MD 143. C – corrosion layer.

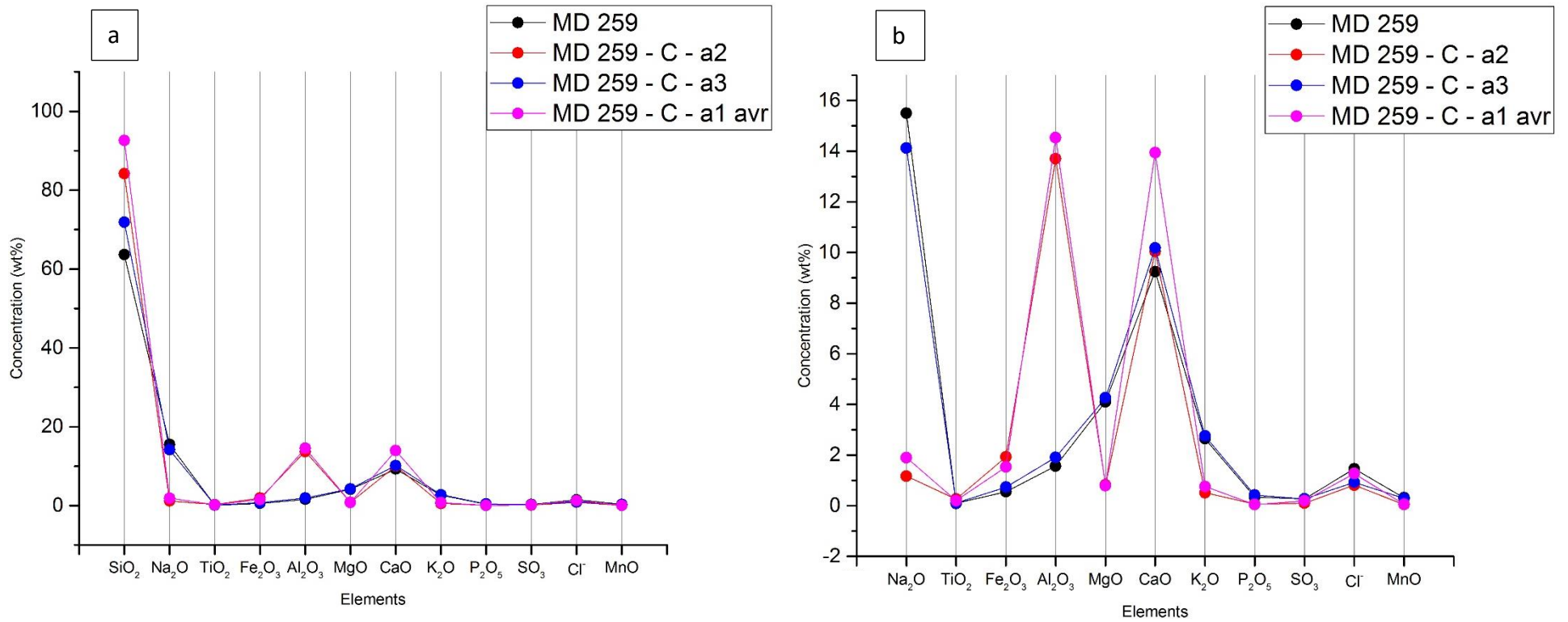


Figure App.4-11 a) and b) Comparison of selected major and minor elements of pristine glass and corrosion layer of MD 259. C – corrosion layer; a – spot name where the corrosion was measured, 1-3 – stratification numbers of the corrosion layer, with 3 being closest to the pristine glass; avr – average.

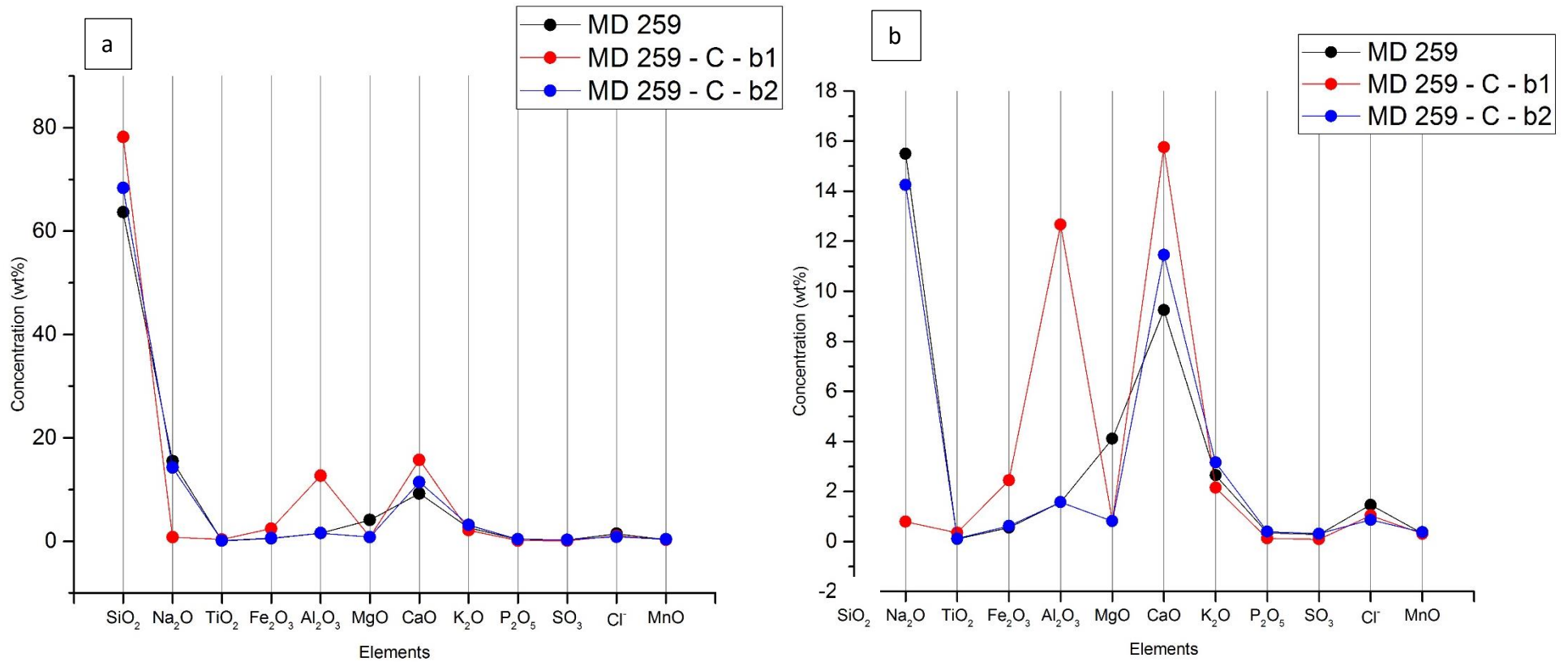


Figure App.4-12 a) and b) Comparison of selected major and minor elements of pristine glass and corrosion layer of MD 259. C – corrosion layer; b – spot name where the corrosion was measured, 1-2 – stratification numbers of the corrosion layer, with 2 being closest to the pristine glass.

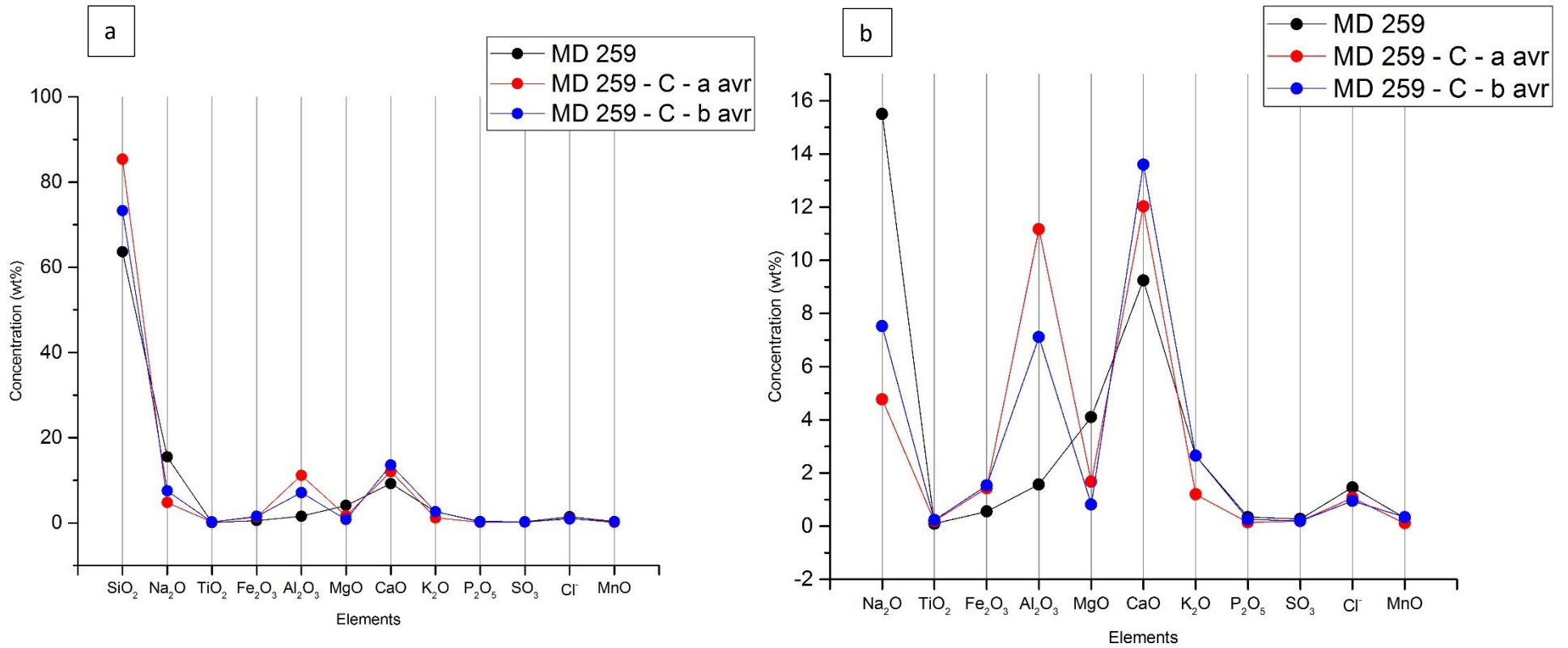


Figure App.4-13 a) and b) Comparison of selected major and minor elements of pristine glass and corrosion layer of MD 259. C – corrosion layer; a and b – spot name where the corrosion was measured; avr - average.

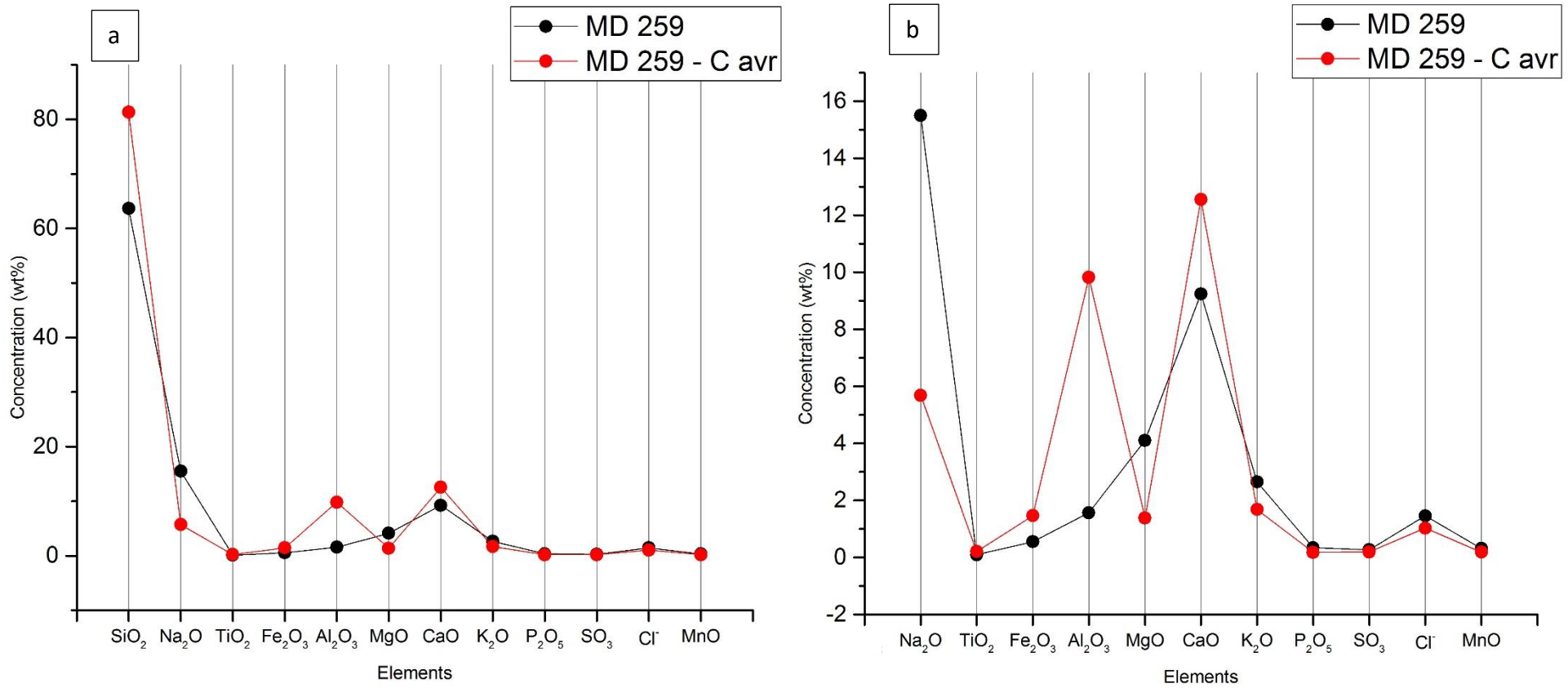


Figure App.4-14 a) and b) Comparison of selected major and minor elements of pristine glass and corrosion layer of MD 259. C – corrosion layer; avr – average of spots a and b.

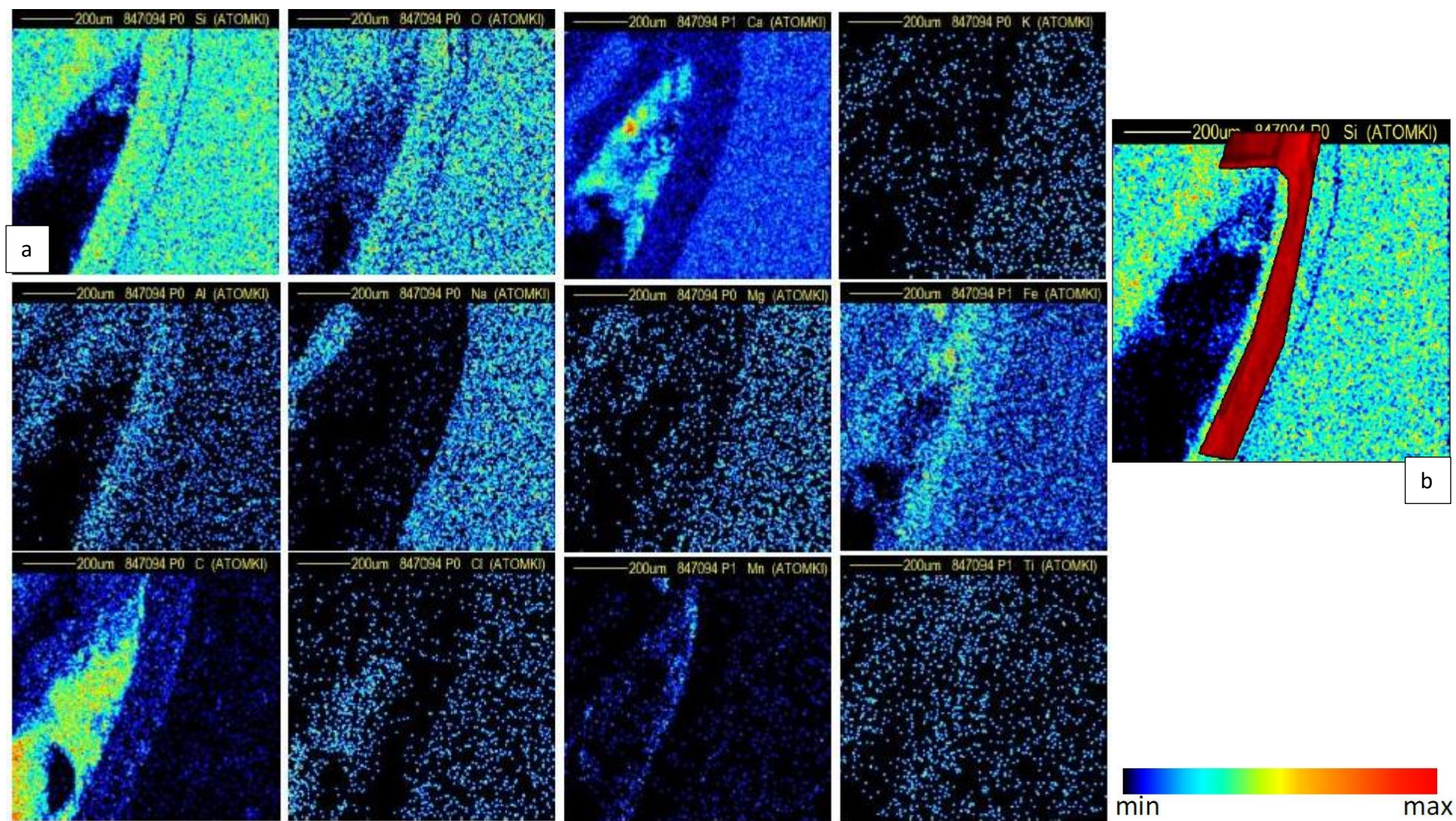


Figure App.4-15 a) Chemical maps of selected elements for the corrosion layer of MD 139; b) the area (spot) that was selected for quantification is marked in red.

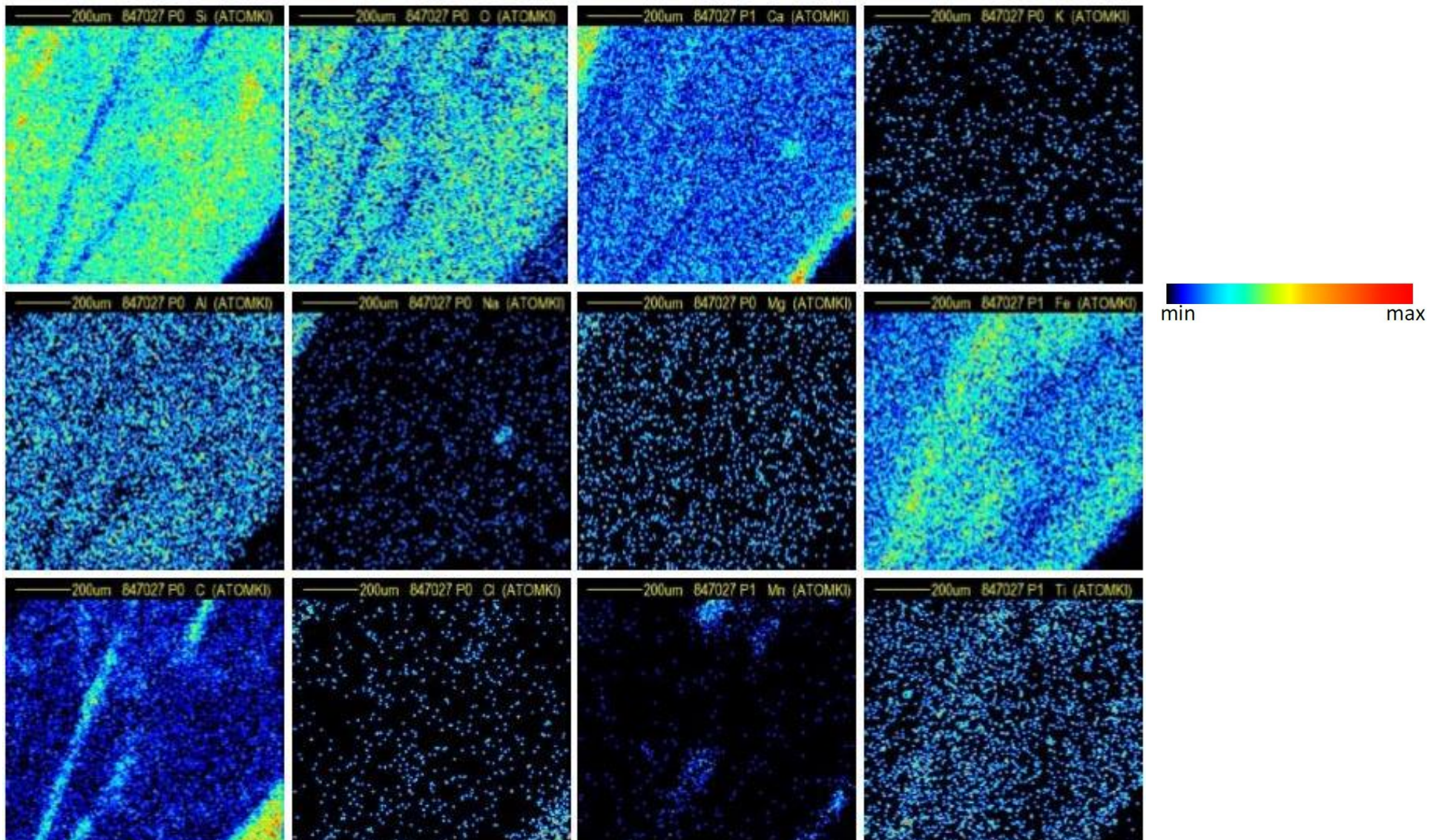


Figure App.4-16 Chemical map of a spot of corrosion layer of MD 139 that has not been quantified.

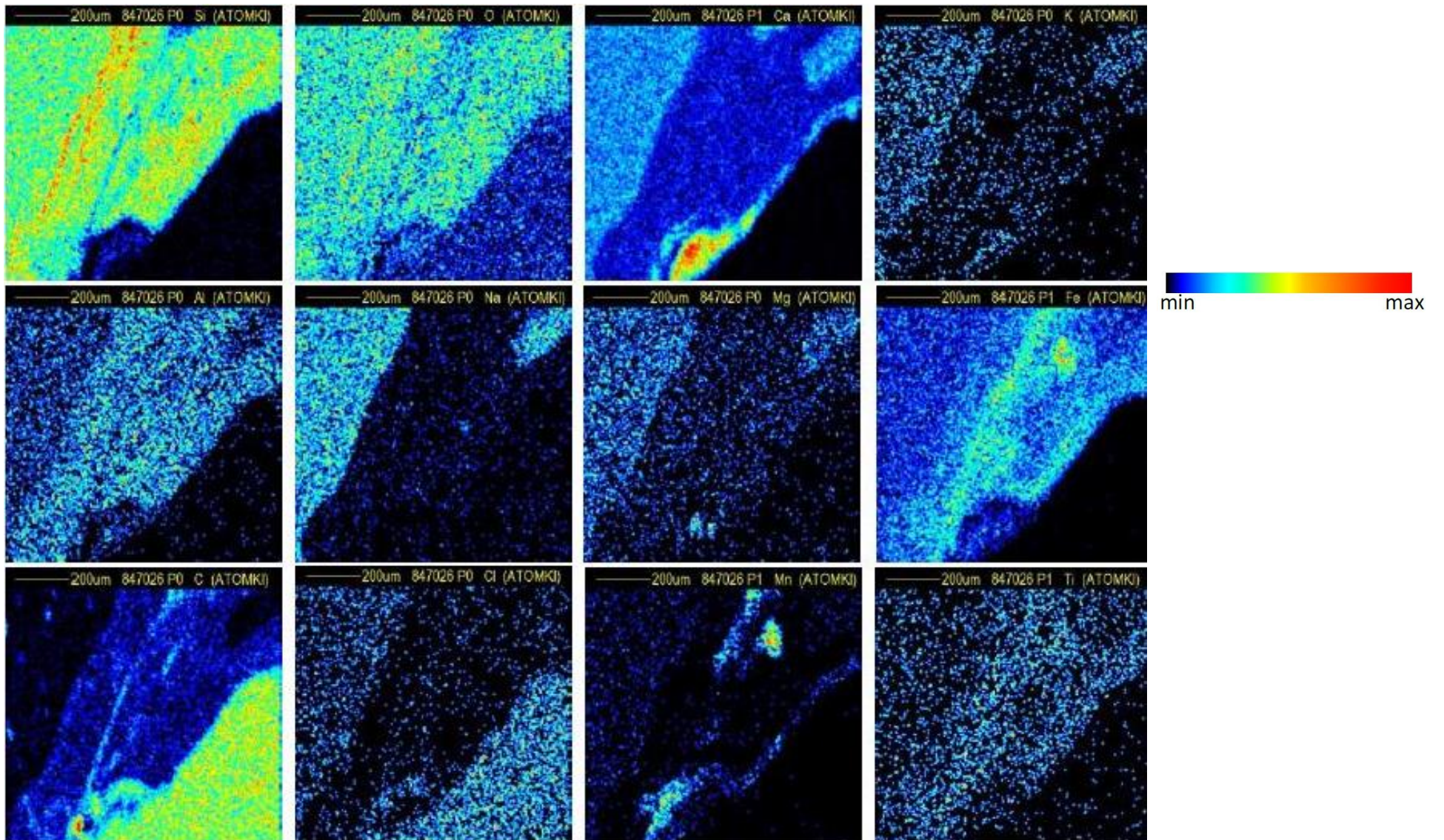


Figure App.4-17 Chemical map of a spot of corrosion layer of MD 139 that has not been quantified.

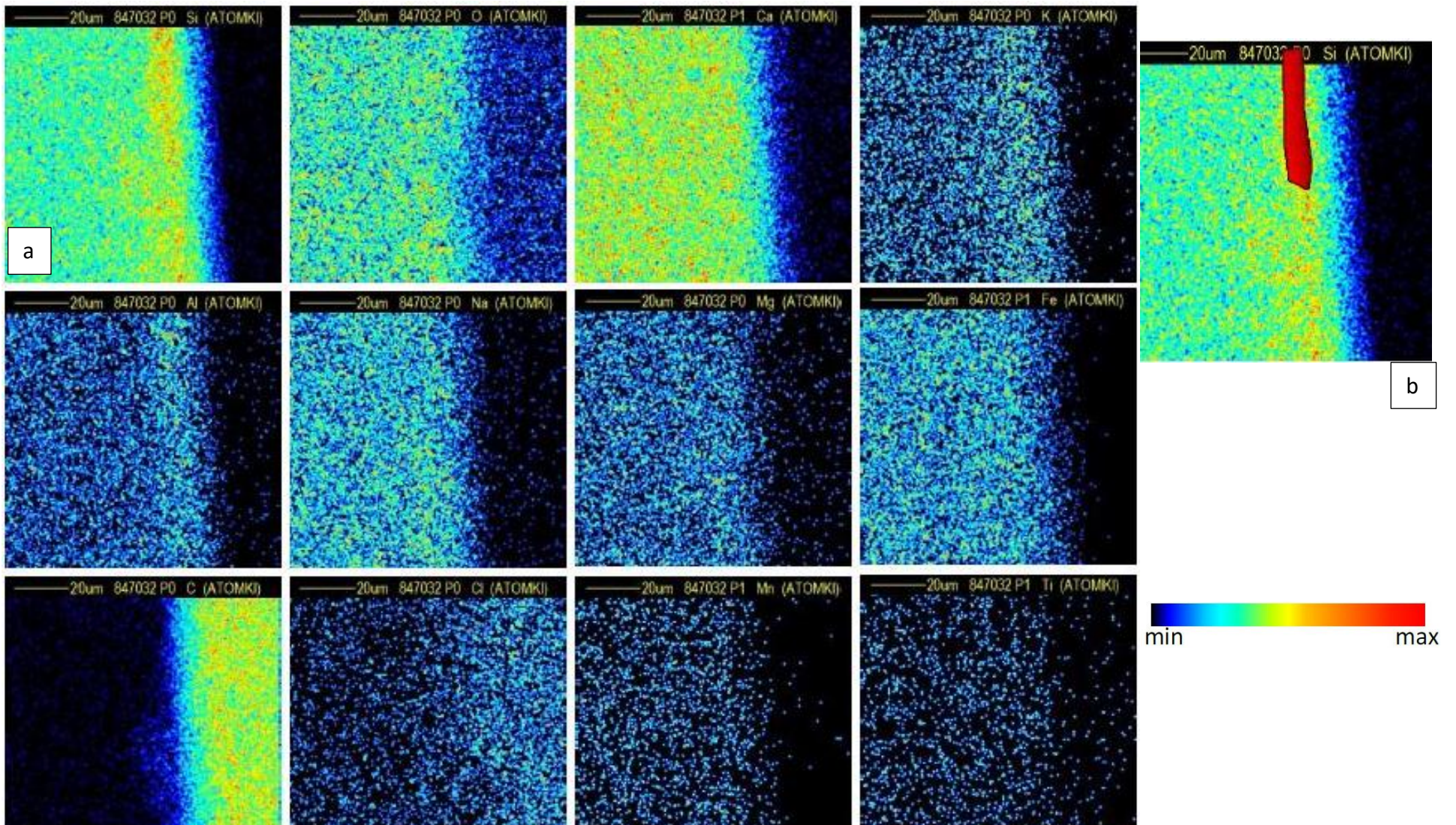


Figure App.4-18 a) Chemical maps of selected elements for the corrosion layer of MD 143; b) the area (spot) that was selected for quantification is marked in red.

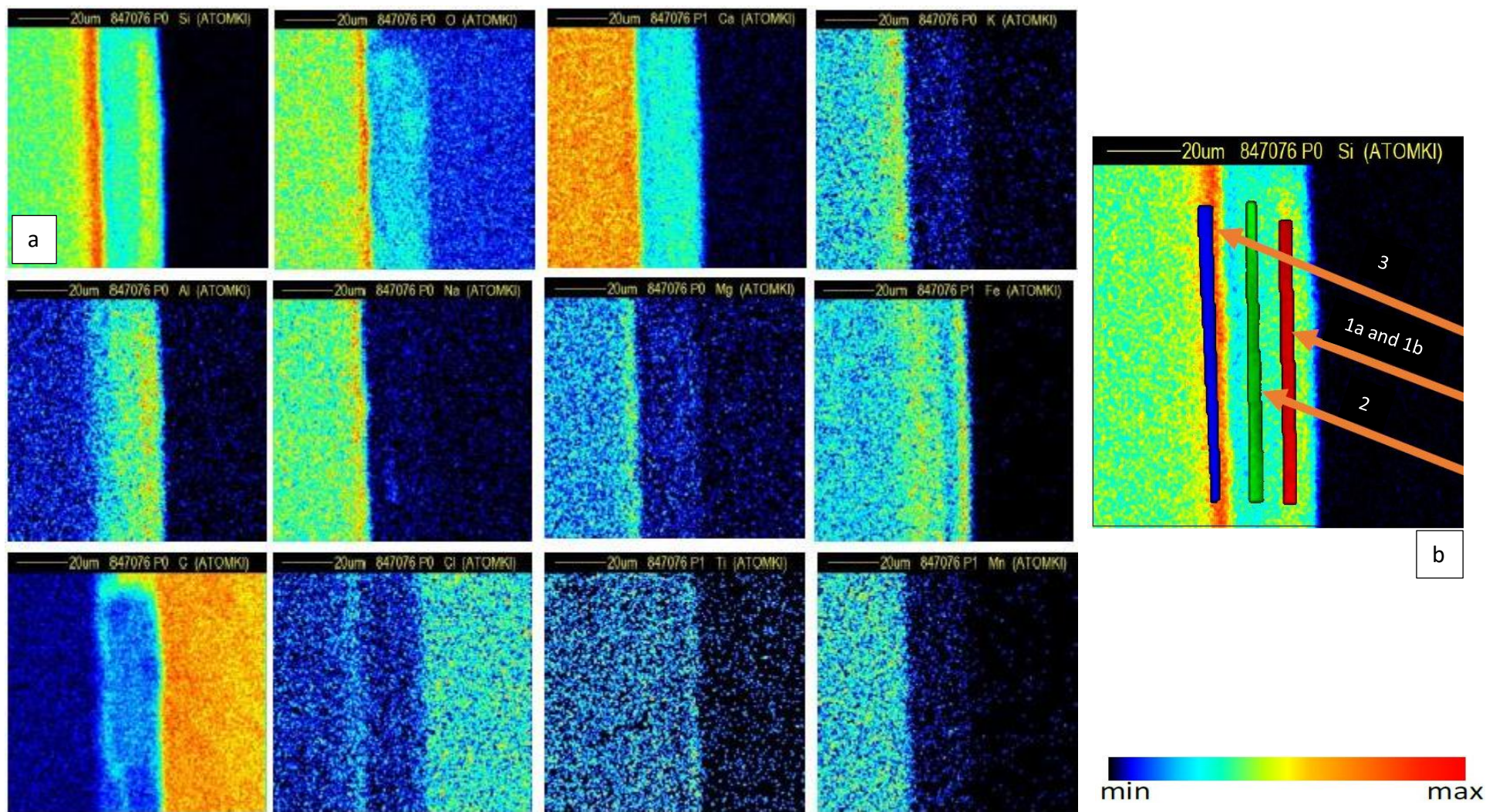


Figure App.4-19 a) Chemical maps of selected elements for the corrosion layer of MD 259 spot a; b) three stratifications of spot a of the corrosion layer of MD 259 marked in red, green and blue. The blue layer is the closest to the pristine glass.

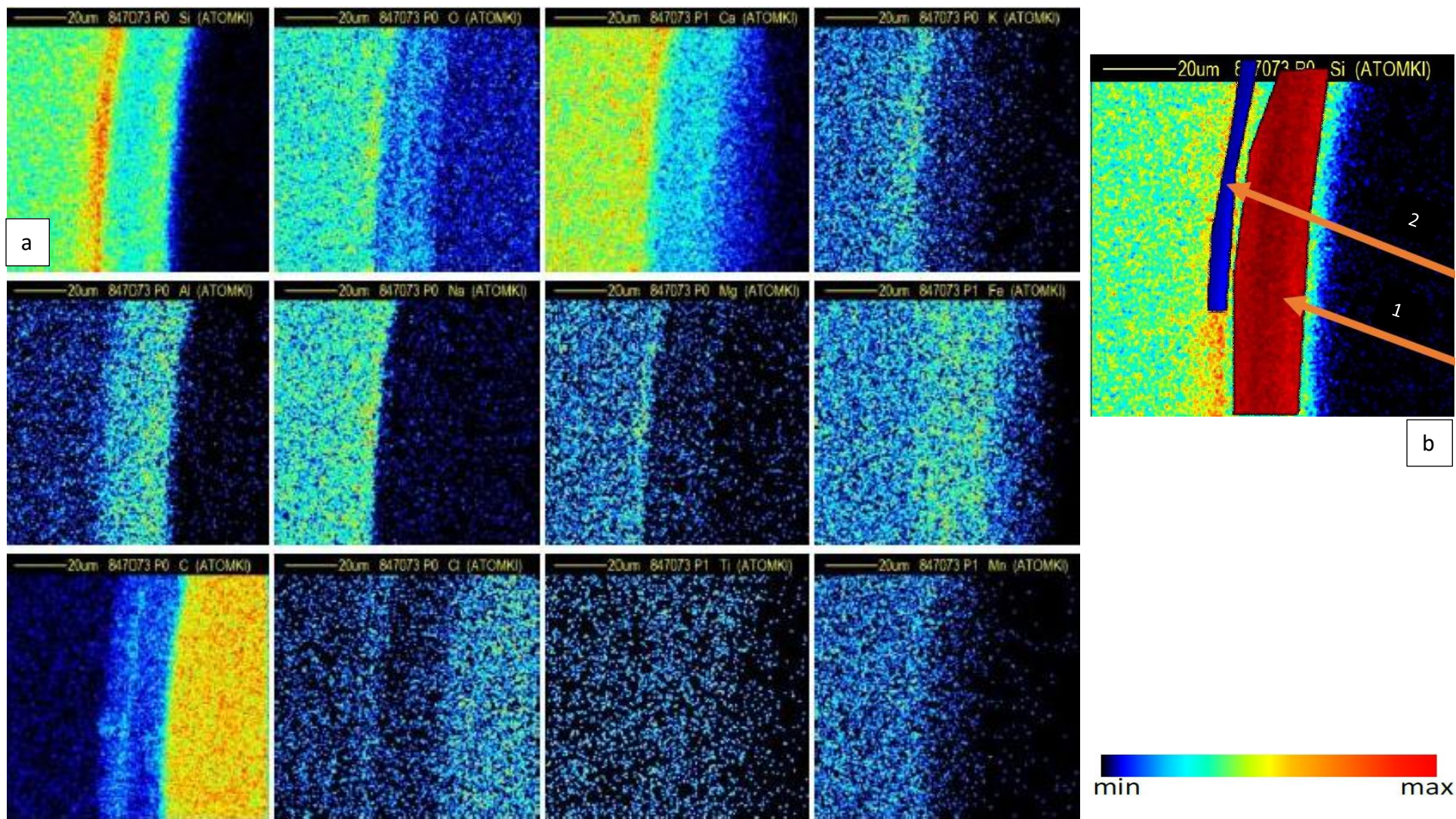


Figure App.4-20 a) Chemical maps of selected elements for the corrosion layer of MD 259 spot b; b) two stratifications of spot b of the corrosion layer of MD 259 marked in red and blue. The blue layer is the closest to the pristine glass.

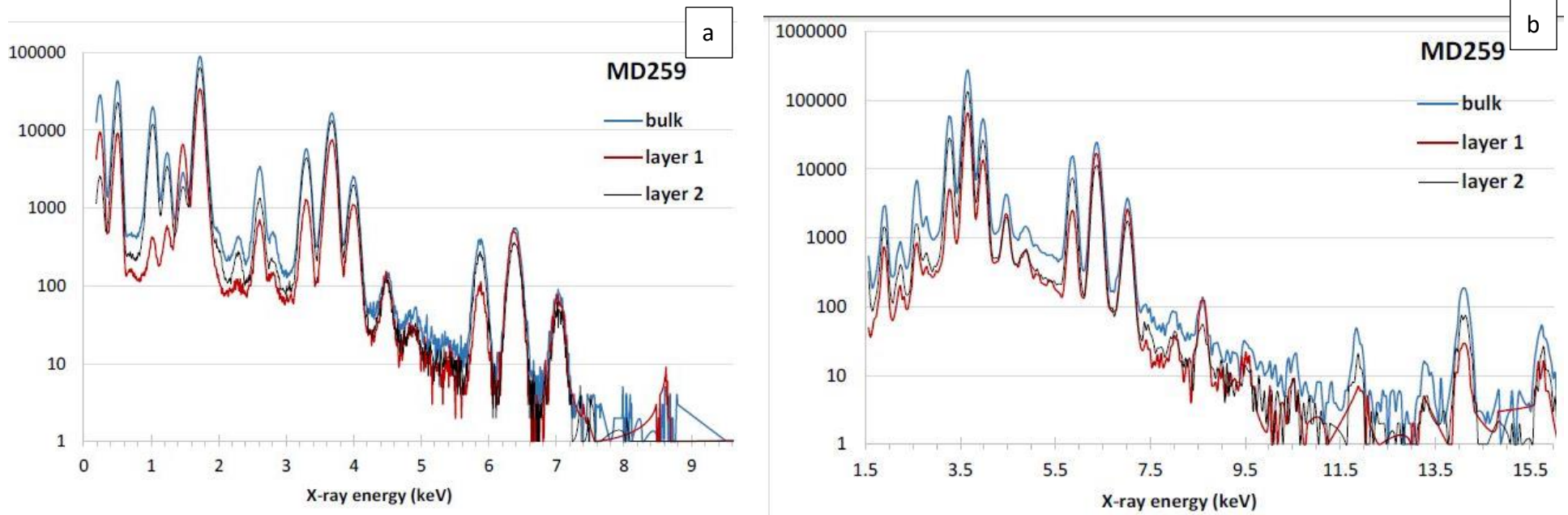


Figure App.4-21 a) and b) Comparison of PIXE/PIGE spectra between the pristine glass (bulk) and two stratifications of corrosion layer in spot b of MD 259.

Appendix 5 – LA-ICP-MS plots

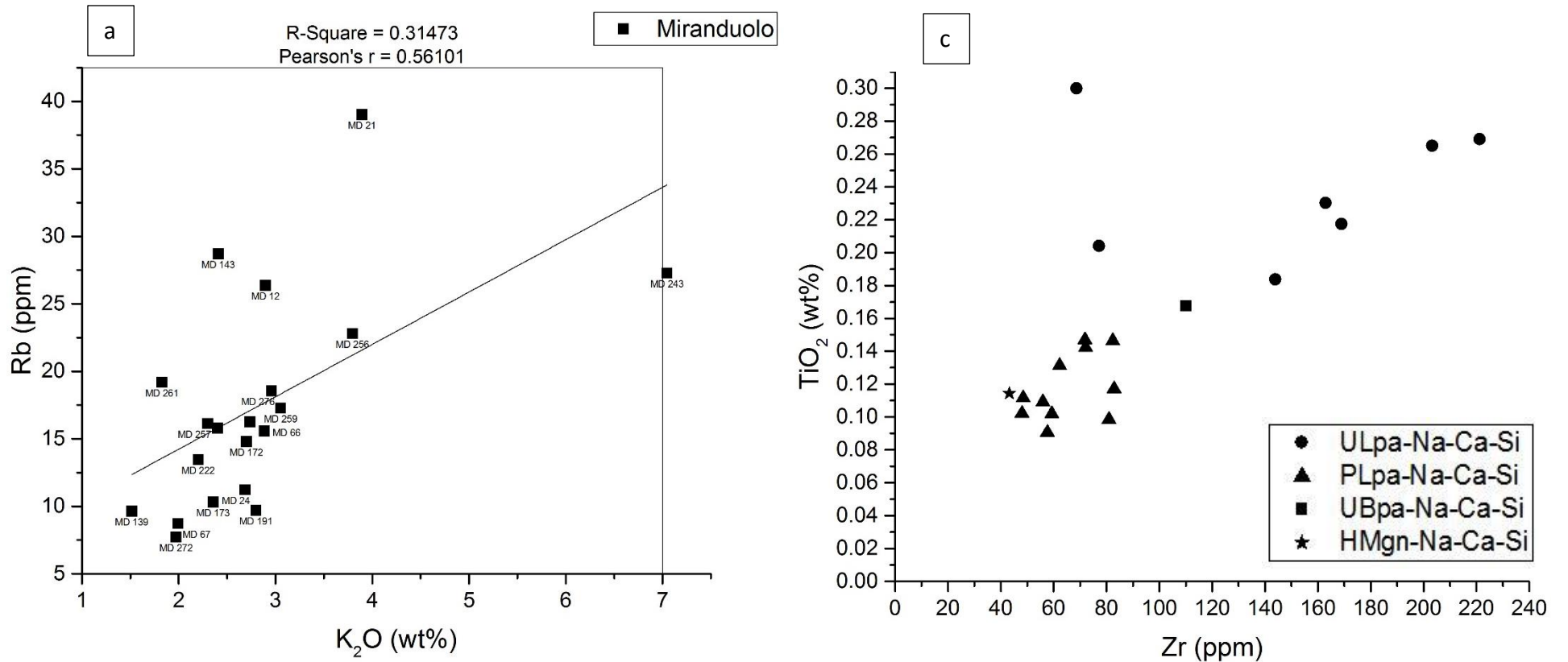


Figure App.5-1 a) Bi-plot of K_2O and Rb with marked Miranduolo sample names and r and r^2 values; b) Bi-plot of Zr and TiO_2 of Miranduolo samples with marked compositional groups.

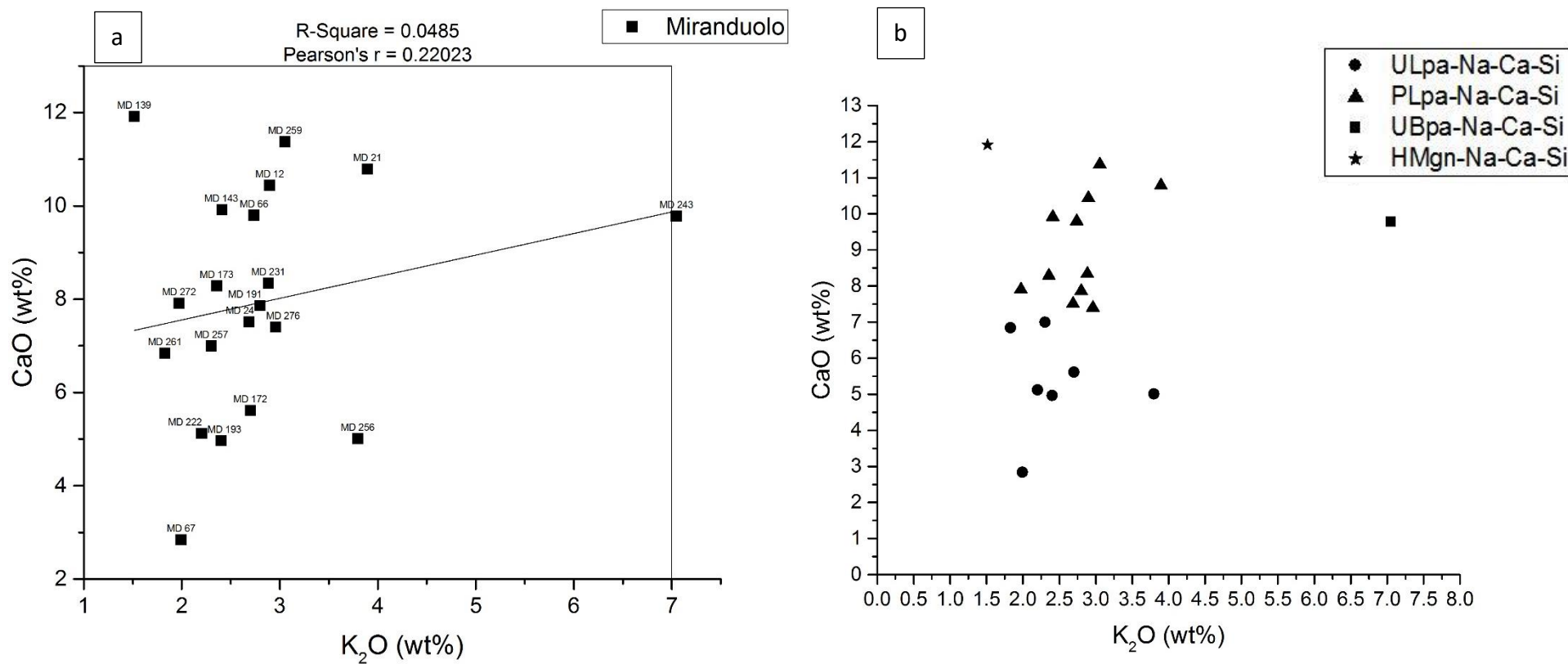


Figure App.5-2 a) Bi-plot of K₂O and CaO with marked Miranduolo sample names and r and r² values; b) Bi-plot of K₂O and CaO of Miranduolo samples with marked compositional groups.

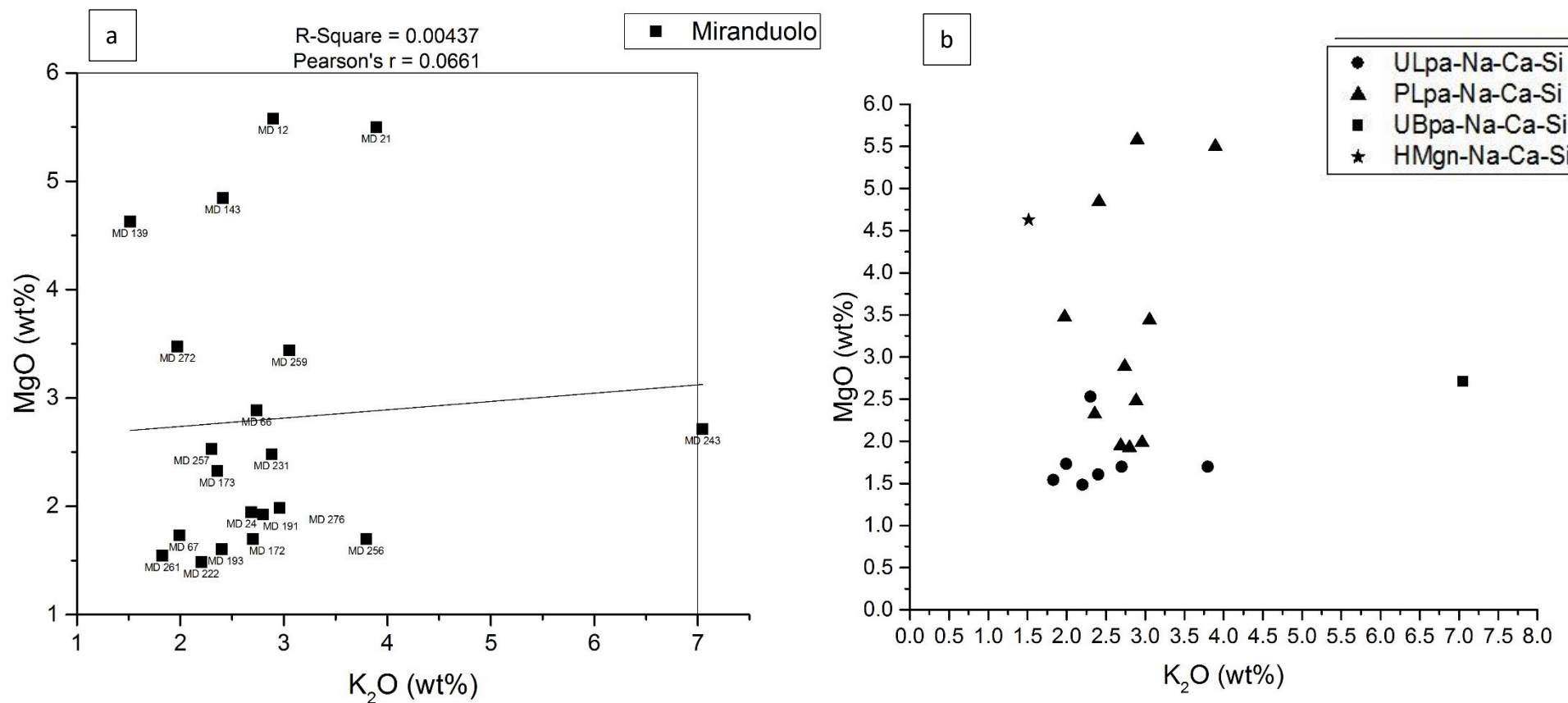


Figure App.5-3 a) Bi-plot of K_2O and MgO with marked Miranduolo sample names and r and r^2 values; b) Bi-plot of K_2O and MgO of Miranduolo samples with marked compositional groups.

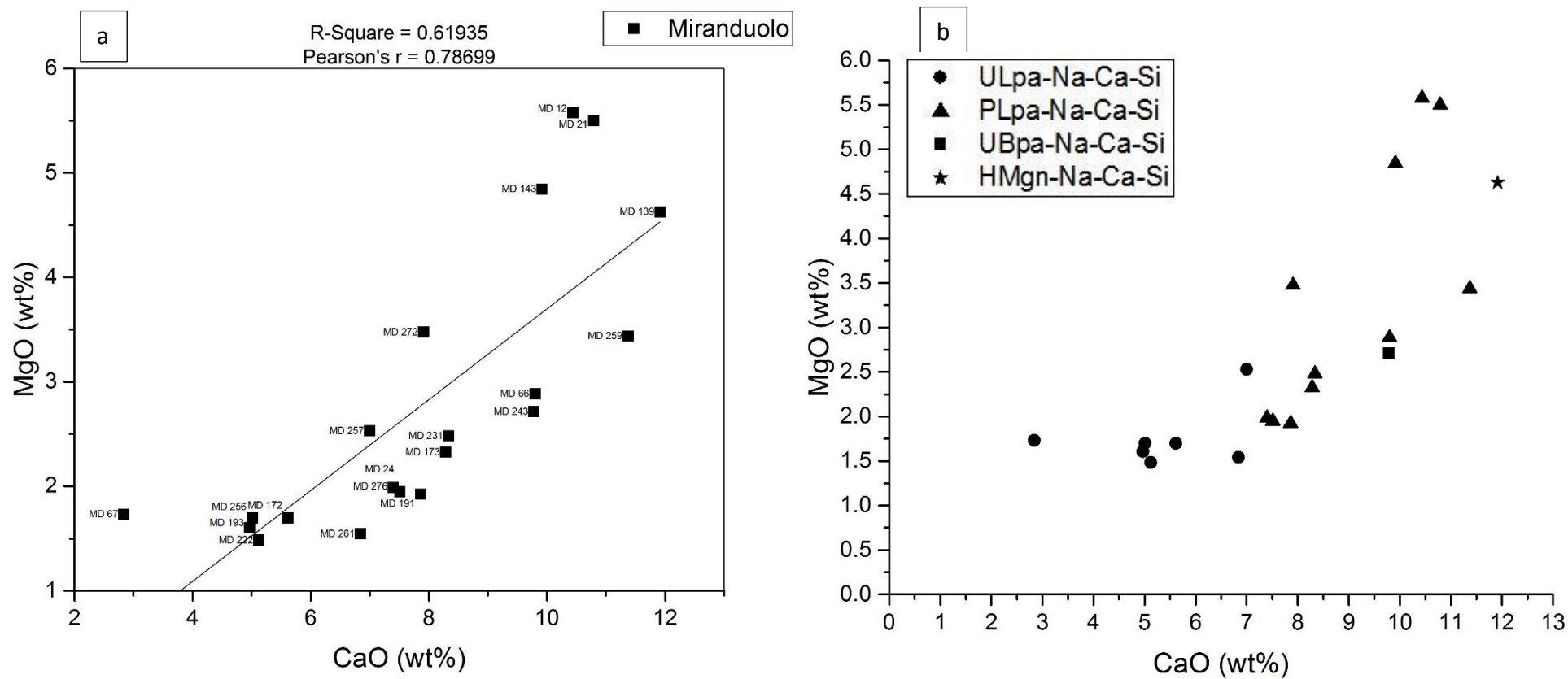


Figure App.5-4 a) Bi-plot of CaO and MgO with marked Miranduolo sample names and r and r^2 values; b) Bi-plot of CaO and MgO of Miranduolo samples with marked compositional groups.

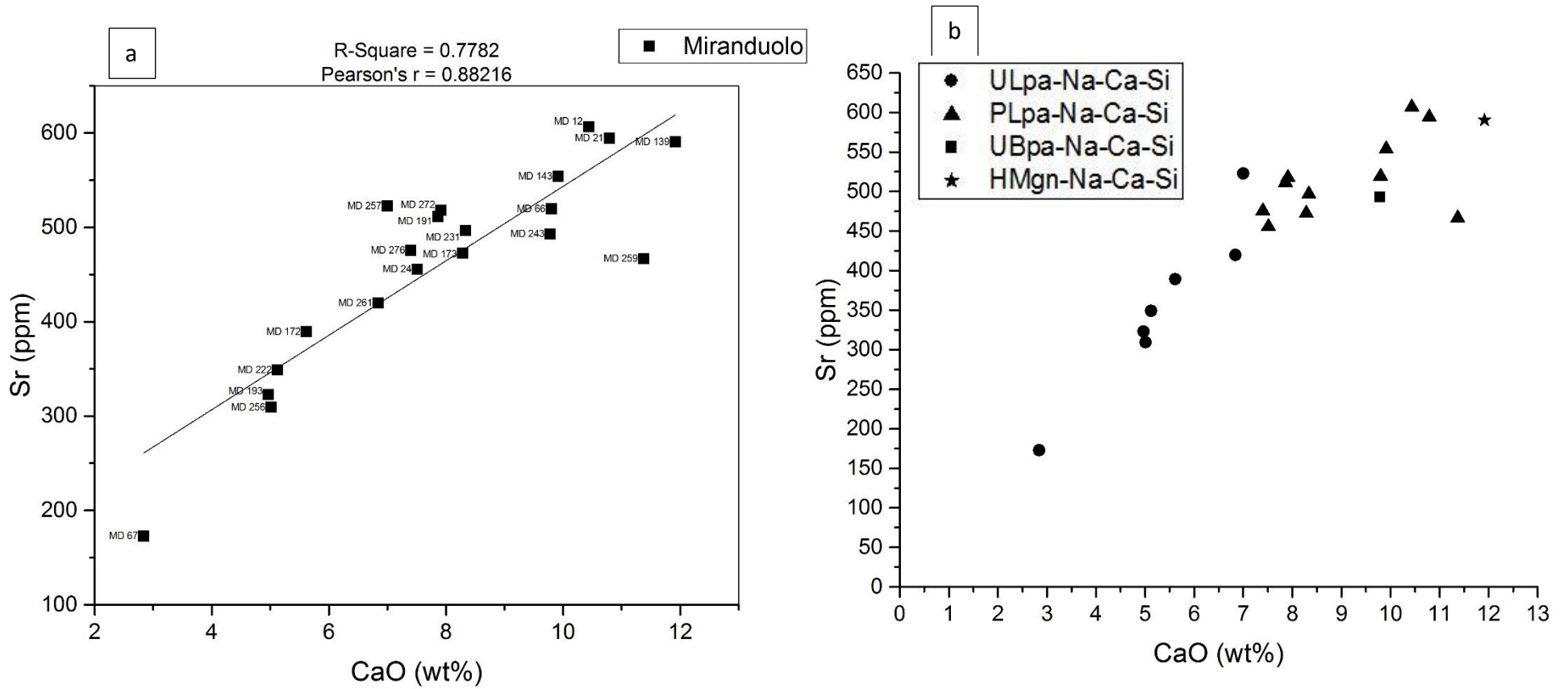


Figure App.5-5 a) Bi-plot of CaO and Sr with marked Miranduolo sample names and r and r² values; b) Bi-plot of CaO and Sr of Miranduolo samples with marked compositional groups.

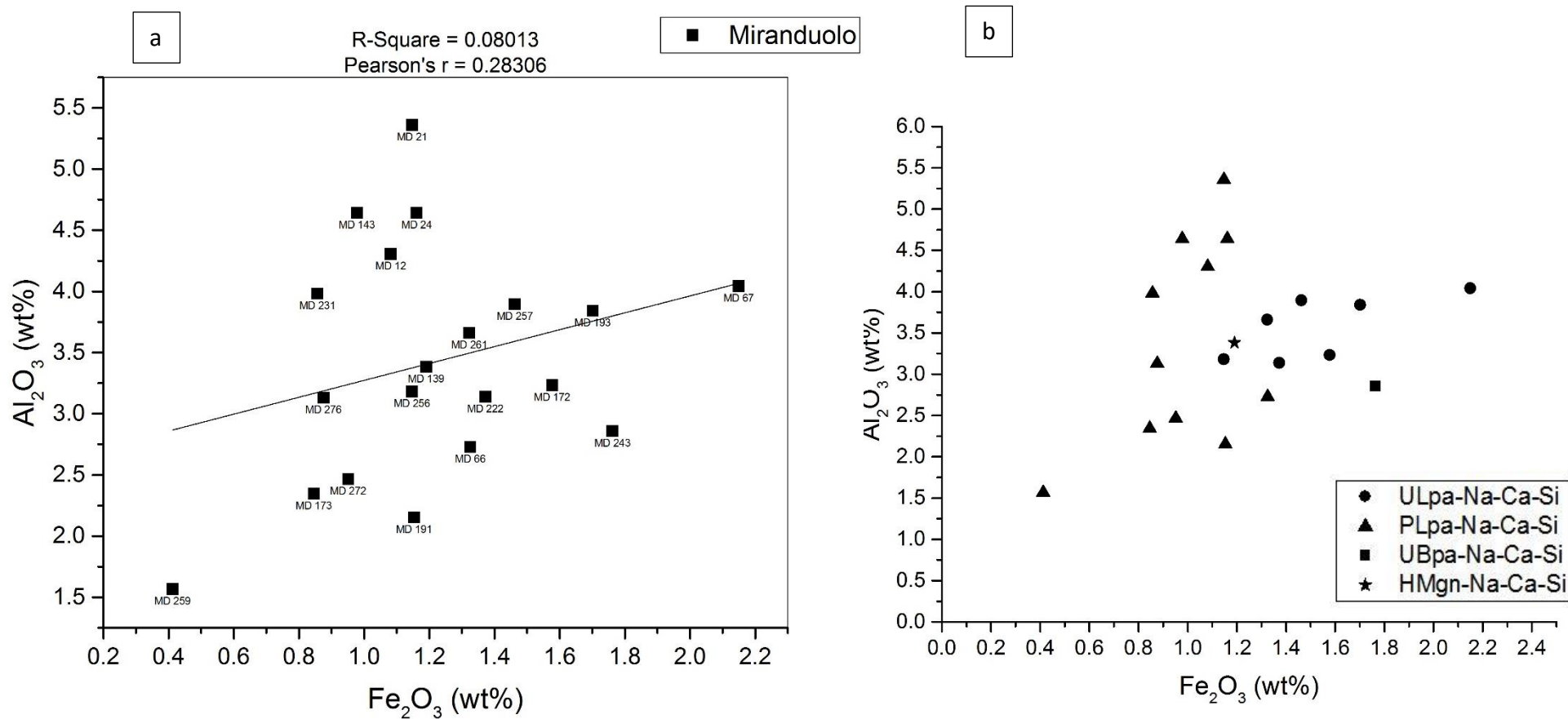


Figure App.5-6 a) Bi-plot of Fe_2O_3 and Al_2O_3 with marked Miranduolo sample names and r and r^2 values; b) Bi-plot of Fe_2O_3 and Al_2O_3 of Miranduolo samples with marked compositional groups.

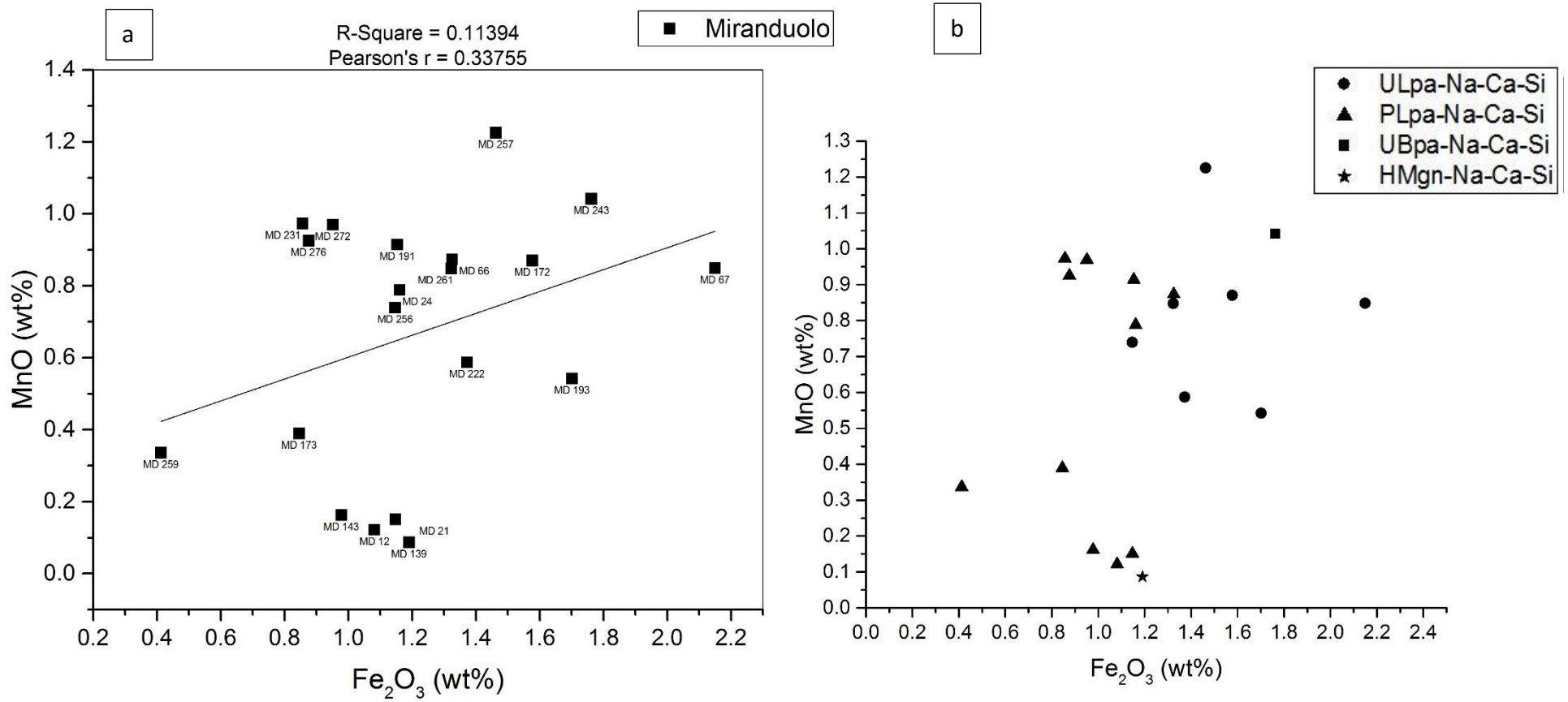


Figure App.5-7 a) Bi-plot of Fe₂O₃ and MnO with marked Miranduolo sample names and r and r² values; b) Bi-plot of Fe₂O₃ and MnO of Miranduolo samples with marked compositional groups.

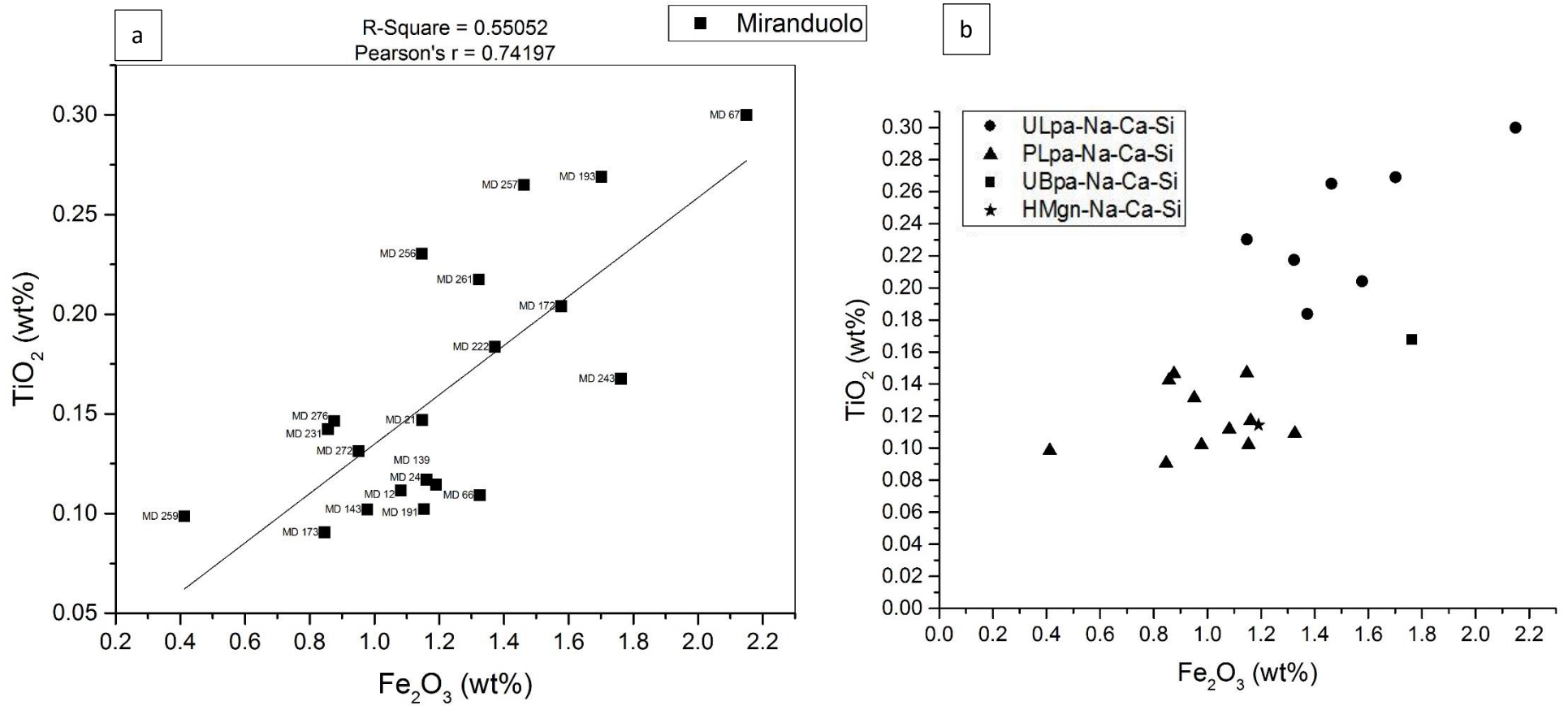


Figure App.5-8 a) Bi-plot of Fe_2O_3 and TiO_2 with marked Miranduolo sample names and r and r^2 values; b) Bi-plot of Fe_2O_3 and TiO_2 of Miranduolo samples with marked compositional groups.

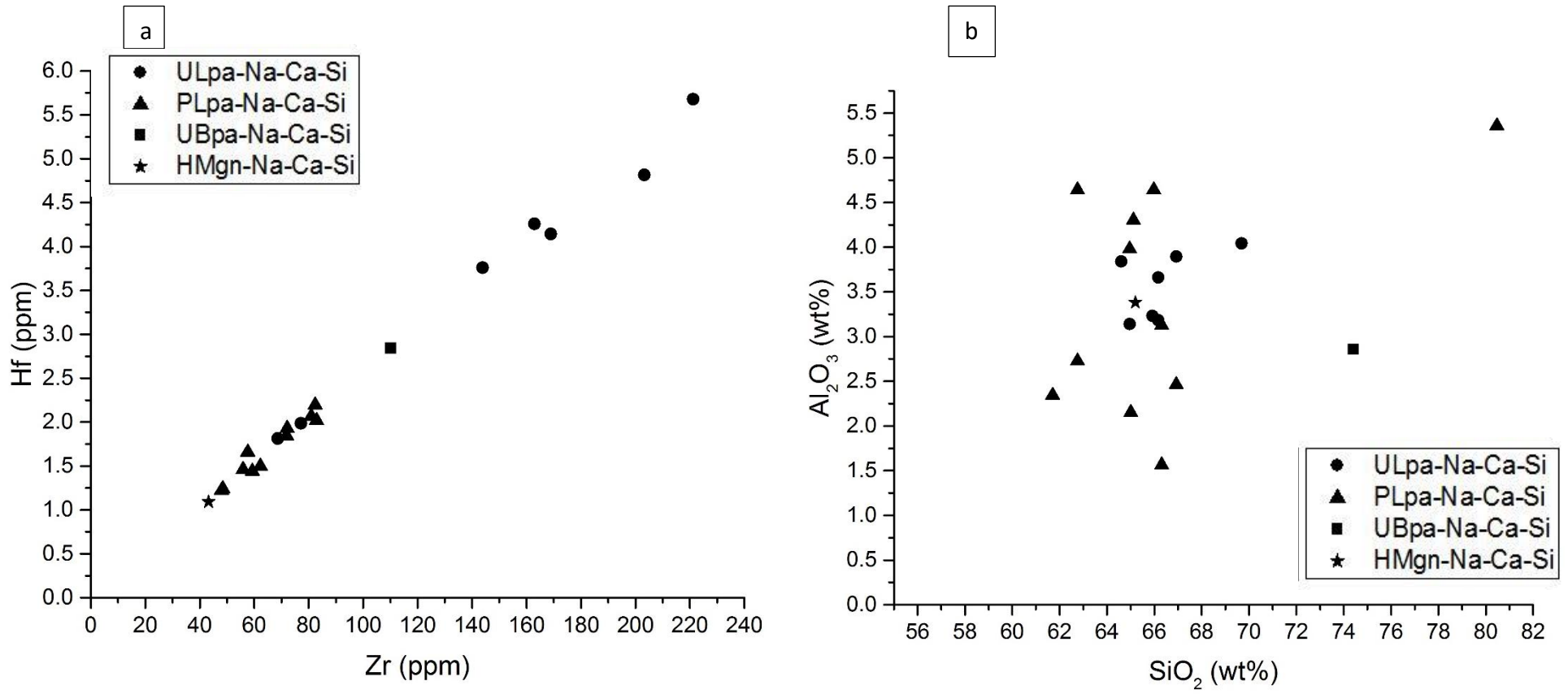


Figure App.5-9 a) Bi-plot of Zr and Hf of Miranduolo samples with marked compositional groups; b) Bi-plot of SiO₂ and Al₂O₃ of Miranduolo samples with marked compositional groups.

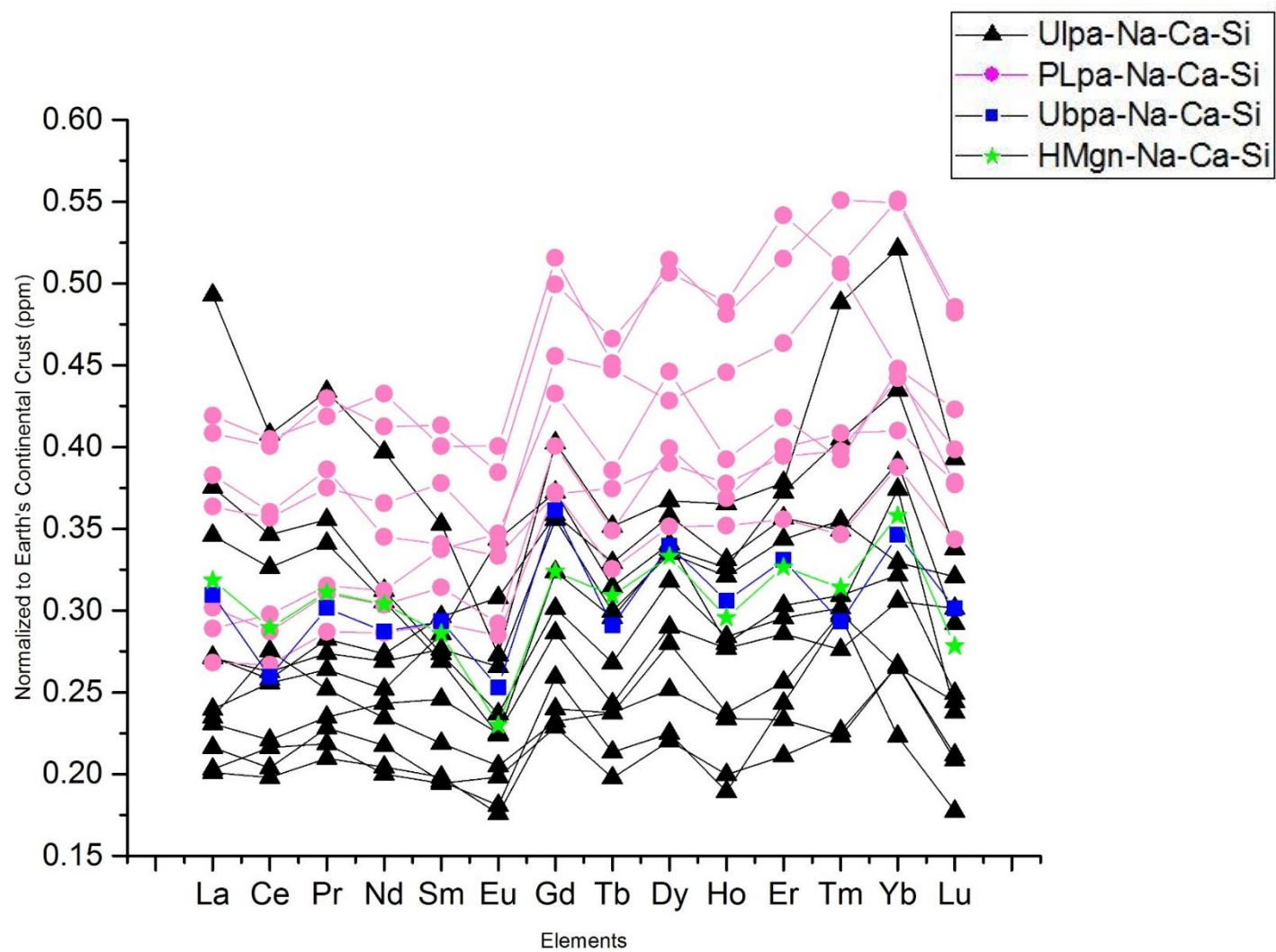


Figure App.5-10 Representation of Miranduolo REE normalized to Earth's Continental Crust with marked compositional groups.

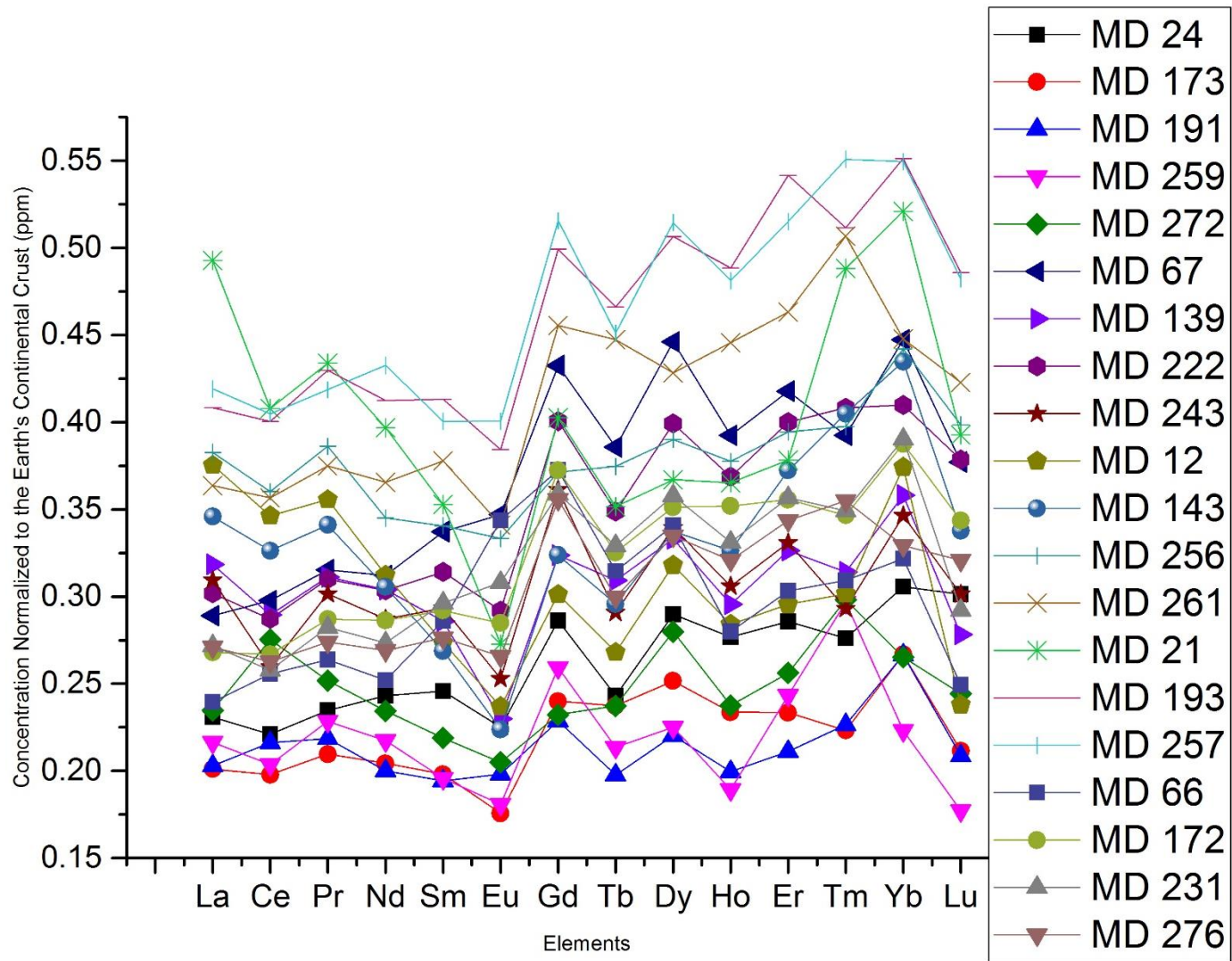


Figure App.5-11 Representation of Miranduolo REE normalized to Earth's Continental Crust with each sample marked.

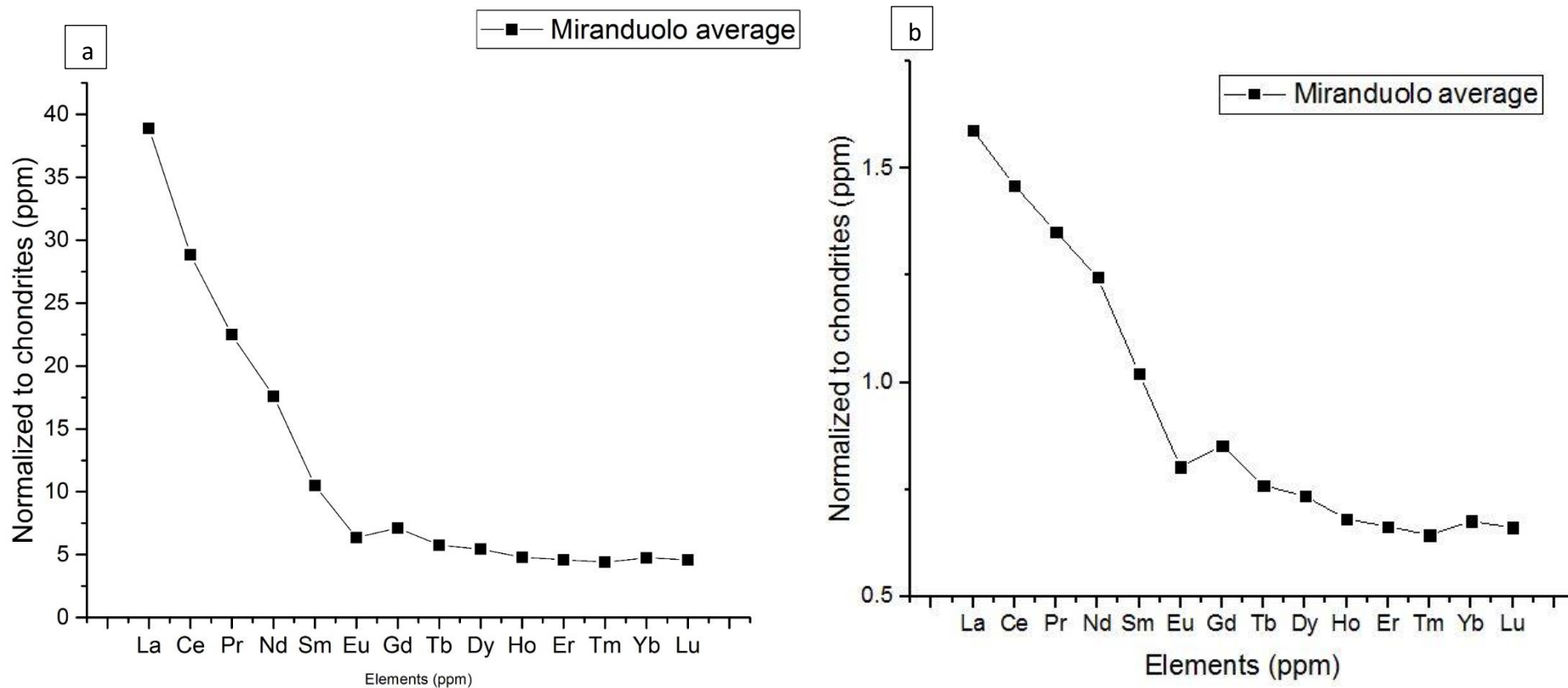


Figure App.5-12 Representation of Miranduolo's average REE normalized to chondrites. b) in logarithmic scale.

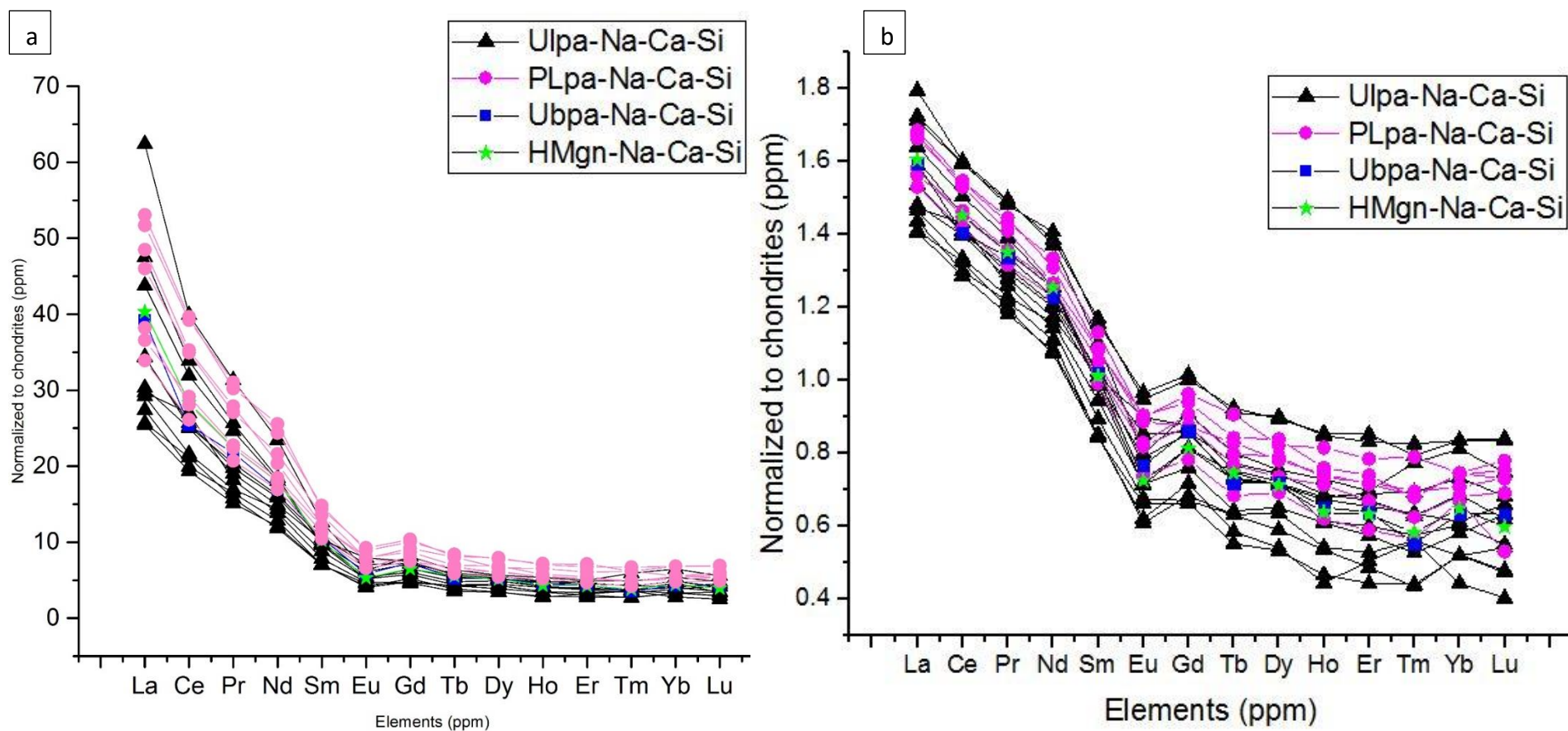


Figure App.5-13 Representation of Miranduolo REE normalized to chondrites with marked compositional groups. b) in logarithmic scale.

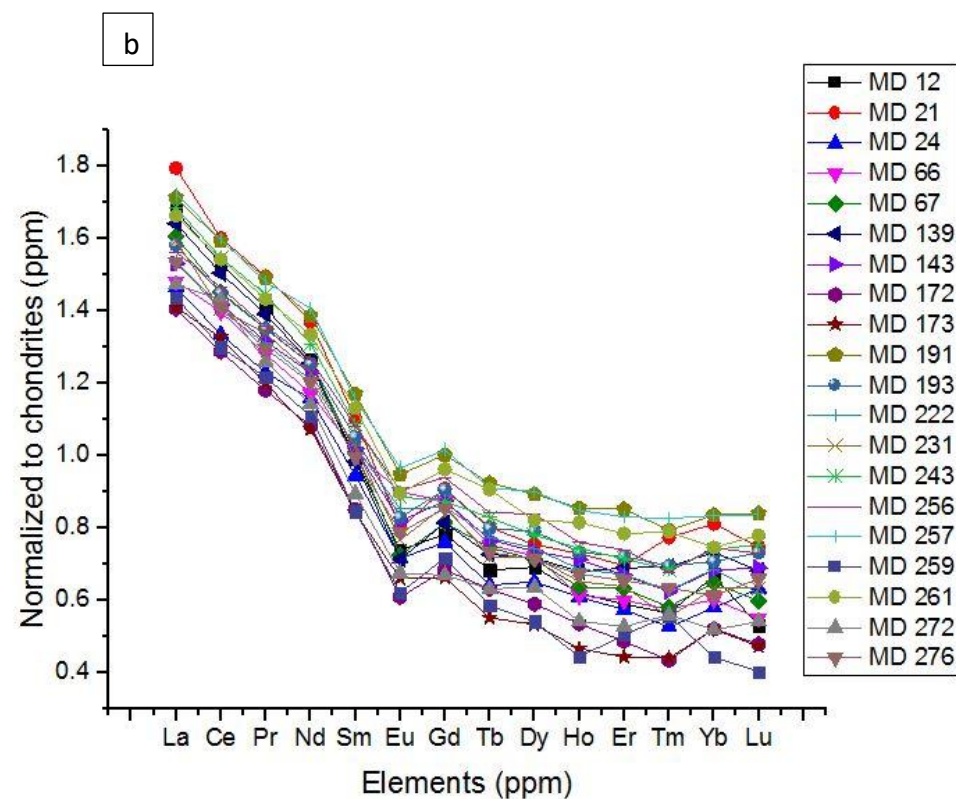
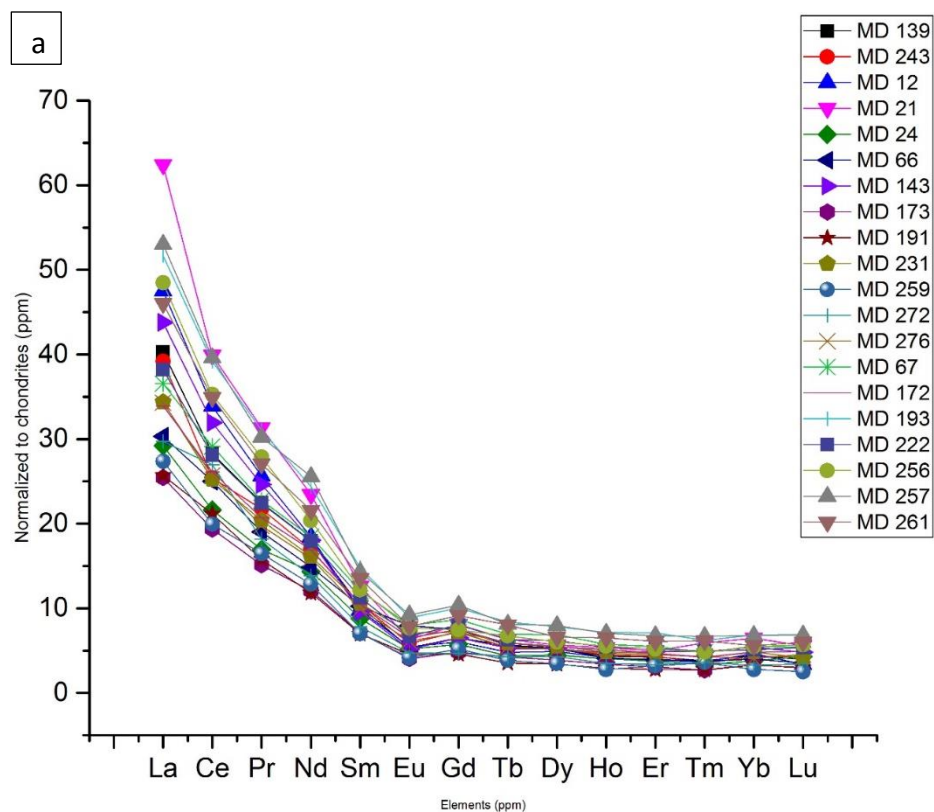


Figure App.5-14 Representation of Miranduolo REE normalized to chondrites with each sample marked. b) in logartithmic scale.

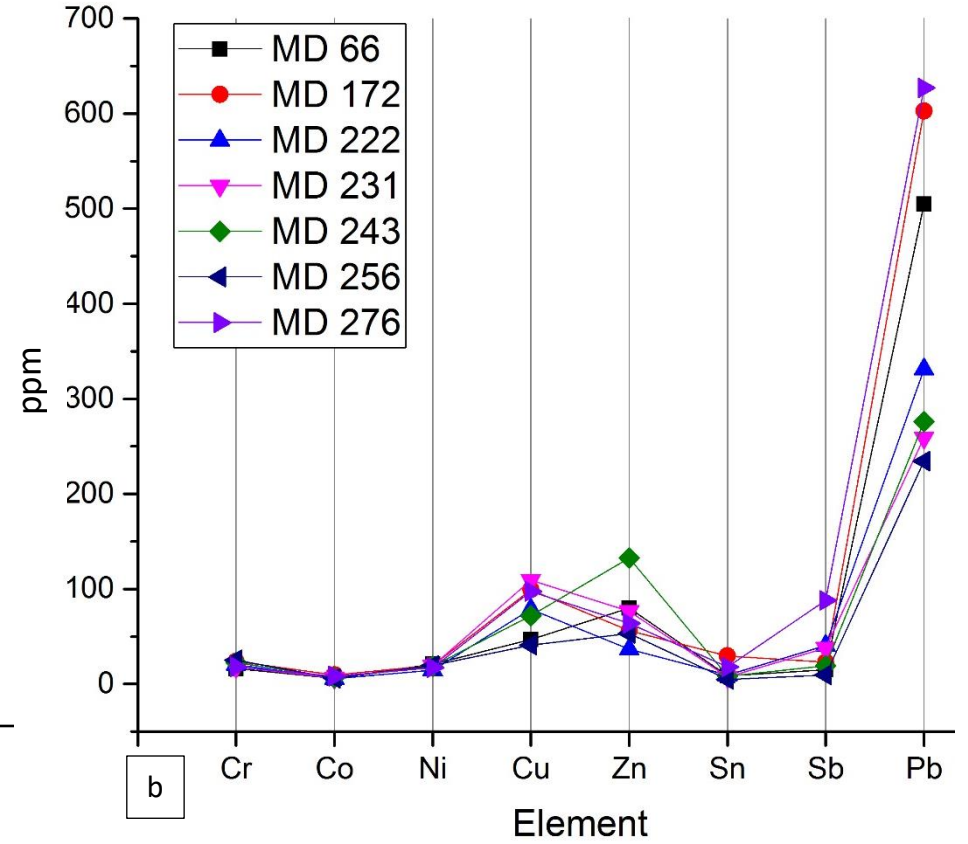
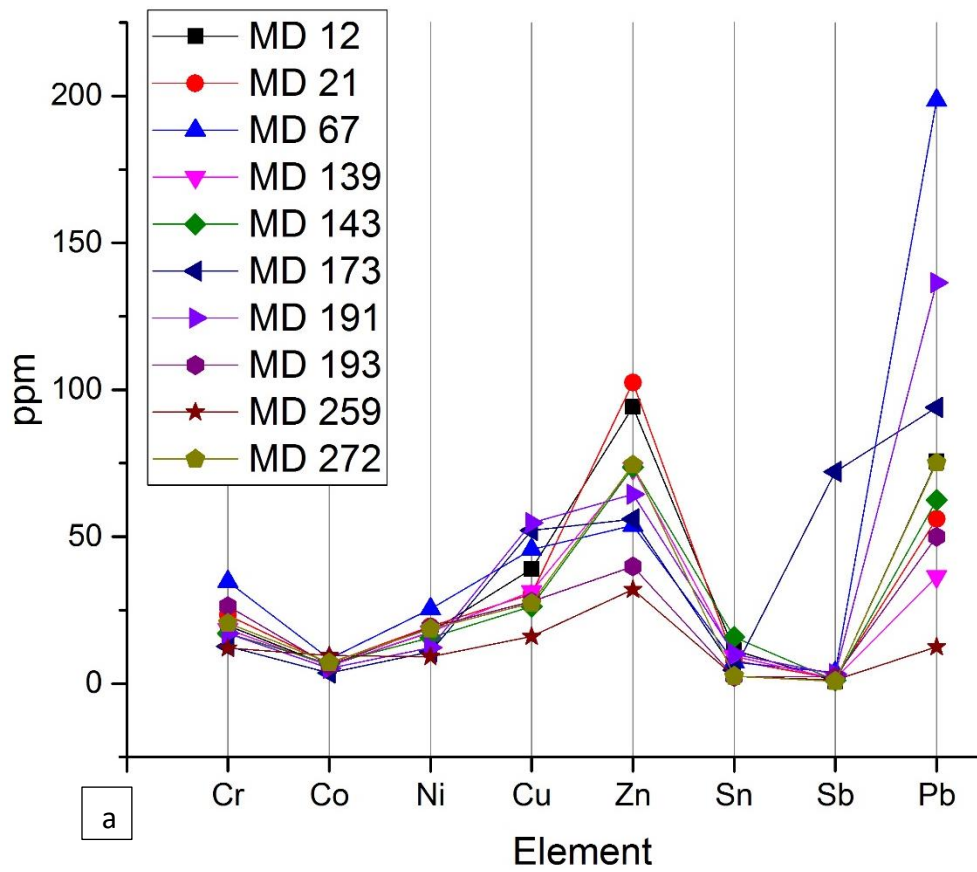


Figure App.5-15 a) and b) Representation of elements that are indicators of recycling for selected Miranduolo samples.

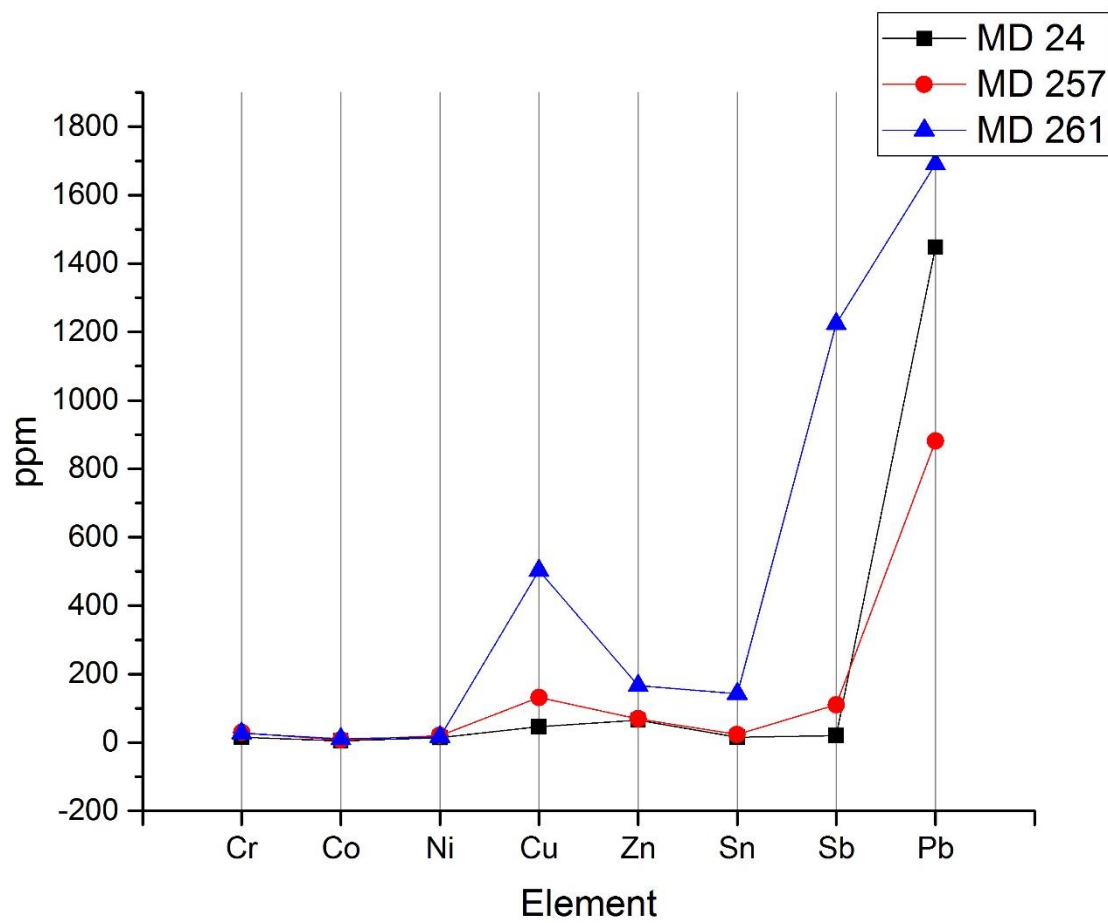


Figure App.5-16 Representation of elements that are indicators of recycling for selected Miranduolo samples.

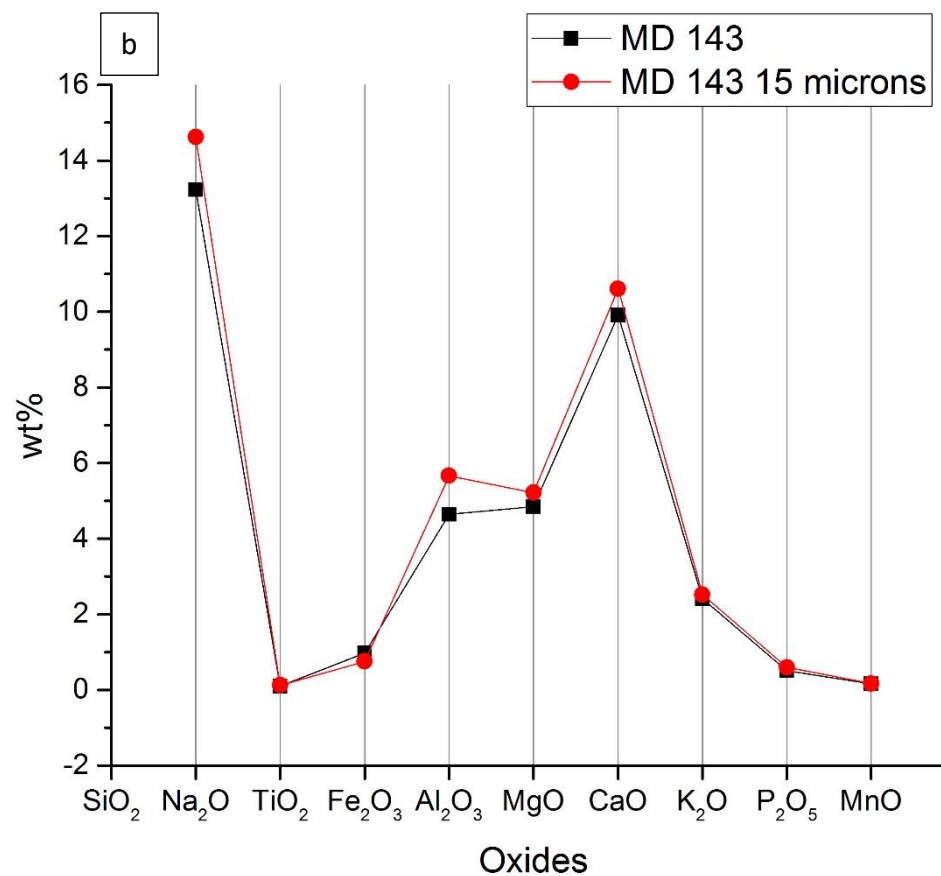
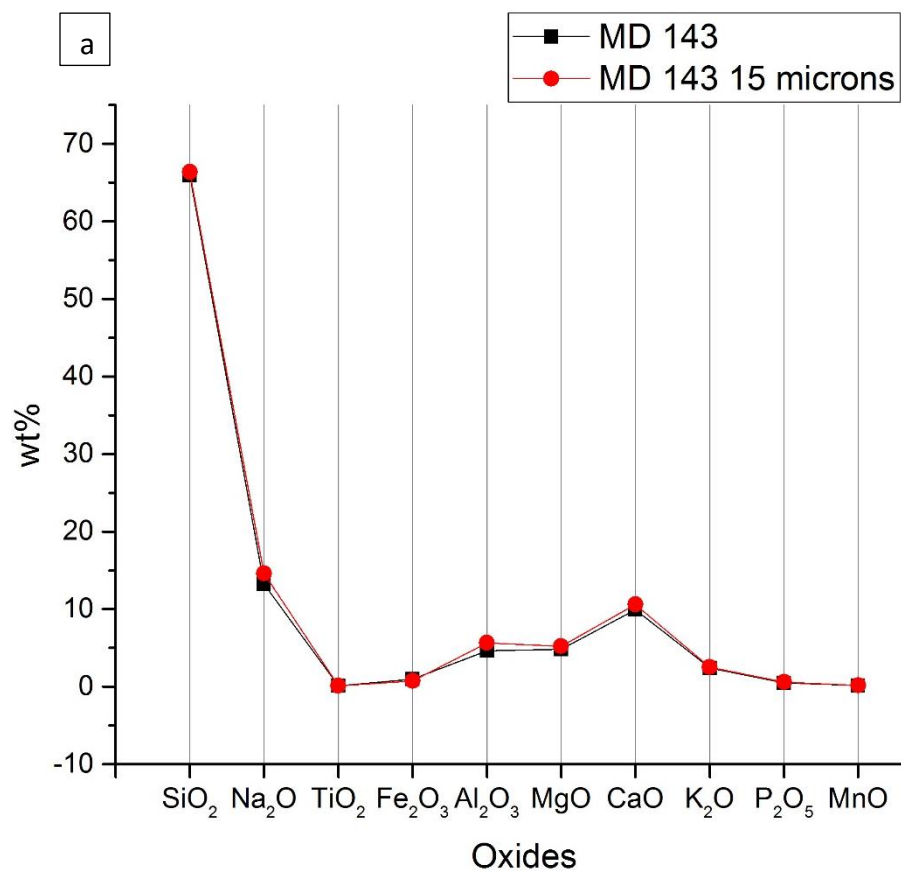


Figure App.5-17 a) and b) Comparison of selected major and minor elements of pristine glass of MD 143 between 50 µm and 15 µm beam size.

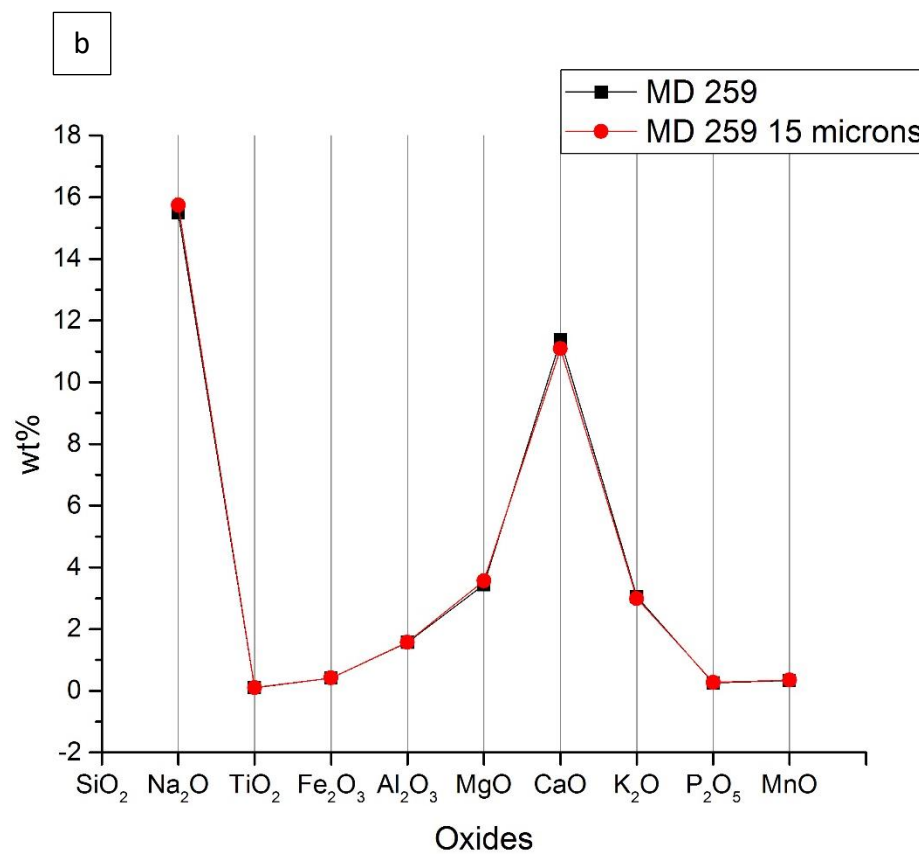
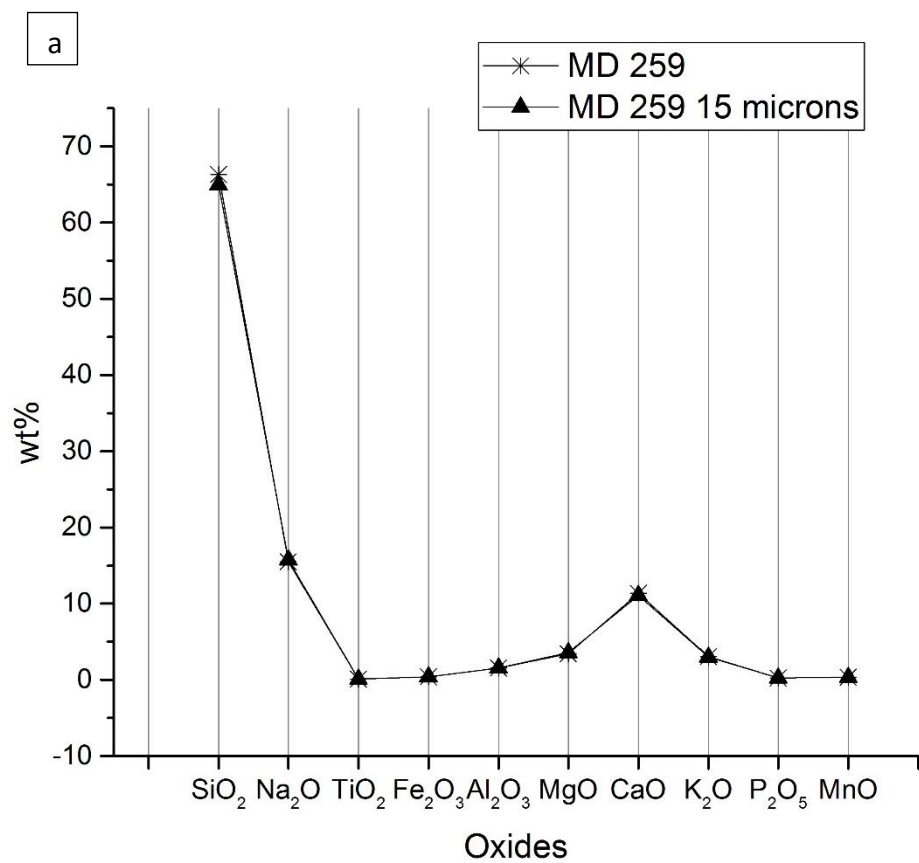


Figure App.5-18 a) and b) Comparison of selected major and minor elements of pristine glass of MD 259 between 50 μm and 15 μm beam size.

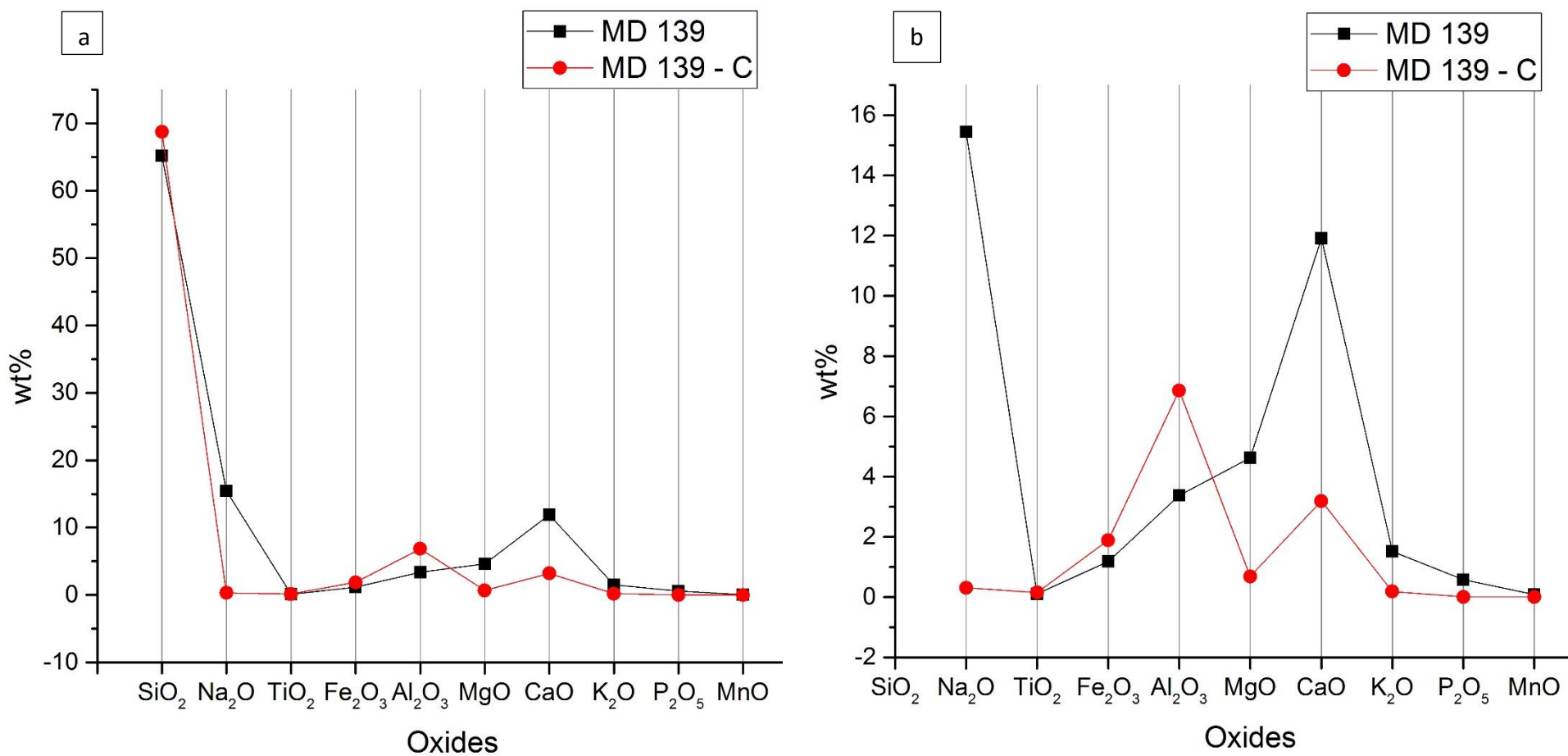


Figure App.5-19 a) and b) Comparison of selected major and minor elements of pristine and corrosion layer of MD 139. C – corrosion.

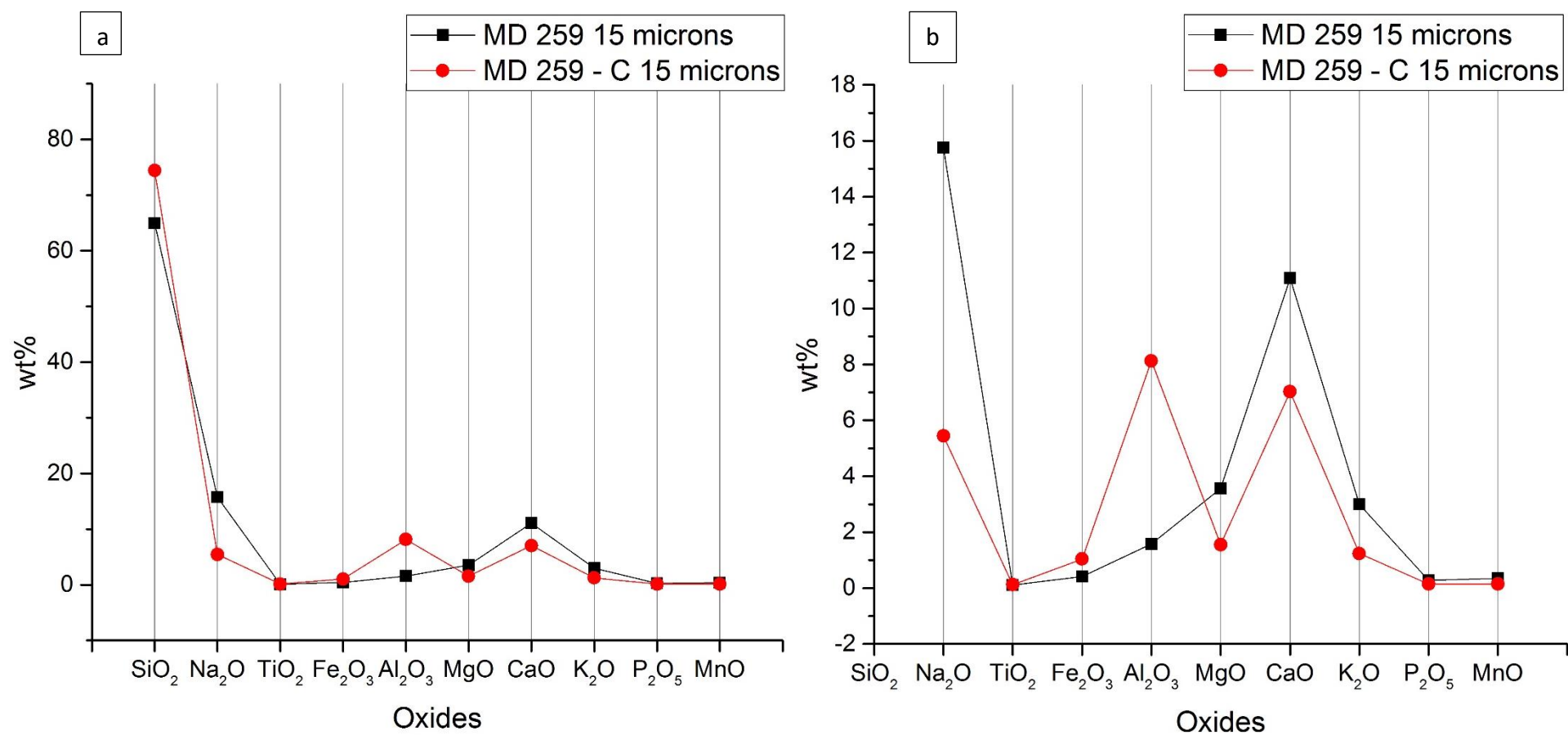


Figure App.5-20 a) and b) Comparison of selected major and minor elements of pristine glass and corrosion layer of MD 259. For pristine glass and the corrosion a 15 μm beam size was used. C – corrosion.

Appendix 6 – Fe₂O₃/MnO ratioTable App.6-1 Comparison of Fe₂O₃ and MnO ratio between PIXE/PIGE and LA-ICP-MS.

wt%	PIXE/PIGE			LA-ICP-MS		
	Fe ₂ O ₃	MnO	Fe ₂ O ₃ /MnO	Fe ₂ O ₃	MnO	Fe ₂ O ₃ /MnO
MD 12	1.04	0.12	8.62	1.08	0.12	8.89
MD 21	1.09	0.14	7.82	1.15	0.15	7.60
MD 24	1.11	0.73	1.52	1.16	0.79	1.47
MD 66	1.17	0.79	1.48	1.33	0.87	1.52
MD 67	1.95	0.80	2.42	2.15	0.85	2.53
MD 139	1.05	0.08	13.17	1.19	0.09	13.73
MD 143	0.96	0.16	5.88	0.98	0.16	6.03
MD 143 – 15 µm				0.76	0.17	4.41
MD 172	1.49	0.87	1.71	1.58	0.87	1.81
MD 173	0.81	0.39	2.06	0.85	0.39	2.17
MD 191	1.03	0.77	1.34	1.15	0.91	1.26
MD 193	1.73	0.59	2.91	1.70	0.54	3.14
MD 222	1.43	0.64	2.25	1.37	0.59	2.34
MD 231	1.16	0.93	1.24	0.86	0.97	0.88
MD 243	2.51	1.02	2.46	1.76	1.04	1.69
MD 256	1.78	0.75	2.36	1.15	0.74	1.55
MD 257	1.78	1.13	1.58	1.46	1.23	1.19
MD 259	0.55	0.32	1.73	0.41	0.34	1.23
MD 259 – 15 µm				0.41	0.35	1.19
MD 261	1.61	0.78	2.07	1.32	0.85	1.56
MD 272	1.22	0.93	1.30	0.95	0.97	0.98
MD 276	1.15	0.89	1.29	0.88	0.93	0.95

Appendix 7 – Comparison of results with contemporary Italian sites

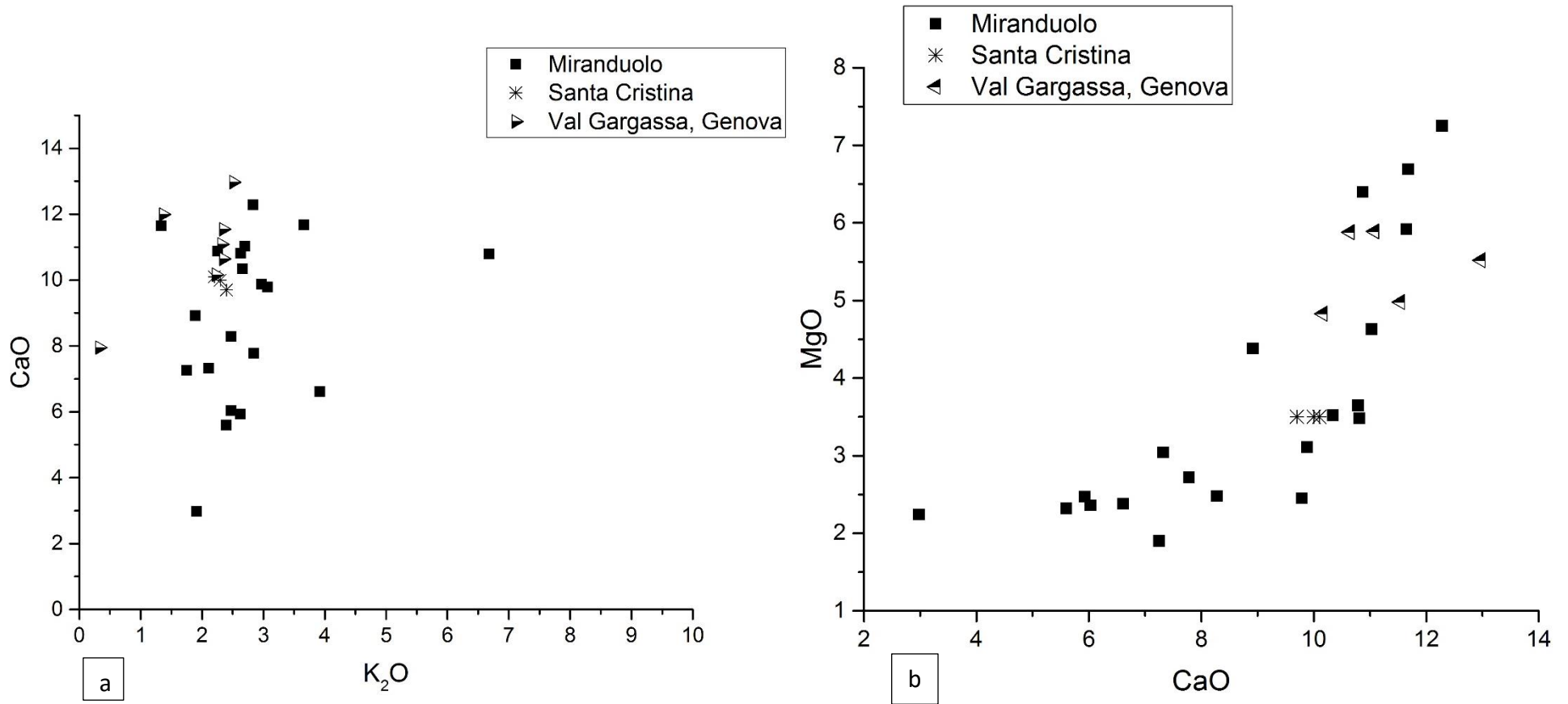


Figure App.7-1 a) EDS Bi-plot of K₂O and CaO with marked 13th-16th century Italian sites; b) EDS Bi-plot of CaO and MgO with marked 13th-16th century Italian sites. Oxides are represented in wt%.

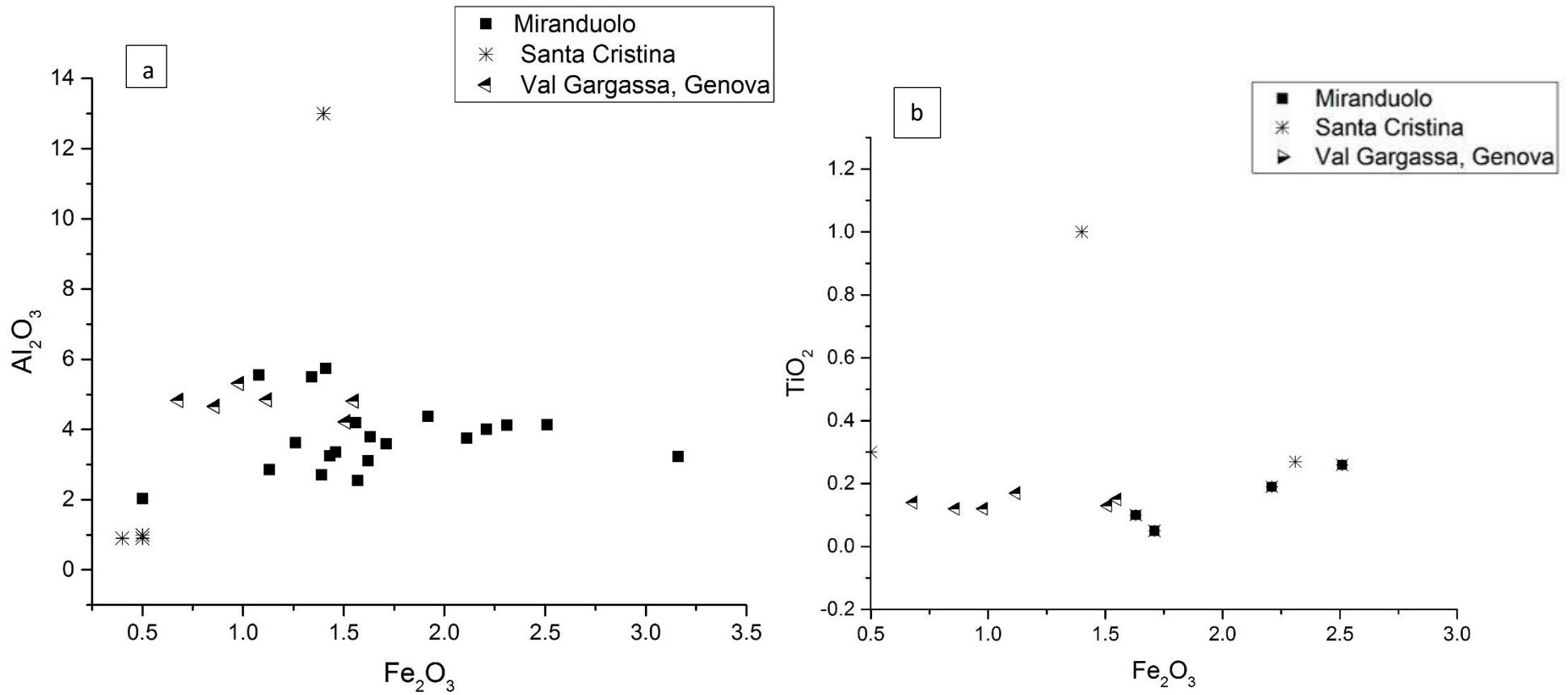


Figure App.7-2 a) EDS Bi-plot of Fe₂O₃ and Al₂O₃ with marked 13th-16th century Italian sites; b) EDS Bi-plot of Fe₂O₃ and TiO₂ with marked 13th-16th century Italian sites. Oxides are represented in wt%.

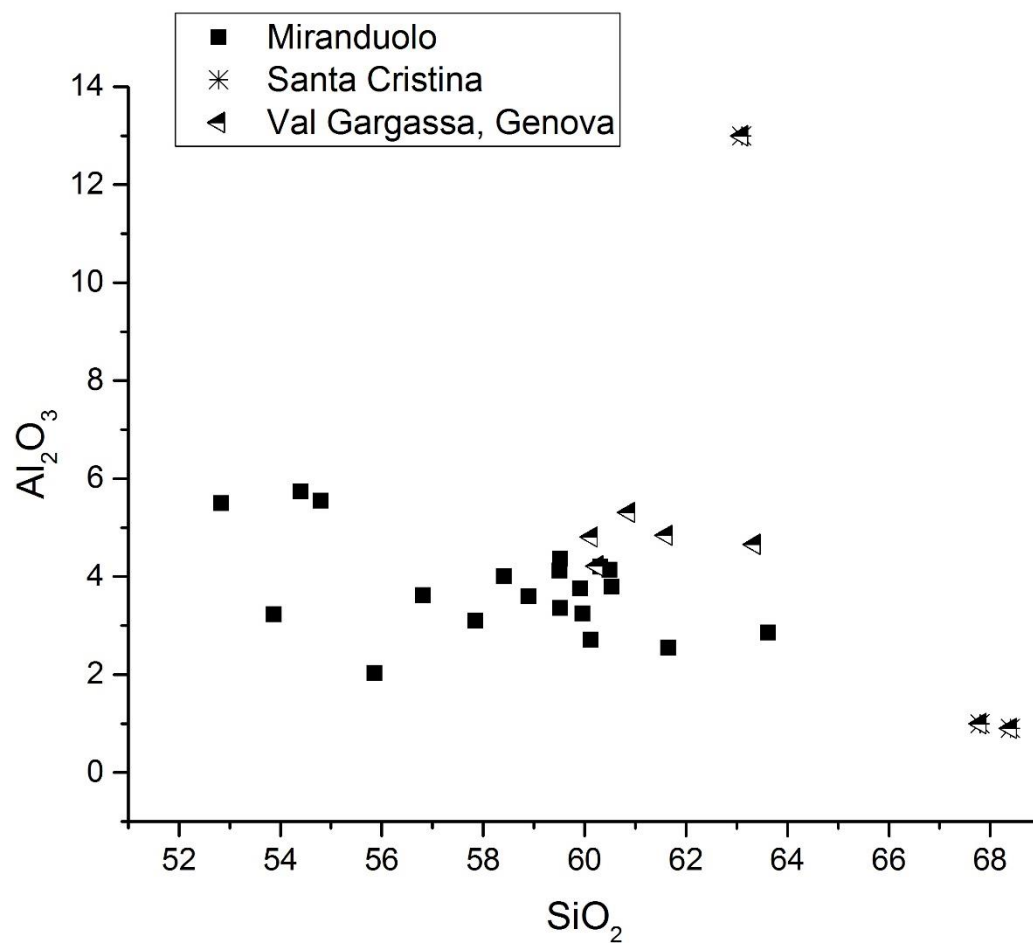


Figure App.7-3 EDS Bi-plot of SiO₂ and Al₂O₃ with marked 13th-16th century Italian sites. Oxides are represented in wt%.

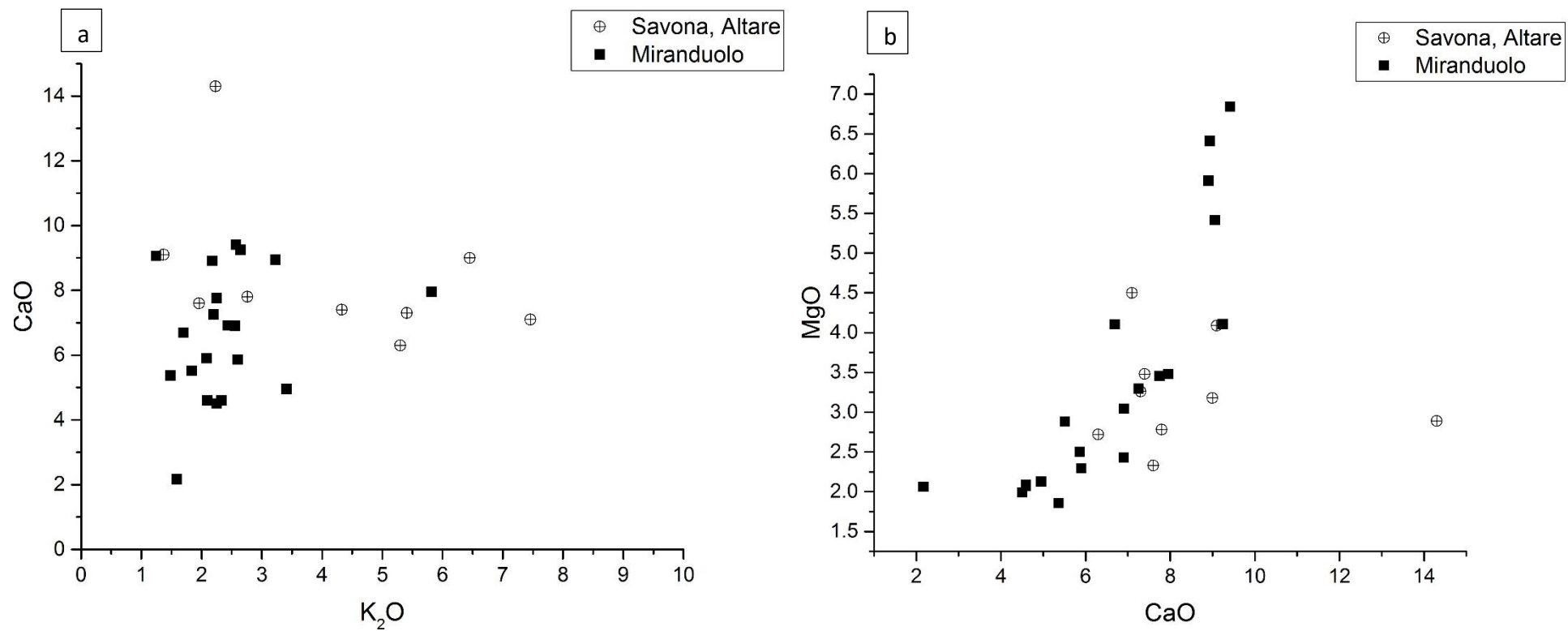


Figure App.7-4 a) PIXE/PIGE bi-plot of K₂O and CaO with marked 13th-14th century Italian sites; b) PIXE/PIGE bi-plot of CaO and MgO with marked 13th-14th century Italian sites. Oxides are represented in wt%.

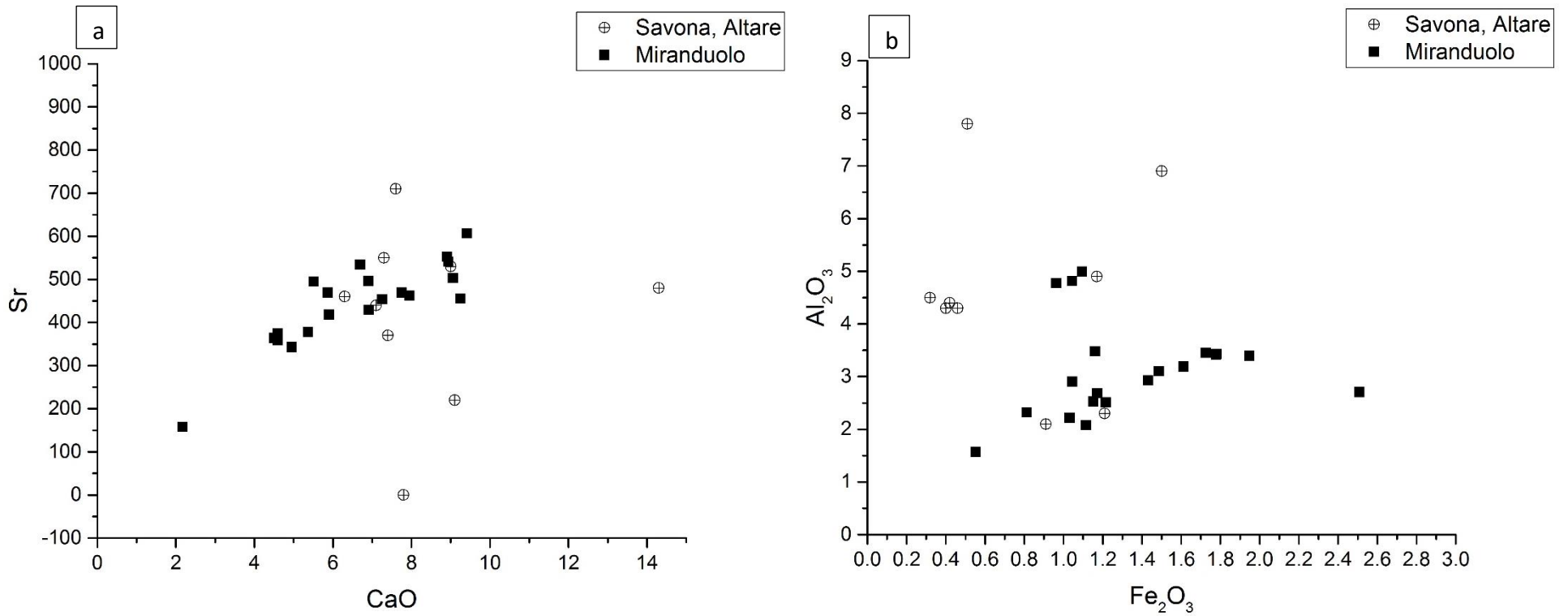


Figure App.7-5 a) PIXE/PIGE bi-plot of CaO and Sr with marked 13th-14th century Italian sites; b) PIXE/PIGE bi-plot of Fe₂O₃ and Al₂O₃ with marked 13th-14th century Italian sites. Oxides are represented in wt%, while elements in ppm.

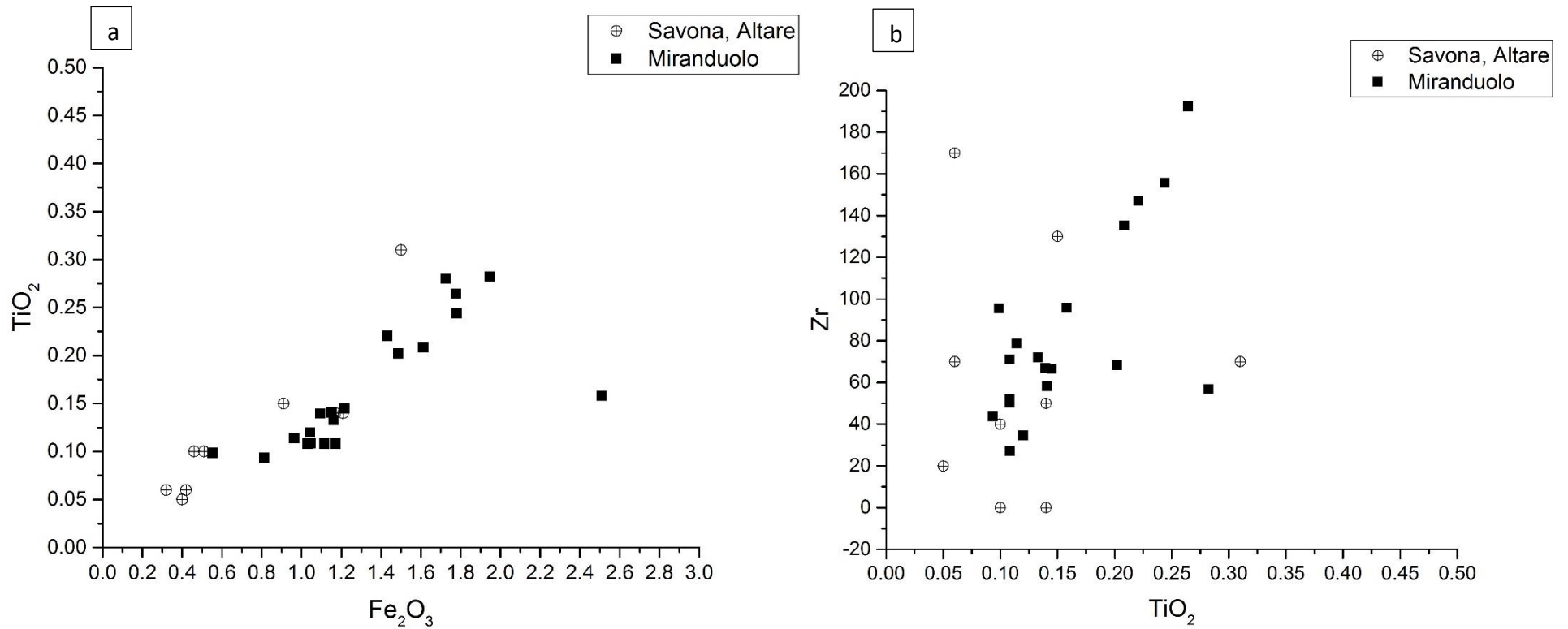


Figure App.7-6 a) PIXE/PIGE bi-plot of Fe_2O_3 and TiO_2 with marked 13th-14th century Italian sites; b) PIXE/PIGE bi-plot of TiO_2 and Zr with marked 13th-14th century Italian sites. Oxides are represented in wt%, while elements in ppm.

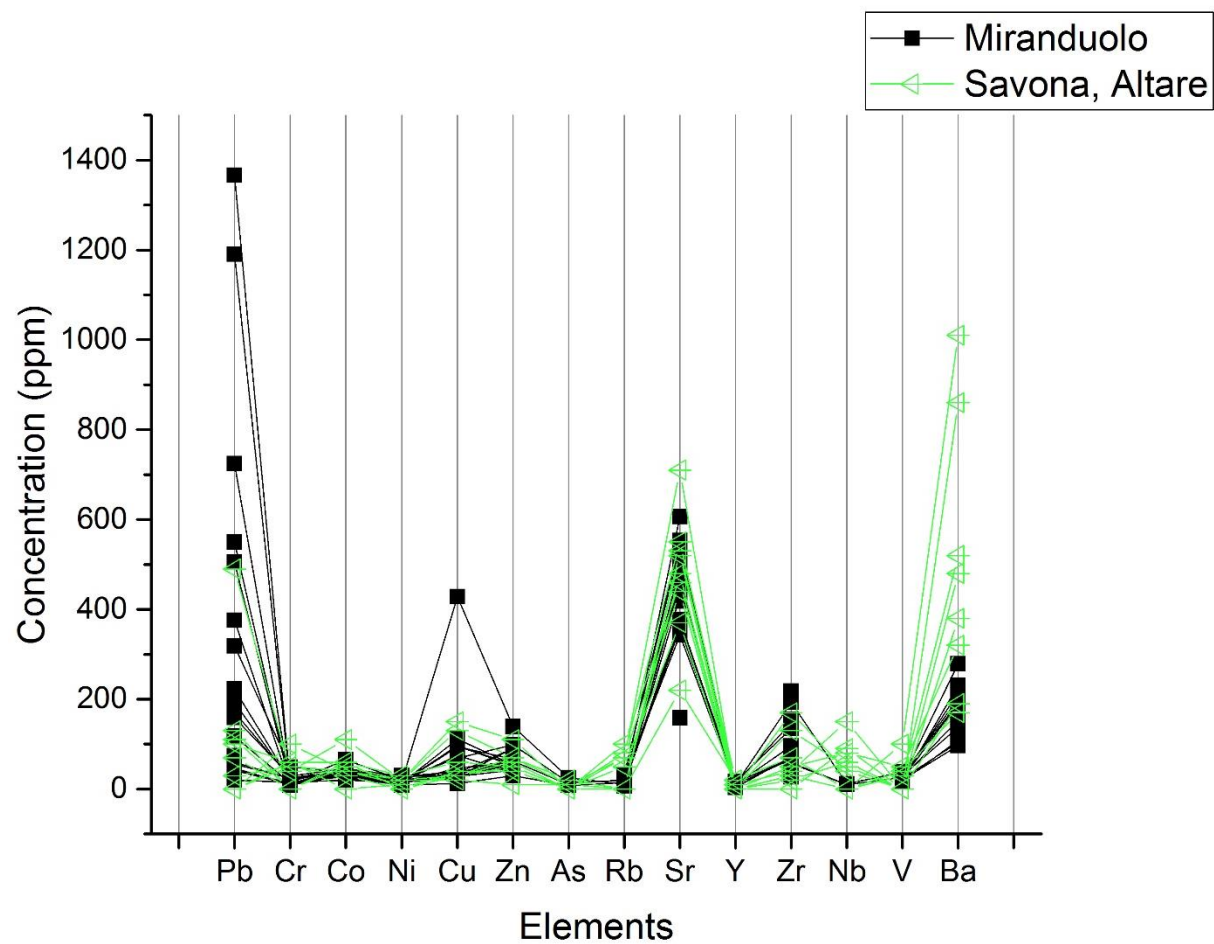


Figure App.7-0-7 PIXE/PIGE comparison of selected elements with marked 13th-14th century Italian sites.

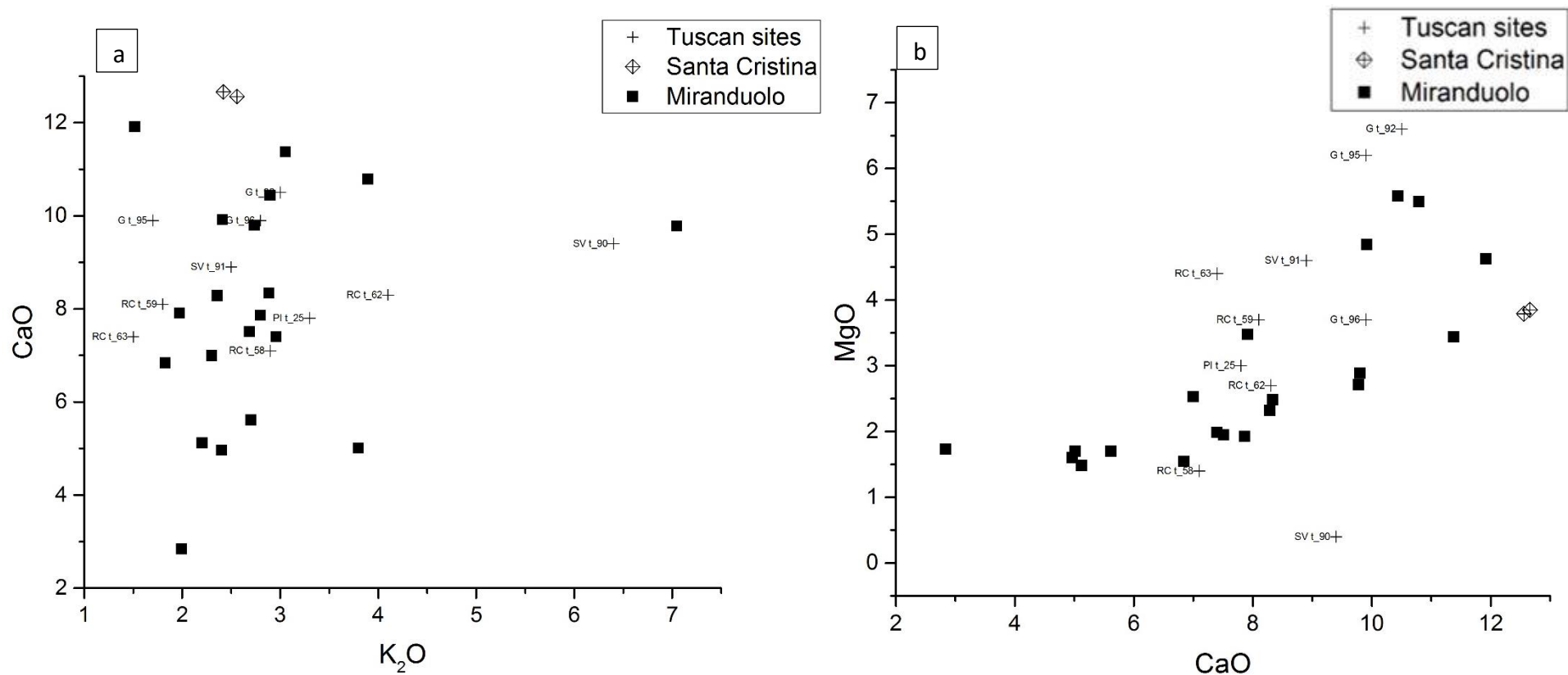


Figure App.7-8 a) LA-ICP-MS bi-plot of K_2O and CaO with marked 13th-14th century Italian sites; b) LA-ICP-MS bi-plot of CaO and MgO with marked 13th-14th century Italian sites. Oxides are represented in wt%. Tuscan sites have marked abbreviations of the sites (except Santa Cristina), with sample names: G- Germagnana, PI – Poggio Imperiale, RC – Rocca di Campiglia and SV – San Vettore.

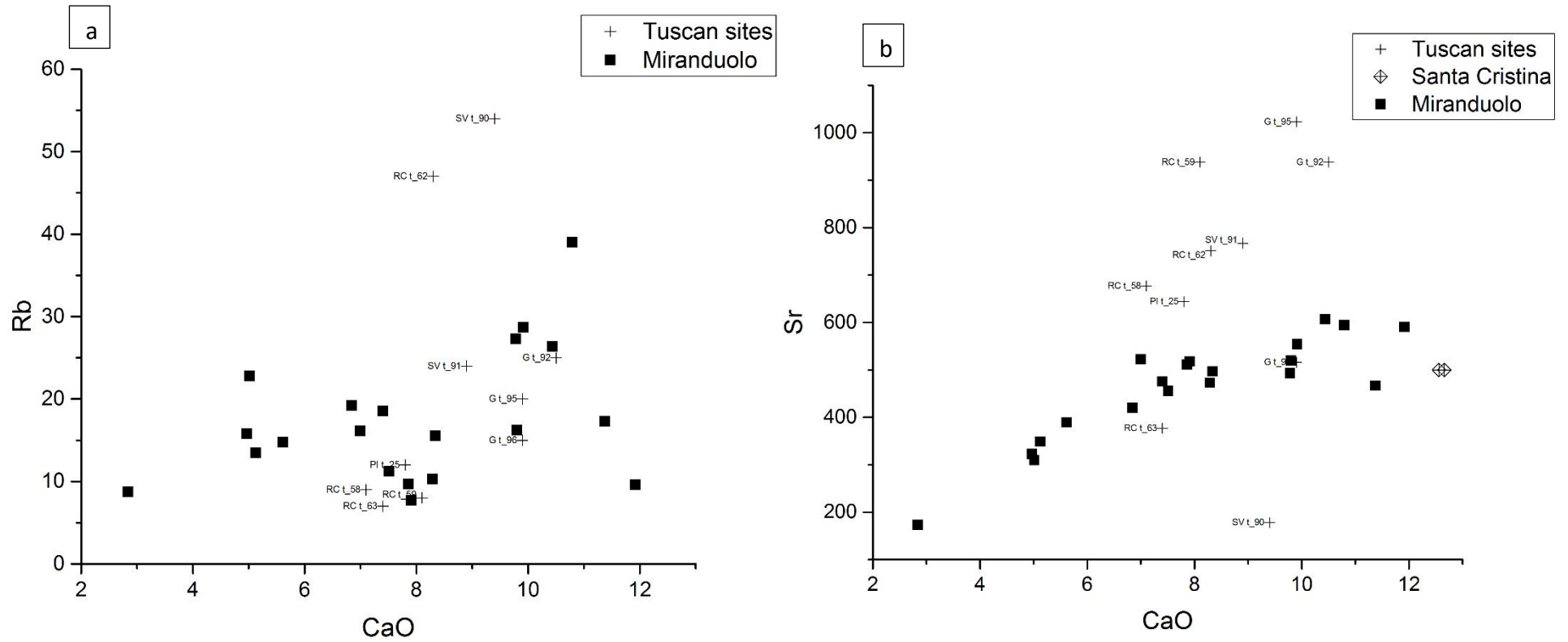


Figure App.7-9 a) LA-ICP-MS bi-plot of CaO and Rb with marked 13th-14th century Italian sites; b) LA-ICP-MS bi-plot of CaO and Sr with marked 13th-14th century Italian sites. Oxides are represented in wt%, while elements in ppm. Tuscan sites have marked abbreviations of the sites (except Santa Cristina), with sample names: G- Germagnana, PI – Poggio Imperiale, RC – Rocca di Campiglia and SV – San Vettore.

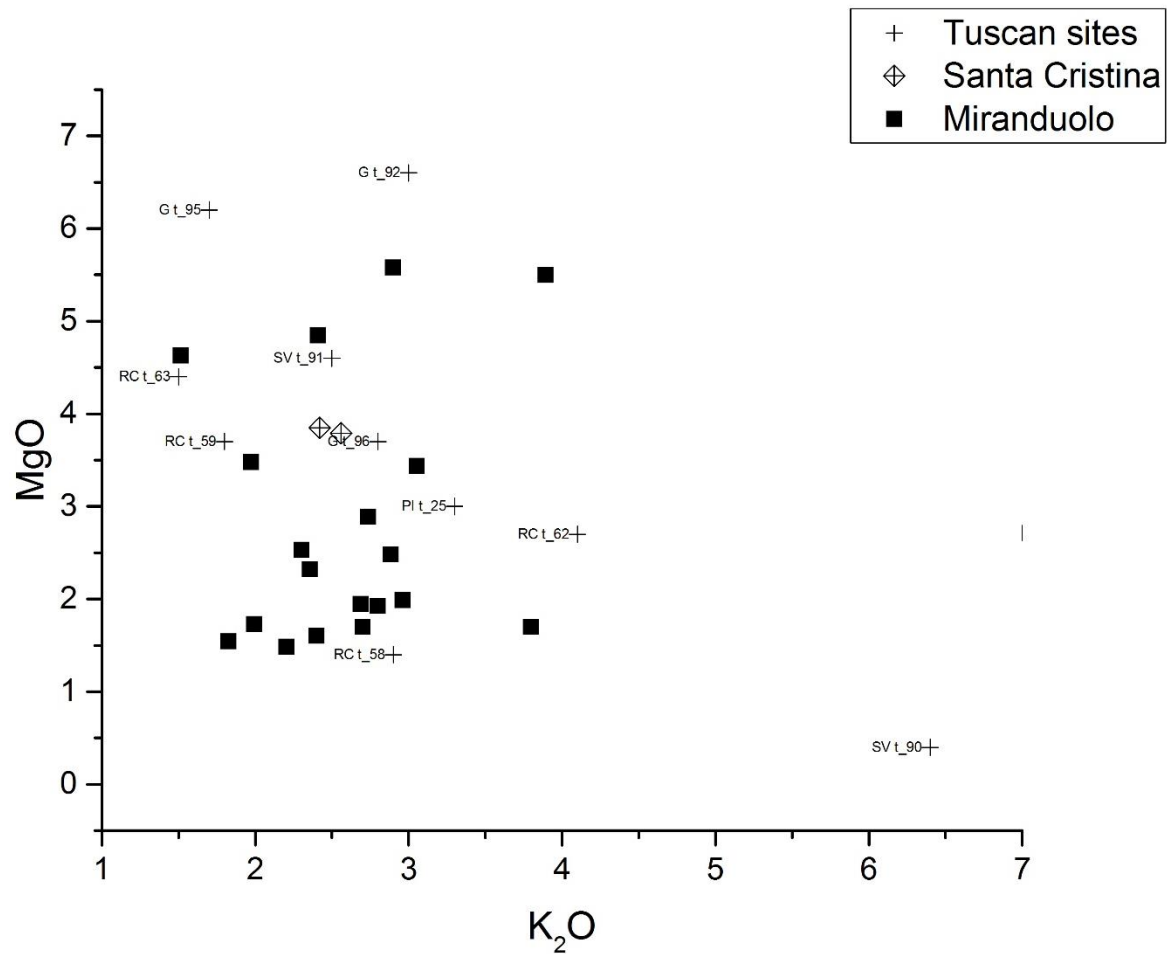


Figure App.7-10 LA-ICP-MS bi-plot of K₂O and MgO with marked 13th-14th century Italian sites. Oxides are represented in wt%. Tuscan sites have marked abbreviations of the sites (except Santa Cristina), with sample names: G- Germagnana, PI – Poggio Imperiale, RC – Rocca di Campiglia and SV – San Vettore.

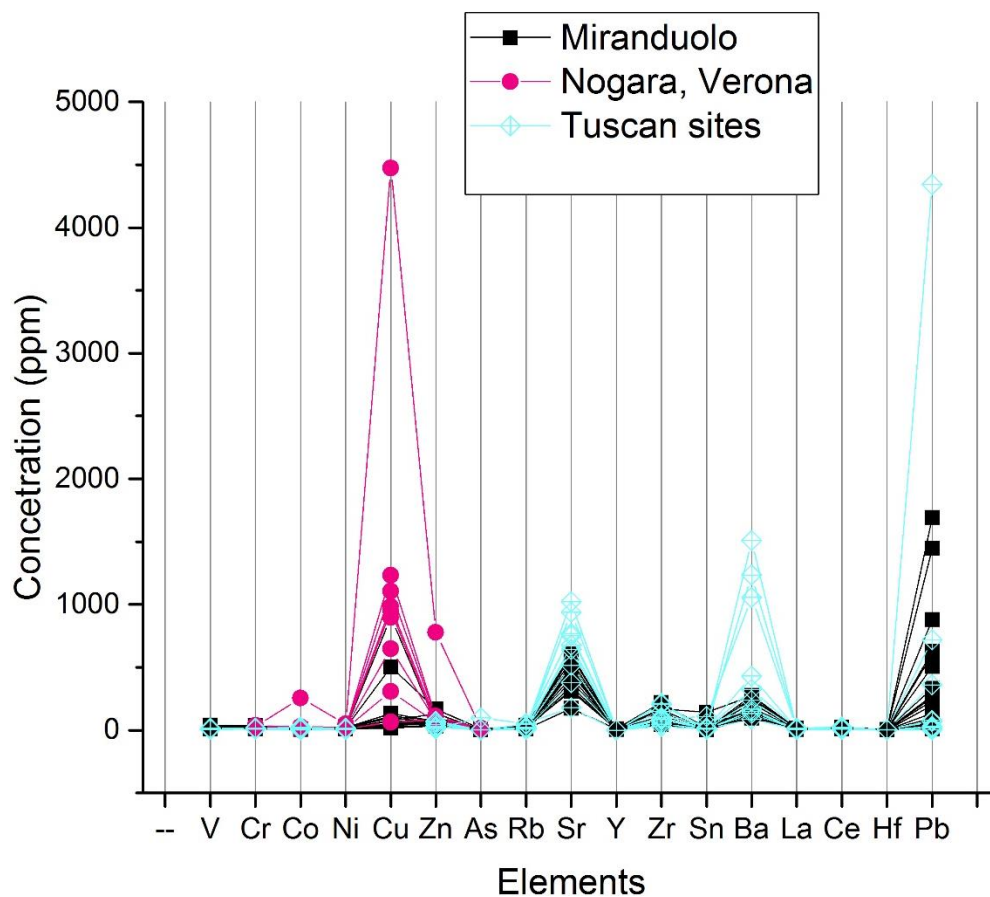


Figure App.7-11 LA-ICP-MS representation of selected results with marked 13th-14th century Italian sites. Not all marked sites have all the elements analyzed, hence could not be presented. Tuscan sites include Germagnana, Poggio Imperiale, Rocca di Campiglia and San Vettore.

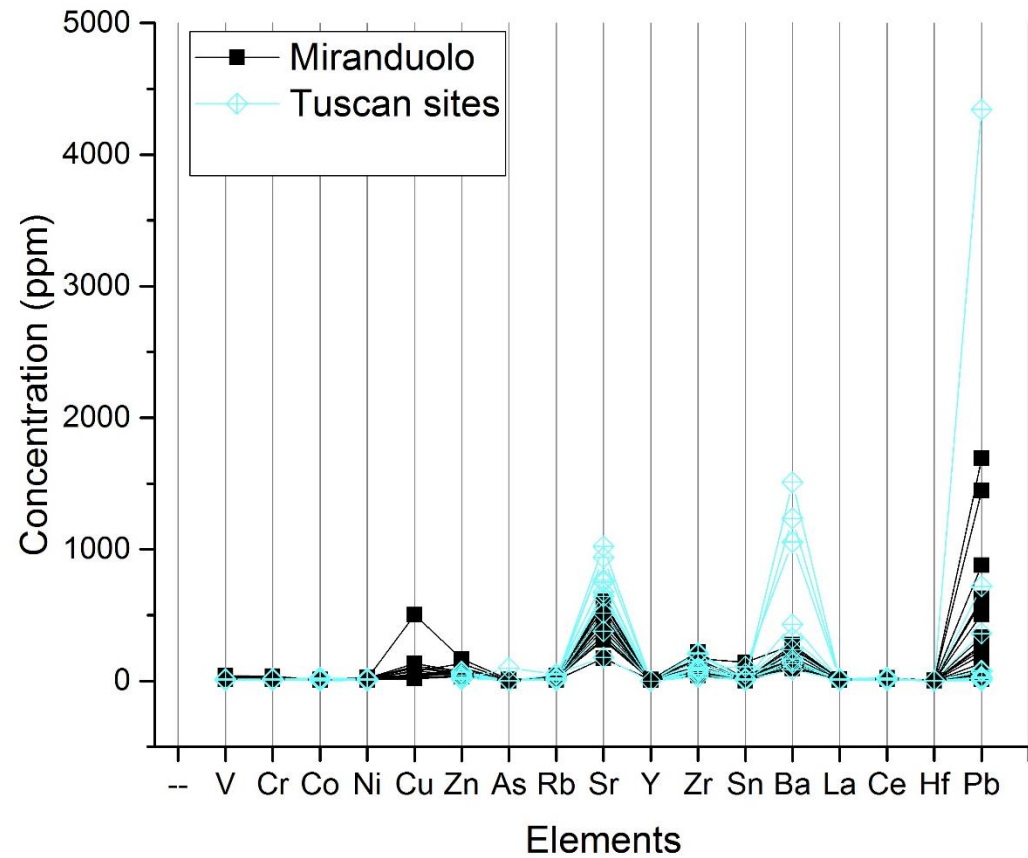


Figure App.7-12 LA-ICP-MS representation of selected results with marked 13th-14th century Italian sites. Not all marked sites have all the elements analyzed, hence could not be presented. Tuscan sites include Germagnana, Poggio Imperiale, Rocca di Campiglia and San Vettore.